Effective field theory flavored paths to beyond the Standard Model dynamics

Tesi Doctoral

Programa de Doctorat en Física

Autor:
Kevin Monsálvez Pozo

Director:
Dr. Jorge Portolés

Departament de Física Teòrica

IFIC, Universitat de València - CSIC

Septembre 2022

A mis padres, a mi hermano
y a María

Jorge Portolés Ibáñez, Científic Titular d'Organismes Públics d'Investigació (CSIC),

Certifica:

Que la present memòria "Effective field theory flavored paths to beyond the Standard Model dynamics" ha sigut realitzada sota la seua direcció a l'Institut de Física Corpuscular, centre mixt de la Universitat de València i del CSIC, per **Kevin Monsálvez Pozo** i constitueix la seua Tesi per a optar al grau de Doctor en Física.

I perquè així conste, en compliment de la legislació vigent, presenta en el Departament de Física Teòrica de la Universitat de València la referida Tesi Doctoral, i firma el present certificat.

València, a 2 de septembre de 2021.

Jorge Portolés Ibáñez

Vist i plau del tutor, Prof. Antonio Pich Zardoya

Acknowledgements

La etapa del doctorado, que culmina con la redacción de esta tesis, ha sido una de las más bonitas de mi vida. Esto se debe tanto a la pasión que despierta en mí la física, como por las personas que me han acompañado en este periodo. He podido viajar, conocer gente y sitios nuevos, además de profundizar en el entendimiento de la física, pero lo más importante es que he podido compartir todo esto con gente fantástica. Me gustaría mostraros mis más sinceros agradecimientos.

Quiero empezar por el inicio, y el mío está en mis padres: mi madre Conso y mi padre Vicente. Sé que no puedo llegar a transmitiros todo el agradecimiento que siento por todo lo que habéis hecho por mí a lo largo de los años. No obstante, espero que estas palabras sirvan para mostraros que sé bien el grandísimo esfuerzo que habéis realizado para darnos lo mejor a Borja y a mí. Muchísimas gracias por todo, por lo material y por lo inmaterial: por la educación que nos habéis impartido, por la libertad que nos habéis dado incluso a una edad temprana, por confiar en nosotros y por animarnos siempre a hacer lo que más nos motivaba. Estoy muy orgulloso de la familia que tengo y eso incluye también a mi hermano Borja. Quiero que sepas que estoy muy orgulloso de ti como persona y del ingeniero en que te has convertido. Y como a los papás, quiero darte las gracias por todos estos años juntos, por tu confianza, por las charlas de hermanos y, en general, por todos los momentos compartidos. Son muchas las cosas que agradecer y seguirán aumentando. Gracias también a ti Paulina por acompañarle en su vida. Gracias también a los Pozo (o *Cucos*) y a los Monsálvez por vuestro apoyo todos estos años y a sus creadores, mis abuelos. Gracias por el orgullo que siempre habéis sentido hacia nosotros y por la infancia que nos disteis, no la cambiaría por ninguna otra.

Vull agrair ara a un dels pilars fonamentals de la meua vida. Si, a tu María. De nou em passa que les paraules se'm queden curtes. Com puc agrair-te el suficient tot el que has fet per mi, el que hem viscut junts i el que he aprés amb tu? Em sent molt afortunat d'haver trobat una companya de viatge com tu. M'has ensenyat molts aquests anys, tant a nivell humà, com psicològic, social i polític, però el més important és que has elegit acompanyar-me, almenys part de la meua vida, i no te'l podria agrair més. Gràcies per tot, per les llargues vesprades (si no dies) de treball junts, per la teua confiança, per donar-me suport en tot el que decidira fer, i estar sempre disposada a ajudar-me. Gràcies per aquest temps.

Un dels principals artífexs que han fet realitat i han donat forma a aquesta etapa ha sigut el meu director: Jorge Portolés. Gràcies Jorge, gràcies per la teua paciència, pels consells, per la llibertat que sempre m'has donat, per la teua sincera implicació, pels llibres que has volgut compartir amb mi... M'has ensenyat com és el món de la investigació en física de partícules i m'has ajudat a introduir-me en ell. Són moltes les coses que m'has ensenyat i per les que he d'agrair-te, però sobretot, que hages aguantat les meues preguntes amb les (llargues) discussions que les seguien. He disfrutat molt d'aquestes i les trobaré a faltar, tant si es tractaven d'algun dubte físic transcendental que em preocupara, com si foren sobre literatura o poesia. Gràcies!

Needless to say, thank you Tomáš, I can *promise* you that it was a real pleasure meeting you and working together. Apart from the nice physics discussions, your insight into Mathematica and your help on it was really invaluable. I am proud of the friendship into which our collaboration has evolved. També vull agrair-te a tu, Toni, que m'obrires la porta del grup i dirigires el meu TFM, va ser una experiència molt enriquidora. Actually, let me thank the whole LHCPHENO group for taking me in, for the meetings and the support I received. En especial, vull donar les gràcies a Ana i Víctor per aguantar les meues preguntes, tant de física com les (innumerables) de HEPfit. Heu estat sempre disposats a donar-me un cop de mà i realment m'heu ajudat moltíssim durant tot el doctorat, no puc estar més agraït. Another colleague at the LHCPHENO I had the opportunity to meet is Luiz. I always have a great time talking to you (regardless of the language we use and despite your gastronomic preferences). The time we worked together was both interesting and fun. Merci pour tout mon pote.

Respecto a mis colaboradores al otro lado del Atlántico: Claudio, Carolina e Iván, solo puedo daros las gracias por acogerme en esa tierra tan bonita que es Chile. Me recibisteis con los brazos abiertos y me guiasteis por el mundo de los neutrinos que yo empezaba a explorar. En este sentido, también quiero agradecer a Martin (Hirsch) por su ayuda desinteresada y las numerosas discusiones sobre estas partículas tan elusivas.

Los siguientes agradecimientos son para Adam, Martín y Víctor. First of all, thank you Adam for hosting me at the IJCLab and give me the opportunity to work with you. Your insight on Physics is incredible and I learnt a lot. Also, you were very open and always willing to help, even when your schedule was tight. Gracias también Martín, me has ayudado mucho con la parte final de la tesis y con tus consejos sobre el mundo académico y los postdocs. De estos meses trabajando juntos me llevo también tu buena intuición física que nos ha hecho avanzar y aprender mucho. Por otro lado, quiero agradecerte, Víctor, todo el trabajo que hemos hecho juntos. Eres una de las personas más trabajadoras que conozco y he disfrutado mucho con nuestras discusiones de física (y también de las de fuera de esta). Thanks again to the three of you.

Manteniéndonos en los dominios de la física, pero vislumbrando la vida más allá, quiero agradecer a mis *pinches*: Navarro, Stefan, Marcos, Pablo y Jose. Gracias por acompañarme estos años, prácticamente día tras día, en la travesía del doctorado en el IFIC. Pero quiero daros las gracias aún más por acompañarme fuera de ella: por todos los planes *de locos*, por las noches planeadas y aún más por las improvisadas, por el Verema, por ser colmena, por los cánticos a la fianza... la lista es larga, pero en resumen, por las risas *al fallo*. Del IFIC me llevo, seguro, unos buenos amigos.

Dins d'aquest selecte grup, vull agrair en especial a qui, des de fa anys, ha sigut com un altre *germà* per a mi: Navarro. De totes les coses que em vaig portar de l'Erasmus, la teua amistat va ser, sense dubte, la millor. Tot el que hem viscut aquests anys junts, viatjant, descobrint coses noves, les llargues converses de la vida, la física, el futur... Totes aquestes experiències (i la muntonà que em deixe) amb algú que pensa de forma tan afí a mi, és algo que no canviaria per res del món. Gràcies *le mec*. Otro descubrimiento de esta etapa has sido tú Stef. Me alegro de que eligieras València para realizar el PhD y haberte conocido. Espero que entre

boda y boda sigas sacando huecos para nosotros. A vosotros dos "solo" me queda deciros una cosa: *o pato*.

De l'altra banda de l'espectre físic: la Universitat, vull agrair de tot cor al trio de Benimaclet: Pau, Andreu i Joan. Sou de les persones més sinceres, autèntiques i amables que conec. He disfrutat molt amb les converses tan interessants i variades que hem tingut, ja fora de política, de jocs, sèries o de la mateixa mecànica quàntica. També m'he divertit moltíssim amb vosaltres, tant jugant a jocs de taula, com eixint a sopar, de festa o en festivals. Sincerament, els sopars dels dijousos es van convertir ràpidament en un dels millors moments de la setmana. A les estivellenques (on englobe a la resta del fantàstic grup que formeu), gràcies també per la vostra amistat aquests anys, no m'estranya que feu tan bona colla tots i totes. No m'oblide de la incorporació estrela al grup uni: Andreu (Masó). Ha sigut un plaer conéixer-te i, com al trio calavera, gràcies per estos anys.

Toca agradecer a otro de mis mejores amigos desde que entré en el mundo de la física: *my frienda* Ferni. Se supone que esto son agradecimientos del PhD, pero como contigo pierdo fácilmente la vergüenza, voy a extenderlos al mismo momento en el que te conocí: gracias por reconocerme y pararme en el metro aquel primer día de la carrera. Lo que hemos vivido juntos daría para un libro, así que simplemente gracias por todo el apoyo, el tiempo compartido y *Topas*.

Siguiendo con amistades unidas por la física, quiero agradecerte, Joan, entre muchas otras cosas, el tiempo que pasamos juntos en París. Durante la carrera ya habíamos congeniado bien, pero se materializó realmente en nuestro *pisito* de Montparnasse: las visitas a los museos, las excursiones de más de cuarenta mil pasos y los más de cuarenta mil restaurantes que probamos (la mitad indios)..., qué fácil fue convivir contigo! Y como no, gracias también a ti Claudia por okuparnos la casa y no perderte una buena comilona.

Jaime y Álex, os toca. Nuestra historia es un poco más larga y con algún que otro bache en el camino (todas los tienen), y aun así, aquí seguimos. Gracias por eso, por seguir ahí a pesar del tiempo y la distancia. Gracias por compartir parte de vuestro tiempo conmigo, por ponerme al día de los cotilleos y por las cervezas en el *Praga*. Gracias por seguir invitándome a Londres a pesar de que siga sin ir, y por querer que trabajemos en crear algo los tres juntos.

Finalmente, quiero agradecer a otras personas que me he dejado arriba, pero también me han acompañado de varias formas durante estos años de doctorado. Gracias Paco por seguir manteniendo la amistad tras tantos años desde el Erasmus y por todo lo compartido juntos. Gracias en general a mis compañeros de despacho. Gracias al grupo IFIC de la ICHEP 2022, disfruté mucho esa conferencia. En especial a Joan i Víctor, dels millors descobriments de la conferència. Thanks also to the IJCLab people, to host me there and being that friendly with me. I enjoyed the time with you so much and I hope our paths will cross again.

Siento si no he podido agradecer a toda la gente que lo merece. No me cabe duda de que me estoy dejando muchas personas que, a lo largo de los años, he conocido, han influido en mí y, por tanto, son partícipes, en mayor o menor medida, de esta tesis. Gracias también a vosotras y vosotros.

Contents

List of Abbreviations

AC	**A**nti-**C**oincident
BRN	**B**eam-**R**elated **N**eutron
BSM	**B**eyond (the) **S**tandard **M**odel
CC	**C**harged **C**urrent
CEνNS	**C**oherent **E**lastic **N**eutrino-**N**ucleus **S**cattering
χPT	**Chi**ral **P**erturbation **T**heory
χSB	**Chi**ral **S**ymmetry **B**reaking
CKM	**C**abibbo-**K**obayashi-**M**askawa
CLFV	**C**harged **L**epton **F**lavor **V**iolation
DAR	**D**ecay **A**t **R**est
DOF	**D**egree(s) **O**f **F**reedom
DV	**D**isplaced **V**ertex
EFT	**E**ffective **F**ield **T**heory
EIC	**E**lectron-**I**on **C**ollider
EOM	**E**quation **O**f **M**otion
EM	**E**lectro**m**agnetic
EW	**E**lectro**w**eak
FCNC	**F**lavor **C**hanging **N**eutral **C**urrent(s)
GIM	**G**lashow-**I**liopoulos-**M**aiani
GUT	**G**rand **U**nified **T**heories
h.c.	**h**ermitian **c**onjugate
HNL	**H**eavy **N**eutral **L**eptons
LEC	**L**ow-**E**nergy **C**onstants
LEFT	**L**ow-energy **E**ffective **F**ield **T**heory
LFV	**L**epton **F**lavor **V**iolation
LHC	**L**aarge **H**adron **C**ollider
LNC	**L**epton **N**umber **C**onserving
LNV	**L**epton **N**umber **V**iolating
LO	**L**eading **O**rder
LQ	**L**epto**q**uark
LY	**L**ight **Y**ield
MCMC	**M**arkov **C**hain **M**onte**c**arlo
NC	**N**eutral **C**urrent
NIN	**N**eutrino-**I**nduced **N**eutron
NLO	**N**ext (to) **L**eading **O**rder
NP	**N**ew **P**hysics
nPDF	**n**uclear **P**arton **D**istribution **F**unctions
NR	**N**on-**R**elativistic

NSI	**N**on-**S**tandard **I**nteractions
OS	**O**pposite-**S**ign
PDF	**P**arton **D**istribution **F**unctions
pdf	**p**robability **d**istribution **f**unctions
PE	**P**hoto**e**lectrons
PMNS	**P**ontecorvo-**M**aki-**N**akagawa-**S**akata
POT	**P**roton **O**n **T**arget
QCD	**Q**uantum **C**hromo**d**ynamics
QD	**Q**uasi-**D**irac
QED	**Q**uantum **E**lectro**d**ynamics
QF	**Q**uenching **F**actor
QFT	**Q**uantum **F**ield **T**heory
QM	**Q**uantum **M**echanics
RGE	**R**enormalization **G**roup **E**quation(s)
r.h.s.	**r**ight **h**and **s**ide
RχT	**R**esonance **Ch**iral **T**heory
ROI	**R**egion **O**f **I**nterest
SD	**S**hort **D**istance
SM	**S**tandard **M**odel
SMEFT	**S**tandard **M**odel **E**ffective **F**ield **T**heory
SNS	**S**pallation **N**eutron **S**ource
SS	**S**ame-**S**ign
SSB	**S**pontaneous **S**ymmetry **B**reaking
SUSY	**Su**per**sy**mmetry
UV	**U**ltra**v**iolet
vev	**v**acuum **e**xpectation **v**alue
WC	**W**ilson **C**oefficient
WEFT	**W**eak **E**ffective **F**ield **T**heory
WIMP	**W**eak **I**nteracting **M**assive **P**article

Preface

The most incomprehensible feature of the universe is that, as far as our understanding of it reaches, it seems to be totally comprehensible. If we accept this well-tested fact to hold true for all physical phenomena, at any energy scale and in every domain of the universe, then we are able (and it is justified) to study, try to understand and describe Nature in its different realms. The nature of this quest, probably one of the largest and most complex endeavors of humankind, is twofold. On one hand, we intend to attain the correct description of the actual content of the universe, which can be traced back to the ancient question: What is the universe made of? On the other hand and related to the first, we search for the laws that such a content obey: the laws of Nature. Both assertions above may be reduced to the colloquial expression: What is there, and how does it behave? The third possible question: Why? It is not yet clear wether it does lie within the reach of science or it actually belongs to the metaphysics realm. For this quest physicists found that their best allies were: *the scientific method*, as a method of research, and the *language of mathematics*, as a way to properly describe the patterns and relations underlying the observed physical phenomena.

The answers to the aforementioned questions have varied throughout the history of science. From classical physics describing the macroscopic objects via the deterministic Newton laws — and all the associated concepts as trajectories and so on — to the quantum description of the universe at the microscopic scale as a wave function of inherent probabilistic nature — with very different concepts as operators, eigenstates, observables.... Another shift in our understanding came from abandoning the traditional view of the rigid and independent space and time, for a more dynamical and highly correlated space-time. All these discoveries led to the developement of *quantum field theory* as the best (current) description of the content of the universe: quantum fields, and their interactions.

Nowadays, our current understanding of Nature provides partial answers to the questions posed above, as it will become clear along this thesis. However, despite what the final description of Nature turns out to be — maybe given in the form of strings or something else entirely new — it will have as low-energy realization a quantum field theory structure. The best QFT description we currently have of the universe at the subatomic level is called the Standard Model of particle physics. It manages to describe three out of the four forces observed in Nature: the strong, electromagnetic and weak forces, achieving the unification of the last two into the electroweak interaction. Whereas the inclusion of gravity within the quantum formalism is still an open question of intense debate.

However, despite all the accomplishments of the Standard Model, it is widely

believed to be an incomplete description of Nature, since it cannot explain all observed physical phenomena. The aim of this thesis is to partially address some of these unknowns by studying the effects of new physics on the predictions of the Standard Model for several observables. The thesis is organized in 3 parts. In Part I we introduce the two frameworks that serve as the building blocks of the material presented in the rest of the text. Part II and III are then devoted to present the core of the work done during the PhD.

Each of the aforementioned parts contains 2 chapters. Hence, the thesis consists of a total of 6 chapters, a summary and a list of appendices that complement some of the calculations presented in the main text. In Chapter 1 the Standard Model of particle physics is reviewed. The basic QFT description of its particle content is given, followed by a detailed description of the strong and electroweak sectors. The spontaneous symmetry breaking mechanism is recalled at the end of the chapter. Chapter 2 focuses on the framework of effective field theories. First, their theoretical underpinnings are explained. Then, Chiral Perturbation Theory, the dual theory of QCD at low energies, is presented together with its extension Resonance Chiral Theory. This is followed by the description of the effective field theory of the Standard Model and its low-energy realization.

Part II collects two strongly related works. Chapter 3 is dedicated to our phenomenological analysis on charged-lepton-flavor violation on tau leptons. After a historical and theoretical introduction of flavor is given, the techniques to compute the observables of interest are presented and the statistical tool used in the analysis is introduced. The corresponding results are given in several sections. These results are later used in Chapter 4 to set bounds on a general leptoquark framework. Such a framework is presented and the relevant interactions contributing to the observables studied in Chapter 3 are highlighted. Then the results are presented for scalar and vector leptoquars separately.

Part III contains two unrelated chapters that deal with neutrino physics. In Chapter 5 the full effective field theory description of the COHERENT experiment with its coherent elastic neutrino-nucleus scattering detection process is provided. The oscillatory behaviour of the neutrinos involved in the experiment is characterized within the QFT formalism. Finally, some preliminary results are shown. The last Chapter 6 deals with a particular extension of the Standard Model addressing the generation of neutrino masses: the linear seesaw model. Within this model, the Quasi-Dirac nature of the extra heavy neutrinos is studied. The chapter ends with a phenomenological analysis that helps to constrain the parameters of the model.

We close with a comprehensive summary of the thesis in Catalan and several appendices.

Part I

Particle physics at the advent of the XXI century

Chapter 1

The Standard Model of particle physics

From the beginning of formal sciences, rooted in the scientific revolution experienced throughout the XVI and XVII centuries, the history of physics has developed in parallel to that of mathematics. Surprisingly enough, each new discovery of physical phenomena was found to be properly described by some mathematical tool. Accordingly, mathematics soon became the language of physics. For instance, first one of the paradigmatic examples as Newton laws of mechanics describing the kinematics and dynamics of macroscopic phenomena and then, its more powerful reformulation by Lagrange, Euler, Hamilton and others into lagrangian (or hamiltonian) mechanics, attained great success in the 18th and 19th centuries, and even nowadays are used on a daily basis in several branches of science.

In the realm of particle physics, we work both at a very short distance scale and with large velocities and energies. Then, the appropriate framework to describe the corresponding phenomena is necessarily a combination of Quantum Mechanics and Special Relativity: Quantum Field Theory (QFT). The QFT formalism describes particles as quantum excitations over the ground state — called vacuum — of an object permeating all the four-dimensional Minkowski space-time: a quantum field. This way, each particle has an associated quantum field. In this formalism, the fundamental particles and their interactions are described as well by a Lagrangian density function[1], whose degrees of freedom (DOF) are the corresponding quantum fields and their derivatives $\psi(x^\alpha)$, $\partial^\mu \psi(x^\alpha)$. Therefore, given the particle content of a theory, these are incorporated within the Lagrangian in terms of combinations of the associated fields into quantum operators, which describe all phenomena of the theory: propagation of particles, their masses, interactions.... Likewise, the symmetries of the theory further restrict the kind of operators there can be present, e.g. Lorentz invariance implies that fermion fields should always appear in even numbers, electric-charge conservation forces the operators to have a total neutral charge and so on.

Within the Lagrangian formalism, a given Lagrangian describing a physical theory has an associated action functional S which is given by

$$S = \int d^4x \mathcal{L} \,, \tag{1.0.1}$$

---

[1] The usual choice of the Lagrangian over the Hamiltonian formalism stems from the fact that the Lagrangian preserves all the symmetries of the theory, as opposed to the Hamiltonian which is not Lorentz invariant.

with the lagrangian density $\mathcal{L}$ that, for short, we will call the Lagrangian. It is interesting to tackle the above equation from a dimensional perspective. Since the action S has dimensions of energy $[S] = E$ and $[d^4x] = E^{-4}$, necessarily the Lagrangian should have dimensions of $[\mathcal{L}] = E^4$. This restricts the amount and type of fields we may use to form the quantum operators of the Lagrangian.

Related to the action S, one of the capital discoveries in physics was the realization that Nature satisfies the principle of least (or stationary) action, i.e. among all possible actions of a physical system — given within the QFT formalism by the different configurations of the fields ψ and their derivatives in the Lagrangian — the physical phenomena realized in Nature are those given by an extremum of the action. Accordingly, the equations of motion (EOM) of the fields can be retrieved by invoking the principle of least action. When applying it in full generality to Eq. (1.0.1), we obtain the celebrated Euler-Lagrange equations

$$\delta S = 0 \qquad \longrightarrow \qquad \partial_\mu \frac{\partial \mathcal{L}}{\partial \left(\partial_\mu \psi \right)} - \frac{\partial \mathcal{L}}{\partial \psi} = 0 \,, \qquad (1.0.2)$$

which provide the EOM of the fields ψ for a given $\mathcal{L}$.

Another fundamental pillar of particle physics is *Group theory*. One of the major discoveries of the past century was to understand that particles are described by irreducible representations of the basic symmetries of Nature, i.e. Lorentz and gauge invariance. Accordingly, for each symmetry there is an associated space over which the corresponding symmetry transformations act. For example, fermions are fundamental representations of the Lorentz group with spin $1/2$ (scalars would be spin-0 representations and so on). More concretely, Dirac fields have four components in Dirac space, over which a given space-time Lorentz boost acts. If such a Dirac field is a quark, those have an extra quantum number called color, the charge of the strong interactions. It turns out that Nature is symmetric under local transformations changing the color of the quarks, these transformations act then on a different vector space: the color space for which the quarks are described in its triplet fundamental representation (see Section 1.2).

In this chapter, the current best description of the known fundamental particles and its interactions in the microscopic domain is reviewed. This thoroughly tested theory goes under the name of: The Standard Model (SM) of Particle Physics. In Section 1.1, the fundamental pillars over which this theory rests are summarized. We do not intend to provide a thorough development from basic principles, but just present some pieces that we think are needed to understand better the framework. Then, in Section 1.2 we describe the theory of the strong interactions felt by quarks and gluons. There, we present for the first time one of the main concepts behind the construction of the Standard Model: the gauge symmetry principle. The other part of the SM describing both the weak and the electromagnetic (EM) interactions: the electroweak sector, is addressed in Section 1.3. Finally, the scalar sector of the SM together with the phenomenon of spontaneous symmetry breaking — providing mass to the SM particles and from which the Higgs field stems — are described in Section 1.4.

Standard Model of Elementary Particles
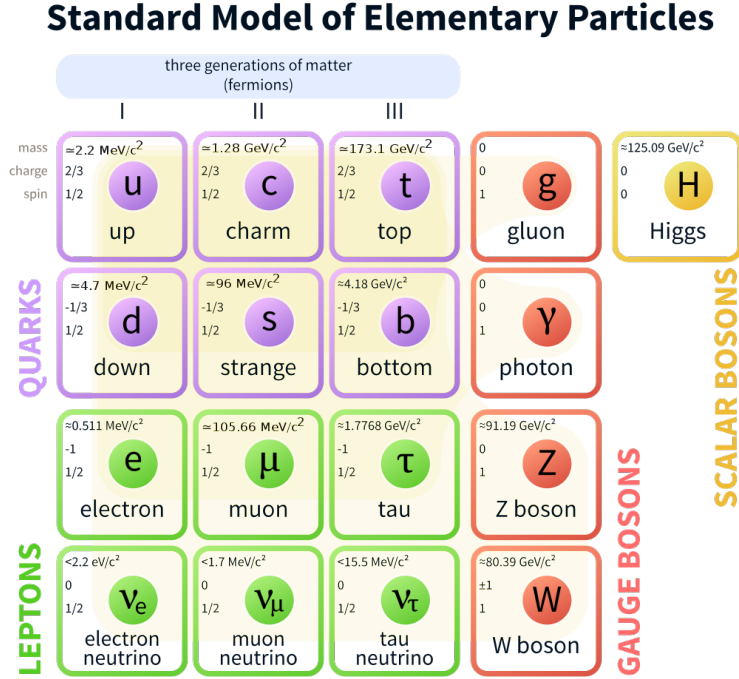
FIGURE 1.1: Diagramatic illustration of the particle content of the Standard Model.

1.1 Basics of the Standard Model within the QFT description

The Standard model of particle physics (whose particle spectrum is collected in Fig. 1.1) is a renormalizable quantum field theory, based on the $\mathrm{SU(3)_C \times SU(2)_L \times U(1)_Y}$ gauge symmetry. On the whole, it contains 12 fermions (with their corresponding antifermions), 12 vector bosons and 1 scalar boson.

1.1.1 Matter content

Regarding fermions, the SM distinguishes between two main categories: quarks and leptons. The former experience all SM interactions while the latter are blind to the strong force. Each category can be divided as well into two subgroups: charged and neutral leptons on one hand, and up-type quarks and down-type quarks on the other. In addition, this scheme is found to be replicated three times in Nature, for particles more and more massive. These are the so-called *families* or *generations* of the SM particles:

$$1^{\mathrm{st}} : \begin{bmatrix} \nu_e & u \\ e^- & d' \end{bmatrix}, \qquad 2^{\mathrm{nd}} : \begin{bmatrix} \nu_\mu & c \\ \mu^- & s' \end{bmatrix}, \qquad 3^{\mathrm{rd}} : \begin{bmatrix} \nu_\tau & t \\ \tau^- & b' \end{bmatrix}, \qquad (1.1.3)$$

where the replicated versions have the same quantum numbers except for the mass and flavor; the latter being assigned only to fermions and being different for each of the 12 of them in the SM[2]. In addition, fermions (denoted in general by ψ) can

---

[2]In Chapter 3 we discuss in more detail the flavor structure of the SM.

have two different chiralities: left-handed $\psi_L \equiv P_L\psi$ and right-handed $\psi_R \equiv P_R\psi$, where we have introduced the chirality operators $P_{R,L} = (1 \pm \gamma_5)/2$, with $\gamma_5 = \gamma^5 \equiv \gamma^0\gamma^1\gamma^2\gamma^3$ and γ^μ are the Dirac gamma matrices. This is important since some SM interactions distinguish between both chiralities, i.e. left- and right-handed fermions do not transform in the same way under the SM symmetries. As we said in the introduction to this chapter, particles are given by irreducible representations of the symmetries of Nature. Accordingly, in the SM left-handed quarks and lepton fields are $SU(2)_L$ doublets, while under this same symmetry their right-handed partners transform as singlets. Regarding the $SU(3)_C$ color symmetry, quark fields — independently of their chirality (see Section 1.2) — are described in its fundamental triplet representation, while leptons transform as singlets. We thus define the chiral quark fields as

$$Q_p \equiv \begin{pmatrix} u_p \\ d_p \end{pmatrix}_L, \qquad u_{Rp}, \qquad d_{Rp}, \tag{1.1.4}$$

and the chiral lepton fields as

$$L_p \equiv \begin{pmatrix} \nu_{\ell_p} \\ \ell_p \end{pmatrix}_L \qquad e_{Rp}, \tag{1.1.5}$$

where $p = 1, 2, 3$ is a flavor index and we have explicitly omitted the right-handed neutrino term since this is a singlet under all SM symmetries and there is no reason to include it in the minimal version of the Standard Model.

The previous discussion entails the following quantum numbers, under the group symmetry $SU(3)_C \times SU(2)_L \times U(1)_Y$, for the matter fields[3] :

$$\begin{aligned} Q_p &= (3, 2, +1/6)\,, & u_{Rp} &= (3, 1, +2/3)\,, & d_{Rp} &= (3, 1, -1/3)\,, \\ L_p &= (1, 2, -1/2)\,, & e_{Rp} &= (1, 1, -1)\,. \end{aligned} \tag{1.1.6}$$

In this thesis we make use of the Dirac description of particles of spin $1/2$ for the fermionic content of the SM (unless stated differently). Hence, all fermion fields above satisfy the Dirac equation

$$(i\gamma^\mu\partial_\mu - m)\psi = 0\,, \tag{1.1.7}$$

for a free particle of mass m, described by the field ψ. Actually, the four-component Dirac field does describe the two left- and right-handed chiralities of a particle and its antiparticle.

The most general solution of the Dirac equation is given by writing the Dirac fermion field — and consequently its Hermitian conjugate (h.c.) — as a superposition of plane waves, i.e. the Fourier decomposition

$$\psi(x^\alpha) = \int \frac{d^3k}{(2\pi)^3} \frac{1}{\sqrt{2E_k}} \sum_{r=1}^{2} \left[a_r(\vec{k}) u_r(\vec{k}) e^{-ik\cdot x} + b_r^\dagger(\vec{k}) v_r(\vec{k}) e^{ik\cdot x} \right]\,,$$

$$\bar{\psi}(x^\alpha) = \int \frac{d^3k}{(2\pi)^3} \frac{1}{\sqrt{2E_k}} \sum_{r=1}^{2} \left[b_r(\vec{k}) \bar{v}_r(\vec{k}) e^{-ik\cdot x} + a_r^\dagger(\vec{k}) \bar{u}_r(\vec{k}) e^{ik\cdot x} \right]\,, \tag{1.1.8}$$

---

[3]The SM quantum numbers of a right-handed neutrino would be $(1, 1, 0)$.

with r the polarization index, $\bar{\psi} \equiv \psi^\dagger \gamma^0$ and we have introduced the four-component (in Dirac space) spinors $u_r(\vec{k})$ and $v_r(\vec{k})$ [1]. Above, $a_r^{(\dagger)}$ and $b_r^{(\dagger)}$ are the annihilation (creation) operators that satisfy the anticommutation relations

$$\left\{ a_r(\vec{k}), a_s^\dagger(\vec{q}) \right\} = \left\{ b_r(\vec{k}), b_s^\dagger(\vec{q}) \right\} = (2\pi)^3 \delta^{(3)}(\vec{k} - \vec{q}) \delta_{rs} \,, \qquad (1.1.9)$$

with the rest of combinations equal to zero. Accordingly, the vacuum $|0\rangle$ of the theory is defined as the state which satisfies

$$a_r(\vec{k})|0\rangle = b_r(\vec{k})|0\rangle = 0 \,. \qquad (1.1.10)$$

Likewise, the one-particle states are defined as excitations over the ground state $|0\rangle$ via

$$|\vec{k}, r, Q\rangle \equiv \sqrt{2E_k}\, a_r^\dagger(\vec{k})|0\rangle \,, \qquad |\vec{k}, r, -Q\rangle \equiv \sqrt{2E_k}\, b_r^\dagger(\vec{k})|0\rangle \,, \qquad (1.1.11)$$

such that the creation operators $a_r^\dagger(\vec{k})$ and $b_r^\dagger(\vec{k})$, when applied onto the vacuum of the theory, create a particle with charge Q and an antiparticle with charge $-Q$ respectively, with momentum $\vec{k}$, energy E_k and polarization r. In the same way, the corresponding annihilation operators remove one-particle states with the same characteristics. Therefore, the field operator $\psi(x^\alpha)(\bar{\psi}(x^\alpha))$, acting on the vacuum, either annihilates a particle or creates the antiparticle (annihilates an antiparticle or creates the particle) at position x^α.

Finally, for completeness, let us also comment that neutral spin-1/2 particles can be either Dirac or Majorana particles. The Majorana field $\chi(x^\alpha)$ is a two-component (instead of four) field which describes the two chiralities of a neutral particle. Besides the Dirac equation (1.1.7), these fields satisfy as well the Majorana condition

$$\chi = \chi^{\mathrm{C}} \equiv C\bar{\chi}^T \,, \qquad \text{with} \qquad C = i\gamma^2\gamma^0 \,, \qquad (1.1.12)$$

where C is the charge conjugation operator. The equation above states that a Majorana fermion is its own antiparticle. This may be the case for the neutrinos of the SM, although there is no enough evidence to do such a claim.

1.1.2 Interactions

Within the Standard Model, fermions experience the fundamental interactions of Nature by the mediation of their associated spin 1 (vector) bosons: the massless photon γ for the electromagnetic interaction, the massive $W^\pm$ and Z bosons as the weak mediators and eight massless colored gluons for the strong force; theoretically a massless graviton would be the spin-2 particle responsible for the gravitational interaction (this is still an open question in physics since gravity lacks a satisfactory quantum implementation: Quantum Gravity).

Massive vector bosons (spin 1) have three possible polarizations, i.e. three degrees of freedom. These are described by a quadrivector $V^\mu(x^\alpha)$, once one DOF is removed by imposing the constraint $\partial_\mu V^\mu = 0$. Therefore, after this consideration is taken into account, their equation of motion becomes the Klein-Gordon equation[4]

$$\left(\Box + m^2\right) V^\mu = 0 \,. \qquad (1.1.13)$$

---

[4]Note that fermions satisfy the Klein-Gordon EOM as well.

In a similar way as for fermions, the most general solution to the Klein-Gordon equation is provided by the Fourier decomposition

$$
V^\mu(x^\alpha) = \int \frac{d^3k}{(2\pi)^3} \frac{1}{\sqrt{2E_k}} \sum_{r=1}^{3} \left[a_r(\vec{k})\epsilon_r^\mu(\vec{k})e^{-ik\cdot x} + b_r^\dagger(\vec{k})\epsilon_r^{\mu*}(\vec{k})e^{ik\cdot x} \right] ,
$$

$$
V^{\mu\dagger}(x^\alpha) = \int \frac{d^3k}{(2\pi)^3} \frac{1}{\sqrt{2E_k}} \sum_{r=1}^{3} \left[b_r(\vec{k})\epsilon_r^\mu(\vec{k})e^{-ik\cdot x} + a_r^\dagger(\vec{k})\epsilon_r^{\mu*}(\vec{k})e^{ik\cdot x} \right] ,
$$

(1.1.14)

where now we have introduced the polarization (quadri-) vectors $\epsilon_r^\mu(\vec{k})$, which describe the three polarizations of the vector boson V^μ. Accordingly, the constraint on the vector field translates into the transverse condition $k_\mu \epsilon_r^\mu(\vec{k}) = 0$ for the vector polarizations. The creation and annihilation operators now satisfy the commutation relations

$$
\left[a_r(\vec{k}), a_s^\dagger(\vec{q}) \right] = \left[b_r(\vec{k}), b_s^\dagger(\vec{q}) \right] = (2\pi)^3 \delta^{(3)}(\vec{k} - \vec{q})\delta_{rs} ,
$$

(1.1.15)

with the rest of combinations equal to zero. A state of a massive vector boson with momentum k^μ, polarization r and charge Q $(-Q)$, is then created by the action of the creation operator $a_r^\dagger(\vec{k})$ $(b_r^\dagger(\vec{k}))$ on the vacuum of the theory

$$
\sqrt{2E_k}\, a_r^\dagger(\vec{k})|0\rangle = |\vec{k}, r, Q\rangle , \qquad\qquad \sqrt{2E_k}\, b_r^\dagger(\vec{k})|0\rangle = |\vec{k}, r, -Q\rangle .
$$

(1.1.16)

For massless vector bosons the situation is a bit more involved, since these particles can only have two polarizations, i.e. two DOFs. Therefore, the fact that we work with a four-component covariant formalism hinders their proper description. In case of the photon field $A^\mu(x^\alpha)$, this entails a freedom which is manifested in the introduction of a gauge[5] fixing term in the Lagrangian, which leads to the following EOM

$$
\left[g^{\mu\nu}\Box + \left(\frac{1}{\xi} - 1 \right) \partial^\mu \partial^\nu \right] A_\nu = 0 .
$$

(1.1.17)

The description of the photon field in terms of plane waves is given by

$$
A^\mu(x^\alpha) = \int \frac{d^3k}{(2\pi)^3} \frac{1}{\sqrt{2E_k}} \sum_{r=0}^{3} \left[a_r(\vec{k})\epsilon_r^\mu(\vec{k})e^{-ik\cdot x} + a_r^\dagger(\vec{k})\epsilon_r^{\mu*}(\vec{k})e^{ik\cdot x} \right] ,
$$

(1.1.18)

where now, since the photon has no electric charge, there are no antiparticle operators $(b_r^{(\dagger)})$ and the field A^μ is as well its h.c.

However, in order to properly quantize the photon field, it turns out that instead of constraining the field operator A^μ, one should introduce restrictions over the states of the theory, namely

1. the Gupta-Bleuler condition: introduces the constraint $\partial_\mu A^\mu|\psi\rangle = 0$, when it is applied to any physical state of the theory. This condition further implies that all physical states have the same number of scalar (time-like) and longitudinal photons,

---

[5]In this case, it refers to the fact that the same electric $\vec{E}$ and magnetic $\vec{B}$ fields can be described by an infinite number of A^μ vector fields, differentiated by the addition of a $\partial^\mu \Lambda$ term, with Λ a scalar field.

2. the possibility to arbitrarily change the number of scalar and longitudinal photons (the two non-physical polarizations of the photon), while satisfying condition 1.

The case of the gluons is yet more involved. First, the field can be decomposed as in Eq. (1.1.18), but adding to the operators and polarization vectors a color index. However, it requires, besides a similar gauge term as for the photon, the introduction of non-physical particles called Ghosts. We are not going to delve more into this issue but refer to [2] for a thorough explanation on the matter.

As we shall see below in Section 1.3, the corresponding Lagrangian description of the electroweak theory based on the $SU(2)_L \times U(1)_Y$ gauge symmetry, forbids all particles to have a mass, since the corresponding mass terms break explicitly the gauge symmetry. Therefore, the Standard Model requires a spontaneous breaking of the $SU(2)_L \times U(1)_Y$ symmetry (see Section 1.4). This phenomenon goes under the name of spontaneous symmetry breaking (SSB) and is performed by a scalar sector — invariant under the same gauge symmetry — which involves an extra physical spin-0 (scalar) neutral boson, the Higgs. Scalar fields $\phi(x^\alpha)$ satisfy as well the Klein-Gordon equation

$$\left(\Box + m^2\right)\phi = 0\,. \tag{1.1.19}$$

Then, the planar-wave decomposition of real scalar fields is given by

$$\phi(x^\alpha) = \int \frac{d^3k}{(2\pi)^3} \frac{1}{\sqrt{2E_k}} \left[a(\vec{k})e^{-ik\cdot x} + a^\dagger(\vec{k})e^{ik\cdot x}\right]\,, \tag{1.1.20}$$

where the commutation relation satisfied by the creation and annihilation operators is

$$\left[a(\vec{k}), a^\dagger(\vec{q})\right] = (2\pi)^3\delta^{(3)}(\vec{k} - \vec{q})\,, \tag{1.1.21}$$

with the rest of combinations equal to zero. The associated scalar neutral boson is created upon the action of the creation operator $a^\dagger$ over the vacuum

$$\sqrt{2E_k}\,a^\dagger(\vec{k})|0\rangle = |\vec{k}\rangle\,. \tag{1.1.22}$$

1.2 Quantum Chromodynamics: QCD

In the second half of the last century, physicists were puzzled by the increasingly growing zoo of particles they were discovering. These were named Hadrons, from the Greek word for "strong", since they seemed to suffer a stronger interaction than the known forces at that time. Those were divided into two groups: Baryons (the "heavy" Greek word) and their anti-particles with half-integer spins, e.g. protons and neutrons enter this category, and mesons (for "medium" heavy) with integer spin, e.g. the pions and kaons. It was soon noticed in 1961 by Murray Gell-Mann, that Hadrons could be conveniently grouped via a SU(3) flavor symmetry in what he called the Eightfold Way [3]. This realization helped later to interpret Hadrons as non-elementary particles, but composite structures made of partons[6]: quarks, antiquarks and gluons. This was done in 1964 by Gell-Mann and George Zweig in

---

[6]Name given by Richard Feynman in the context of deep inelastic scattering.

their quark model [4,5], but they were very reluctant to see quarks as real physical entities rather than some mathematical tools to describe some not well-understood phenomena. Nowadays, the physical existence of quarks is widely proved.

Under the quark model, the Eightfold Way was explained by assuming that mesons were made out of a pair quark-antiquark, and baryons out of three quarks. Besides, in the first version of the quark model in Refs. [4,5], they considered the existence of three quark flavors (u, d and s), which would thus explain the SU(3) flavor symmetry of the Eightfold Way (see Section 2.2.2). The fourth charm quark was soon considered in Ref. [6] (see Chapter 3 for more details about the discovery of quarks). Currently, the Standard Model contains 6 quarks (u, d, s, c, b, t, ordered by mass from light to heavy). However, it was necessary to include an extra quantum number for the model to consistently describe Hadrons as composite objects of quarks: the *color*. As we will see below, it turns out that color can be seen as the charge associated to the strong force and hence, the gauge theory which describes the strong interactions is called Quantum Chromodynamics (QCD).

Mesons play an important role in the work presented in this thesis, let us then delve a bit more on its quark nature. Mesons are constituted of a quark-antiquark $q\bar{q}$ pair. As dictated by the superposition principle of Quantum Mechanics, the total spin vector $\vec{J}$ of the meson is formed by adding the spins of its constituents and their angular orbital momentum $\vec{\ell}$. Denoting the sum of the quark spins as $\vec{s} = \vec{q} + \vec{\bar{q}}$, the total spin vector is $\vec{J} = \vec{\ell} + \vec{s}$. Since quarks are spin-1/2 fermions, their individual spin projections may take the values of $1/2$ or $-1/2$. Accordingly, the $q\bar{q}$ quantum numbers are $s = 0$ or 1 and $\ell = 0, 1, 2, \ldots$. The angular momentum $\vec{\ell}$, represents the oscillation modes of the $q\bar{q}$ pair along its axis (see Fig. 1.2). Then, mesons with $\ell > 0$ correspond to orbital excitations of the ground state $\ell = 0$. From this discussion it is trivial to see that the meson spin j takes integer values within

$$|\ell - s| \leq j \leq \ell + s . \tag{1.2.23}$$

Apart from orbital excitations, the $q\bar{q}$ pair can also feel radial excitations (usually called vibrations), which are denoted by the quantum number $n \geq 1$. All in all, the quantum numbers of a meson are typically given following one of the two notations

$$n^{2s+1}\ell_j \text{ or } I^G(J^{PC}) . \tag{1.2.24}$$

The first notation shows explicitly which are the aforementioned quantum numbers of a given meson: s, n the orbital excitation ℓ_J, with J the total meson spin; while the second notation focuses more on the charge (C), parity (P) and G parity (G) transformations of the meson, as well as its isospin (I) and total spin J. For instance, by taking the lightest three quarks satisfying the SU(3) flavor symmetry of the Eightfold Way explained above, the ground state ($\ell = 0$ and $n = 1$) mesons that can be built, correspond to the nine pseudoscalar mesons with quantum numbers $1^1 S_0$ (or $J^{PC} = 0^{-+}$): $\left(\pi^0, \pi^+, \pi^-, K^0, K^+, \bar{K}^0, K^-, \eta, \eta'\right)$, and the nine vector mesons with quantum numbers $1^3 S_1$ (or $J^{PC} = 1^{--}$): $\left(\rho^0, \rho^+, \rho^-, K^{*0}, K^{*+}, \bar{K}^{*0}, K^{*-}, \phi, \omega\right)$. Therefore, we notice that the pseudoscalar mesons are those $q\bar{q}$ pair configurations with antiparallel (opposite) quark spins, while the vector meson resonances correspond to parallel quark spins. In Section 2.2.2 of the next chapter, we provide a more thorough description of mesons within QCD.
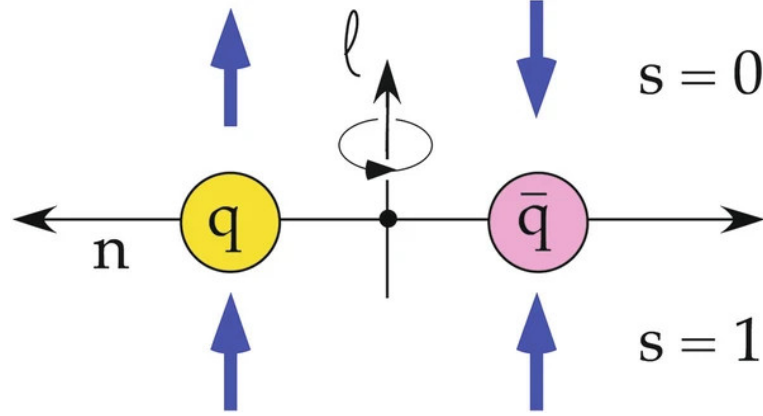
FIGURE 1.2: A $q\bar{q}$ meson pair may be in a spin-singlet state (s=0, antiparallel quark spins) or in a spin-triplet state (s=1, parallel quark spins). Excited states are obtained by switching angular momentum $\ell > 0$ within the $q\bar{q}$ pair (orbital excitations) or by inducing vibrations $n > 1$ (radial excitation). Image taken from Ref. [7].

Let us now move to present the formal derivation of the QCD Lagrangian and explain the gauge principle over which the Standard Model is built. First, the construction of QCD relies on the following properties of the strong interactions:

(i) conserve flavor and do not depend on it,

(ii) are parity and (electric) charge invariant,

(iii) its charge can be identified as the color (in analogy to the electromagnetic charge of QED).

Keeping that in mind, we can construct the QCD Lagrangian departing — within the Lagrangian formalism — from the Dirac free Lagrangian (which provides the Dirac EOM in Eq. (1.1.7)) for the quark fields:

$$\mathcal{L}_0 = \sum_f \bar{q}_f \left(i\gamma^\mu \partial_\mu - m_f \right) q_f \,, \tag{1.2.25}$$

where the quark field q_f of flavor f, is indeed a quark vector in color space $q_f^T \equiv (q_f^1, q_f^2, q_f^3)$, with the superindex $i = 1, 2, 3$ denoting the quark color.

The above Lagrangian is invariant under arbitrary global $SU(3)_C$ transformations acting over the quark fields in color space. Under this symmetry quark fields transform as

$$q_f^i \longrightarrow q_f^{i\prime} = U^i_{\;j} q_f^j \,, \qquad \text{with} \qquad UU^\dagger = U^\dagger U = 1 \,, \qquad \text{and} \qquad \det(U) = 1 \,, \tag{1.2.26}$$

where U are the $SU(3)_C$ matrices and are usually given by

$$U = \exp\left\{ i\frac{\lambda^a}{2} \theta_a \right\} \,, \tag{1.2.27}$$

with λ^a the Gell-Mann matrices. The expression above describes global symmetry transformations, since the θ_a parameters are constant in all the space-time (remind that fields are defined in the whole space-time $q_f^i(x^\alpha)$).

For instance, group theory tells us that transformation matrices associated to the symmetry group SU(N), for arbitrary N, can all be expressed in terms of the generators of the fundamental representation of SU(N), the N×N $\lambda^a/2$ matrices above, and an equivalent number of arbitrary parameters θ_a. In the case at hand, the generators of $SU(3)_C$ are the 3×3 Gell-Mann matrices. Nedless to say, the generators of $SU(3)_C$ act as well in color space, so that a is a color index. These are traceless matrices and satisfy the commutation relations

$$\left[\frac{\lambda^a}{2}, \frac{\lambda^b}{2}\right] = if^{abc}\frac{\lambda^c}{2}, \tag{1.2.28}$$

where f^{abc} are the real and totally antisymmetric structure constants of $SU(3)_C$. The fact that the generators of the SU(N) algebra do not commute, classifies these symmetries as *non-abelian*.

The free Lagrangian in Eq. (1.2.25) lacks an explanation of the (strong) interactions suffered by quarks. Gauge symmetry provides a natural and elegant way to introduce those missing interactions. The basic procedure consists on gauging the $SU(3)_C$ symmetry: promoting it to a local symmetry via $\theta_a = \theta_a(x^\alpha)$. However, by doing such a promotion, the Lagrangian (1.2.25) is no longer invariant under local $SU(3)_C$ transformations since

$$\partial_\mu q_f \xrightarrow{SU(3)_C} \exp\left\{i\frac{\lambda^a}{2}\theta_a(x^\alpha)\right\}\left(\partial_\mu + i\frac{\lambda^a}{2}\partial_\mu\theta_a(x^\alpha)\right)q_f. \tag{1.2.29}$$

However, the global transformation (1.2.27) can be seen as providing a mere change of phase for the quark field in Eq. (1.2.26), driven by the θ_a parameters. Therefore, the non-invariance of the Lagrangian under local $SU(3)_C$ transformations, just means that the choice of a phase convention (a given θ_a) at some arbitrary point x_0^μ necessarily implies the same convention in the whole space-time. This is not general whatsoever.

Accordingly, to obtain a more general Lagrangian invariant under such local transformations, we should add another piece that, after the symmetry transformation is applied, cancels out the extra term $i\frac{\lambda^a}{2}\partial_\mu\theta_a$. The requirement that the $SU(3)_C$ phase invariance holds locally is indeed the *gauge principle*. This is fixed by the transformation in Eq. (1.2.29) and, since the extra terms are eight colored Lorentz vectors $(\partial_\mu\theta_a)$, we need to introduce eight new colored spin-1 fields $G_a^\mu(x^\alpha)$, the so-called gluons. Consequently, we should change the quark derivative by a covariant object that actually remains invariant under the local $SU(3)_C$ transformations. This covariant derivative is defined as

$$D^\mu q_f \equiv \left[\partial^\mu + ig_s\frac{\lambda^a}{2}G_a^\mu\right]q_f \equiv \left[\partial^\mu + ig_sG^\mu\right]q_f, \tag{1.2.30}$$

where a 3×3 color identity matrix is implicit in the derivative term. We need $D^\mu q_f$ to transform in the same way as q_f, such that the term $\bar{q}_f D^\mu q_f$ becomes invariant. This entails the following transformation properties of the gauge fields

$$D^\mu \longrightarrow D^{\mu\prime} = UD^\mu U^\dagger, \qquad G^\mu \longrightarrow G^{\mu\prime} = UG^\mu U^\dagger + \frac{i}{g_s}(\partial^\mu U)U^\dagger, \tag{1.2.31}$$

where we have dropped the space-time dependence of the gluon fields. The previous relations ensure the invariance of the Lagrangian under local $SU(3)_C$ transformations.

Therefore, we are just left with the inclusion of a gauge-invariant kinetic term for the gluons to finish our QCD Lagrangian. These are introduced via the field strengths

$$G^{\mu\nu} \equiv -\frac{i}{g_s}[D^\mu, D^\nu] = \partial^\mu G^\nu - \partial^\nu G^\mu + ig_s[G^\mu, G^\nu] \equiv \frac{\lambda^a}{2} G_a^{\mu\nu}, \qquad (1.2.32)$$

which transforms under $SU(3)_C$ as

$$G^{\mu\nu} \longrightarrow G^{\mu\nu\prime} = U G^{\mu\nu} U^\dagger, \qquad (1.2.33)$$

so that the color trace $\text{Tr}(G^{\mu\nu}G_{\mu\nu}) = \frac{1}{2}G_a^{\mu\nu}G_{\mu\nu}^a$ remains invariant. Finally, the Lagrangian of Quantum Chromodynamics is

$$\mathcal{L}_{\text{QCD}} = -\frac{1}{4}G_a^{\mu\nu}G_{\mu\nu}^a + \sum_f \bar{q}_f \left(i\gamma^\mu D_\mu - m_f\right) q_f. \qquad (1.2.34)$$

Several comments are in order: first, $\mathcal{L}_{\text{QCD}}$ does not contain a gluon mass term of the kind $\frac{1}{2}m_G^2 G_a^\mu G_\mu^a$, since it is not invariant under the $SU(3)_C$ transformations of the gluon fields in Eq. (1.2.31); second, due to the non-abelian character of the $SU(3)_C$ symmetry group, the kinetic $G_a^{\mu\nu}G_{\mu\nu}^a$ term gives rise to cubic and quartic gluon self-interactions; third, the strength of the strong interactions is given by just a single free coupling g_s.

Finally, gauge invariance allows for another term in the QCD Lagrangian, the so-called θ term [2]

$$\mathcal{L}_{\theta_{\text{QCD}}} = -\theta_{\text{QCD}}\frac{g_s^2}{32\pi^2}\tilde{G}_a^{\mu\nu}G_{\mu\nu}^a, \qquad (1.2.35)$$

where we have introduced the dual $\tilde{G}_a^{\mu\nu} \equiv \frac{1}{2}\epsilon^{\mu\nu\alpha\beta}G_{a\,\alpha\beta}$. The Lagrangian above explicitly violates CP and introduces an extra free parameter θ_{QCD}. However, the bound on the electric dipole moment of the neutron entails a strong constraint on the value of $\theta_{\text{QCD}} \sim 0$.

1.3 The electroweak unification

The development of the theory of electroweak (EW) interactions was linked to the particle discoveries along the last century, which we review in some detail in Chapter 3, together with the growing understanding of the phenomena involving electromagnetic and weak interactions. It had its culmination in the determination of the structure of the electroweak theory by Weinberg [8], Glashow [9] and Salam [10], which unifies both the electromagnetic and the weak interactions. This structure has been later extended to include the rest of the particle spectrum of the SM.

One of the crucial observations was that charged and neutral currents had different behaviour in electroweak interactions:

Charged currents (mediated by the $W^\pm$ bosons) in EW interactions

- are only left-handed for fermions or right-handed for antifermions, i.e. only left-handed particles experience EW charged-current interactions,

- do totally violate parity and charge conjugation. However, the combined transformation CP is almost conserved[7],

- occur for the pairs of fermions within the same doublet (see Eqs. (1.1.4) and (1.1.5)), where the electric charges of the two fermions differ in one unit,

- have the same universal strength, i.e. the $W^\pm$ bosons have the same coupling to all fermion doublets .

  Neutral currents (mediated by the Z and γ (photon) bosons) in EW interactions

- if mediated by the Z boson, they distinguish (have different couplings) between left- and right-handed fermions,

- are flavor conserving, i.e. there are no flavor-changing neutral currents (FCNC) in the SM at tree level. Then, necessarily both mediators (γ and Z) couple to a fermion and its antifermion,

- couple depending on the fermion electric charge Q_f. Accordingly, fermions sharing the same Q_f, couple to the Z or γ with the same universal strength[8].

In order to accommodate the aforementioned features of the electroweak interactions and the particle content with the structure described in Section 1.1.1 within a single gauge invariant framework, we proceed as follows. First, we should find the proper symmetry group. Since we are working with doublets, the simplest group with such a representation is SU(2). Besides, we should include as well electromagnetic interactions, this can be provided by the addition of a U(1) group[9]. From the fact that only left-handed fermions appear in doublets, the appropriate symmetry group of the EW interactions is

$$G \equiv \mathrm{SU(2)_L} \times \mathrm{U(1)_Y} \,, \tag{1.3.36}$$

where L stands for left-handed fields and Y refers to a new quantum number named as hypercharge.

Let us focus on a single family of fermions, say the first one ($p = 1$ in Eqs. (1.1.4) and (1.1.5)), and further on particularize to quarks to simplify the discussion. Obviously, the whole derivation below applies for leptons and the three families of the SM. We follow a similar procedure as for the derivation of QCD, with the difference that now all fermions (except the absent right-handed neutrino) feel the electroweak interactions. The free Lagrangian is

$$\mathcal{L}_0 = i\bar{Q}\gamma^\mu \partial_\mu Q + i\bar{u}_R \gamma^\mu \partial_\mu u_R + i\bar{d}_R \gamma^\mu \partial_\mu d_R \,, \tag{1.3.37}$$

---

[7]The existence of three families of fermion fields leads to a slight violation of CP as we will see in the last section of this chapter.

[8]Neutrinos have zero charge and as such, do not experience electromagnetic interactions, but they do couple to the Z boson.

[9]This will not be the usual symmetry group of QED U(1)$_\mathrm{QED}$, but the latter will be recovered once the spontaneous symmetry breaking takes place (see below).

which is invariant under global G transformations in flavor space

$$Q \xrightarrow{G} Q' \equiv \exp\{iy_Q\beta\} U_L Q\,,$$
$$u_R \xrightarrow{G} u_R' \equiv \exp\{iy_u\beta\} u_R\,, \tag{1.3.38}$$
$$d_R \xrightarrow{G} d_R' \equiv \exp\{iy_d\beta\} d_R\,,$$

with U_L the unitary matrix of $\mathrm{SU}(2)_L$ transformations given by

$$U_L \equiv \exp\left\{i\frac{\sigma_j}{2}\alpha^j\right\} \qquad \text{with} \qquad j=1,2,3\,, \tag{1.3.39}$$

where $\sigma_j/2$ are the generators of the SU(2) symmetry group (to be compared with the Gell-Mann matrices $\lambda^a/2$ in Eq. (1.2.27) for SU(3)), i.e. the three Pauli matrices, and α^j are three arbitrary parameters characterizing the concrete symmetry transformation. The symmetry transformation group G is non-abelian as in QCD, thus the generators of G do not conmute, but follow the usual commutation relations for the Pauli matrices. Above, the y parameters are called hypercharges, in analogy to the $\mathrm{U}(1)_{\mathrm{QED}}$ similar phase transformation.

Applying the gauge principle, we now impose the Lagrangian to be invariant under local $\mathrm{SU}(2)_L \times \mathrm{U}(1)_Y$ gauge transformations, i.e. we promote the α and β parameters to functions in space-time $\alpha(x^\mu)$ and $\beta(x^\mu)$. This entails to change fermion derivatives by covariant derivatives which, again, should transform as fermion fields. For each gauge parameter we need an extra gauge boson, hence four vector fields are needed:

$$D_\mu Q \equiv \left[\partial_\mu + ig\widetilde{W}_\mu + ig'y_1 B_\mu\right] Q\,,$$
$$D_\mu u_R \equiv \left[\partial_\mu + ig'y_2 B_\mu\right] u_R\,, \tag{1.3.40}$$
$$D_\mu d_R \equiv \left[\partial_\mu + ig'y_3 B_\mu\right] d_R\,,$$

with

$$\widetilde{W}_\mu \equiv \frac{\sigma_i}{2} W_\mu^i \qquad \text{with} \qquad i=1,2,3 \tag{1.3.41}$$

a $\mathrm{SU}(2)_L$ matrix field. Together, the $W_\mu^i(x^\alpha)$ and $B_\mu(x^\alpha)$ add up to four, the needed vector bosons to describe the two charged $W^\pm$, and two neutral Z and γ bosons. However, we cannot yet do the identification of those fields.

The requirement that the covariant derivatives transform as the fermion fields, fixes the transformation properties of the gauge fields

$$B_\mu \xrightarrow{G} B_\mu' = B_\mu - \frac{1}{g'}\partial_\mu\beta\,,$$
$$\widetilde{W}_\mu \xrightarrow{G} \widetilde{W}_\mu' = U_L W_\mu' U_L^\dagger + \frac{i}{g}\partial_\mu U_L U_L^\dagger\,. \tag{1.3.42}$$

Note that the $\mathrm{SU}(2)_L$ W_μ^i transforms in an analogous way as the gluon fields of QCD. The non-linearity of the $\mathrm{SU}(2)_L$ commutation relations constrains their associated couplings, such that there can only be one free coupling g. This is not the case for the $\mathrm{U}(1)_Y$ symmetry that, while there is only one g', the hypercharges y are arbitrary free parameters (as it happens in QED for the electric charges).

We are just left with the construction of the kinetic terms for the gauge fields. As we did for the gluons of QCD, we introduce the field strengths

$$B_{\mu\nu} \equiv \partial_\mu B_\nu - \partial_\nu B_\mu \tag{1.3.43}$$

$$\widetilde{W}_{\mu\nu} \equiv \partial_\mu \widetilde{W}_\nu - \partial_\nu \widetilde{W}_\mu + ig \left[\widetilde{W}_\mu, \widetilde{W}_\nu \right] , \tag{1.3.44}$$

$$\widetilde{W}_{\mu\nu} \equiv \frac{\sigma_i}{2} W^i_{\mu\nu} \qquad \text{with} \qquad W^i_{\mu\nu} = \partial_\mu W^i_\nu - \partial_\nu W^i_\mu + g\epsilon^{ijk} W^j_\mu W^k_\nu . \tag{1.3.45}$$

The $\mathrm{SU(2)_L \times U(1)_Y}$ transformation properties of the field strength tensors are then

$$B_{\mu\nu} \xrightarrow{G} B_{\mu\nu} , \qquad \widetilde{W}_{\mu\nu} \xrightarrow{G} U_L \widetilde{W}_{\mu\nu} U_L^\dagger . \tag{1.3.46}$$

Let us point out that, due to the quadratic pieces contained in the field strengths $W^i_{\mu\nu}$, the kinetic Lagrangian provides with cubic and quartic self-interactions among the gauge fields. However, the magnitude of these interactions is also controlled by the $SU(2)_\mathrm{L}$ coupling g that appeared before (1.3.40). We do not show them explicitly here but refer to Ref. [11] for the Lagrangian expressions.

The full one-family electroweak Lagrangian — invariant under the $\mathrm{SU(2)_L \times U(1)_Y}$ symmetry — is then

$$\mathcal{L}_{\mathrm{EW}} = -\frac{1}{4} B_{\mu\nu} B^{\mu\nu} - \frac{1}{4} W^i_{\mu\nu} W^{\mu\nu}_i + i \sum_j \bar\psi_j \slashed{D} \psi_j , \tag{1.3.47}$$

where the first two pieces on the right-hand side (r.h.s.) above are the kinetic terms of the gauge bosons containing the field strengths and $W^i_{\mu\nu} W^{\mu\nu}_i = 2\mathrm{Tr}\left[\widetilde{W}_{\mu\nu} \widetilde{W}^{\mu\nu} \right]$. For the fermionic pieces we have also included the lepton fields — which transform in the same way as quark fields in Eq. (1.3.40) — introducing the notation $\psi = \{Q, u_R, d_R, L, e_R\}$. We also employed the usual notation $\slashed{D} \equiv \gamma_\mu D^\mu$ for the covariant derivatives defined in Eq. (1.3.40). The matter part of the Lagrangian $\mathcal{L}_{EW}$ appears replicated three times in Nature, one for each family of quarks and leptons.

Note that the electroweak Lagrangian (1.3.47) does not include mass terms, either for gauge bosons or fermions. Both are forbidden by the gauge symmetry. A fermionic mass term $-m_\psi \left(\bar\psi_L \psi_R + \bar\psi_R \psi_L \right)$, with ψ any quark or lepton field, mixes both left and right chiralities, which transform differently under the symmetry group G, and consequently breaks explicitly the $\mathrm{SU(2)_L \times U(1)_Y}$ gauge symmetry.

Charged-current interactions

The covariant derivatives in the EW Lagrangian (1.3.47) contain the interactions among the fermion matter fields and the gauge bosons. Particularizing for the charged currents, these are driven by the terms containing the $\mathrm{SU(2)_L}$ matrix $\widetilde{W}_\mu$. By presenting it in its matrix form

$$\widetilde{W}_\mu = \frac{\sigma^i}{2} W^i_\mu = \frac{1}{2} \begin{pmatrix} W^3_\mu & \sqrt{2} W^\dagger_\mu \\ \sqrt{2} W_\mu & -W^3_\mu \end{pmatrix} , \tag{1.3.48}$$

we may identify the combinations $W_\mu \equiv (W_\mu^1 + iW_\mu^2)/\sqrt{2}$ and its complex conjugate $W_\mu^\dagger \equiv (W_\mu^1 - iW_\mu^2)/\sqrt{2}$, as the quantum fields of the gauge bosons $W^\pm$. The new W_μ^3 field will contribute to neutral-current interactions described in next section. The charged-current (CC) interactions are then given for any family of quarks and leptons by

$$\mathcal{L}_{\mathrm{CC}} = -\frac{g}{2\sqrt{2}} \left\{ W_\mu^\dagger \left(\bar{u}\gamma^\mu(1 - \gamma_5)d + \bar{\nu}_e\gamma^\mu(1 - \gamma_5)e \right) + \text{ h.c.} \right\} . \qquad (1.3.49)$$

The Lagrangian above provides the reason why we observe a universal charged-current weak interaction: they all share the same coupling constant g.

Neutral-current interactions

As for charged currents, the covariant derivatives of Eq. (1.3.47) contain the neutral gauge bosons W_μ^3 and B_μ, which provide the neutral-current (NC) interactions. However, these cannot be simply identified with the observed Z and γ, but instead, the following rotation is needed

$$\begin{pmatrix} W_\mu^3 \\ B_\mu \end{pmatrix} = \begin{pmatrix} \cos\theta_{\mathrm{W}} & \sin\theta_{\mathrm{W}} \\ -\sin\theta_{\mathrm{W}} & \cos\theta_{\mathrm{W}} \end{pmatrix} \begin{pmatrix} Z_\mu \\ A_\mu \end{pmatrix} , \qquad (1.3.50)$$

with θ_{W} being the weak mixing (also called Weinberg) angle. Therefore, the actual physical Z and γ bosons are a combination of the initial W_μ^3 and B_μ. The neutral-current Lagrangian then becomes

$$\mathcal{L}_{\mathrm{NC}} = -\sum_i \bar{\psi}_i \left\{ \slashed{A} \left[g\frac{\sigma_3}{2}\sin\theta_{\mathrm{W}} + g'y_j\cos\theta_{\mathrm{W}} \right] + \slashed{Z} \left[g\frac{\sigma_3}{2}\cos\theta_{\mathrm{W}} - g'y_j\sin\theta_{\mathrm{W}} \right] \right\} \psi_i ,$$
$$(1.3.51)$$

where we have employed again the notation $\psi = \{Q, u_R, d_R, L, e_R\}$. The above Lagrangian can also be writen as

$$\mathcal{L}_{\mathrm{NC}} = \mathcal{L}_{\mathrm{QED}} + \mathcal{L}_{\mathrm{NC}}^Z \qquad (1.3.52)$$

The first term on the r.h.s. of Eq. (1.3.51) becomes the interacting QED piece

$$\mathcal{L}_{\mathrm{QED}} = -eA_\mu \sum_i \bar{\psi}_i\gamma^\mu Q_i\psi_i \equiv -eA_\mu J_{\mathrm{EM}}^\mu , \qquad (1.3.53)$$

with J_{EM}^μ the electromagnetic current, after imposing

$$g\sin\theta_{\mathrm{W}} = g'\cos\theta_{\mathrm{W}} = e, \qquad Y = Q - T_3 . \qquad (1.3.54)$$

Above, the first expression relates the $\mathrm{SU(2)_L}$ and $\mathrm{U(1)_Y}$ couplings g and g' to the electromagnetic coupling e; $T_3 = \sigma_3/2$ and Q stands for the electromagnetic charge operator. The latter applies to quark and lepton fields in Eqs. (1.1.4) and (1.1.5) in the following way

$$Q_{Q(L)} = \begin{pmatrix} Q_{u(\nu)} & 0 \\ 0 & Q_{d(e)} \end{pmatrix} , \qquad Q_{u_R} = Q_u , \qquad Q_{d_R(e_R)} = Q_{d(e)} \qquad (1.3.55)$$

This way, the second expression in Eq. (1.3.54) gives us the fermion hypercharges in terms of their electric charge and weak isospin quantum numbers as

Quarks: $y_Q = Q_u - \dfrac{1}{2} = Q_d + \dfrac{1}{2} = \dfrac{1}{6}$, $y_u = Q_u = \dfrac{2}{3}$, $y_d = Q_d = -\dfrac{1}{3}$,

Leptons: $y_L = Q_\nu - \dfrac{1}{2} = Q_e + \dfrac{1}{2} = -\dfrac{1}{2}$, $y_\nu = Q_\nu = 0$, $y_e = Q_e = -1$,

where we have written explicitly the resulting null hypercharge and electric charge of a right-handed neutrino y_ν, Q_ν to show that such a particle would not have any gauge interaction in the SM and as such, it is not included[10].

The remaining piece of the neutral-current Lagrangian then reads

$$\mathcal{L}_{\rm NC}^Z = -\frac{e}{2\sin\theta_{\rm W}\cos\theta_{\rm W}} Z_\mu \sum_f \bar{f}\gamma^\mu(v_f - a_f\gamma_5)f, \qquad (1.3.56)$$

where f stands for any fermion field in the SM, and we have defined $a_f = T_3^f$ and $v_f = T_3^f(1 - 4|Q_f|\sin^2\theta_{\rm W})$, which depend on the given fermion f.

1.4 Spontaneous symmetry breaking: the scalar sector

The gauge symmetry principle provides a simple and elegant way to describe the electroweak interactions via the $\mathrm{SU(2)_L \times U(1)_Y}$ symmetry within the Lagrangian formalism. However, this same symmetry forbids the addition of mass terms for any of the physical particles: mass terms break explicitly the gauge symmetry. Therefore, we need some mechanism that is able to break the symmetry and gives masses to bosons and fermions while keeping the goodness of the gauge symmetry: the spontaneous symmetry breaking [12–14].

1.4.1 SSB and the Nambu-Goldstone theorem

In order to understand well the spontaneous symmetry breaking mechanism, let us address first the concept of symmetry in quantum mechanics (QM). We should distinguish first between the symmetries of the laws of Nature or, equivalently, the equations of motion and the symmetries of the states of the theory. Since the dynamics of the quantum states stem from the Hamiltonian (Lagrangian), symmetries of the EOM correspond as well to symmetries of the Hamiltonian (Lagrangian).

A symmetry transformation is represented in the Hilbert space of quantum mechanics by a unitary transformation U. A state $|\psi\rangle$ is symmetric under the symmetry transformation U if it satisfies

$$U|\psi\rangle = e^{i\varphi}|\psi\rangle, \qquad (1.4.57)$$

where the phase factor φ appears due to the fact that, in QM, the total phase of a quantum state is not measurable. However, for our purpose we can ignore that phase.

---

[10]Since right-handed neutrinos do not feel SM gauge interactions, we could just add as many as we wished instead of just one. Actually, we could add as many non-interacting fermions or bosons and we will never see them. This is why in the minimal SM a right-handed neutrino is not included.

Any quantum operator A is invariant under a symmetry transformation U if $U^\dagger A U = A$ or, what is the same, if they commute $[U, A] = 0$. A unitary transformation U is then a symmetry of the Hamiltonian if it holds $[U, H] = 0$. In that case, eigenstates of the Hamiltonian are also eigenstates of $U^\dagger A U = A$. Accordingly, we may use them as a complete basis of energy eigenstates. It is straightforward to realize that if a state $|\psi\rangle$ of the aforementioned basis has an eigenvalue E_ψ, then the transformed state $U|\psi\rangle$ — which is an eigenstate of the same basis as well — has the same eigenvalue:

$$H\left(U|\psi\rangle\right) = U H |\psi\rangle = U E_\psi |\psi\rangle = E_\psi \left(U|\psi\rangle\right). \qquad (1.4.58)$$

However, in case the corresponding energy eigenstate $|\psi\rangle$ is not symmetric, all states reached by the application of the symmetry transformation U are thus degenerated in energy. The transformation U allows us then to move between the subset of degenerated eigenstates.

More concretely, for a given group G of field transformations under which the Lagrangian is invariant, we have already seen that the unitary operator can be written as $U = \exp\{i\theta^a \mathcal{Q}_a\}$, with $\mathcal{Q}_a$ some conserved charges derived from the conserved Noether currents j_a^μ, that act as the generators of the symmetry transformations. In the Wigner-Weyl realization of the symmetry — for which both the states and the Lagrangian are invariant under G — the charges annihilate the vacuum $\mathcal{Q}_a|0\rangle = 0$, which hence remains invariant under U as well: $U|0\rangle = |0\rangle$. The other possible realization of the symmetry — for which the vacuum state of the theory is not invariant under G — presents the phenomenon called *spontaneous symmetry breaking*. In this case the Lagrangian is invariant under the symmetry group G, but the vacuum of the theory remains invariant only under a subgroup $H \subset G$. In other words, the spontaneous symmetry breaking occurs when a subset of physical states have "less symmetry" than the laws of Nature that govern them.

In the SSB situation of $G \to H$, the Nambu-Goldstone theorem [15,16] applies. It states that, given a conserved current $j_a^\mu(x^\alpha)$ derived from the continuous symmetry G, and the corresponding conserved charge $\mathcal{Q}_a(x^\alpha)$, if there exists some operator $\mathcal{O}$ such that $v_a \equiv \langle 0|[\mathcal{Q}_a, \mathcal{O}]|0\rangle \neq 0$, then the spectrum of the theory contains as many massless states as generators $\mathcal{Q}_a$ are broken ($N = \dim(G) - \dim(H)$), i.e. generators of G which do not belong to H. These states share the same quantum numbers as the broken generators.

Let us illustrate it with a simple example given by the Lagrangian of a complex scalar field $\phi(x^\alpha)$

$$\mathcal{L} = \partial_\mu \phi^\dagger \partial^\mu \phi - V(\phi), \qquad V(\phi) = \mu^2 \phi^\dagger \phi + \lambda \left(\phi^\dagger \phi\right)^2. \qquad (1.4.59)$$

The above Lagrangian is invariant under the symmetry group $G \equiv \mathrm{U}(1)$ of global phase transformations of the scalar field

$$\phi \longrightarrow \phi' \equiv \exp\{i\theta\}\phi. \qquad (1.4.60)$$

The potential $V(\phi)$ is characterized by two free parameters λ and μ. The existence of a ground state requires the potential to be bounded from below, this forces λ to be positive $\lambda > 0$. Then, depending on the sign of μ^2 we end up with two different

$V(\phi)$ describing very distinct physics, which are illustrated in Fig. 1.3. The vacuum of the theory can be obtained by minimizing the potential with respect to the field ϕ

$$\left. \frac{\partial V}{\partial \phi} \right|_{\phi=\phi_0} = 0 \, , \qquad (1.4.61)$$

where we have defined the vacuum expectation value (vev) of the field ϕ as $\phi_0 \equiv \langle 0|\phi|0 \rangle$. The usual Wigner-Weyl realization (see Fig. 1.3 (A)) corresponds to $\mu^2 > 0$, which entails a single minimum for the potential at $\phi = 0$ and describes a massive scalar particle with mass μ. The case of interest is given by $\mu^2 < 0$ (see Fig. 1.3 (B)). This potential presents the pattern of SSB with a minimum given by the field configurations satisfying

$$|\phi_0| = \sqrt{\frac{-\mu^2}{2\lambda}} \equiv \frac{v}{\sqrt{2}} > 0 \, , \qquad V(\phi_0) = -\frac{\lambda}{4}v^4 \, . \qquad (1.4.62)$$

The Lagrangian U(1) symmetry entails an infinite number of degenerated vacuum states given by $\phi_0 = \frac{v}{\sqrt{2}} \exp\{i\theta\}$. However, the choice of a concrete solution (given by θ) for the actual vacuum of the theory, breaks spontaneously the symmetry, since the particular value is not symmetric anymore. The field ϕ can be parametrized as

$$\phi \equiv \frac{1}{\sqrt{2}} \left[v + \varphi_1 + i\varphi_2 \right] \, , \qquad (1.4.63)$$

such that we are explicitly parametrizing the excitations over the ground state via the real φ_1 and φ_2 fields. In terms of these fields the potential looks like

$$V(\phi) = V(\phi_0) - \mu^2\varphi_1^2 + \lambda\,v\,\varphi_1\left(\varphi_1^2 + \varphi_2^2\right) + \frac{\lambda}{4}\left(\varphi_1^2 + \varphi_2^2\right)^2 \, , \qquad (1.4.64)$$

showing that φ_1 is indeed a massive field with $m_{\varphi_1}^2 = -2\mu^2$ and φ_2 is massless. The emergence of a massless field is exactly the result of the Nambu-Goldstone theorem. We started with a symmetric Lagrangian under G, where $\dim(G) = 1$; the particular choice of the vev breaks this symmetry spontaneously, so that the states of the theory are not symmetric anymore. From the Nambu-Goldstone theorem we have then $N = 1 - 0 = 1$ massless Goldstone bosons, the φ_1.

1.4.2   The Higgs sector and the gauge bosons

The realization of the spontaneous symmetry breaking in the Standard Model occurs via a similar scalar sector as the example above. Indeed, even though we have seen that, in general, one of the results is the appearance of a massless extra mode, when the pattern of SSB happens for a local gauge theory, it naturally provides masses to the gauge bosons and allows for fermion mass terms as well.

The extra scalar field should be now a $SU(2)_{\rm L}$ doublet of complex scalar fields

$$\phi \equiv \begin{pmatrix} \phi^{(+)} \\ \phi^{(0)} \end{pmatrix} \, . \qquad (1.4.65)$$

(A) Potential with $\mu^2 > 0$.

(B) 2D and 3D potentials with $\mu^2 < 0$.
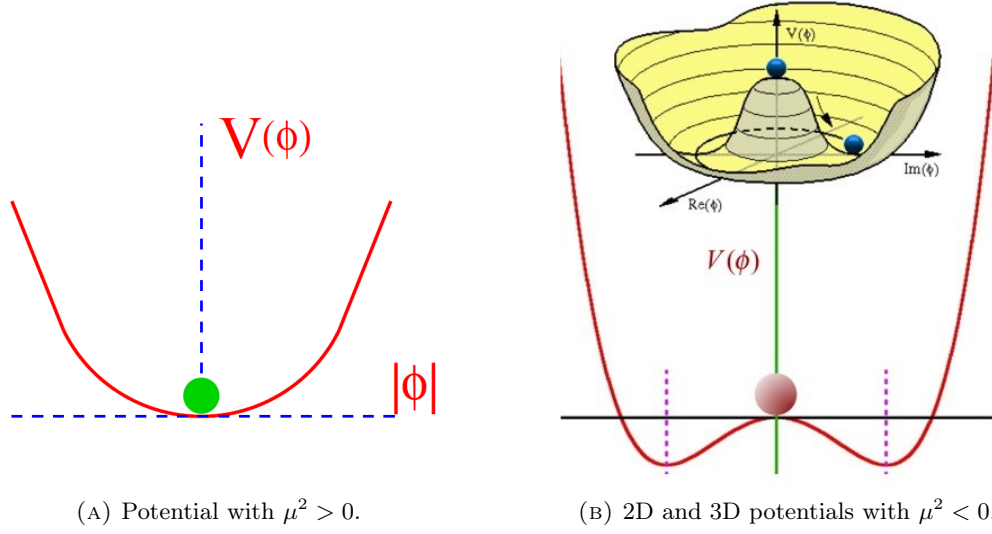
FIGURE 1.3: Different cases of the Higgs potential in terms of μ^2.

Then, introducing the scalar sector of Eq. (1.4.59) with the new doublet scalar field and gauging it, we obtain

$$\mathcal{L}_{\mathrm{S}} = \left(D_\mu \phi\right)^\dagger D^\mu \phi - \mu^2 \phi^\dagger \phi - \lambda \left(\phi^\dagger \phi\right)^2 , \qquad (1.4.66)$$

with the conditions $\lambda > 0$, $\mu^2 < 0$, that we studied earlier, and where the covariant derivative D^μ is the one defined in Eq. (1.3.40) for $SU(2)_{\mathrm{L}}$ doublets. The corresponding hypercharge is given by imposing the correct couplings between the scalar field ϕ and the photon field A^μ: $y_\phi = Q_\phi - T_3 = 1/2$. Therefore, $\mathcal{L}_S$ is invariant under local $SU(2)_{\mathrm{L}} \times U(1)_{\mathrm{Y}}$ transformations.

In order to obtain the vacuum of the theory, we should first note that the electric charge is a conserved quantity. Accordingly, only the neutral component $\phi^{(0)}$ can acquire a vacuum expectation value. This is given by

$$\phi_0 \equiv |\langle 0|\phi^{(0)}|0\rangle| = \sqrt{\frac{-\mu^2}{2\lambda}} \equiv \frac{v}{\sqrt{2}} , \qquad (1.4.67)$$

where v is more customarily referred to as the vev, and so we call it from now on.

As in the example above, there is an infinite set of degenerated states that share the same vev (we will see below how those states may be reached). The particular choice of the ground state among the infinite symmetric possibilities, is what provides the necessary SSB breaking pattern of the SM symmetry to the electromagnetic subgroup

$$SU(2)_{\mathrm{L}} \times U(1)_{\mathrm{Y}} \xrightarrow{\mathrm{SSB}} U(1)_{\mathrm{QED}} , \qquad (1.4.68)$$

which by construction still remains a good symmetry of the vacuum. The Nambu-Goldstone theorem then tells us that, since three generators of the $SU(2)_{\mathrm{L}} \times U(1)_{\mathrm{Y}}$ symmetry have been broken, there are three associated massless states.

In Fig. 1.3 (B) we provide the scalar potential in Eq. (1.4.66) as function of ϕ. This presents the usual mexican hat shape. In order to understand better the role

of the Goldstone bosons, it is illustrative to parametrize the scalar doublet field (via a polar decomposition) as

$$\phi = \exp\left\{i\frac{\sigma_i}{2}\theta^i\right\}\frac{1}{\sqrt{2}}\begin{pmatrix} 0 \\ v + H \end{pmatrix}, \qquad (1.4.69)$$

which contains the three real fields $\theta^i(x^\alpha)$ in the exponential and another real field $H(x^\alpha)$. Accordingly, by applying a suitable $SU(2)_L$ transformation, we can rotate away the dependence on the θ^i fields. These correspond then to the three massless Goldstone modes, which in the parametrization above appear as a phase of the field ϕ. Therefore, the Goldstone bosons are the responsibles for the excitations around the flat valley of the potential in Fig. 1.3 (B), i.e. into states with the same energy as the chosen vacuum state. The correspondence between the massless fields and excitations over same energy levels is then clear. Radial excitations are then given by the field H, which by the same arguments corresponds to a massive field, the Higgs field.

Let us study now the coupling of the gauge bosons to the scalar field. This is provided, as usual, by the covariant derivative D^μ. By taking the physical *unitary gauge* $\theta^i = 0$, the kinetic piece of $\mathcal{L}_S$ becomes

$$\left[(D_\mu\phi)^\dagger D^\mu\phi\right](\theta^i = 0) = \frac{1}{2}\partial_\mu H\partial^\mu H + (v + H)^2\left\{\frac{g^2}{4}W_\mu^\dagger W^\mu + \frac{g^2}{8\cos^2\theta_W}Z_\mu Z^\mu\right\}.$$
$$(1.4.70)$$

The vacuum expectation value of the doublet neutral scalar then generates the masses of the $W^\pm$ and Z gauge bosons

$$M_W = \frac{1}{2}vg\,, \qquad M_Z = \frac{1}{2\cos\theta_W}vg\,, \qquad (1.4.71)$$

while the photon remains massless, and the total electroweak Lagrangian is still invariant under the gauge $SU(2)_L \times U(1)_Y$ symmetry, which ensures the renormalizability of the Standard Model. Furthermore, the SSB mechanism relates the gauge boson masses and, at tree level, they satisfy the relation

$$\rho \equiv \frac{M_W^2}{M_Z^2\cos^2\theta_W} = 1\,. \qquad (1.4.72)$$

Note as well that the tree level couplings of the gauge bosons and the Higgs are completely fixed and are proportional to the square mass of the former[11].

The spontaneous symmetry breaking mechanism, thus generates the masses of the gauge bosons by a trade-off between the massless Goldstone modes and the longitudinal polarizations of the $W^\pm$ and Z bosons, characteristic of massive particles. This is colloquially addressed as a process where the Goldstone bosons are "eaten" by the gauge fields to acquire mass. However, this is not the only physical effect of the SSB pattern in the SM. In addition, it predicts the existence of a new neutral scalar boson described by the remaining scalar field H in the unitary gauge: the

---

[11] Since the Higgs couples via the mass of the other particles, there is no tree level coupling to the photon. This, however, is coupled via loop interactions.

Higgs boson. After many years of search, it was finally discovered[12] by the AT-LAS [17] and CMS [18] collaborations in 2012. The interactions of the Higgs boson are described by scalar Lagrangian, which in the unitary gauge becomes

$$\mathcal{L}_S = \mathcal{L}_H + \mathcal{L}_{HG^2} \,, \tag{1.4.73}$$

where $\mathcal{L}_{HG^2}$ contains the Higgs-gauge bosons interactions given in Eq. (1.4.70) and the corresponding kinetic term as well as the rest of Higgs self-interactions are included in

$$\mathcal{L}_H = \frac{1}{2}\partial_\mu H \partial^\mu H - \frac{1}{2}M_H^2 H^2 - \frac{M_H^2}{2v}H^3 - \frac{M_H^2}{8v^2}H^4 \,, \tag{1.4.74}$$

where the Higgs mass is given as

$$M_H = \sqrt{-2\mu^2} = \sqrt{2\lambda}v \,. \tag{1.4.75}$$

Note that the Higgs interactions always depend on the mass of the coupled boson and, as such, it allows up to quartic Higgs self-interactions.

1.4.3 Yukawa sector and flavor dynamics

Gauge symmetry forbids, as well, fermion mass terms. However, the same doublet scalar field giving rise to gauge boson masses, also allows to generate fermion masses, although in a less restrictive manner. Let us consider the three generations of the SM fermions, denoted in the weak basis[13] with a prime: u'_p, d'_p, ν'_p and ℓ'_p. We can write the gauge-invariant fermion-scalar interacting Yukawa-like Lagrangian as

$$\mathcal{L}_Y = -\sum_{p,r}\left\{\left(\bar{u}'_p\ \bar{d}'_p\right)_L\left[Y_{pr}^{(d)}\begin{pmatrix}\phi^{(+)}\\\phi^{(0)}\end{pmatrix}d'_{R\,r} + Y_{pr}^{(u)}\begin{pmatrix}\phi^{(0)*}\\-\phi^{(-)}\end{pmatrix}u'_{R\,r}\right]\right.$$
$$\left. + \left(\bar{\nu}'_p\ \bar{\ell}'_p\right)_L Y_{pr}^{(\ell)}\begin{pmatrix}\phi^{(+)}\\\phi^{(0)}\end{pmatrix}e'_{R\,r}\right\} + \text{ h.c.}\,, \tag{1.4.76}$$

where the $Y_{pr}^{(d)}$, $Y_{pr}^{(u)}$ and $Y_{pr}^{(\ell)}$ are arbitrary Yukawa matrices, and we have introduced the C conjugate scalar field $\phi^C \equiv i\sigma_2\phi^*$.

In the unitary gauge, the Lagrangian above becomes

$$\mathcal{L}_Y = -\left(1 + \frac{H}{v}\right)\left\{\bar{d}'_L M'_d d'_R + \bar{u}'_L M'_u u'_R + \bar{\ell}'_L M'_\ell \ell'_R + \text{ h.c.}\right\}\,, \tag{1.4.77}$$

where we have collected the three fermion families in a 3-dimensional vector in flavor space denoted in bold face. The matrices M' are defined in terms of the Yukawa couplings as

$$(M'_d)_{pr} \equiv Y_{pr}^{(d)}\frac{v}{\sqrt{2}}\,, \qquad (M'_u)_{pr} \equiv Y_{pr}^{(u)}\frac{v}{\sqrt{2}}\,, \qquad (M'_\ell)_{pr} \equiv Y_{pr}^{(\ell)}\frac{v}{\sqrt{2}}\,. \tag{1.4.78}$$

---

[12]The complete identification of the Higgs particle with that discovered at CERN in 2012 is still a work in progress. Up to now though, both share the same quantum numbers and all indications point to the predicted Higgs boson.

[13]The weak basis is defined as the fermion eigenstates which interact in the electroweak Lagrangian with the corresponding gauge bosons, i.e. with definite transformations properties under the gauge group. To be distinguished below from the mass basis, defined as the eigenstates with a definite mass.

A matrix A can be generally decomposed as $A = S^\dagger \mathcal{A} S U$, where U and S are unitary matrices and the resulting $\mathcal{A}$ is diagonal, Hermitian and positive definite. Therefore, we can diagonalize the matrices M' in the same way: $M' = S^\dagger \mathcal{M} S U$, with different S and U matrices for the different fermion species u, d and ℓ. The corresponding diagonal mass matrices can then be expressed in terms of the fermion masses as

$$\mathcal{M}_d = \mathrm{diag}(m_d, m_s, m_b)\,, \quad \mathcal{M}_u = \mathrm{diag}(m_u, m_c, m_t)\,, \quad \mathcal{M}_\ell = \mathrm{diag}(m_e, m_\mu, m_\tau)\,. \tag{1.4.79}$$

Inserting the expression for M', in terms of the diagonal $\mathcal{M}$, in Eq. (1.4.76) we arrive to the Yukawa Lagrangian expressed in the mass basis of the fermion fields

$$\mathcal{L}_Y = -\left(1 + \frac{H}{v}\right) \left\{ \bar{\boldsymbol{d}} \mathcal{M}_d \boldsymbol{d} + \bar{\boldsymbol{u}} \mathcal{M}_u \boldsymbol{u} + \bar{\boldsymbol{\ell}} \mathcal{M}_\ell \boldsymbol{\ell} \right\}\,, \tag{1.4.80}$$

with the mass eigenstates defined as

$$\begin{aligned} \boldsymbol{d}_L &\equiv S_d \boldsymbol{d}'_L\,, & \boldsymbol{u}_L &\equiv S_u \boldsymbol{u}'_L\,, & \boldsymbol{\ell}_L &\equiv S_\ell \boldsymbol{\ell}'_L\,, \\ \boldsymbol{d}_R &\equiv S_d U_d \boldsymbol{d}'_R\,, & \boldsymbol{u}_R &\equiv S_u U_u \boldsymbol{u}'_R\,, & \boldsymbol{\ell}_R &\equiv S_\ell U_\ell \boldsymbol{\ell}'_R\,, \end{aligned} \tag{1.4.81}$$

The mixing of flavor eigenstates provided by Eq. (1.4.81) has further consequences in other sectors of the Standard Model. The strong interactions, being flavor blind, remain unaffected by this change of basis. In the electroweak sector, due to the general $\overline{\psi'_{L(R)}} \psi'_{L(R)} = \overline{\psi_{L(R)}} \psi_{L(R)}$ structure of the neutral currents, the mixing matrices above cancel for all fermion combinations, thus precluding the existence, at tree level, of flavor-changing neutral currents in the SM (GIM mechanism [6]). The charged-current interactions are another matter. These interactions (see Eq. (1.3.49)) mix (independently) quark and lepton flavors via terms of the form

(i) $\bar{\boldsymbol{u}'}_L \boldsymbol{d}'_L = \bar{\boldsymbol{u}}_L S_u S_d^\dagger \boldsymbol{d}_L \equiv \bar{\boldsymbol{u}}_L V \boldsymbol{d}_L$,

(ii) $\bar{\boldsymbol{\nu}'}_L \boldsymbol{\ell}'_L = \bar{\boldsymbol{\nu}'}_L S_\ell^\dagger \boldsymbol{\ell}_L \equiv \bar{\boldsymbol{\nu}}_L \boldsymbol{\ell}_L$.

Therefore, working in the mass basis introduces a charged-current quark-flavor mixing (see (i) above) driven by the unitary 3×3 mixing matrix V, the so-called Cabibbo-Kobayashi-Maskawa (CKM) matrix [19, 20]. This is consequently of the form:

$$V = \begin{pmatrix} V_{ud} & V_{us} & V_{ub} \\ V_{cd} & V_{cs} & V_{cb} \\ V_{td} & V_{ts} & V_{tb} \end{pmatrix}\,, \tag{1.4.82}$$

and is customarily used in the down-quark sector to switch between the weak and mass basis

$$\begin{pmatrix} d' \\ s' \\ b' \end{pmatrix} = \begin{pmatrix} V_{ud} & V_{us} & V_{ub} \\ V_{cd} & V_{cs} & V_{cb} \\ V_{td} & V_{ts} & V_{tb} \end{pmatrix} \begin{pmatrix} d \\ s \\ b \end{pmatrix}\,, \tag{1.4.83}$$

while fixing the identification of the up-quark weak eigenstates with the mass eigenstates. Let us point out that we may use the unobservable phase redefinitions of the quark fields to reduce the number of free parameters in V, from the most general

9 real parameters for a unitary 3×3 matrix to the actual 4 physical CKM components: 3 angles and 1 phase. The latter constitutes the only complex phase of the SM Lagrangian and, consequently, it is the only possible source of CP violation.

On the other hand, the absence of a right-handed neutrino precludes the existence of a corresponding neutrino mass term. This means that for neutrinos there is no difference between mass and flavor eigenstates. Therefore, we may use this freedom to redefine neutrino flavors in a suitable way, such that it removes the mixing in the lepton sector (see (ii) above). However, if a right-handed neutrino is added to the SM particle content, the same discussion as for quarks applies here. Accordingly, the charged-current sector presents as well lepton-flavor mixing and the corresponding unitary mixing matrix for neutrinos is in this case the Pontecorvo-Maki-Nakagawa-Sakata (PMNS) [21, 22] — in the diagonal charged-lepton flavor basis. Note though that neutrinos do actually have mass and, as such, they do present an oscillation pattern among the flavor states: neutrino oscillations. Nonetheless, since on one hand, right-handed neutrinos do not feel the SM gauge interactions and, on the other, their corresponding Yukawas may be seen as unnaturally small (in view of their measured tiny masses), there are actually other better motivated neutrino mass-generating mechanisms. These tend to enlarge the PMNS matrix, due to the addition of other (usually) heavy neutral leptons (HNL), and hence to spoil the unitarity of the 3×3 sub-block (see Chapter 6) corresponding to the mixing of the light neutrinos of the SM.

All in all, the charged-current Lagrangian of the SM in the mass basis is given by

$$\mathcal{L}_{\text{CC}} = -\frac{g}{2\sqrt{2}} \left\{ W_\mu^\dagger \left[\sum_{p,r} \bar{u}_p \gamma^\mu (1 - \gamma_5) V_{pr} d_r + \sum_e \bar{\nu}_e \gamma^\mu (1 - \gamma_5) e \right] + \text{ h.c.} \right\}, \tag{1.4.84}$$

thus providing the aforementioned charged-current quark flavor mixing.

Switching to the mass basis and performing suitable quark phase redefinitions, has allowed us to use the freedom we have in the definition of the fermion fields to reduce (via Eqs. (1.4.81) and (1.4.84)) the initial free 54 parameters — introduced by the most general 3×3 Yukawa matrices $Y_{pr}^{(u)}$, $Y_{pr}^{(d)}$ and $Y_{pr}^{(\ell)}$ — to the free 9 fermion masses and 4 CKM components, to be determined experimentally. Hence, the total number of free parameters in the Standard Model Lagrangian adds up to 19 if one takes also into account the $\theta_{\text{QCD}} \sim 0$ parameter.

Chapter 2

Effective field theories

The Standard Model described in the previous section as a consistent renormalizable theory, stands as one of the best theories ever built to understand and explain the physical phenomena, at subatomic level, observed in Nature. Despite the success of this particular quantum field theory, there are still several open questions of both observational and theoretical nature.

Among the former kind, there are several observed phenomena which have no explanation within the SM framework, e.g. the mass of neutrinos (absent in the SM) observed via the oscillations of their flavor eigenstates in weak processes; the large missing fraction of the total mass of the universe, which the current dominant paradigm tends to explain via the so-called dark matter; the observed dominance of matter over antimatter in the universe, for which the SM only accounts for a small part of it, and others.

The theoretical issues, although do not necessarily entail inconsistencies within the SM framework itself, lack a fundamental understanding. The customary example is the naturalness problem, whose realization in the SM is threefold:

(i) the notable hierarchy problem or naturalness of the Higgs mass, characterized by the seemingly needed fine-tuning of its physical (measured) mass stemming from the subtle cancellation between the bare parameter of the Lagrangian and its quantum radiative corrections,

(ii) the Strong CP problem or naturalness of the theta parameter of QCD, being its experimental value compatible with zero but with no explanation whatsoever within the SM,

(iii) the cosmological constant problem or naturalness of the cosmological constant, found to be between 40 and 100 orders of magnitude smaller than the naive expectations within the SM.

Apart from naturalness, there are other theoretical hints pointing to a richer physics scenario within the apparent "desert" between the electroweak scale and the Planck mass $\mathcal{M}_{\mathrm{Plank}} \sim 10^{18}$ GeV — where gravitational effects start to be relevant at short distances and a consistent description of gravity within the quantum formalism is needed. One of these indications is the running behaviour of the SM coupling constants, which even though approach each other at very large energies $E \sim 10^{15} - 10^{16}$ GeV, fail to exactly converge within the SM formalism. This observation provides a hint of the unification of the SM interactions at those energies, but points to the

necessity of new physics (NP) to reach such convergence. These new physics scenarios (unfortunately with new dynamics arising typically at those scales, so directly unobservable at current experimental energies) extend the symmetry group of the SM to explain all phenomena in terms of a unified interaction. Consequently, the generated new dynamics shift the running behavior of the SM coupling constants, such that at the above characteristic scale these converge and behave as only one physical constant. To a lesser extent, another example is provided by the requirement of renormalizability onto the SM. This restriction leads to the appearance of accidental global symmetries as global lepton and baryon number conservation. As we will see below, the inclusion of non-renormalizable terms in a more general theory may naturally break this symmetry. Although experimental data — up to the current precision — confirms the SM framework in this matter as well, the existence of accidental symmetries lack a more profound explanation.

In view of these unanswered questions and the deeper insight gained into the QFT formalism (see next section), in the recent years a consensus has been reached about the understanding of the SM as a low-energy realization of a complete high-energy theory, customarily referred to as its Ultraviolet (UV) completion.

Accordingly, on the *theoretical* side, the physics community has witnessed a proliferation of beyond the Standard Model (BSM) physics scenarios addressing one or several of the aforementioned issues. For instance, neutrino masses may be explained via different seesaw mechanisms (see Chapter 5). The hierarchy problem has been typically solved in supersymmetric (SUSY) extensions of the SM, while the axion field provides a dynamical mechanism to explain the null value of the theta parameter of QCD. Gran Unified Theories (GUT) provide an extended symmetry framework with a natural unification of the SM interactions at the characteristic GUT energy scales $E_{\mathrm{GUT}} \sim 10^{15} - 10^{16}$ GeV. The minimal supersymmetric extension of the SM (MSSM) also manage to reach the convergence of the SM coupling constants but with new dynamics arising at a much lower energy scale. Many theoretical ideas have arisen in the quest to explain the origin of dark matter, from the well-known weak interacting massive particles (WIMPs) or the increasingly famous axion-like particles, to the very exotic idea of primordial black holes accounting for the missing (only-)gravitationally interacting mass. Gauging baryon and lepton number — thus promoting to local gauge symmetries part of the building blocks of the theory — has been among others a usual approach to face the experimental results confirming the conservation of these global symmetries in the SM Lagrangian. These models make predictions of physical observables in terms of their parameters (masses and couplings), either along the existing SM contributions or driving new phenomena not present in the SM.

From the *experimental* perspective, many collaborations around the globe have already gathered a vast amount of data on low and high-energy processes. These can be classified in three categories[1]:

(i) precise measurements of observables already existing within the SM,

(ii) not quite precise but novel measurements of expected (but difficult to measure) SM processes,

---

[1] The work presented in this thesis focuses on aspects of the phenomenology related to the last two.

(iii) constraints on (or possible observations of) forbidden processes in the SM.

Indeed, the largest and more powerful particle accelerator in the world exploring the highest achievable energy regimes in physics, the Large Hadron Collider (LHC), in its first two runs of data acquisition has performed impressively well. It provided the major milestone of the discovery of the Higgs particle, novel measurements of expected observables and the most precise determinations of several SM parameters. However, contrary to the general preexisting feeling expecting to find a zoo of SUSY particles or other more exotic phenomena, apart from the discovery of the Higgs, no new particles have been found so far.

In view of the null results provided by *direct searches* in finding new degrees of freedom pointing to a concrete UV completion of the SM, a complementary path to look for new physics comes from studying the (quantum) effects of higher energy dynamics into existing or forbidden SM observables. These *indirect searches* rely on the idea that the existence of heavy degrees of freedom embedded in a higher-energy BSM framework, may manifest in deviations of the SM predictions for physical observables at low (currently observable) energies.

Clearly, in order to extract relevant information from experiments, one has to process — within the model of interest — the raw data acquired in the detectors. On account of the large amount of models and the required resources, the endeavor of performing dedicated analyses for each theoretical model is unattainable.

Are we then compelled to analyze model by model under the appropriate sub-set of experimental data? Or there is a way to make use of all experimental data and systematically explore all possible deviations from the Standard Model? Effective field theories (EFTs) provide negative and affirmative answers respectively for those questions. EFTs can be regarded as tools that allow us to systematically characterize deviations of the theory upon which they are built and as such, it retains its main aspects, as particle content and symmetries. The basic qualitative idea behind EFTs is that, in the description of a given phenomenon taking place at a characteristic energy scale μ, one can separate the relevant ingredients (long-distance effects with $E \lesssim \mu$) from subleading terms (short-distance effects with $E \gg \mu$), which can be ignored assuming a (controlled) loss in precision.

In this chapter we focus on the effective field theory formalism and present some EFTs that will be used along the thesis. Concretely, in Section 2.1 we describe the theoretical pillars over which the EFT formalism is derived, its consistency, and how the EFTs are related to the underlying more fundamental theory. Then, in Section 2.2 we present in detail the low-energy effective field theory of QCD: Chiral Perturbation Theory, which is extended by the so-called Resonance Chiral Theory, to account for the resonances populating the QCD non-perturbative region, in Section 2.4. The EFT of the SM is presented up to $d = 6$ operators in Section 2.5. There, some important aspects regarding its practical use as well as its renormalization are discussed. Finally, Section 2.6 is devoted to present the lower-energy realization of the SMEFT, for which we go even further and compute its non-relativistic limit.

2.1 Basics of the EFTs

In Chapter 1 we started with a discussion about the lagrangian formalism. In summary, we saw that physical theories can be described by a Lagrangian built out of operators made of particle fields. From dimensional analysis, the dimension of the resulting operators together with the lagrangian parameters should always add up to four. In addition, those operators are also restricted by the symmetries of the theory, both continuous as gauge transformations or discrete symmetries as charge or parity conjugation[2], to pose some examples. This whole discussion applies to effective field theories as well.

2.1.1 General principles of the EFTs: the bottom-up approach

In general terms, EFTs can be defined as a procedure to encode the effects of a more fundamental QFT, that allow us to parametrize in a consistent manner the (less-relevant) effects at low energies of unknown physics present beyond a given energy scale[3]. One of the fundamental requirements of any EFT to properly account for such effects, is the existence of a sufficiently large energy gap between both low and high-energy regimes, e.g. the effective Fermi theory of weak interactions describes well phenomena at energies much lower than the mass of the W (high energies), while the SMEFT formalism, in view of current experimental results pointing to the absence of new physics up to the TeV range, may describe well deviations of SM dynamics at scales of the order $E \sim v$ — with $v \equiv \langle 0|\varphi|0\rangle$ the vacuum expectation value of the Higgs (see Chapter 1) in the SM — that originate in new dynamics at a higher energy scale.

The generality of EFTs lies in a theorem that applies to quantum field theories as a whole. This theorem was first mentioned by Weinberg [23] and states that, although individual QFTs as QED, QCD or the SM itself, have indeed a good deal of content, i.e. they accommodate a specific particle spectrum, describe their behavior, make predictions based on a small number of couplings etc, by themselves have no content beyond:

- the symmetries we may impose;

- the basic principles required by the foundational theories of Special Relativity and Quantum Mechanics, i.e. Lorentz invariance, analyticity, unitarity and cluster decomposition.

The latter is just the modern version of locality in Special Relativity, and refers to the fact that two or more experiments made at a sufficiently large distance cannot affect each other, in other words that their results are uncorrelated.

The aforementioned theorem provides the reason why, given some particle content and a symmetry group, the Lagrangian resulting from considering all possible invariant operators necessarily encompasses — when working to all orders in perturbation theory — all possible dynamics experienced by the specified fields, since

---

[2]We leave out time reversal since the CPT theorem states that QFTs are invariant under the total CPT transformation by construction, what establishes a relation between the CP and T symmetries.

[3]In this context, the meaning of low and high energy varies depending on the characteristic energy scale at which the studied process takes on.

we are just assuming, besides the symmetry group, the previously stated principles of the theories underlying the QFT construction. From this very general discussion, any effective field theory may be expressed via the following Lagrangian:

$$\mathcal{L}_{\text{EFT}} = \sum_{d=2}^{\infty} \left(\sum_i \frac{C_i^{(d)}}{\Lambda^{d-4}} \mathcal{O}_i^{(d)} \right) , \qquad (2.1.1)$$

where the $C_i^{(d)}$ are dimensionless parameters that receive the name of Wilson coefficients (WC), and we are summing over the dimension index d, which takes integer values. For each given d there is a finite subset of operators, built out of the field content of the theory, of dimension $[\mathcal{O}_i^{(d)}] = E^d$, which are spanned by the sum over i. Therefore, the superindex in parentheses d labels the dimension of the operators and the corresponding Wilson coefficients. Due to dimensional arguments, to compensate the dimensions of the operators in the Lagrangian, a power $d-4$ of the mass term Λ, with $[\Lambda] = E$, is always present in the denominator.

From the general EFT Lagrangian of Eq. (2.1.1), we can distinguish three kinds of operators in terms of their dimensionality: Relevant ($d < 4$), Marginal ($d = 4$) and Irrelevant ($d > 4$) operators. This classification responds to the low-energy behavior of the operators, including the mass term in the denominator. *Relevant* operators are thus accompanied by a coupling of positive mass dimension, in consequence their effects become larger at energies lower than the scale of that coupling. For instance, this is the case of massive terms for bosons ($d = 2$) and fermions ($d = 3$), whose effects are negligible at high energies ($E \gg m$) but turn out to be important at energies close to and below the mass of these particles. *Marginal* operators are those of $d = 4$ whose corresponding coupling is hence dimensionless. These operators are in principle equally important irrespective of the energy scale. However, quantum corrections may change their behavior at different energy scales, as it is the case for gauge couplings like the fine structure constant α of QED or the strong coupling α_s of QCD, increasing or decreasing respectively their magnitude at higher energies. *Irrelevant* operators are those of dimensionality $d > 4$, which are consequently suppressed by terms of $\mathcal{O}\left(1/\Lambda^{(d-4)}\right)$, with Λ representing a characteristic heavy scale of the system. More concretely, matrix elements of irrelevant operators between initial $|i\rangle$ and final $\langle f|$ states, behave qualitatively as

$$\langle f | \mathcal{O}_i^{(d)} | i \rangle \sim E^{(d-4)+a} \quad d > 4 , \qquad (2.1.2)$$

where E stands for the characteristic energy scale at which the processes are taken place and a is fixed by the external states, e.g. for a given operator $\mathcal{O}_i^{(d)}$, a would differ for matrix elements with different initial and final states. Therefore, since anyhow for a given observable the parameter a is a common term for all kind of operators, the long-distance contribution of any irrelevant operator is suppressed by factors of $\mathcal{O}\left((E/\Lambda)^{(d-4)}\right)$ relative to the leading terms, i.e. relevant and marginal terms. Likewise, the higher the energy, the less suppressed it becomes, up to a point where irrelevant operators start to be more "relevant" and the main requirement of EFTs about the existence of a gap between the low and high-energy theories is lost.

In any case, at low energies one can truncate the infinite sum over the dimension parameter d at some value n, making an error of $\mathcal{O}\left((E/\Lambda)^{(n-4)}\right)$. This is actually

the reason why EFTs are such a powerful tool when studying long-distance effects stemming from short-distance dynamics: one does not have to compute the contributions from the whole tower of operators in Eq. (2.1.1), since we know higher order terms are more and more suppressed. On the contrary, when working with EFTs, one may ideally compute as many higher-order terms as accuracy on the calculation is desired, neglecting thus the subleading contributing terms in the series. However, in practice, the further we go in the expansion of Eq. (2.1.1), the more unknown WC are introduced, thus losing predictability and requiring more and more experimental inputs to fix or constrain them.

Historically until recent times, effective field theories received minor attention due to its apparent lack of renormalizability. The renormalizable nature (in the old sense) of a theory was early identified as due to the dimensionality of its couplings [24]. Therefore, theories containing a finite number of operators with $d = 4$, i.e. marginal operators, received the status of renormalizable theories. In these kind of theories, the infinities arising from the divergent integrals over the momentum space in the calculation involving loop diagrams, can be canceled at every order in the perturbative expansion by just redefining all parameters of the theory in terms of the so-called renormalized quantities. On the other hand, theories containing operators of higher dimension ($d > 4$), i.e. with coupling constants of negative mass dimension, were classified as non-renormalizable theories and as such, non appropriate to describe Nature. However, this classification and the understanding derived from it are outdated. We now know that non-renormalizable theories — containing an infinite tower of operators in increasing dimension — are just as renormalizable as renormalizable theories, provided all allowed (infinite) terms by the symmetries of the theory are included. Schematically, the ultraviolet divergences arising in loop diagram computations, can be canceled by counterterms stemming from the higher order terms in the (dimensional) expansion. This holds at all orders in perturbation theory: the further one goes, the more loops are faced and higher dimensional counter terms are thus needed [25]. One may claim though, that in order to have a consistent renormalizable theory, we should pay the price of ending up with an infinite Lagrangian. However, from the previous discussion, we know that only a finite number of terms are needed to compute any physical process up to a desired precision of $\mathcal{O}\left((E/\Lambda)^{(n-4)}\right)$, such that subleading terms may be neglected. This is indeed the reason why renormalizable theories as the Standard Model have attained great success: they contain all relevant ingredients to properly describe physical phenomena, while systematically neglecting[4] terms suppressed by powers of E/Λ.

Notice that, in the discussion above, we have not yet addressed those operators with positive mass-dimension couplings. In general, from Eq. (2.1.1), we could expect those couplings to be of order Λ^n, with $n > 0$, meaning the order of the fundamental higher-energy scale, thus being by definition very large. The only one term in the Standard Model Lagrangian, before SSB takes place, with such a coupling is the bare mass of the Higgs particle. From the previous reasoning, one would hence expect the mass of the Higgs to lie around the GUT or even the Planck

---

[4]Note though that if the scale of new physics Λ lived not much far away from current experimental energies E, the corresponding corrections E/Λ would become large enough to see deviations from the SM predictions in the experiments.

scales $E \sim 10^{16} - 10^{18}$ GeV, if considered as fundamental scales. Needless to say, this does not correspond to the 125 GeV Higgs observed at the LHC. This discrepancy is the so-called naturalness problem of the Higgs, for which we do not have yet a clear explanation. The same effect happens for the other known positive mass-dimension coupling, the cosmological constant, observed to be much smaller than expected by naive considerations.

Nevertheless, on one side the observed phenomena lacking an explanation within the renormalizable SM and, on the other, our current understanding of both the Standard Model and the effective field theory formalism, has brought us to think of the SM as merely an effective low-energy realization of a more fundamental theory — perhaps not in the form of a QFT. Assuming the existence of a sufficiently large energy gap between the SM and its UV completion, the former has to be consequently extended by an infinite tower of local operators of increasing dimension, into the well-known SMEFT (see Section 2.5).

2.1.2 Integrating out heavy degrees of freedom: the top-down approach

The path followed in the previous discussion to construct the most general EFT represents the so-called bottom-up approach: we made no assumptions on the short-distance dynamics and built the EFT Lagrangian of Eq. (2.1.1) departing directly from the known symmetries and particle content of the low-energy theory. In that manner, based on the general QFT theorem (generally ascribed to Weinberg) stated above and despite the huge amount of possible UV completions, we are able to capture all relevant information from the dynamics of the heavy degrees of freedom — as deviations of the predictions at low-energies for the physical observables — in terms of the parameters of the EFT.

A natural question thus arise, how is the information from the UV theory encoded in the EFT parameters? In other words, how the EFT of Eq. (2.1.1) can be (partially) recovered from a given higher-energy theory? A formal answer is provided by the object called generating functional (of correlation functions), which lies on the basis of the path integral formulation of QFT.

For a simple theory describing the dynamics of a field $\phi(x^\mu)$ via the action $S[\phi]$, the generating functional $\mathcal{Z}$ provides the vacuum matrix elements[5] of the theory and is given by [26]

$$\langle 0|0 \rangle = \int \mathcal{D}\phi \exp\left\{ iS[\phi] \right\} \equiv \mathcal{Z}\,, \qquad (2.1.3)$$

where $\mathcal{D}\phi$ stands for the measure of integration over all possible configurations of the field ϕ, i.e. is the generalization to continuous functions (the fields) of the differential dx for discrete vectors. Likewise, the argument of the functional S is given in brackets to denote their nature as a function.

In the presence of an external classical source $J(x^\mu)$ coupled to the field ϕ, the generating functional looks like

$$\mathcal{Z}[J] = \int \mathcal{D}\phi \exp\left\{ iS[\phi] + i \int d^4x J\phi \right\}, \qquad (2.1.4)$$

---

[5]As sketched in the previous chapter, asymptotic particle states are derived from the vacuum state of the theory.

which reduces to Eq. (2.1.3) for $J = 0$. It can be shown that, from the generating functional of a given theory, one can calculate all relevant n-point functions via

$$(-i)^n \frac{1}{Z[0]} \frac{\partial^n Z}{\partial J(x_1) \dots \partial J(x_n)} \bigg|_{J=0} = \langle 0 | T \{\phi(x_1) \dots \phi(x_n)\} | 0 \rangle . \qquad (2.1.5)$$

Let us now consider a UV theory which contains a light field φ of mass m_φ and a heavy degree of freedom ϕ with mass M_ϕ, such that $M_\phi \gg m_\varphi$. At energies below the mass threshold of the heavy particle ($E \ll M_\phi$), this particle decouples and the low-energy behaviour of the theory is described by an EFT Lagrangian containing only the light state φ [27]. The corresponding effective action is then defined by the following relation between the generating functionals of the UV and effective theories

$$\int \mathcal{D}\varphi \exp\left\{ i \int d^4x \mathcal{L}_{\text{eff}}[\varphi] \right\} = \int \mathcal{D}\varphi \mathcal{D}\phi \exp\left\{ i \int d^4x \mathcal{L}_{\text{UV}}[\varphi, \phi] \right\} , \qquad (2.1.6)$$

where the EFT Lagrangian only contains the light state of the theory φ, and we have fully integrated out (to all orders) the heavy field ϕ.

The complete effective theory is obtained from the full integration of the heavy field ϕ in Eq. (2.1.6). The leading order (LO) of the EFT is provided by the classical limit. In order to do so, we have to recover the Planck constant $\hbar$ in the expression for $\mathcal{Z}$. Again, for a single field ϕ

$$\mathcal{Z}[0] = \int \mathcal{D}\phi \exp\left\{ \frac{i}{\hbar} S[\phi] \right\} , \qquad (2.1.7)$$

such that taking the classical limit $\hbar \to 0$ entails that the integral above is dominated by the field configuration ϕ for which $S[\phi]$ has an extremum. This is indeed the condition that brought us to the Euler-Lagrange equations as explained in the previous chapter. Accordingly, the field configurations that take $S[\phi]$ far from its minimum, lead to integrate over phases oscillating infinitely fast, that in average contributes zero, and the remaining main contribution corresponds to the classical solution of the EOM. This corresponds to the so-called method of steepest descent, for which one computes the EOM of the heavy field — to be integrated away — from the UV action, perform an expansion over its (large) mass and then obtain some substituting rules for this field in terms of the light degrees of freedom. Such procedure provides us with the integration of a heavy field at tree level, i.e. the leading order of the effective Lagrangian. However, as stated above, the complete effective theory is retrieved only by performing the full integration of the heavy field from the generating functional as presented in Eq. (2.1.6).

The information on the dynamics of the UV theory is transferred into the Wilson coefficients $C_i^{(d)}$ ($d > 4$) of the EFT Lagrangian, e.g. the coupling constants of the higher-energy theory, while the Λ parameter receives contributions from the masses of the heavy states (see Eq. (2.1.1)). The infrared dynamics are then absorbed into the matrix elements of the EFT operators $\langle f | \mathcal{O}_i^{(d)} | i \rangle$ ($d > 4$) [28]. With this in mind, the EFT Lagrangian is better described by

$$\mathcal{L}_{\text{EFT}} = \sum_{d=2}^{\infty} \left(\sum_i \frac{C_i^{(d)}(\mu)}{\Lambda^{d-4}} \mathcal{O}_i^{(d)}(\mu) \right) . \qquad (2.1.8)$$

where we have suitably expressed the EFT Lagrangian in terms of the renormalized operators $\mathcal{O}_i^{(d)}(\mu)$ and Wilson coefficients $C_i^{(d)}(\mu)$, for which the characteristic energy scale μ of the process under study is as well used as the renormalization scale (see Section 2.5.3). From Eq. (2.1.8), we may notice that, as stated by the decoupling theorem [27], the couplings and fields of the renormalizable part of the EFT Lagrangian with $d = 4$, do indeed receive information from the high-energy physics via the renormalization procedure. This is for instance how GUT and SUSY theories modify the running of the SM couplings to reach their convergence at high-energy scales.

The previously described procedure is known as the top-down approach: we start from a renormalizable high-energy theory and, by integrating away the heavy degrees of freedom, we obtain a set of correlated local operators built out of the remaining light states, which we can identify as the EFT non-renormalizable operators. The corresponding identification between the parameters of the UV theory and the Wilson coefficients as well as the masses of the heavy states and the characteristic high-energy scale of the EFT Λ, goes under the name of *matching*. For instance, performing the path integral over a heavy degree of freedom as in Eq. (2.1.6), is indeed a way of matching. Other matching mechanisms are extensively described in Ref. [26]. Furthermore, note that in general, after integrating away the heavy degrees of freedom in a UV theory, we may end up with a subset of redundant operators. However, in Refs. [29] and [30], it was shown that via the classical equations of motion of the light fields, any effective Lagrangian can be reduced to a canonical form consisting of a smaller set of independent operators that respect the symmetries of the theory and are unrelated by the EOM.

The total integration of a heavy field in the UV theory provides an infinite tower of local operators as shown in Eq. (2.1.8). However, we have already seen that when making use of EFTs, we do not have to consider the infinite tower of operators to compute physical observables, in fact we do truncate that sum to a desired accuracy in the calculation assuming an error of $\mathcal{O}\left((E/\Lambda)^{n-4}\right)$. Likewise, in the integration of a heavy state, since at low energies fluctuations around its classical configuration are highly suppressed due to its large mass, we can approximate the field by its classical equations of motion. Accordingly, performing a Taylor expansion over the inverse of its (large) mass, we obtain the series of local operators of the EFT in Eq. (2.1.8). The higher-order terms in the mass expansion are then the responsibles for the higher-dimensional terms in the EFT Lagrangian. For instance, identifying the heavy field with its classical equation of motion corresponds to taking the steepest descent approximation in the path integral. Nonetheless, as seen above, in order to perform the integration at all orders of the heavy field, we should compute the path integral of Eq. (2.1.6) exactly.

2.2   Phenomenological Lagrangians

In the previous section we presented the general principles of the effective field theory formalism. Now, we will particularize to a subset of EFTs, namely those stemming from strongly-coupled higher-energy theories displaying as well a pattern

of spontaneous symmetry breaking. More concretely, we will study the effective field theory of QCD at low energies: Chiral Perturbation Theory (χPT) [31–33].

2.2.1 The linear sigma model

The need of an EFT to describe the long-distance phenomena of QCD arises from the non-perturbative character of the strong interactions at energies $E \lesssim 2.5$ GeV. The renormalization group equations for the strong coupling shows that α_s grows as the energy decreases. Eventually α_s gets large enough such that perturbation theory — based on the expansion over this coupling constant — fails to provide the right results. Furthermore, also as a consequence of the running of α_s, at low energies the QCD interactions become so strong (hence the name of strong interactions) that the relevant degrees of freedom we observe phenomenologically are no longer quarks and gluons but the combinations of those in terms of mesons and baryons, i.e. hadrons.

Accordingly, one may be tempted to find a theory that contains the hadronic relevant DOF describing the strong interactions at low energies, and for which we may apply the perturbative program, i.e. a dual theory of QCD at low energies. A first step on this enterprise was taken by Weinberg, who tried to obtain a (phenomenological) Lagrangian to ease the work on the computation of pion matrix elements [34] — which involved at that time the current algebra formalism. He started with the linear sigma model, where the pion is found in a multiplet of four real scalar fields $\Phi(x)^T \equiv (\vec{\pi}(x), \sigma(x))$. Its dynamics is described by the Lagrangian

$$\mathcal{L}_\sigma = \frac{1}{2}\partial_\mu \Phi^T \partial^\mu \Phi - \frac{\lambda}{4}\left(\Phi^T \Phi - v^2\right)^2 , \qquad (2.2.9)$$

with λ and v constants of the potential. Note that $\mathcal{L}_\sigma$ is invariant under global SO(4) rotations acting on the components of Φ.

Let us now make a change of field variables from the four vector Φ to the 2×2 matrix $\Sigma(x) \equiv \sigma(x)I_2 + i\vec{\tau}\vec{\pi}(x)$, where I_2 is the 2×2 identity matrix and $\vec{\tau}$ the three Pauli matrices. Under this change of variables the Lagrangian of Eq. (2.2.9) looks like

$$\mathcal{L}_\sigma = \frac{1}{4}\langle \partial_\mu \Sigma^\dagger \partial^\mu \Sigma \rangle - \frac{\lambda}{16}\left(\langle \Sigma^\dagger \Sigma \rangle - 2v^2\right)^2 , \qquad (2.2.10)$$

where $\langle A \rangle$ denotes the trace of the matrix A in the flavor space. Now $\mathcal{L}_\sigma$ is invariant under global transformations of the group $G \equiv \text{SU(2)}_\text{L} \times \text{SU(2)}_\text{R}$, such that[6]

$$\Sigma \xrightarrow{G} g_\text{R}\Sigma g_\text{L}^\dagger , \qquad g_\text{L}, g_\text{R} \in \text{SU(2)}_\text{L,R} . \qquad (2.2.11)$$

Then, we have two different scenarios depending on the sign of v^2,

1. $v^2 < 0$: the symmetry is realized à la Wigner-Weyl. The potential has one minimum that gives the vacuum of the theory as

$$\langle 0|\Sigma|0\rangle = 0 \qquad \left(\langle 0|\sigma|0\rangle = 0, \langle 0|\vec{\pi}|0\rangle = 0\right) , \qquad (2.2.12)$$

---

[6]Since the physical content of the two Lagrangian notations is necessarily the same, the change of field variables shows the equivalence between the SO(4) and $\text{SU(2)}_\text{L} \times \text{SU(2)}_\text{R}$ groups.

and the theory contains four degenerate states with mass $m = -\lambda v^2$. Since the vacuum is the trivial zero point in field space, it is invariant under the symmetries of the Lagrangian.

2. $v^2 > 0$: the potential has a continuous set of minima for all field configurations satisfying $\langle \Sigma^\dagger \Sigma \rangle = 2v^2$. Accordingly, the vacuum is given by

$$\langle 0|\Sigma|0\rangle = vI_2 \qquad \left(\langle 0|\sigma|0\rangle = v, \langle 0|\vec{\pi}|0\rangle = 0\right), \qquad (2.2.13)$$

which remains invariant only under a subgroup H of the symmetry group of the Lagrangian G, namely those transformations[7] that satisfy $g_{\mathrm{L}} = g_{\mathrm{R}}$: $H \equiv \mathrm{SU(2)}_{L+R}$. This second case suffers then from the following pattern of spontaneous symmetry breaking

$$\mathrm{SU(2)}_{\mathrm{L}} \times \mathrm{SU(2)}_{\mathrm{R}} \longrightarrow \mathrm{SU(2)}_{\mathrm{L+R}}. \qquad (2.2.14)$$

We now focus on the second scenario above. Due to the Nambu-Goldstone theorem [15, 16], the SSB of Eq. (2.2.14) has associated three massless fields, i.e. the same number as generators are broken in the SSB procedure. The quantum numbers of these fields follow from those of the broken generators as well, in this case the axial $A = L - R$ generators of G. With this in mind, we can do another change of variables by taking the polar decomposition of the complex-valued function Σ (in the same sense as we did for the Higgs field in Eq (1.4.69) of Section 1.4.1), which is further motivated by the spherical shape of the potential of the theory,

$$\Sigma(x) = [v + S(x)]\, U(\vec{\phi}), \qquad U(\vec{\phi}) = \exp\left\{ i\frac{\vec{\tau}}{v}\vec{\phi}(x) \right\}. \qquad (2.2.15)$$

Above, $S(x)$ is a scalar field invariant under the symmetry group G and $U(\vec{\phi})$ is a function of the Nambu-Goldstone pseudoscalar fields $\vec{\phi}$, which has the same transformation properties under the chiral rotations G as Σ in Eq. (2.2.11). As a consequence, the fields $\vec{\phi}$ transform non-linearly, as the phase of chiral rotations.

The Lagrangian in therms of $S(x)$ and $U(\vec{\phi})$ takes now the form of

$$\mathcal{L}_\sigma = \frac{v^2}{4}\left(1 + \frac{S}{v}\right)^2 \langle \partial_\mu U^\dagger \partial^\mu U \rangle + \frac{1}{2}\left(\partial_\mu S \partial^\mu S - M^2 S^2\right) + \mathcal{O}(S^3). \qquad (2.2.16)$$

From the above Lagrangian we see that the potential is driven by the radial field $S(x)$, which describes a massive particle of $M^2 = 2\lambda v^2$. At sufficiently low energies, there exists an energy gap between the massless Goldstone bosons $\vec{\phi}$ and the massive field $S(x)$, such that the latter can be integrated out. The resulting Lagrangian then reduces to

$$\mathcal{L} = \frac{v^2}{4}\langle \partial_\mu U^\dagger \partial^\mu U \rangle + \mathcal{O}\left(\frac{1}{M^2}\right), \qquad (2.2.17)$$

which describes the low-energy dynamics of the pion fields — via an infinite number of interactions among the $\vec{\phi}$ fields due to the non-linear functional form of $U(\vec{\phi})$ — as Nambu-Goldstone bosons stemming from the SSB of the $\mathrm{SU(2)}_{\mathrm{L}} \times \mathrm{SU(2)}_{\mathrm{R}}$ chiral symmetry into $\mathrm{SU(2)}_{\mathrm{L+R}}$.

---

[7]Upon a transformation G acting over the vacuum state $\langle 0|\Sigma|0\rangle \xrightarrow{G} \langle 0|g_{\mathrm{R}}\Sigma g_{\mathrm{L}}^\dagger|0\rangle = g_{\mathrm{R}}\langle 0|\Sigma|0\rangle g_{\mathrm{L}}^\dagger = vg_{\mathrm{R}}I_2 g_{\mathrm{L}}^\dagger \neq vI_2$.

2.2.2   Massless QCD and its symmetries

In Ref. [23], Weinberg tells how Julian Schwinger suggested him that a similar phenomenological Lagrangian as in Eq. (2.2.17), may be constructed without passing by the linear sigma model, but just assuming from the beginning non-linear transformation for pion fields and the symmetries of the higher-energy underlying theory, i.e. in a similar way as we proceeded to derive the EFT Lagrangian in Eq. (2.1.1). Therefore, in order to obtain the proper EFT of QCD we should study its symmetries, understand how the relevant degrees of freedom at low energies arise from them and which is their best characterization.

Let us start recalling the massless QCD Lagrangian

$$\mathcal{L}^0_{\text{QCD}} = -\frac{1}{4} G^{\mu\nu}_a G^a_{\mu\nu} + i \sum_q \bar{q}_L \gamma^\mu D_\mu q_L + i \sum_q \bar{q}_R \gamma^\mu D_\mu q_R \,, \qquad (2.2.18)$$

where the QCD covariant derivative D_μ is given in Eq. (1.2.30) and we are summing over the n quark flavors and three colors. In the Lagrangian above we have separated explicitly the left and right chiralities of the quark fields. Accordingly, the massless QCD Lagrangian is invariant under global $G \equiv \text{SU}(n)_\text{L} \times \text{SU}(n)_\text{R}$ transformations acting independently on left- and right-handed quarks in flavor space.

In Nature, we find three light quarks (u, d, s) for which we might expect the chiral symmetry G above to be fulfilled up to a good extent. However, when looking at the light hadronic spectrum, that should a priori inherit this symmetry, we find something else. On one hand, to consider a larger isospin global symmetry from SU(2) rotations in a two-flavor space $\begin{pmatrix} u & d \end{pmatrix}^T$ (see previous discussion on the symmetries of the linear sigma model), to SU(3) rotations in a three-flavor space $\begin{pmatrix} u & d & s \end{pmatrix}^T$, allows us to extend the description of the pion fields (within a triplet) to include the lightest pseudoscalar mesons in an octet $(\pi^0, \pi^+, \pi^-, K^0, K^+, \bar{K}^0, K^-, \eta_8) \equiv (\vec{\pi}, \vec{K}_{S=1}, \vec{K}_{S=-1}, \eta_8)$, where in the last step we have grouped in isospin vectors, mesons with similar masses and equal strange number S. The flavor symmetry SU(3) (also called isospin symmetry for SU(2)) in the quark flavor space then explains the corresponding quantum numbers of the resulting degenerated mesons within the octet (triplet) [7]. The realization of the chiral symmetry à la Wigner-Weyl — with the invariance of the Lagrangian as well as the vacuum, and thereby the states of the theory — would consequently entail the existence of two degenerated multiplets of opposite chiralities, i.e. $(\vec{\pi}, \vec{K}_{S=1}, \vec{K}_{S=-1}, \eta_8)_\text{L+R}$ and $(\vec{\pi}, \vec{K}_{S=1}, \vec{K}_{S=-1}, \eta_8)_\text{L-R}$ for $\text{SU}(3)_\text{L} \times \text{SU}(3)_\text{R}$. This is not though what we find phenomenologically, where only one multiplet with axial $L - R$ quantum numbers is present. On the other hand, we observe the existence of a large gap between the lightest octet of pseudoscalar mesons and the rest of the hadronic spectrum.

These empirical facts, in analogy with the previous discussion on the linear sigma model, point to the understanding of the previous octet as the Goldstone bosons originated by the dynamical symmetry breaking of the group G into its subgroup H:

$$G \equiv \text{SU}(3)_\text{L} \times \text{SU}(3)_\text{R} \longrightarrow H \equiv SU(3)_\text{L+R} \,. \qquad (2.2.19)$$

In a similar way as for the SSB driven by the Higgs field in the SM (see Section 1.4), in this case the chiral symmetry is broken (χSB) by the physical vacuum of QCD, which remains symmetric under $SU(3)_{L+R} \equiv SU(3)_V$. This means 8 broken generators, i.e. $n^2 - 1$ for $n = 3$. Accordingly, from the Nambu-Goldstone theorem, there exist eight Nambu-Goldstone bosons that share the quantum numbers of the broken generators of $SU(3)_{L-R} \equiv SU(3)_A$. This can be then identified with the aforementioned light octet of pseudoscalars, which in turn receive their different masses due to the (small) explicit breaking of the global chiral symmetry induced by the quark-mass terms.

2.3 Chiral perturbation theory

We have realized in the previous section that there exists a "sufficiently large" mass gap between the lightest states and the rest of the stable hadronic spectrum. Furthermore, we saw that at low energies the particles suffering the strong interactions, quarks and gluons, are confined into the relevant degrees of freedom at those energies, the hadrons. All these ingredients make of the EFT formalism a very suitable framework to study QCD at low energies. Following the discussion of Section 2.1.1, here we will build the most general EFT describing the interactions of the relevant DOFs: the octet of pseudoscalar bosons. In order to do that, we should first find the best parametrization of the Nambu-Goldstone modes as we did in the non-linear sigma model. As we showed for that model and shall see below, a suitable parametrization will ease both the physical understanding of the theory and the calculations.

2.3.1 Non-linear realization of Goldstone bosons and its EFT

We saw in Section 2.2.1 that Weinberg found — via the matrix $U(x)$ in the non-linear sigma model — a very convenient non-linear realization of the chiral symmetry $SU(2)_L \times SU(2)_R$ [35]. This was later generalized to arbitrary groups in Refs. [36] and [37]. Here, we will not delve much into this issue, but will just sketch why those non-linear realizations of the pseudoscalar fields present such a good parametrization (for a detailed explanation see Ref. [38]).

Let us first consider a generalized version of the linear sigma model with N real scalar fields: $\vec{\Phi}(x)^T \equiv (\varphi_1, \varphi_2, \ldots, \varphi_N)$. The model is described by the same Lagrangian of Eq. (2.2.9) and has thus a global $\mathcal{O}(N)$ symmetry described by the group G, under which $\vec{\Phi}(x)$ transforms as an $\mathcal{O}(N)$ vector. The potential of the theory presents a set of degenerated ground-states made of all field configurations satisfying $|\vec{\Phi}|^2 = \sum_i \varphi_i^2 = v^2$, i.e. a $N-1$-dimensional hypersphere in a N- dimensional space. By performing an appropriate $\mathcal{O}(N)$ rotation, one may assign to the vector field the following vacuum expectation value

$$\vec{\Phi}_0^T \equiv \langle 0|\vec{\Phi}|0\rangle^T = (0, \ldots, 0, v) \;, \qquad (2.3.20)$$

with $v \equiv \langle 0|\varphi_N|0\rangle$. The choice of the vev in Eq. (2.3.20) remains invariant under the subgroup $H \equiv \mathcal{O}(N-1)$ acting on the first $N-1$ field coordinates. The model

presents a $G \to H$ ($\mathcal{O}(N) \to \mathcal{O}(N-1)$) spontaneous symmetry breaking, with $N-1$ broken generators. Accordingly, there exists $N-1$ Nambu-Goldstone bosons that parametrize the rotations of the vev $\vec{\Phi}_0$ over the $N-1$ dimensional vacuum space.

Likewise we did for the linear sigma model, now we can perform a change to polar coordinates such that $\vec{\Phi}$ may be expressed as

$$\vec{\Phi}(x) = \left(1 + \frac{S(x)}{v}\right) U(x)\vec{\Phi}_0 \, , \qquad (2.3.21)$$

where again $S(x)$ is a radial excitation and the $N-1$ Nambu-Goldstone bosons $\vec{\phi}(x)$ are parametrized within the matrix $U(x)$ as follows

$$U(x) = \exp\left\{i\vec{T}\,\frac{\vec{\phi}(x)}{v}\right\} . \qquad (2.3.22)$$

Above, $\vec{T}$ are the broken $N-1$ generators that induce rotations over the $N-1$-dimensional hypersphere representing the vacuum field configurations and v is included to compensate the dimension of the real scalar fields $\vec{\phi}(x)$. Therefore, the matrix $U(x)$ provides a general parametrization of the $N-1$-dimensional vacuum space.

In group theoretical terms, the Nambu-Goldstone fields can be identified with the elements of the left coset space G/H [38]. For each field configuration $\vec{\phi}(x)$, we may choose any group element $\xi(\vec{\phi}) \in G$ as a coset representative. The crucial step connecting the idea of coset representative and the parametrization of the pseudoscalar fields, is the choice of the matrix $U(x)$ as the coset representative involving only the Nambu-Goldstone modes.

Now we particularize to the case of χPT, with the pattern of chiral symmetry breaking

$$G \equiv \mathrm{SU}(3)_\mathrm{L} \times \mathrm{SU}(3)_\mathrm{R} \xrightarrow{SSB} H \equiv \mathrm{SU}(3)_\mathrm{V} \, , \qquad (2.3.23)$$

leading to eight Nambu-Goldstone bosons $\vec{\phi}(x)$. As stated above, a general choice of coset representative gives $\xi(\vec{\phi}) \equiv \left(\xi_\mathrm{L}(\vec{\phi}), \xi_\mathrm{R}(\vec{\phi})\right) \in G$. In order to obtain the appropriate transformation laws of the matrix $U(x)$ under G, i.e. those of Eq. (2.2.11), we should define it in the following way [38]

$$U(\vec{\phi}) \equiv \xi_\mathrm{R}(\vec{\phi})\xi_\mathrm{L}^\dagger(\vec{\phi}) \xrightarrow{G} g_\mathrm{R}U(\vec{\phi})g_\mathrm{L}^\dagger. \qquad (2.3.24)$$

Finally, following the requirement that the coset representative involves only the broken axial generators — so that it pertains to the left coset G/H — we make the canonical choice $\xi_\mathrm{R}(\vec{\phi}) = \xi_\mathrm{L}^\dagger(\vec{\phi}) \equiv u(\vec{\phi})$. Consequently, the 3×3 unitary matrix

$$U(\vec{\phi}) = u(\vec{\phi})^2 = \exp\left\{i\sqrt{2}\frac{\Phi}{F}\right\} , \qquad \Phi(x) \equiv \frac{\vec{\lambda}}{\sqrt{2}}\vec{\phi}, \qquad (2.3.25)$$

entails a very convenient parametrization of the pseudoscalar bosons resulting of the pattern of SSB in Eq. (2.3.23). In Eq. (2.3.25) above, λ^i are the generators of

SU(3), i.e. the Gell-Mann matrices and F some characteristic scale to compensate the dimension of the (pseudo) scalar fields. Hence

$$\Phi = \begin{pmatrix} \frac{1}{\sqrt{2}}\pi^0 + \frac{1}{\sqrt{6}}\eta_8 & \pi^+ & K^+ \\ \pi^- & -\frac{1}{\sqrt{2}}\pi^0 + \frac{1}{\sqrt{6}}\eta_8 & K^0 \\ K^- & \bar{K}^0 & -\frac{2}{\sqrt{6}}\eta_8 \end{pmatrix}, \qquad (2.3.26)$$

that reduces to the upper-left 2×2 submatrix with only pion fields for two quark flavors, i.e. under the symmetry $\mathrm{SU(2)_L \times SU(2)_R}$. Again, although $U(\vec{\phi})$ transforms linearly under the chiral symmetry, the induced transformations on the fields $\vec{\phi}$ are non-lineal.

The studied pattern of symmetry breaking has provided us with a very convenient parametrization of the relevant DOFs of QCD at low energies. Now, in the spirit of Section 2.1.1, in order to build the most general EFT that describes the low-energy ($E \ll M_\rho$) dynamics of the octet of pseudoscalar bosons, we should consider all possible operators that can be made out of the $U(x)$ matrix satisfying as well the symmetries of QCD[8]. Furthermore, similarly to the role of $1/\Lambda^2$ in the Lagrangian of Eq. (2.1.1), our EFT also needs some small expansion parameter to ensure that higher effects can be safely neglected in the expansion. Since we are working at very low energies, we can make an expansion over the characteristic momenta involved in these interactions. In other words, we can organize the Lagrangian in terms of increasing number of derivatives of the fields.

With the premises above, the first order in the momentum expansion of the most general effective Lagrangian, built out of the non-linear realization $U(\vec{\phi})$ of the pseudoscalar Nambu-Goldstone fields, and satisfying Lorentz, parity and global chiral invariance is given by

$$\mathcal{L}_\chi^{(2)} = \frac{F^2}{4}\langle \partial_\mu U^\dagger \partial^\mu U \rangle, \qquad (2.3.27)$$

where the superindex (2) stands for the second order in the derivative expansion, since the first order is forbidden by parity conservation. The coupling F is the usual pion decay constant, which has dimensions of mass.

2.3.2 χPT Lagrangian

We aim at constructing a more realistic effective field theory of QCD at low energies. In order to do so, we should consider several missing pieces. First, we know that the remaining symmetry group $H = \mathrm{SU(3)_V}$ is explicitly broken in Nature by the non-zero quark masses. On top of that, electroweak interactions in the SM also drive chiral symmetry breaking explicitly, and we may expect in general new physics dynamics not respecting this global symmetry whatsoever. All in all, we should include all possible sources of explicit symmetry breaking in our formalism. This is achieved by attaching to the massless QCD Lagrangian of Eq. (2.2.18), the possible sources — in terms of their Lorentz structure — as external fields coupled to the

---

[8]Notice that the information on the pattern of symmetry breaking is already included in the non-linear characterization of the pseudoscalar Goldstone bosons within the matrix $U(x)$.

quark currents. Therefore, we add the auxiliary fields $v_\mu = v_\mu^i \lambda^i/2$, $a_\mu = a_\mu^i \lambda^i/2$, $s = s_i \lambda^i$, $p = p_i \lambda^i$ and $\bar{t}^{\mu\nu} = \bar{t}_{\mu\nu}^i \lambda^i/2$, which are Hermitian matrices in flavor space[9] [31–33]

$$\mathcal{L}_{\text{QCD}}^{\text{ext}} = \mathcal{L}_{\text{QCD}}^0 + \bar{q}\gamma_\mu \left(v^\mu + a^\mu \gamma_5\right) q - \bar{q}\left(s - ip\gamma_5\right) q + \bar{q}\sigma_{\mu\nu}\bar{t}^{\mu\nu} q\,. \tag{2.3.28}$$

For example, the explicit χSB induced by the quark masses is parametrized via the external sources above as

$$s = \mathcal{M}\,, \qquad \text{with} \qquad \mathcal{M} = \text{diag}(m_u, m_d, m_s)\,. \tag{2.3.29}$$

Likewise, within the SM, the v_μ field parametrizes the electromagnetic interactions; the charged- and neutral-current interactions, via the $W^\pm$ and Z bosons, can be incorporated into v_μ and a_μ, and the Higgs Yukawa interactions may be accounted by s as well. Accordingly, depending on the Lorentz structure of BSM dynamics, if coupled to quarks they will contribute via some of those external sources. Note though that these external sources are classical: they serve us as a tool to compute the quark current hadronizations (see below) in semileptonic decays, but cannot be used, for instance, to compute the contributions from a virtual photon, Z or $W^\pm$.

We may now gauge the chiral symmetry $G = \text{SU}(3)_{\text{L}} \times \text{SU}(3)_{\text{R}}$, by imposing the invariance of the Lagrangian in Eq. (2.3.28) under the corresponding transformations $(g_{\text{L}}, g_{\text{R}}) \in G$. By doing so, we promote the external sources to gauge fields that are enforced to transform as

$$\begin{aligned}
\ell_\mu \equiv v_\mu - a_\mu &\xrightarrow{G} g_{\text{L}}\ell_\mu g_{\text{L}}^\dagger + ig_{\text{L}}\partial_\mu g_{\text{L}}^\dagger \\
r_\mu \equiv v_\mu + a_\mu &\xrightarrow{G} g_{\text{R}}r_\mu g_{\text{R}}^\dagger + ig_{\text{R}}\partial_\mu g_{\text{R}}^\dagger \\
s + ip &\xrightarrow{G} g_{\text{R}}(s + ip)g_{\text{L}}^\dagger \\
t_{\mu\nu} &\xrightarrow{G} g_{\text{R}}t_{\mu\nu}g_{\text{L}}^\dagger
\end{aligned} \tag{2.3.30}$$

Thanks to the above gauging of the SU(3) chiral symmetry, we may now extend the effective Lagrangian of Eq. (2.3.27) to include arbitrary external sources. Thus, the first order in the derivative expansion of the most general effective Lagrangian — built out of the non-linear realization $U(\vec{\phi})$ of the pseudoscalar Nambu-Goldstone fields and (gauge) external field sources — and satisfying Lorentz, parity and local chiral invariance is given by

$$\mathcal{L}_\chi^{(2)} = \frac{F^2}{4}\langle D_\mu U^\dagger D^\mu U + U^\dagger \chi + \chi^\dagger U\rangle\,, \tag{2.3.31}$$

with D_μ the covariant derivative

$$D_\mu U = \partial_\mu U + iU\ell_\mu - ir_\mu U\,, \qquad D_\mu U^\dagger = \partial_\mu U^\dagger - i\ell_\mu U^\dagger + iU^\dagger r_\mu\,, \tag{2.3.32}$$

and

$$\chi = 2B_0(s + ip)\,, \tag{2.3.33}$$

___
[9] For practical purposes, in the tensor case we define the $t_{\mu\nu}$ and $t_{\mu\nu}^\dagger$ external fields by $\bar{\psi}\sigma_{\mu\nu}\bar{t}^{\mu\nu}\psi = \bar{\psi}_L\sigma^{\mu\nu}t_{\mu\nu}^\dagger\psi_R + \bar{\psi}_R\sigma^{\mu\nu}t_{\mu\nu}\psi_L$ [39].

where B_0 can be shown [38] to be related to the quark vacuum condensate via

$$\langle 0|\bar{q}^j q^i|0\rangle = -F^2 B_0 \delta^{ij}\,. \tag{2.3.34}$$

The gauge fields v_μ and a_μ can also appear through the field strength tensors:

$$F_L^{\mu\nu} = \partial^\mu \ell^\nu - \partial^\nu \ell^\mu - i[\ell^\mu, \ell^\nu]\,, \qquad F_R^{\mu\nu} = \partial^\mu r^\nu - \partial^\nu r^\mu - i[r^\mu, r^\nu]\,. \tag{2.3.35}$$

Several comments regarding the χPT Lagrangian are in order:

(i) As a consequence of the gauging procedure, the Lagrangian of Eq. (2.3.31) is now invariant under local chiral transformations. In the absence of external sources, this Lagrangian recovers the form of Eq. (2.3.27).

(ii) The addition of scalar and pseudoscalar sources entails another invariant chiral tensor χ in the Lagrangian, with another coupling constant B_0. This, as well as F, cannot be obtained by symmetry requirements alone, but should be retrieved from the non-perturbative behaviour of QCD. More concretely, B_0 is related to the quark condensate and F to the SSB mechanism itself.

(iii) By fixing the external source fields to a specific value, the chiral symmetry gets broken explicitly. The symmetry is broken in exactly the same way for both the effective Lagrangian in Eq. (2.3.31) and the fundamental Lagrangian of Eq. (2.3.28), what confirms the validity of the EFT chiral Lagrangian to describe QCD at low energies.

(iv) Operators involving tensor fields do not appear at the LO in the momentum expansion, but start at next-to-leading order (NLO) as we will see in next section.

Let us now show for completeness the full χPT Lagrangian extending that of Eq. (2.3.31). It reads

$$\mathcal{L}_{\chi\text{PT}} = \mathcal{L}_\chi^{(2)} + \sum_{i=1}^{16} L_i \mathcal{O}_i^{(4)} + \sum_{j=1}^{94} C_j \mathcal{O}_j^{(6)} + \dots\,, \tag{2.3.36}$$

where $\mathcal{L}_\chi^{(2)}$ is given in Eq. (2.3.31) and L_i and C_j receive the name of low-energy constants (LEC). Above, $\mathcal{O}_i^{(4)}$ are the operators of the Gasser and Leutwyler Lagrangian [32], where we have also included the tensor operators [39]; the $\mathcal{O}(p^6)$ Lagrangian has also been studied in Ref. [40]. We can distinguish several common features to any EFT Lagrangian:

- We have an infinite expansion which is ordered in this case in terms of the number of derivatives and mass terms present in the operators, labeled by the superscript in parentheses.

- In analogy to the EFT Lagrangian of Eq. (2.1.1), we may distinguish a higher-energy scale of χSB Λ_χ above which the EFT does not work anymore. This is usually expected to be of the order of the light-quark resonance mass $M_\rho \simeq M_\rho(770)$ — the next degree of freedom found in the hadronic spectrum. In

addition, χPT presents another characteristic energy scale, that of the NLO contributions via loop diagrams involving the pseudoscalar Goldstone bosons; it can be estimated from these amplitudes to be $\Lambda_\chi \sim 4\pi F \sim 1.2$ GeV [38]. This fact may show that contributions from resonances may be more important than higher-order terms in the perturbative expansion.

- The LECs of the theory $(L_i, C_j, \dots)$ cannot be extracted by symmetry requirements alone, since they contain the information from high-energy dynamics.

Finally, we have all the needed tools to match both theories and thus compute the low-energy realizations of the QCD currents: the hadronization of quark currents. This is provided by the generating functional of QCD $Z[v, a, s, p, t]$, in analogy to Eq. (2.1.6) via the path-integral formula

$$e^{i\mathcal{Z}[v,a,s,p,t]} = \int \mathcal{D}q \mathcal{D}\bar{q} \mathcal{D}G_\mu \exp\left\{i \int d^4x \mathcal{L}_{\mathrm{QCD}}\right\} = \int \mathcal{D}U \exp\left\{i \int d^4x \mathcal{L}_{\mathrm{eff}}\right\}.$$
$$(2.3.37)$$

However, even though the method presented below gives good results for the hadronization of the quark bilinears, we do not know how to solve explicitly the path integral. In the following section, within the more complete framework of Resonance Chiral Theory, we compute the hadronization of the quark currents of interest explicitly, which will be needed in the phenomenological analysis of Chapters 3, 4 and 6.

2.4   Resonance chiral theory

The Chiral Perturbation Theory framework allows us to describe the low-energy interactions of the lightest octet of pseudoscalar bosons in the hadronic spectrum. The success of χPT at low energies, lies in the existence of a sufficiently large energy gap between the mass of its DOFs and the next relevant energy scale, gap that is in turn explained by the SSB of the chiral symmetry. However, as already pointed out in the previous section, this EFT is only valid up to energies much below the mass of the lightest resonance $\rho(770)$. The energy region above $M_\rho \simeq 775$ MeV turns out to be populated by many hadronic resonances whose dynamics are far to be perfectly understood. This for instance, poses a problem to study QCD-involved physical processes taking place at those energies, e.g. hadronic tau decays, with a characteristic energy scale of the mass of the decaying particle $m_\tau \simeq 1.78$ GeV; or any decay of any possible BSM particle with a mass lying in this energy region, for example heavy extra neutrinos in neutrino-mass generating models. Both specified cases before are addressed in this thesis in Chapters 3 and 6 respectively, and consequently, we should understand correctly how to deal with this non-perturbative QCD regime. In the literature there exists several approaches to address this issue. For instance, one can just compute the relevant Green functions of the quark currents needed in those observables, without specifying any Lagrangian at all. Lattice gauge theory stands as another good candidate. In this thesis though, we follow the EFT-phenomenological approach of Resonance Chiral Theory (RχT), which is presented in this section. We first explain the basic concepts underlying its construction,

2.4.1 Basics of RχT

In contrast to the situation within the χPT framework, the region from $E \sim M_\rho$ to the perturbative continuum of QCD $E \gtrsim 2.5$ GeV shows a very rich jungle of hadron resonances. The lack of a mass gap between those relevant DOFs and the perturbative energy regime where we can properly describe the dynamics of quarks and gluons, entails then a problem for the construction of an EFT at those energies, as we will see below. However, the RχT phenomenological framework based on the dynamics driven by effective field theories and the chiral symmetry of QCD has proved to be very fruitful to describe this intermediate energy region [41–43].

From its EFT inspiration of a dual theory of QCD at low energies, RχT is based on the limit of large number of colors (large-$N_{\rm C}$):

- In this limit, we enlarge the color symmetry of the SM SU(3) to SU($N_{\rm C}$) and take $N_{\rm C} \to \infty$. Then, we take the inverse of the number of colors $1/N_{\rm C}$ as a perturbative expansion parameter. Likewise, next-to-leading order corrections in the $1/N_{\rm C}$ expansion, involve loop calculations within the RχT framework.

- This was motivated by the results of Refs. [44, 45], where it was shown that QCD in the limit of $N_{\rm C} \to \infty$ shares similar features as for $N_{\rm C} = 3$. For instance, meson dynamics can be described by an effective Lagrangian in the $N_{\rm C} \to \infty$ limit.

- By construction, the large-$N_{\rm C}$ limit involves an infinite number of narrow hadronic states. However, in RχT we cut the spectrum to the lightest hadron multiplets which dominate the dynamics and remain in the large-$N_{\rm C}$ limit. Note that the dynamics of these extra hadronics states cannot be generated simply by loops of the light pseudoscalar mesons. Since the perturbative parameter is $1/N_{\rm C}$ loop contributions tend to zero, as opposed to resonance contributions that, by definition, remain in this limit.

Therefore, the Resonance Chiral Lagrangian is built out of the chiral symmetry of QCD, and extends the model-independent χPT scheme by adding to the theory the lightest fields of nonets of hadron resonances[10] of the type

$$J^{PC} : V(1^{--}), A(1^{++}, 1^{+-}), S(0^{++}), P(0^{-+}), T(2^{++}), \qquad (2.4.38)$$

where J is the total spin, P the parity and C the charge of the resonance. This Lagrangian $\mathcal{L}(U, V, A, S, P, T)$ describes as well the couplings of mesons resonances to the Nambu-Goldstone bosons via operators analogous to

$$\mathcal{O} \sim \langle R\chi(p^n) \rangle, \langle RR\chi(p^n) \rangle, \dots \qquad (2.4.39)$$

where R stands for a generic resonance field and $\chi(p^n)$ for a chiral structured tensor of order n in derivatives, which involves both the pseudoscalar Goldstone bosons and the external currents (2.3.30).

---

[10]Even though we have a perturbative expansion parameter $1/N_{\rm C}$, the RχT framework lacks an EFT expansion parameter that limits the number of operators involving resonance fields, in analogy to the role of momenta (derivatives) and masses in χPT or the mass parameter Λ in the general EFT of Eq. (2.1.1).

2.4.2   RχT Lagrangian

In order to construct $\mathcal{L}(U, V, A, S, P, T)$ we should study how the resonance fields transform under the chiral symmetry. Since the symmetry is broken by the vacuum, which remains invariant under the subgroup $H \equiv \mathrm{SU(3)_V}$, we are interested in resonances transforming as fundamental representations of H, i.e. octets or singlets under this symmetry. For a general resonance denoted as $R_8 = \vec{\lambda}\vec{R}/\sqrt{2}$ (octet) and R_1 (singlet), with λ^i again the Gell-Mann matrices, it transforms under G as

$$R_8 \xrightarrow{G} h R_8 h^\dagger \,, \qquad\qquad R_1 \xrightarrow{G} R_1 \,, \qquad\qquad (2.4.40)$$

with $h \in H$. Actually, in the large-N_C limit, both octets and singlets are degenerated in the chiral limit, and so we can collect them within a nonet

$$R \equiv R_8 + \frac{1}{\sqrt{3}} R_0 I_3 \,, \qquad\qquad (2.4.41)$$

with I_3 the 3×3 identity matrix. Following the gauging procedure of the chiral symmetry group G as in the previous section, we define a covariant derivative of the resonance field as

$$\nabla_\mu R_8 = \partial_\mu R + [\Gamma_\mu, R] \,, \qquad\qquad (2.4.42)$$

where the connection is given by

$$\Gamma_\mu = \frac{1}{2} \left\{ u^\dagger \left(\partial_\mu - i r_\mu \right) u + u \left(\partial_\mu - i \ell_\mu \right) u^\dagger \right\} \,, \qquad\qquad (2.4.43)$$

with ℓ_μ and r_μ the external currents defined in Eq. (2.3.30) and u the canonical choice of coset representative that defined the matrix $U(\vec{\phi})$ and is given in Eq. (2.3.25) as $U = u^2$.

In the previous section, our χPT Lagrangian of Eq. (2.3.31) was built out of the matrix $U(\vec{\phi})$ containing the Nambu-Goldstone modes, and the spurion external currents included both in the covariant derivative and χ. However, those terms do not transform under G in the same way as the resonances in Eq. (2.4.40). Therefore, in order to build invariant terms in the Lagrangian containing both the pseudoscalar fields and the external currents coupled to the resonance mesons, it is convenient to define out of the pseudoscalar fields, the following covariant quantities that transform as in Eq. (2.4.40):

$$\begin{aligned} u_\mu &\equiv i u^\dagger \left(D_\mu U \right) u^\dagger = u_\mu^\dagger \,, & \chi_\pm &\equiv u^\dagger \chi u^\dagger \pm u \chi^\dagger u \,, \\ f_\pm^{\mu\nu} &\equiv u F_\mathrm{L}^{\mu\nu} u^\dagger \pm u^\dagger F_\mathrm{R}^{\mu\nu} u \,, & t_\pm^{\mu\nu} &\equiv u^\dagger t^{\mu\nu} u^\dagger \pm u\, t^{\mu\nu\,\dagger} u \,. \end{aligned} \qquad (2.4.44)$$

A final remark before presenting the RχT Lagrangian is in order. Resonance Chiral Theory tries to be an interpolating representation between the high-energy QCD and the long-distance χPT frameworks. As such, it is possible to integrate out the new degrees of freedom introduced by the RχT formalism — keeping the chiral symmetry — and recover the local low-energy χPT Lagrangian. Qualitatively, at leading order the procedure is as follows. One departs from the solution of the resonance equation of motion

$$\left(\nabla^2 + M_R^2 \right) R = \chi_R \,, \qquad\qquad (2.4.45)$$

which can be expanded over the inverse of its (large) mass M_R in terms of the local chiral operator χ_R containing only light fields, such as

$$R = \frac{1}{M_R^2}\chi_R + \mathcal{O}\left(\frac{p^4}{M_R^4}\right). \tag{2.4.46}$$

Plugging the previous expression in the RχT Lagrangian defined below as $\mathcal{L}_{\mathrm{R}\chi\mathrm{T}}$, we arrive to the LO contributions of the resonance fields to the $\mathcal{O}(p^4)$ χPT Lagrangian. For instance, it was shown in Refs. [41] and [42] that the LECs of the $\mathcal{O}(p^4)$ χPT Lagrangian were saturated by the contribution of the resonances in the RχT Lagrangian upon its integration.

Finally, the relevant RχT Lagrangian is

$$\mathcal{L}_{\mathrm{R}\chi\mathrm{T}} = \mathcal{L}_{\mathrm{GB}} + \mathcal{L}_{\mathrm{S}} + \mathcal{L}_{\mathrm{P}} + \mathcal{L}_{\mathrm{V}} + \mathcal{L}_{\mathrm{T}}, \tag{2.4.47}$$

where

$$\mathcal{L}_{\mathrm{GB}} = \frac{F^2}{4}\langle u_\mu u^\mu + \chi_+ \rangle + \sum_{i=1}^{12} L_i^{\mathrm{SD}} O_i^{(4)} + \Lambda_1^{\mathrm{SD}}\langle t_+^{\mu\nu} f_{+\,\mu\nu}\rangle - i\,\Lambda_2^{\mathrm{SD}}\langle t_+^{\mu\nu} u_\mu u_\nu\rangle + \mathcal{O}(p^6), \tag{2.4.48}$$

is the chiral Lagrangian of Eq. (2.3.31) involving only the octet of pseudoscalar Goldstone fields and the external auxiliary fields, but given in terms of the covariant quantities defined in Eq. (2.4.44). The first term in Eq. (2.4.48) corresponds to the $\mathcal{O}(p^2)$ Lagrangian of χPT, while the higher-order operators have the same structure as those of the chiral Lagrangian, but with different couplings. The couplings in Eq. (2.4.48) (of $\mathcal{O}(p^n)$ for $n > 2$) labeled "SD" do not have contributions that could be obtained upon integration of the resonance fields in $\mathcal{L}_{\mathrm{R}\chi\mathrm{T}}$ — since the latter are already explicit in the theory — and are, a priori, unknown. In this way, double counting is avoided. In other words, those couplings are the part of the χPT LECs in Eq. (2.3.36) that cannot be recovered upon integration of the resonance fields, but receive information directly from the short-distance QCD dynamics. As a consequence, they may be retrieved via the implementation of QCD short-distance constraints (see below). Above, $O_i^{(4)}$ are the operators of the Gasser and Leutwyler Lagrangian [32] and the tensor-involved operators have been recalled from Ref. [39]. The resonance terms [41,46,47] are[11] of the type $\langle R\chi(p^2)\rangle$ (see Eq. (2.4.39)), including their kinetic terms,

$$\begin{aligned}
\mathcal{L}_{\mathrm{S}} &= \frac{1}{2}\langle \nabla^\mu S \nabla_\mu S - M_S^2 S^2 \rangle + \langle S\chi_S\rangle, \\
\mathcal{L}_{\mathrm{P}} &= \frac{1}{2}\langle \nabla^\mu P \nabla_\mu P - M_P^2 P^2 \rangle + \langle P\chi_P\rangle, \\
\mathcal{L}_{\mathrm{V}} &= -\frac{1}{2}\langle \nabla^\lambda V_{\lambda\mu}\nabla_\nu V^{\nu\mu} - \frac{M_V^2}{2}V_{\mu\nu}V^{\mu\nu}\rangle + \langle V_{\mu\nu}\chi_V^{\mu\nu}\rangle, \\
\mathcal{L}_{\mathrm{T}} &= -\frac{1}{2}\langle T_{\mu\nu}D_T^{\mu\nu,\rho\sigma}T_{\rho\sigma}\rangle + \langle T_{\mu\nu}\chi_T^{\mu\nu}\rangle,
\end{aligned} \tag{2.4.49}$$

---

[11]We use the antisymmetric representation for spin-1 fields [41]. In this realization, there is no mixing of axial-vector resonances and pseudoscalar fields.

where $D_T^{\mu\nu,\rho\sigma}$ is given in Appendix A of Ref. [46]. Here, the interaction is provided by the following $\mathcal{O}(p^2)$ chiral tensors:

$$
\begin{aligned}
\chi_S &= c_d\, u_\mu\, u^\mu \,+\, c_m\, \chi_+\,, \\
\chi_P &= i\, d_m\, \chi_-\,, \\
\chi_V^{\mu\nu} &= \frac{F_V}{2\sqrt{2}}\, f_+^{\mu\nu} \,+\, i\, \frac{G_V}{\sqrt{2}}\, u^\mu\, u^\nu \,+\, T_V\, t_+^{\mu\nu}\,, \\
\chi_T^{\mu\nu} &= g_T\, \{\, u^\mu, u^\nu\,\} \,+\, \beta\, g^{\mu\nu}\, u^\alpha\, u_\alpha \,+\, \gamma\, g^{\mu\nu}\, \chi_+\,.
\end{aligned}
\tag{2.4.50}
$$

As it is well known, the identification of those multiplets with the experimentally determined resonances in the PDG [48] is relatively clear in all cases except for the scalars; see Ref. [49] and references therein. We provide the corresponding identifications in Appendix A. Let us just recall that we are including only those resonances that remain in the $N_{\mathrm{C}} \to \infty$ limit.

2.4.3 Hadronization of quark bilinears

Let us now present the practical implementation of the RχT framework. In practice, we have typically to compute the amplitude of a desired process, which will be driven by light-quark bilinears. However, at low energies the final and intermediate states are not quarks or gluons, but the hadrons that we have studied. Therefore, we need to hadronize those quark bilinears into the relevant DOFs. This is indeed a matching procedure between the short-distance theory QCD and the low-energy EFT description given by RχT. The matching is achieved by equating both generating functionals given by the path-integral formulae

$$
\int \mathcal{D}q\mathcal{D}\bar{q}\mathcal{D}G_\mu \exp\left\{ i \int d^4x \mathcal{L}_{\mathrm{QCD}} \right\}
$$
$$
= \int \mathcal{D}U\mathcal{D}V\mathcal{D}A\mathcal{D}S\mathcal{D}P\mathcal{D}T \exp\left\{ i \int d^4x \mathcal{L}(U,V,A,S,P,T) \right\}.
\tag{2.4.51}
$$

On one hand, we identify the scalar, pseudoscalar, vector, axial-vector and tensor currents as:

$$
\begin{aligned}
S^i &= -\bar{q}\,\lambda^i\, q\,, & P^i &= \bar{q}\, i\gamma_5\,\lambda^i\, q\,, \\
V_\mu^i &= \bar{q}\,\gamma_\mu\frac{\lambda^i}{2}\, q\,, & A_\mu^i &= \bar{q}\,\gamma_\mu\gamma_5\frac{\lambda^i}{2}\, q\,, \\
T^{i\,\mu\nu} &= \bar{q}\,\sigma^{\mu\nu}\frac{\lambda^i}{2}\, q\,, & T_5^{i\,\mu\nu} &= \bar{q}\,\sigma^{\mu\nu}\gamma_5\frac{\lambda^i}{2}\, q\,,
\end{aligned}
\tag{2.4.52}
$$

where λ^i, $i = 0, \ldots, 8$ are the Gell-Mann matrices. The chiral currents are defined as is customary: $J_{\mathrm{L}}^i = (S^i - iP^i)/2$, $J_{\mathrm{R}}^i = (S^i + iP^i)/2$, $J_{\mathrm{L}}^{i\,\mu} = (V^{i\,\mu} - A^{i\,\mu})/2$, $J_{\mathrm{R}}^{i\,\mu} = (V^{i\,\mu} + A^{i\,\mu})/2$, $T_{\mathrm{L}}^{i\,\mu\nu} = (T^{i\,\mu\nu} - T_5^{i\,\mu\nu})/2$, $T_{\mathrm{R}}^{i\,\mu\nu} = (T^{i\,\mu\nu} + T_5^{i\,\mu\nu})/2$.

On the other hand, the identification of Eq. (2.4.51), allows us to carry out the hadronization of the quark bilinears via functional derivatives, with respect to the

external sources, of the RχT Lagrangian above. We thus obtain for the different Lorentz-structured currents

$$S^i = \frac{\partial \mathcal{L}_{\text{R}\chi\text{T}}}{\partial s^i}\bigg|_{j=0}, \qquad\qquad P^i = \frac{\partial \mathcal{L}_{\text{R}\chi\text{T}}}{\partial p^i}\bigg|_{j=0},$$

$$V^i_\mu = \frac{\partial \mathcal{L}_{\text{R}\chi\text{T}}}{\partial v^i_\mu}\bigg|_{j=0}, \qquad\qquad A^i_\mu = \frac{\partial \mathcal{L}_{\text{R}\chi\text{T}}}{\partial a^i_\mu}\bigg|_{j=0}, \qquad\qquad (2.4.53)$$

$$T^i_{\mu\nu} = \frac{\partial \mathcal{L}_{\text{R}\chi\text{T}}}{\partial (t^{i\dagger}_{\mu\nu} + t^i_{\mu\nu})}\bigg|_{j=0},$$

where the RχT Lagrangian is the one in Eq. (2.4.47). The "$j = 0$" notation indicates that after the derivatives are calculated, all external currents are set to zero. We obtain

$$S^i = -B_0 \langle \lambda^i \Phi^2 \rangle + 8\frac{B_0}{F^2} L_5^{\text{SD}} \langle \lambda^i \partial_\mu \Phi \partial^\mu \Phi \rangle + 4 B_0 c_m \langle \lambda^i S \rangle$$
$$+ 4 \frac{B_0}{F^2}\frac{d_m^2}{M_P^2} \left[2 \langle \lambda^i \Phi M_p \Phi \rangle + \langle \lambda^i \{ M_p, \Phi^2 \} \rangle \right] + 4 B_0 \gamma\, g^{\mu\nu} \langle \lambda^i T_{\mu\nu} \rangle,$$

$$P^i = \sqrt{2}\, B_0\, F \langle \lambda^i \Phi \rangle - 4\sqrt{2}\,\frac{B_0}{F}\frac{d_m^2}{M_P^2} \langle \lambda^i \{ M_p, \Phi \} \rangle,$$

$$V^i_\mu = \frac{i}{2} \langle \lambda^i \left[(\partial_\mu \Phi)\, \Phi - \Phi\, \partial_\mu \Phi \right] \rangle - \frac{F_V}{\sqrt{2}} \langle \lambda^i \partial^\nu V_{\nu\mu} \rangle,$$

$$A^i_\mu = -\frac{F}{\sqrt{2}} \langle \lambda^i \partial_\mu \Phi \rangle,$$

$$T^i_{\mu\nu} = -i\frac{\Lambda_2^{\text{SD}}}{2\,F^2} \langle \lambda^i \left[(\partial_\mu \Phi)\, \partial_\nu \Phi - (\partial_\nu \Phi)\, \partial_\mu \Phi \right] \rangle + \frac{T_V}{2} \langle \lambda^i V_{\mu\nu} \rangle,$$

$$(2.4.54)$$

with Φ being the octet of Goldstone fields, and

$$M_p = \begin{pmatrix} m_\pi^2 & & \\ & m_\pi^2 & \\ & & 2m_K^2 - m_\pi^2 \end{pmatrix}. \qquad\qquad (2.4.55)$$

These are not the final results for the hadronization of the quark bilinears. The resonance chiral Lagrangian provides additional interactions that allow to introduce resonance contributions to the currents above. For example, if we were interested in the hadronization of a vector quark current into two pseudoscalars $P_1 P_2$, besides the direct contribution from the first term on the r.h.s. of the vector current V^i_μ in Eq. (2.4.54), within the RχT framework we would have to consider as well the hadronization via the second term $(T_V/2\langle \lambda^i V_{\mu\nu}\rangle)$ into a vector resonance, and its subsequent decay into the pair $P_1 P_2$ as given by $\mathcal{L}_V$ in Eq. (2.4.49).

2.4.4 Short distance constraints

Apart from the L_i^{SD} couplings in $\mathcal{L}_{\text{GB}}$, we have several couplings involving the resonances, namely c_d, c_m, d_m, F_V, G_V, T_V, g_T, β and γ. Some of these couplings

could be fixed from the phenomenology: for instance, F_V could be determined from $\rho \to e^+ e^-$. However, the real strength of RχT resides in obtaining as much information on those couplings from the high-energy QCD structure as possible via the implementation of short-distance constraints [42, 50–52].

Most of this work has already been done [43, 46, 51]. We get

$$F_V\, G_V \;=\; F^2\,, \qquad\qquad 4\,c_d\, c_m \;=\; F^2\,,$$
$$\beta \;=\; -g_T\,, \qquad\qquad 8\,(c_m^2 - d_m^2) \;=\; F^2\,. \qquad (2.4.56)$$

The interacting term for the pseudoscalar resonance (proportional to d_m) from Eqs. (2.4.49) and (2.4.50) produces a mixing between the resonance and the pseudoscalar Goldstone bosons. We can avoid this mixing through a redefinition of the pseudoscalar resonance: $P \to P + i\,\frac{d_m}{M_P^2}\,\chi_-$. The d_m term in χ_P from Eq. (2.4.50) is canceled, but the local contribution that we have to consider is generated[12]:

$$\mathcal{L} \;=\; L_8^P\, O_8^{(4)} \,+\, L_{12}^P\, O_{12}^{(4)} \;=\; -\frac{d_m^2}{2M_P^2}\,\Big(O_8^{(4)} - 2\,O_{12}^{(4)} \Big) \;=\; -\frac{d_m^2}{2M_P^2}\,\langle \chi_-^2 \rangle\,. \quad (2.4.57)$$

We notice that our redefinition of the pseudoscalar resonance field implies that it is being integrated out from our Lagrangian. Accordingly, we recover the pseudoscalar resonance contributions to L_8 and L_{12} from Ref. [41].

We have noticed that in the hadronization of the scalar current the contribution of the spin-2 resonances spoils its high-energy behaviour [53]. To solve this problem, we fix

$$L_5^{\rm SD} \;=\; -\frac{2}{3}\,\frac{\beta\,\gamma}{M_T^2}\,, \qquad\qquad (2.4.58)$$

where M_T is the octet mass of the spin-2 resonances. In addition,

$$L_i^{\rm SD} \;=\; 0\,, \qquad i \neq 5\,. \qquad\qquad (2.4.59)$$

Furthermore, when using this framework to compute the hadronization of the quark currents present in hadronic τ decays in Chapter 3, in the hadronization of the tensor current (3.3.6), the $\Lambda_2^{\rm SD}$ coupling from Eq. (2.4.48) appears. There is no a priori knowledge on the short-distance component of this coupling. However, the same hadronized tensor current in Eq. (3.3.6) gives us an answer. Requiring the appropriate high energy behaviour of this current [53] we obtain

$$\Lambda_2^{\rm SD} \;=\; 0\,. \qquad\qquad (2.4.60)$$

In fact, we can also determine the vector-resonance contribution to the χPT coupling Λ_2, namely $\Lambda_2^{\rm R}$, upon its integration between the G_V and T_V terms from Eq. (2.4.50). We get

$$\Lambda_2^{\rm R} \;=\; \sqrt{2}\,\frac{T_V\, G_V}{M_V^2}\,. \qquad\qquad (2.4.61)$$

The value of Λ_2 has been determined in Ref. [54]: $\Lambda_2 = (11.1 \pm 0.4)\,{\rm MeV}$ (see also [55]). If we assume resonance saturation, we can, in fact, use this relation to

---

[12]The L_{12} χPT coupling corresponds to H_2 in the Gasser and Leutwyler Lagrangian [32].

get a value[13] for the coupling T_V:

$$T_V \approx 0.1147\,\mathrm{GeV}^2\,. \tag{2.4.62}$$

This gives $f_V^\perp \approx 0.148\,\mathrm{GeV}$ to be compared with the result from Ref. [47], $f_V^\perp(1\,\mathrm{GeV}) = 0.165 \pm 0.031\,\mathrm{GeV}$.

2.5 The Standard Model effective field theory: SMEFT

We have already motivated in the introduction of this chapter, why the SM is commonly seen as the low-energy realization of a more fundamental higher-energy theory. In other words, why the SM can be considered as the first terms in the expansion of a more general effective field theory provided by Eq. (2.1.1). In this section we present the SM effective field theory usually called SMEFT, focusing on the first two terms of the expansion, i.e. the full set of $d = 5$ and $d = 6$ operators. We will briefly recall under which conditions the SMEFT can really capture the infrared information of physics beyond the SM and will sketch as well the main steps to properly use this framework to analyze experimental data. Then, we will show the basic ideas to go to NLO and perform the renormalization of the SMEFT operators. Finally, the relevant parts for our work of the lower-energy realization of the SMEFT, for which the heavier particle spectrum in the SM is integrated out, i.e. the top, Higgs and weak bosons $W^\pm$ and Z, is presented. This EFT goes under the name of weak or low-energy EFT (WEFT or LEFT).

2.5.1 The SMEFT in the Warsaw basis

The SMEFT Lagrangian — following the discussion of Section 2.1 — is constructed out of the SM fields and incorporates the SM gauge symmetry $\mathrm{SU}(3)_\mathrm{C} \times \mathrm{SU}(2)_\mathrm{L} \times \mathrm{U}(1)_\mathrm{Y}$, before the spontaneous symmetry breaking has taken place. Therefore, it presents the usual SM Higgs field as a $\mathrm{SU}(2)_\mathrm{L}$ doublet. Due to the increasing suppression of operators with dimension greater than 4, the SMEFT Lagrangian can be organized by an expansion in the dimension of the operators. In analogy to Eq. (2.1.1), it reads

$$\mathcal{L}_{\mathrm{SMEFT}} = \mathcal{L}_{\mathrm{SM}}^{(4)} + \frac{1}{\Lambda}\sum_i C_i^{(5)}\mathcal{O}_i^{(5)} + \frac{1}{\Lambda^2}\sum_i C_i^{(6)}\mathcal{O}_i^{(6)} + \mathcal{O}\left(\frac{1}{\Lambda^3}\right)\,, \tag{2.5.63}$$

where $\mathcal{L}_{SM}^{(4)}$ is the usual renormalizable SM Lagrangian presented in Chapter 1; the Wilson coefficients $C_i^{(d)}$ contain the information on the couplings of the integrated heavy degrees of freedom; the low-energy information is encoded in terms of the "light" SM fields in the operators $\mathcal{O}_i^{(d)}$; Λ parametrizes the characteristic high-energy scale of the fundamental theory, and is usually identified with the mass of the lightest integrated heavy particle because, although it receives in general information from the whole higher-energy spectrum, at low energies the dominant contribution stems from the lightest heavy state, not included in the Lagrangian.

---

[13]For numerical inputs, we use the values from Appendix B.

The SMEFT framework described by the Lagrangian (2.5.63), can properly account for the IR limit of a wide range of BSM models given that

1. The heavier degrees of freedom of the BSM theory reside at scales larger than either the electroweak scale ($\Lambda \gg v$) or the characteristic energy scale of the process under study, e.g. in experiments at the LHC involving energies $E > v$ the requirement thus becomes $\Lambda \gg E$. In the most general case, the Lagrangian that applies is (2.5.63) in the form of (2.1.8);

2. There are not light hidden states yet to be found and accordingly, all the light fields are accounted for in $\mathcal{L}_{\text{SMEFT}}$. Otherwise, in the presence of other light fields as extra sterile neutrinos, axion-like particles or possible dark matter candidates, new operators would have to be considered in the EFT description of the new SM framework including those light states.

Should those two points be satisfied, the SMEFT thus provides a consistent framework to systematically combine low- and high-energy experimental data for the program of narrowing down the origin of new physics. Assuming the validity of the two requirements above, most of the work of this thesis is framed within that program. In the following chapters we will work with $d = 6$ operators at most, so we present here the whole basis of independent operators $\mathcal{O}_i^{(5)}$ and $\mathcal{O}_i^{(6)}$. Their independence stems from the fact that no linear combination of them and their Hermitian conjugates can be removed by use of the equations of motion. We follow the notation of Ref. [56] up to trivial modifications.

The basis of $d = 5$ operators $\mathcal{O}_i^{(5)}$ is quite reduced, it comprises just one single type of operator after imposing the SM gauge symmetries, the so-called Weinberg neutrino mass operator [57]

$$\mathcal{O}_{\nu\nu}^{pr} = \epsilon_{jk}\epsilon_{mn}\varphi^j \varphi^m \left(L_p^k\right)^T C L_r^n + \text{h.c.} \equiv \left(\tilde{\varphi}^\dagger L_p\right)^T C \left(\tilde{\varphi}^\dagger L_r\right) + \text{h.c.}, \qquad (2.5.64)$$

where j, k, m, n are isospin indices, p, r are flavor indices which label as well the different operators and Wilson coefficients $C_{\nu\nu}^{pr}$ and $C = i\gamma^2\gamma^0$ is the charge conjugation matrix. In the last step above we have used the relation $\tilde{\varphi}^j = \epsilon_{jk}\left(\varphi^k\right)^*$, with ϵ_{jk} being the totally antisymmetric tensor and $\epsilon_{12} = +1$. Operators of odd dimension are the only ones that violate lepton number, as such $\mathcal{O}_{\nu\nu}^{pr}$, after the electroweak symmetry breaking has taken place and the Higgs has been assigned a vev, is the first operator generating neutrino masses and mixing.

A first counting of $d = 6$ operators was conducted in Ref. [58], the authors arrived at a result of 80 operators. However, some of these operators were redundant, in the sense that they could be related by means of the SM equations of motion and field redefinitions. The complete independent basis of $d = 6$ operators of the SMEFT was given for the first time in Ref. [56] and is now known as the Warsaw basis[14]. Forgetting about flavor combinations, it contains a total of 59 independent operators if baryon number (B) conservation is imposed, and 64 otherwise. These are presented in Tables 2.1 and 2.2 following the same conventions as in Chapter 1 and same notation as in Ref. [56], up to apparent changes like for left $SU(2)_L$ doublets $l(q) \to L(Q)$. There, operators are classified depending on their field content

---

[14]For the complete list of $d = 7$ operators see Ref. [59].

and chiralities into 10 classes (11 if B violation is included): 3 classes of (hermitian) bosonic operators $X^3, X^2\varphi^2, \varphi^6$ and $\varphi^4 D^2$, 3 of mixed fermion-bosonic operators $\psi^2\varphi^3, \psi^2 X\varphi, \psi^2\varphi^2 D$ and 4 (5) of pure fermionic operators labeled by their chiralities as $(\bar{L}L)(\bar{L}L), (\bar{R}R)(\bar{R}R), (\bar{L}L)(\bar{R}R), (\bar{L}R)(\bar{R}L)$ and $(\bar{L}R)(\bar{L}R)$ (B-violating). The Hermitian conjugate should be added as well for operators involving fermions. The Wilson coefficients share the same notation with the associated operators, just substituting $\mathcal{O} \to C$. Furthermore, in full generality, the WCs are matrices in flavor space. Hence, even though we have simplified the notation in Tables 2.1 and 2.2, the label of the operators as well as their WCs should include flavor indices, e.g. $C_{eB}^{pr}\mathcal{O}_{eB}^{pr}$ or $C_{LeQu}^{(3)\,prst}\mathcal{O}_{LeQu}^{(3)\,prst}$.

2.5.2 Good practices in the SMEFT

We have extended the SM Lagrangian presented in Chapter 1 by local $d = 5$ and $d = 6$ operators. This has some implications in the computation of observables. For instance, performing analyses within the SMEFT takes yet several extra steps which involve [60]:

- the choice of a flavor assumption on the operators,

- the normalization and diagonalization of all kinetic terms,

- the choice of an input parameter scheme,

for which we will focus on the relevant operators used in this thesis: $d = 6$ operators.

Regarding flavor assumptions, we have introduced 59 operators defined with free flavor indices. This means a total of 2499 extra real parameters, what clearly reduces the applicability of the general framework, further when, for theoretical consistency, we should consider the full independent set of operators. However, in practice one works with reduced parameter sets, either because only a subset of operators contribute to the studied observables and the rest are assumed to be zero or by making well-motivated flavor symmetry assumptions, e.g. via the U(3)^5 symmetry on fermion flavor space, which reduces to 81 real parameters, or by assuming an alignment with the flavor structure of the SM, the so-called minimal flavor violation (MFV) SMEFT. We apply the EFT formalism in two chapters along the thesis. In Chapter 3 we merge both approaches: a restricted set of operators inducing the interested phenomena is considered and some flavor assumptions are made as well. In Chapter 5, we make no flavor assumptions, but we restrict our analysis to the operators involved in the studied processes.

The last two operations stated above, induce corrections stemming from $\mathcal{L}^{(6)}$ of $\mathcal{O}\left(C^{(6)}/\Lambda^2\right)$. When they are applied to the $d = 6$ operators themselves, these become of $\mathcal{O}\left(\left(C^{(6)}/\Lambda^2\right)^2\right)$ and can then be neglected since they contribute effectively to $\mathcal{L}^{(8)}$. Accordingly, working up to $d = 6$, we should consider the proper normalization and diagonalization of kinetic terms as well as the effects of a given choice of input parameter scheme in the $d = 4$ Standard Model Lagrangian.

The extension of the SM into the SMEFT given in Eq. (2.5.63), spoils, after the spontaneous symmetry breaking takes place, the behaviour of the kinetic terms of

$(\bar{L}L)(\bar{L}L)$		$(\bar{R}R)(\bar{R}R)$		$(\bar{L}L)(\bar{R}R)$	
$\mathcal{O}_{LL}$	$(\bar{L}_p\gamma_\mu L_r)(\bar{L}_s\gamma^\mu L_t)$	$\mathcal{O}_{ee}$	$(\bar{e}_p\gamma_\mu e_r)(\bar{e}_s\gamma^\mu e_t)$	$\mathcal{O}_{Le}$	$(\bar{L}_p\gamma_\mu L_r)(\bar{e}_s\gamma^\mu e_t)$
$\mathcal{O}_{QQ}^{(1)}$	$(\bar{Q}_p\gamma_\mu Q_r)(\bar{Q}_s\gamma^\mu Q_t)$	$\mathcal{O}_{uu}$	$(\bar{u}_p\gamma_\mu u_r)(\bar{u}_s\gamma^\mu u_t)$	$\mathcal{O}_{Lu}$	$(\bar{L}_p\gamma_\mu L_r)(\bar{u}_s\gamma^\mu u_t)$
$\mathcal{O}_{QQ}^{(3)}$	$(\bar{Q}_p\gamma_\mu\tau^I Q_r)(\bar{Q}_s\gamma^\mu\tau^I Q_t)$	$\mathcal{O}_{dd}$	$(\bar{d}_p\gamma_\mu d_r)(\bar{d}_s\gamma^\mu d_t)$	$\mathcal{O}_{Ld}$	$(\bar{L}_p\gamma_\mu L_r)(\bar{d}_s\gamma^\mu d_t)$
$\mathcal{O}_{LQ}^{(1)}$	$(\bar{L}_p\gamma_\mu L_r)(\bar{Q}_s\gamma^\mu Q_t)$	$\mathcal{O}_{eu}$	$(\bar{e}_p\gamma_\mu e_r)(\bar{u}_s\gamma^\mu u_t)$	$\mathcal{O}_{Qe}$	$(\bar{Q}_p\gamma_\mu Q_r)(\bar{e}_s\gamma^\mu e_t)$
$\mathcal{O}_{LQ}^{(3)}$	$(\bar{L}_p\gamma_\mu\tau^I L_r)(\bar{Q}_s\gamma^\mu\tau^I Q_t)$	$\mathcal{O}_{ed}$	$(\bar{e}_p\gamma_\mu e_r)(\bar{d}_s\gamma^\mu d_t)$	$\mathcal{O}_{Qu}^{(1)}$	$(\bar{Q}_p\gamma_\mu Q_r)(\bar{u}_s\gamma^\mu u_t)$
		$\mathcal{O}_{ud}^{(1)}$	$(\bar{u}_p\gamma_\mu u_r)(\bar{d}_s\gamma^\mu d_t)$	$\mathcal{O}_{Qu}^{(8)}$	$(\bar{Q}_p\gamma_\mu T^A Q_r)(\bar{u}_s\gamma^\mu T^A u_t)$
		$\mathcal{O}_{ud}^{(8)}$	$(\bar{u}_p\gamma_\mu T^A u_r)(\bar{d}_s\gamma^\mu T^A d_t)$	$\mathcal{O}_{Qd}^{(1)}$	$(\bar{Q}_p\gamma_\mu Q_r)(\bar{d}_s\gamma^\mu d_t)$
				$\mathcal{O}_{Qd}^{(8)}$	$(\bar{Q}_p\gamma_\mu T^A Q_r)(\bar{d}_s\gamma^\mu T^A d_t)$

$(\bar{L}R)(\bar{R}L)$ and $(\bar{L}R)(\bar{L}R)$		B-violating	
$\mathcal{O}_{LedQ}$	$(\bar{L}_p^j e_r)(\bar{d}_s Q_t^j)$	$\mathcal{O}_{duQ}$	$\varepsilon^{\alpha\beta\gamma}\varepsilon_{jk}\,[(d_p^\alpha)^T C u_r^\beta]\,[(Q_s^{\gamma j})^T C L_t^k]$
$\mathcal{O}_{QuQd}^{(1)}$	$(\bar{Q}_p^j u_r)\varepsilon_{jk}(\bar{Q}_s^k d_t)$	$\mathcal{O}_{QQu}$	$\varepsilon^{\alpha\beta\gamma}\varepsilon_{jk}\,[(Q_p^{\alpha j})^T C Q_r^{\beta k}]\,[(u_s^\gamma)^T C e_t]$
$\mathcal{O}_{QuQd}^{(8)}$	$(\bar{Q}_p^j T^A u_r)\varepsilon_{jk}(\bar{Q}_s^k T^A d_t)$	$\mathcal{O}_{QQQ}^{(1)}$	$\varepsilon^{\alpha\beta\gamma}\varepsilon_{jk}\varepsilon_{mn}\,[(Q_p^{\alpha j})^T C Q_r^{\beta k}]\,[(Q_s^{\gamma m})^T C L_t^n]$
$\mathcal{O}_{LeQu}^{(1)}$	$(\bar{L}_p^j e_r)\varepsilon_{jk}(\bar{Q}_s^k u_t)$	$\mathcal{O}_{QQQ}^{(3)}$	$\varepsilon^{\alpha\beta\gamma}(\tau^I\varepsilon)_{jk}(\tau^I\varepsilon)_{mn}\,[(Q_p^{\alpha j})^T C Q_r^{\beta k}]\,[(Q_s^{\gamma m})^T C L_t^n]$
$\mathcal{O}_{LeQu}^{(3)}$	$(\bar{L}_p^j\sigma_{\mu\nu} e_r)\varepsilon_{jk}(\bar{Q}_s^k\sigma^{\mu\nu} u_t)$	$\mathcal{O}_{duu}$	$\varepsilon^{\alpha\beta\gamma}\,[(d_p^\alpha)^T C u_r^\beta]\,[(u_s^\gamma)^T C e_t]$

TABLE 2.1: Four-fermion operators.

gauge bosons and the Higgs itself. On one hand, the Higgs, G_μ^A, W_μ^I and B_μ kinetic terms receive contributions — in the unitary gauge (see Section. 1.4.2) — from $C_{\varphi\square}$ and $C_{\varphi D}$, $C_{\varphi G}$, $C_{\varphi W}$ and $C_{\varphi B}$ respectively. Moreover, the operator associated to $C_{\varphi WB}$ induce an extra mixing between the W_μ^I and B_μ fields. All in all, suitable

X^3		φ^6 and $\varphi^4 D^2$		$\psi^2\varphi^3$	
$\mathcal{O}_G$	$f^{ABC}G_\mu^{A\nu}G_\nu^{B\rho}G_\rho^{C\mu}$	$\mathcal{O}_\varphi$	$(\varphi^\dagger\varphi)^3$	$\mathcal{O}_{e\varphi}$	$(\varphi^\dagger\varphi)(\bar{L}_p e_r \varphi)$
$\mathcal{O}_{\widetilde{G}}$	$f^{ABC}\widetilde{G}_\mu^{A\nu}G_\nu^{B\rho}G_\rho^{C\mu}$	$\mathcal{O}_{\varphi\square}$	$(\varphi^\dagger\varphi)\square(\varphi^\dagger\varphi)$	$\mathcal{O}_{u\varphi}$	$(\varphi^\dagger\varphi)(\bar{Q}_p u_r \widetilde{\varphi})$
$\mathcal{O}_W$	$\varepsilon^{IJK}W_\mu^{I\nu}W_\nu^{J\rho}W_\rho^{K\mu}$	$\mathcal{O}_{\varphi D}$	$(\varphi^\dagger D^\mu\varphi)^\star(\varphi^\dagger D_\mu\varphi)$	$\mathcal{O}_{d\varphi}$	$(\varphi^\dagger\varphi)(\bar{Q}_p d_r \varphi)$
$\mathcal{O}_{\widetilde{W}}$	$\varepsilon^{IJK}\widetilde{W}_\mu^{I\nu}W_\nu^{J\rho}W_\rho^{K\mu}$				

$X^2\varphi^2$		$\psi^2 X\varphi$		$\psi^2\varphi^2 D$	
$\mathcal{O}_{\varphi G}$	$\varphi^\dagger\varphi\, G_{\mu\nu}^A G^{A\mu\nu}$	$\mathcal{O}_{eW}$	$(\bar{L}_p\sigma^{\mu\nu}e_r)\tau^I\varphi W_{\mu\nu}^I$	$\mathcal{O}_{\varphi L}^{(1)}$	$(\varphi^\dagger i\overleftrightarrow{D}_\mu\varphi)(\bar{L}_p\gamma^\mu L_r)$
$\mathcal{O}_{\varphi\widetilde{G}}$	$\varphi^\dagger\varphi\, \widetilde{G}_{\mu\nu}^A G^{A\mu\nu}$	$\mathcal{O}_{eB}$	$(\bar{L}_p\sigma^{\mu\nu}e_r)\varphi B_{\mu\nu}$	$\mathcal{O}_{\varphi L}^{(3)}$	$(\varphi^\dagger i\overleftrightarrow{D}_\mu^I\varphi)(\bar{L}_p\tau^I\gamma^\mu L_r)$
$\mathcal{O}_{\varphi W}$	$\varphi^\dagger\varphi\, W_{\mu\nu}^I W^{I\mu\nu}$	$\mathcal{O}_{uG}$	$(\bar{Q}_p\sigma^{\mu\nu}T^A u_r)\widetilde{\varphi}\, G_{\mu\nu}^A$	$\mathcal{O}_{\varphi e}$	$(\varphi^\dagger i\overleftrightarrow{D}_\mu\varphi)(\bar{e}_p\gamma^\mu e_r)$
$\mathcal{O}_{\varphi\widetilde{W}}$	$\varphi^\dagger\varphi\, \widetilde{W}_{\mu\nu}^I W^{I\mu\nu}$	$\mathcal{O}_{uW}$	$(\bar{Q}_p\sigma^{\mu\nu}u_r)\tau^I\widetilde{\varphi}\, W_{\mu\nu}^I$	$\mathcal{O}_{\varphi Q}^{(1)}$	$(\varphi^\dagger i\overleftrightarrow{D}_\mu\varphi)(\bar{Q}_p\gamma^\mu Q_r)$
$\mathcal{O}_{\varphi B}$	$\varphi^\dagger\varphi\, B_{\mu\nu} B^{\mu\nu}$	$\mathcal{O}_{uB}$	$(\bar{Q}_p\sigma^{\mu\nu}u_r)\widetilde{\varphi}\, B_{\mu\nu}$	$\mathcal{O}_{\varphi Q}^{(3)}$	$(\varphi^\dagger i\overleftrightarrow{D}_\mu^I\varphi)(\bar{Q}_p\tau^I\gamma^\mu Q_r)$
$\mathcal{O}_{\varphi\widetilde{B}}$	$\varphi^\dagger\varphi\, \widetilde{B}_{\mu\nu} B^{\mu\nu}$	$\mathcal{O}_{dG}$	$(\bar{Q}_p\sigma^{\mu\nu}T^A d_r)\varphi\, G_{\mu\nu}^A$	$\mathcal{O}_{\varphi u}$	$(\varphi^\dagger i\overleftrightarrow{D}_\mu\varphi)(\bar{u}_p\gamma^\mu u_r)$
$\mathcal{O}_{\varphi WB}$	$\varphi^\dagger\tau^I\varphi\, W_{\mu\nu}^I B^{\mu\nu}$	$\mathcal{O}_{dW}$	$(\bar{Q}_p\sigma^{\mu\nu}d_r)\tau^I\varphi\, W_{\mu\nu}^I$	$\mathcal{O}_{\varphi d}$	$(\varphi^\dagger i\overleftrightarrow{D}_\mu\varphi)(\bar{d}_p\gamma^\mu d_r)$
$\mathcal{O}_{\varphi\widetilde{W}B}$	$\varphi^\dagger\tau^I\varphi\, \widetilde{W}_{\mu\nu}^I B^{\mu\nu}$	$\mathcal{O}_{dB}$	$(\bar{Q}_p\sigma^{\mu\nu}d_r)\varphi\, B_{\mu\nu}$	$\mathcal{O}_{\varphi ud}$	$i(\widetilde{\varphi}^\dagger D_\mu\varphi)(\bar{u}_p\gamma^\mu d_r)$

TABLE 2.2: Dimension-six operators other than the four-fermion ones.

redefinitions of all these fields should be made to bring them into a canonical normalized form, which absorbs the extra WC dependencies generated by the $d = 6$ SMEFT operators into the kinetic terms. In this thesis, none of these operators are considered, they are then set to zero and the usual gauge bosons as well as the Higgs are assumed to be the canonically normalized fields, i.e. those providing properly normalized kinetic terms in the usual way.

The effects induced by the choice of an input parameter scheme within the SMEFT framework are a bit more subtle. From a general perspective, we start with a Lagrangian $\mathcal{L}_{\text{SM}}$ (for convenience we stick to the SM Lagrangian, but the following discussion applies to any Lagrangian formalism) containing a number of unknown parameters $(g, g', g_s, v, Y_f, \dots)$. This Lagrangian is used to compute physical observables as functions of those parameters (e.g. cross sections $\sigma(g, g', g_s, \dots)$). Upon a measurement of the former, the inverse process can be followed to extract values for the relevant parameters entering the calculation. More concretely, we make use of some input measurements (e.g. the electroweak m_Z, the measurement of the fine-structure constant α_{em} and the decay of $\mu \to e\nu_e\nu_\mu$, the Higgs-related masses of the Higgs and fermions among others) to extract numerical values of the associated Lagrangian parameters (e.g. the electroweak g, g', the Higgs-related v, λ and the Yukawas among others). These numbers can then be used within the same framework — via SM theoretical relations — to compute and obtain numerical predictions for other observables. Within the SM, this cyclic procedure entails a check of its input-output consistency. However, when the SM is extended into the SMEFT, the list of Lagrangian parameters increases considerably. Therefore, the original relations between the input measurements and the Lagrangian parameters

are not longer valid. Now, the physical observable of interest should be computed as a function of the SM parameters as well as the Wilson coefficients of the SMEFT. As before, the measurement of this observable allows us to express the parameters of the SM Lagrangian as functions of the experimental value and the WCs. Therefore, within the SMEFT, the SM parameters are shifted by the Wilson coefficients, with respect to the previously (only $d = 4$ operators) settled value given by the experimental input measurement.

Let us exemplify the above discussion by means of the usual determination of the Fermi constant G_F. This is customarily extracted from muon decay $\mu^- \to e^- \bar{\nu}_e \nu_\mu$, whose decay width at LO in the SM is given by

$$\Gamma_{\text{SM}} \left(\mu^- \to e^- \bar{\nu}_e \nu_\mu \right) = \frac{G_F^2 m_\mu^5}{192\pi^3} \,. \tag{2.5.65}$$

The value of the width comes from the experimental determination of the muon Lifetime τ_μ^{exp} via $\Gamma_\mu^{\text{exp}} = 1/\tau_\mu^{\text{exp}} = 3 \times 10^{-19}$ GeV, which in turn provides the value of $G_F = (1.1663787 \pm 0.0000006) \times 10^{-5}$ GeV^{-2} [48] via an improved expression of Eq. (2.5.65). The same theoretical computation within the SMEFT framework leads to

$$\Gamma_{\text{SMEFT}} \left(\mu^- \to e^- \bar{\nu}_e \nu_\mu \right) = \Gamma_{\text{SM}} \left\{ 1 + 2v^2 \frac{\left(C_{\varphi L}^{(3)\,22} + C_{\varphi L}^{(3)\,11} - C_{LL}^{1221} \right)}{\Lambda^2} \right\} . \tag{2.5.66}$$

In order to extract now G_F from the experimental value Γ_μ^{exp}, we perform a series expansion over the necessarily small ratio C/Λ^2 arriving at

$$\sqrt{\frac{192\pi^3 \Gamma_\mu^{\text{exp}}}{m_\mu^5}} \equiv G_F \left\{ 1 + \sqrt{2}\Delta G_F \right\} , \tag{2.5.67}$$

where we have defined the shift induced by the $d = 6$ WCs on G_F as ΔG_F:

$$\sqrt{2}\Delta G_F = v^2 \frac{\left(C_{\varphi L}^{(3)\,22} + C_{\varphi L}^{(3)\,11} - C_{LL}^{1221} \right)}{\Lambda^2} \,, \tag{2.5.68}$$

This shift affects other SM parameter determinations that relied on G_F via theoretical relations, e.g. the vev v.

The Standard Model has a total of 19 parameters to be fixed by the experiment: 9 fermion masses, 4 CKM-matrix parameters, 2 describing the strong interactions and 4 in the electroweak and scalar sectors. Accordingly, one needs 19 input measurements to fix these parameters and make numerical predictions. Let us now focus on the electroweak sector to show how to properly manage the shifts induced by the higher dimensional SMEFT operators. The electroweak sector has 3 independent parameters: v, g, g', which are typically fixed by choosing 3 precise input measurements among the 4: $\hat{G}_F, \hat{\alpha}_{\text{EM}}, \hat{m}_Z$ and $\hat{m}_W$, where the hat indicates that these are the measured physical quantities, i.e. the value that these quantities acquire in the SM alone. A concrete choice thus entails an input parameter scheme. The usual SM relations lead to the usual values of the independent parameters labeled as

$\hat{v}, \hat{g}, \hat{g}'$, e.g. $\hat{v} = 1/\sqrt{\sqrt{2}\hat{G}_F} = 246$ GeV. On the other hand, within the SMEFT we have seen that the input parameter-SM identification is shifted by the WCs, e.g. $\hat{G}_F = G_F \left\{ 1 + \sqrt{2}\Delta G_F \right\}$. Accordingly, this shift translates into the derived independent parameters, which will be now function of the WCs as well and are then denoted with a bar in the Lagrangian, e.g. $\bar{v} = \frac{1}{\sqrt{\sqrt{2}G_F}} = \hat{v}\left(1 + \frac{\Delta G_F}{\sqrt{2}}\right)$. Therefore, in general, once the input parameter scheme is settled, we proceed by expressing them as functions of the $\mathcal{L}_{\text{SM}}^{(4)}$ parameters and the Wilson coefficients:

$$\left[\hat{G}_F, \hat{\alpha}_{\text{EM}}, \hat{m}_Z, \hat{m}_W\right] = f\left(\bar{v}, \bar{g}, \bar{g}', \vec{C}\right), \qquad (2.5.69)$$

where $\vec{C}$ contains the actual WC dependence given by the concrete shifts on the input parameters. Finally, we can solve those equations for $\{\bar{v}, \bar{g}, \bar{g}'\}$ in terms of their known SM-valued partners $\{\hat{v}, \hat{g}, \hat{g}'\}$ and the WCs [60]. This should be consistently applied, once an input parameter scheme is chosen, to all derived quantities.

The above discussion actually refers to the effect stemming from the fact that the usual processes we use to determine the SM parameter values, may be contaminated by new physics as well. Hence, the experimental value would be a combination of the SM parameters and the Wilson coefficients of the SMEFT. When we make use of the values provided by the PDG in other independent calculations, we are actually introducing the new-physics contamination entering the physical process from which the parameter value is obtained. The general procedure above shows how to deal with this issue. In this thesis, we find in Chapter 3 no effect from this contamination since there we study a forbidden phenomenon in the SM. Therefore, new-physics entering those calculations cannot enter in other SM parameter determinations and, since we consider the rest of $d = 6$ operators to vanish, the shifts of the input parameters are zero. This is not the case in Chapter 5, where we make use of the muon and pion decay widths, which receives indeed contributions from new physics, and we will see that this has a very important consequence in our results.

2.5.3 RGE of SMEFT operators

Let us now move to higher-order terms in the perturbative expansion. It is a well established fact that, when computing beyond tree level, some loop diagrams give rise to infinite contributions. In the first half of the XX century, these infinities were a symptom that QFTs were sick theories, not valid to describe physical phenomena. It was later understood that there were theories for which those infinities were just due to a not well-defined starting point within the Lagrangian theory in terms of the so-called (unphysical) bare quantities: bare fields, bare couplings constants and bare masses. Therefore, the solution came by the redefinition of those bare objects via the absorption of the unphysical infinities in a process called *renormalization*. This led to the understanding that indeed, from the beginning, the bare objects were divergent in a way that should cancel the arising UV divergences to give finite physical results. Renormalizable theories (see also Section 2.1.1) were named those that had the exact number of bare quantities needed to absorb all infinities from the divergent loop diagrams. Non-renormalizable theories were dubbed those that contained an

infinite number of operators. However, some well-constructed non-renormalizable theories as the SMEFT contain as well an infinite number of bare parameters to deal with the divergences arising in the calculation of physical observables.

We focus here on the renormalization procedure of non-renormalizable theories, i.e. of effective field theories and more concretely of the SMEFT. Let us recall that EFTs are built out of operators made of the light spectrum present in the low-energy regime, which have associated dimensionless parameters called Wilson coefficients (see Eq. (2.1.1)). Therefore, in addition to the renormalization constants — denoted here as Z — introduced in the renormalization procedure of the light fields, coupling constants and masses within the "renormalizable" sector of the theory ($\mathcal{L}_{\text{SM}}^{(4)}$ in the SMEFT), we introduce as many extra renormalization constants as operators are added. These Z are given by the divergent loop calculations involving the local operators and are absorbed via the renormalization procedure of the bare operators

$$\mathcal{O}_{i,0}^{(d)} = \sum_j Z_{ij}^{(d)}(\mu)\mathcal{O}_j^{(d)}(\mu) \tag{2.5.70}$$

where the subscript 0 denote the bare operators (those of Eq. (2.1.1) before renormalization); the operators on the r.h.s. are the renormalized operators. The renormalization procedure introduces an artificial dependence on the energy for the renormalized operators, which propagates to the Wilson coefficients (see Eq. (2.1.8)). Note that the renormalization of the bare operators introduces, in general, operator mixing via the sum over j in Eq. (2.5.70). This is explained by the fact that in the renormalization of the bare operator $\mathcal{O}_{i,0}^{(d)}$, other operators $\mathcal{O}_j^{(d)}(\mu)$ with $j \neq i$ are needed as counterterms. A very important point that should be emphasized here is that, in the renormalization of EFTs the most convenient regularization scheme is dimensional regularization, since it ensures no mixing between operators of different dimension d. Accordingly, in the following we omit the superscript labeling the dimension (d).

The running and mixing of the renormalized operators are characterized by their anomalous dimension. This can be computed by taking advantage of the scale independence of the bare operators on the left-hand side in Eq. (2.5.70). Taking the derivative over the characteristic energy μ

$$\frac{dZ_{ij}(\mu)}{d\ln\mu}\mathcal{O}_j(\mu) + Z_{ij}(\mu)\frac{d\mathcal{O}_j(\mu)}{d\ln\mu} = 0, \tag{2.5.71}$$

where sum over repeated indices is assumed. The solution to the previous equation is given by

$$\frac{d\mathcal{O}_k(\mu)}{d\ln\mu} = -\left(Z^{-1}\right)_{ki}(\mu)\frac{dZ_{ij}(\mu)}{d\ln\mu}\mathcal{O}_j(\mu) \equiv -\gamma_{kj}(\mu)\mathcal{O}_j(\mu), \tag{2.5.72}$$

which can be expressed in matrix notation as

$$\frac{d\vec{\mathcal{O}}_j(\mu)}{d\ln\mu} = -\boldsymbol{\gamma}\vec{\mathcal{O}}_j(\mu), \qquad \text{with} \qquad \boldsymbol{\gamma} = \mathbf{Z}^{-1}(\mu)\frac{d\mathbf{Z}}{d\ln\mu}, \tag{2.5.73}$$

where boldface is used to denote matrices. $\boldsymbol{\gamma}$ is the so-called anomalous-dimension matrix of the renormalized operators. Let us point out that the elements of $\boldsymbol{\gamma}$ can

be directly obtained from the divergent part of $\boldsymbol{Z}$, i.e. the coefficient in front of the typical $1/\epsilon$ pole.

Now that we have the evolution and mixing of the operators we are left with the computation of the *renormalization group equations* (RGE) of the Wilson coefficients, i.e. the equations describing their running with the energy and their mixing. We will take advantage again of the fact that the general Lagrangian as given in Eq. (2.1.8) should be independent of the characteristic energy scale μ. Taking the derivative over this scale and making use of the relation given by Eq. (2.5.72), one arrives at

$$\left[\frac{dC_i(\mu)}{d\ln\mu}\delta_{ij} - C_i(\mu)\gamma_{ij}(\mu)\right]\mathcal{O}_j(\mu) = 0\,. \tag{2.5.74}$$

Since we are working with an independent complete basis of dimension d operators, the relation above should be satisfied for all operators $\mathcal{O}_j(\mu)$, such that it follows

$$\frac{dC_j(\mu)}{d\ln\mu} - C_i(\mu)\gamma_{ij}(\mu) = 0\,, \tag{2.5.75}$$

what provides the renormalization group differential equations of the Wilson coefficients via their anomalous dimension. In matrix notation is looks

$$\frac{d\vec{C}(\mu)}{d\ln\mu} = \boldsymbol{\gamma}^T(\mu)\vec{C}(\mu)\,. \tag{2.5.76}$$

The Warsaw basis presented in Tables 2.1 and 2.2 has been completely renormalized at the one-loop level in three papers [61, 62] and [63]. In Ref. [63], the explicit RGE of all WCs are given as differential equations relating them in Appendix C, which we refer again in Chapter 3.

2.6 Working at low energies: Cascade of EFTs

The SMEFT framework presented in the previous section stands as the current paradigm to search for new physics effects in a model independent way. It contains the same degrees of freedom as the SM and allows us to combine both low- and high-energy experimental data to constrain the higher-energy dynamics all within a single framework. However, there are experiments taking place at much lower energies ($E \ll v$), where the heavier states present in the SM play a secondary role, since they cannot be created on-shell but contribute just as virtual particles. In line with the EFT spirit of Section 2.1, we can integrate out the heavy SM states and obtain a more suitable EFT to describe the experiment, which contains only the relevant DOFs at the energies at play. The resulting EFT at $E \ll 1$ GeV receives the name of Weak effective field theory or low-energy EFT and contains only the lightest fields ($e, \mu, \nu_\alpha, u, d, g, \gamma$), with $\alpha = e, \mu, \tau$. The electroweak gauge bosons ($W^\pm, Z$), the Higgs boson h and the heaviest quarks t, b and c are integrated out. Accordingly, the remaining gauge group of the LEFT is $\mathrm{SU}(3)_\mathrm{C} \times \mathrm{U}(1)_\mathrm{QED}$. A thorough explanation of the LEFT, how is recovered from the SMEFT and a complete classification up to $d = 6$ of their operators is given in Ref. [64][15]. The

---

[15]Note that in Ref. [64] the LEFT is defined slightly different, containing the quarks c and b.

work of that reference is extended to the computation of the anomalous dimensions and the matching at one loop of the LEFT in Refs. [65] and [66] respectively. In this section we just recall the relevant part of the WEFT Lagrangian for the work presented in Chapter 5.

In Chapter 5 we are interested in the coherent elastic neutrino-nucleus scattering process (CEνNS). The neutrinos that scatter off the material of the detector are produced via charged-current interactions from pion and muon decay. Considering only left-handed neutrinos the parts of the WEFT Lagrangian contributing to pion decay are

$$
\begin{aligned}
\mathcal{L}_{\mathrm{WEFT}}^{\mathrm{CC}} \supset -\frac{2V_{ud}}{v^2}\Big\{ & [\mathbf{1} + \epsilon_L]_{\alpha\beta}\left(\bar{u}\gamma^\mu P_L d\right)\left(\bar{l}_\alpha\gamma_\mu P_L \nu_\beta\right) + [\epsilon_R]_{\alpha\beta}\left(\bar{u}\gamma^\mu P_R d\right)\left(\bar{l}_\alpha\gamma_\mu P_L \nu_\beta\right) \\
& + \frac{1}{2}\left[\epsilon_S\right]_{\alpha\beta}\left(\bar{u}d\right)\left(\bar{l}_\alpha P_L \nu_\beta\right) - \frac{1}{2}\left[\epsilon_P\right]_{\alpha\beta}\left(\bar{u}\gamma_5 d\right)\left(\bar{l}_\alpha P_L \nu_\beta\right) \\
& + \frac{1}{4}\left[\epsilon_T\right]_{\alpha\beta}\left(\bar{u}\sigma^{\mu\nu}P_L d\right)\left(\bar{l}_\alpha\sigma_{\mu\nu}P_L \nu_\beta\right) + \mathrm{h.c.}\Big\},
\end{aligned}
\tag{2.6.77}
$$

where we have denoted the Wilson coefficients by ϵ. These are matrices in leptonic flavor space, and unidimensional in quark flavor space since we are considering only two quark flavors. The muon decay can be characterized by

$$
\begin{aligned}
\mathcal{L}_{\mathrm{WEFT}}^{\mathrm{CC}} \supset -\frac{2}{v^2}\Big[& \left(\delta_{\alpha a}\delta_{\beta b} + [\rho_L]_{a\alpha\beta b}\right)\left(\bar{l}_a\gamma^\mu P_L \nu_\alpha\right)\left(\bar{\nu}_\beta\gamma_\mu P_L l_b\right) \\
& - 2\left[\rho_R\right]_{a\alpha\beta b}\left(\bar{l}_a P_L \nu_\alpha\right)\left(\bar{\nu}_\beta P_R l_b\right)\Big],
\end{aligned}
\tag{2.6.78}
$$

where $[\rho_L]_{a\alpha\beta b}^* = [\rho_L]_{b\beta\alpha a}$ for the Lagrangian to be hermitian.

The CEνNS itself is driven by neutral-current interactions involving neutrinos and quarks. However, at the energies involved in the process, the relevant degrees of freedom are not quarks but the nucleons (protons and neutrons) conforming the nucleus. Therefore, as we did in Sections 2.2 and 2.4, we should trade the quark currents by the nucleon fields. Considering again only left-handed neutrinos, the WEFT Lagrangian terms contributing to CEνNS are

$$
\mathcal{L}_{\mathrm{WEFT}}^{\mathrm{NC}} \supset -\frac{1}{v^2}\sum_{q=u,d}\sum_{\alpha,\beta=e,\mu,\tau}(\bar{\nu}_\alpha\bar{\sigma}_\mu\nu_\beta)\left\{[g_V^q]_{\alpha\beta}(\bar{q}\gamma^\mu q) + [g_A^q]_{\alpha\beta}(\bar{q}\gamma^\mu\gamma_5 q)\right\}.
\tag{2.6.79}
$$

Above we are employing a hybrid notation where the quarks q are 4-component Dirac spinors, and the neutrinos ν_α are 2-component spinors. For a complete review on the two-component spinor formalism see Ref. [67]. The convenience of this notation will be clear below when obtaining the low-energy EFT. The Wilson coefficients measured on the detection side of the CEνNS are the four 3×3 matrices $[g_{V/A}^q]_{\alpha\beta}$. In the SM limit these become

$$
[g_V^q]_{\alpha\beta}^{\mathrm{SM}} = \left[T_q^3 - 2Q_q\sin^2\theta_{\mathrm{W}}\right]\delta_{\alpha\beta}, \qquad [g_A^q]_{\alpha\beta}^{\mathrm{SM}} = -T_q^3\delta_{\alpha\beta}.
\tag{2.6.80}
$$

The next step is to match the WEFT Lagrangian in (2.6.79) to a lower energy EFT where the degrees of freedom are nucleons (protons and neutrons) rather than

quarks. To this end, we need the matrix elements of the quark operators between the nucleon states. Let us denote the incoming nucleon momentum k, and the outgoing nucleon momentum k'. In the zero recoil limit, $q \equiv k - k' = 0$, we have

$$\langle N(k, s') | \bar{q} \gamma^\mu q | N(k, s) \rangle = F_1^{q,N} \bar{u}(k, s') \gamma^\mu u(k, s),$$
$$\langle N(k, s') | \bar{q} \gamma^\mu \gamma_5 q | N(k, s) \rangle = g_A^{q,N} \bar{u}(k, s') \gamma^\mu \gamma_5 u(k, s), \quad (2.6.81)$$

where $N = p, n$, and $u(k, s)$ are the usual Dirac spinor wave functions (see Eq. (1.1.8)). Isospin symmetry implies $F_1^{u,p} = F_1^{d,n}$ and $F_1^{u,n} = F_1^{d,p}$, and the same applies to $g_A^{q,N}$. For the vector part, imposing conservation of the electromagnetic current we arrive at

$$\langle p(k, s') | (2/3) \bar{u} \gamma^\mu u - (1/3) \bar{d} \gamma^\mu d | p(k, s) \rangle = (+1) \bar{u}(k, s') \gamma^\mu u(k, s),$$
$$\langle n(k, s') | (2/3) \bar{u} \gamma^\mu u - (1/3) \bar{d} \gamma^\mu d | n(k, s) \rangle = 0. \quad (2.6.82)$$

Thus, in the limit where the strange content of the nucleon is ignored we have $2F_1^{u,n} = F_1^{d,n}$ ($2F_1^{d,p} = F_1^{u,p}$) and $(2/3)F_1^{u,p} - (1/3)F_1^{d,p} = 1$, what leads to

$$F_1^{d,p} = F_1^{u,n} = 1, \qquad F_1^{u,p} = F_1^{d,n} = 2. \quad (2.6.83)$$

For the axial part we do not have any symmetry principle to fix the normalization as in Eq. (2.6.82). Instead, the nucleon charges $g_A^{q,N}$ needs to be determined phenomenologically.

Using these matrix elements, we can write down the effective Lagrangian with nucleon degrees of freedom as

$$\mathcal{L}_{\text{nucleon}}^{\text{NC}} \supset - \sum_{N=p,n} \sum_{\alpha,\beta=e,\mu,\tau} (\bar{\nu}_\alpha \bar{\sigma}_\mu \nu_\beta) \left\{ [C_V^N]_{\alpha\beta} (\bar{N} \gamma^\mu N) + [C_A^N]_{\alpha\beta} (\bar{N} \gamma^\mu \gamma_5 N) \right\}, \quad (2.6.84)$$

where the leading order matching of the Wilson coefficients of the two EFTs reads

$$[C_V^N]_{\alpha\beta} = \frac{1}{v^2} \sum_{q=u,d} F_1^{q,N} [g_V^q]_{\alpha\beta},$$
$$[C_A^N]_{\alpha\beta} = \frac{1}{v^2} \sum_{q=u,d} g_A^{q,N} [g_A^q]_{\alpha\beta}. \quad (2.6.85)$$

In the SM limit we have

$$[C_V^p]_{\alpha\beta}^{\text{SM}} = \frac{1}{2v^2} \left[1 - 4 \sin^2 \theta_W \right] \delta_{\alpha\beta},$$
$$[C_V^n]_{\alpha\beta}^{\text{SM}} = -\frac{1}{2v^2} \delta_{\alpha\beta},$$
$$[C_A^p]_{\alpha\beta}^{\text{SM}} = -\frac{1}{2v^2} \left[g_A^{u,p} - g_A^{d,p} \right] \delta_{\alpha\beta} = -\frac{g_A}{2v^2} \delta_{\alpha\beta}, \quad (2.6.86)$$
$$[C_A^n]_{\alpha\beta}^{\text{SM}} = -\frac{1}{2v^2} \left[g_A^{u,n} - g_A^{d,n} \right] \delta_{\alpha\beta} = \frac{g_A}{2v^2} \delta_{\alpha\beta}.$$

Note that, due to the fact that $\sin^2 \theta_W \sim 1/4$, the accidental cancellation in the first term of Eq. (2.6.86) makes vector interactions approximately protophobic. The

Lagrangian of Eq. (2.6.84) thus provides an EFT description of the neutral-current neutrino-nucleus interactions at the nucleon level.

However, the very low energies involved in this process allow us to descend more in this cascade of EFTs. For instance, the neutrino scattering translates into a very low-energy (observable) recoil of the nucleus. The tiny momenta of the outgoing nucleus allows to characterize it better in the non-relativistic (NR) limit. The NR limit of the relevant operators in the Lagrangian (2.6.84) gives

$$\begin{aligned}
\bar{N}\gamma^0 N &= \psi_N^\dagger \psi_N + \mathcal{O}(\nabla^2)\,, \\
\bar{N}\gamma^0\gamma_5 N &= \mathcal{O}(\nabla)\,, \\
\bar{N}\gamma^k N &= \mathcal{O}(\nabla)\,, \\
\bar{N}\gamma^k\gamma_5 N &= \psi_N^\dagger \sigma^k \psi_N + \mathcal{O}(\nabla^2),
\end{aligned} \tag{2.6.87}$$

where $k = 1\ldots 3$ and ψ_N are the non-relativistic nucleon fields, which satisfy the Schrödinger equations of motion. The non-relativistic EFT for nucleons at the zero-recoil level is thus described by the Lagrangian

$$\mathcal{L}_{\rm NR}^{\rm NC} \supset \sum_{N=p,n} \sum_{\alpha,\beta=e,\mu,\tau} \left\{ -[C_V^N]_{\alpha\beta}(\psi_N^\dagger \psi_N)(\bar{\nu}_\alpha \bar{\sigma}^0 \nu_\beta) + [C_A^N]_{\alpha\beta}(\psi_N^\dagger \sigma^k \psi_N)(\bar{\nu}_\alpha \bar{\sigma}^k \nu_\beta) \right\}, \tag{2.6.88}$$

which will be of great use in Chapter 5 when analyzing the CEνNS.

Part II

Charged-lepton-flavor violation of τ involved processes and the role of leptoquarks

Chapter 3

Charged-lepton-flavor violation and the τ lepton

Lepton-flavor violation (LFV) is a widely studied phenomenon both from the theoretical and experimental fields. Its importance and interest relies on the absence of such dynamics in the Standard Model with massless neutrinos, thus providing a unique window to new physics with no theoretical background[1]. Neutrino oscillation experiments have proven the SM to be incomplete, requiring the neutrinos to acquire mass somehow. Similarly to the quark-flavor dynamics in the SM ruled by the CKM matrix (see Section 1.4.3), neutrino masses drive in turn the violation of the flavor in the neutral-lepton sector, i.e. neutrino oscillations. However, despite the continuous observations of this effect in the neutral sector, and the great effort made to find its charged counterpart, no signal of charged-lepton-flavor violation (CLFV) has been observed so far, and only limits on the branching ratios of these processes can be set. This poses us a question: Why is there such a pronounced effect on the neutral leptons while, on the other hand, this phenomenon is remarkably suppressed (if not prohibited) for their charged partners? Since there is no LFV in the Standard Model with massless neutrinos, the answer to this question lies in the concrete extension of the SM addressing this issue: CLFV may be intrinsically linked to the neutrino-mass generating mechanism, however, it might not be the only source of this phenomenon. For instance, many of these extensions naturally yield non-negligible CLFV rates, as it is the case of extended scalar sectors as the two-Higgs doublet models, supersymmetric UV completions, models with large extra dimensions, little Higgs models, leptoquarks.... In this sense, for example leptoquarks (LQs) can mediate flavor-violating transitions, for both quarks and leptons, without being necessarily the source of the neutrino masses (although there exist mechanisms relating both, see Chapter 4).

This question has been extensively studied in the literature (see for example the reviews [68–70]) concerning mainly the first two lepton families, the electron and the muon, whereas the tau lepton has received a minor attention due to the experimental complications arising in its production and detection: they are not produced in great abundance and have a much shorter lifetime as compared to muons, so that one cannot talk about τ beams to be used in experiments. Therefore, despite an a priori enhanced experimental sensitivity due to its larger mass, the limits on CLFV

---

[1]From the theoretical point of view, LFV observables stand as very clean environments to look for NP, since SM dynamics give null predictions for them and consequently there is no SM contamination.

τ-involved processes are usually obtained from non-dedicated experiments. Notwithstanding, CLFV processes with the τ lepton present an exceptional opportunity to look for new physics that will be exploited by the next generation of B-factories as Belle II [71] (already taking data) and other complementary experiments as the NA64 experiment at CERN. On a longer time scale, the τ sector may be deeply studied by several facilities like the possible successor of LEP in this matter[2], a TeraZ facility of a future FCC-ee [72], the Super τ-Charm Facility (STCF) and the Electron-Ion Collider (EIC) [73].

In this chapter we present a model-independent analysis of the lepton-flavor-violating processes involving tau leptons, within the framework of the Standard Model Effective Field Theory up to dimension 6 operators (see Section 2.5). We start by briefly reviewing the history of flavor and the role of the tau lepton in this picture. Then, we give an overview of the (C)LFV phenomena in the Standard Model and how they arise in some extensions, and show the systematic way to study these phenomena under the model-independent procedure provided by the SMEFT. The two main processes thoroughly studied in this analysis are presented in the following two sections, i.e. hadronic τ decays and ℓ-τ conversion in nuclei. This is followed by a description of the statistical tools used to extract bounds on the parameters of the SMEFT. Finally, the results from the analysis are presented and some conclusions are given. Most of the content of this chapter is based on our Ref. [74].

3.1   A history of flavor and the τ lepton

Within the Standard Model, the concept of flavor is used to denominate the existence of twelve different species of elementary particles, the basic constituents of matter: six quarks and six leptons, each with a given flavor, and altogether conforming the group of elementary fermions. These are as well grouped in three families or generations (see Chapter 1), whose only difference stems from the Yukawa interactions with the Higgs field (see Section 1.4.3), i.e. their masses[3]. However, in our present understanding of the SM, the structure of flavor is somewhat arbitrary. There is no known mechanism that dictates there should be three heavier copies (or any number at all) of the same gauge representations of the lepton and quark fields. Indeed, this structure responds just to the content of matter observed in nature and the similar properties among families, i.e. they share the same gauge quantum numbers but differ in the mass (and obviously their flavors). The very existence of these replications is one of the pieces of the so-called SM puzzle, one which has strong consequences like the existence of $\mathcal{CP}$ as we saw in Section 1.4.3. Another piece of this puzzle is the lack of a basic (symmetry) principle that explains the pattern of

---

[2]The production mechanism of tau pairs would be the same for both LEP and TeraZ: via the decay at rest of a Z, what entails controllable systematic uncertainties and relatively low backgrounds.

[3]This is indeed a more subtle point. In several extensions of the Standard Model, the SM Yukawa couplings constitute just a fraction of the total mass of the particles. The latter then receives contributions also from other new physics sources, such as other Yukawa couplings to extra Higgs fields. In this sense, in order to assess the validity or the limit of the SM mass-generation mechanism, at the LHC, a program is being conducted to measure the coupling of the Higgs field to fermions, i.e. the same mass-generating Yukawas within the SM; see Ref. [75] and references therein.

the SM Yukawa couplings and, accordingly, the resulting masses and mixings (see e.g. Ref. [68] for a detailed explanation).

The first indication of the existence of these replicas appeared in 1937 with the discovery of the muon in cosmic-ray showers by Anderson and Neddermeyer [76]. The most plausible hypothesis to explain the observed penetrating particles, coming from this cosmic radiation, was asserted to be the existence of "higher mass states of ordinary electrons". However, the dominating idea at that time became to relate this particle to the mediator of the strong force predicted by Yukawa [77]. It was not until a decade later in 1947 that this possibility was ruled out by the CPP experiment [78]. Hence, the origin of flavor is usually traced back to a letter sent the same year by Bruno Pontecorvo to Gian-Carlo Wick [70]. In this letter he made the hypothesis that this particle could be a "sort of isomer" of the electron. This idea was reinforced by the discovery of the two-step decay of the pion into a muon and a following electron, by the group of Powell [79], which helped to differentiate the pion (π), as the aforementioned Yukawa mediator, and the muon (μ), a possible second generation of the electron.

The history concerning the neutral sector of leptons took another path. The existence of the first generation of neutral leptons (the electronic neutrino ν_e) was first postulated by Wolfgang Pauli in 1930 to explain beta decay — the decay of a neutron into a proton, an electron and an electronic anti-neutrino $n \to p\,e\,\bar{\nu}_e$ — without requiring Bohr's idea about the violation of the principle of energy conservation [80]. This elusive particle was detected for the first time in 1956 in the Cowan-Reines neutrino experiment [81]. The postulation of a second generation of neutrinos came from an interplay between theory and experiment. In 1958, it was shown by Feinberg [82] that if there existed some heavy charged bosons mediating the weak interactions — as it was suggested by the discovery of parity violation by the Wu experiment [83] in 1957 — these would increase the branching ratio of $\mu^+ \to e^+\gamma$ above the experimental limit at that time. This enhancement was due to a loop contribution involving the $W^\pm$ gauge bosons and the single electronic neutrino (see Fig. 3.4). Therefore, a well-motivated way out was proposed by Pontecorvo in 1959 [84], the two-neutrino hypothesis. This postulated the existence of a second neutrino that would only couple to the muon and not to the electron (and the opposite for the electronic neutrino), in such a way that the process $\mu^+ \to e^+\gamma$ would be forbidden. The scheme with a second-neutrino generation was confirmed experimentally in 1962 at the Brookhaven National Laboratory [85].

To talk about the star of this chapter, the τ lepton, first we should briefly introduce the other half of the flavor spectrum: the quarks. In the quark sector the understanding of the presence of different families — and the existence of the quarks themselves — was done implicitly, through the non-elementary particles where the quarks are always confined in at low energies (E $\lesssim$ 2 GeV): the hadrons.

In parallel to the realization that the muon was not the mediator of the strong force, but a possible heavier cousin of the electron, in 1947 Rochester and Butler discovered an unknown signal of two opposite-charged tracks forming a V pattern [86]. This signal was the product of the decay of a neutral particle that would take some time to identify as the neutral Kaon. Therefore, this discovery presented the first

observation of the existence of a second-generation quark, the strange quark, although it took until 1964 for Murray Gell-Mann and George Zweig to postulate the very existence of quarks [4, 5] as the fundamental constituents of the hadrons. The charm quark made his first appearance in 1970 in the model proposed by Sheldon Glashow, John Iliopoulos, and Luciano Maiani for the weak interactions [6]. In this model with four quarks, the absence of flavor-changing neutral currents (at treee level) arose naturally in what has been latter called the GIM mechanism. Over the summer of 1974, the charm quark was discovered independently by two groups one at SLAC [87] and the other at the Brookhaven National Laboratory (BNL) [88], via the observation of a new (composed) particle the J/ψ meson comprising a pair of $c\bar{c}$ quarks. Hence, the second family of fermions was completed. The first experimental indication of the existence of a third generation of quarks came in 1964 from the observation of CP violation in the decay of neutral kaons [89]. Such an effect could not be possible in the previously described framework of two families, but a third generation was needed as was shown by Kobayashi and Maskawa in 1973 [20], thus completing Cabibbo's analysis [19] of transitions — mediated by the weak interaction — between different generations of quarks (flavor violation in the quark sector). Then, the b quark was discovered in 1977 [90], but we had to wait almost 20 years, until 1995, to have the first evidence of its weak isodoublet partner, the massive top quark, hence completing the third and heaviest quark family [91, 92].

In 1972, it was shown for Weinberg's model of the weak and electromagnetic interactions [8], that in order to obtain a theory free of Adler-Bell-Jackiw axial anomalies [93, 94] — where the currents stemming from the SM gauge symmetries are non-anomalous — the same number of leptons and quarks is needed [95]. This is a profound result pointing to a possible unification of matter, although the specific implementation in an ultra-violet completion of the SM that nature might adopt (if any) is still unknown. This realization, together with the state of development of particle physics described above, led physicists in the seventies to believe that there may exist heavier leptons and its observation could be feasible in new e^+e^- colliders [96]. In this spirit, in 1975, the Mark I detector at the e^+e^- collider in SLAC detected 24 anomalous $e\mu$ events of the form $e^+ + e^- \rightarrow e^\pm + \mu^\mp + \geq$ 2 undetected particles [97]. The collaboration ascribed this anomaly to the existence of a pair of new particles, each with a mass $M \sim 2$ GeV, and explained the 24 events through their production and subsequent decay. We now know they observed the production of two tau leptons $e^+e^- \rightarrow \tau^+\tau^-$ with the subsequent decays $\tau^+ \rightarrow e^+\nu_e\bar{\nu}_\tau$ and $\tau^- \rightarrow \mu^-\bar{\nu}_\mu\bar{\nu}_\tau$. Accordingly, the existence of a tau neutrino ν_τ was also considered. However, it was not until 1977, at the DORIS e^+e^- storage ring at DESY, that the PLUTO collaboration confirmed this hypothesis narrowing it down to charged leptons of spin 1/2 [98]. In 1990, using the ARGUS detector at the DORIS II e^+e^- storage ring, the V$-$A Lorentz structure of the tau vertex in weak interactions as well as further confirmation of e-μ-τ universality was established [99]. Finally, direct evidence of the tau neutrino was given by the dedicated DONUT experiment at Fermilab in 2000 [100].

The tau lepton has a unique position within the Standard Model, namely it is the only known lepton with enough mass to decay into light flavored hadrons. Concretely, due to baryon number conservation — a global symmetry of the SM

— the tau can only decay into mesons, since otherwise there would not be enough phase space for the decay into two baryons and baryon number would be violated. Therefore, the tau provides a rich source of very interesting phenomenology, which is usually used twofold: one can either study the SM dynamics involving the strong interactions at low energies, e.g. the hadronization of quarks into mesons, or given the appropriate QCD data from somewhere else, the copious phenomenology can be used to study physics beyond the Standard Model that would manifest in deviations of the predicted SM tau dynamics. However, as described above, its shorter lifetime as compared to its lighter cousins hinders its large production. This problem has been somehow surpassed by the B-meson factories, e.g. at the end of the past century by the CLEO experiment at the Cornell Electron Storage Ring (CESR) [101], but it is in the advent of this century when the tau physics program has experimented a boost with BaBar at SLAC [102], Belle at KEK [103,104] and the currently ongoing Belle II experiment at SuperKEKB (an upgrade of Belle) [71]. The B-factories work at the center-of-mass energy $\sqrt{s} = 10.58$ GeV to optimally produce the $\Upsilon(4S)$ resonance, made out of a pair of $b\bar{b}$ quarks, that decays mainly ($> 96\%$) into a pair of $B\bar{B}$ mesons. At these energies, the cross section to produce a pair of $\tau^+\tau^-$ is 90% that of producing the $b\bar{b}$ pair [70], what makes of B-factories also very efficient τ factories. The most up-to-date experiment studying, among others, hadronic tau decays is Belle II. The B-factory started to collect data in 2019 and it is expected to increase the sensitivity to these decays at least one order of magnitude.

3.2 CLFV in the SM and beyond

In Chapter 1, we saw how the Yukawa couplings of the quarks, in the scalar sector of the Standard Model, provided non-trivial flavor dynamics based on the structure of the CKM matrix. This, in turn, provides a richer phenomenology that is, however, absent in the leptonic sector. In this regard, the difference between quarks and leptons stems from the absence of a right-handed neutrino. Such a neutral lepton transforms as a singlet with zero hypercharge under the SM gauge-group symmetries (with the group transformation properties (1,1,0)). Given also the fact that it has never been observed in nature, its addition to the theory would be procured ad hoc.

Let us approach this issue from a more general perspective: in terms of symmetry principles. The matter content of the Standard Model — as representations of the gauge symmetries — can be regarded as a single SM family $(Q, L, u_{\mathrm{R}}, d_{\mathrm{R}}, e_{\mathrm{R}})$, see Section 1.1.1. In the absence of Yukawa interactions, the whole theory is invariant under the global symmetry

$$\mathrm{U}(3)^5 \equiv \mathrm{U}(3)_{Q_{\mathrm{L}}} \times \mathrm{U}(3)_{L_{\mathrm{L}}} \times \mathrm{U}(3)_{u_{\mathrm{R}}} \times \mathrm{U}(3)_{d_{\mathrm{R}}} \times \mathrm{U}(3)_{\ell_{\mathrm{R}}} , \qquad (3.2.1)$$

acting on the family indices of each of the (five) inequivalent gauge representations stated above. Namely, providing an example, for massless leptons the Standard Model Lagrangian would be symmetric under a global $\mathrm{U}(3)_{\ell_{\mathrm{R}}}$ transformation on the

family vector of the right-handed lepton $(\text{SU}(2)_\text{L} \times \text{U}(1)_\text{Y}$ singlet) ℓ_R:

$$
\begin{pmatrix} e' \\ \mu' \\ \tau' \end{pmatrix}_\text{R} = U_{\ell_R} \begin{pmatrix} e \\ \mu \\ \tau \end{pmatrix}_\text{R} , \tag{3.2.2}
$$

with U_{ℓ_R} the 3×3 matrix representation of the $\text{U}(3)_{\ell_\text{R}}$ symmetry transformation. This means that in the massless SM Lagrangian, the gauge interactions are independent of the specific choice of basis in flavor space for every field in the SM family.

Once the Yukawa sector is included, the global $\text{U}(3)^5$ flavor symmetry is explicitly broken. Likewise, the degeneracy of the three families is removed with the elementary fermions acquiring different masses related to their Yukawa interactions. On the one hand, in the quark sector, the Yukawa matrices of the up and down quarks totally break this symmetry giving rise to different masses for the different families and, after mass diagonalization, inducing quark-flavor violation as described by the CKM matrix (see Section 1.4.3). On the other hand, the Yukawa matrices present in the leptonic sector break the corresponding lepton symmetries in $\text{U}(3)^5$ and are the responsibles for the masses of the charged leptons. However, the omission of the right-handed neutrinos and the neutrino-Yukawa matrices associated to them, results in the "softer" breaking of the $\text{U}(3)^5$ symmetry to the subgroup

$$
L \equiv \text{U}(1)_e \times \text{U}(1)_\mu \times \text{U}(1)_\tau , \tag{3.2.3}
$$

such that the Standard Model Lagrangian remains invariant under global rotations of the individual lepton fields. This invariance implies a conserved charge for each lepton family: L_e for (e, ν_e), L_μ for (μ, ν_μ) and L_τ for (τ, ν_τ). Accordingly, Eq. (3.2.3) is, in symmetry language, the statement for lepton-flavor conservation.

The global symmetry L is an accidental symmetry of the Lagrangian since it is not one of the building blocks of the theory, but appears by chance once the renormalized Standard Model is constructed (as opposed to the SM gauge symmetries). Therefore, considering the SM as an effective field theory (see Chapter 2), one could expect higher-dimensional non-renormalizable terms — describing new-physics interactions taking place at higher energy scales — to violate this accidental symmetry, hence mediating LFV. Another straightforward way L may be broken is via the simple addition of a right-handed neutrino Dirac term. Such a term provides masses to the neutrinos and breaks the individual L_e, L_μ and L_τ symmetries, although it conserves the total lepton number, i.e. invariance under common-global phase rotations of the three lepton fields. Note that, upon the inclusion of a right-handed neutrino within the SM matter content, nothing forbids the addition of a Majorana mass term violating also the total lepton number, we will delve into the Dirac/Majorana nature of the neutrinos in Chapter 6.

Lepton-flavor violation has been already observed in neutrino oscillation experiments. Therefore, we do know that neutrinos have mass and the L global symmetry is broken in nature. However, no direct observation of this breaking in the charged sector has been made so far. There are, nonetheless, some relevant experimental hints pointing to non-trivial lepton dynamics. These come in the form of notorious discrepancies with the universality SM predictions for some decays of the B mesons:
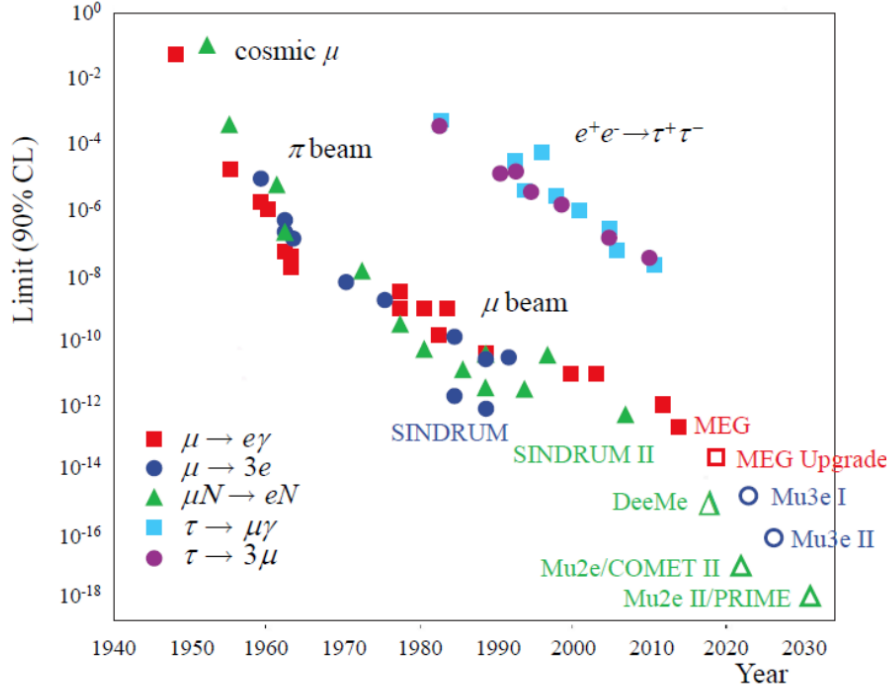
FIGURE 3.1: History of the development of the limits on several CLFV processes, from the beginning of the second half of the past century until the end of the current decade. The filled geometric figures stand for the currently established limits, while the empty ones for the future expected sensitivities on these processes of the corresponding experiments labeled next to them [126].

$R_{D^{(*)}}$ [105–112], R_K [113–120] together with very recent $R_{K_S^0}$ and $R_{K^{*+}}$ [121] — the so-called B anomalies [122] — as well as the anomalous magnetic moment $(g - 2)$ of the muon [123, 124]. Depending on the anomaly, different lepton families are involved. However, in this chapter we will mainly focus on the third family, the tau lepton, due to the aforementioned reasons, besides the fact that the situation relating the first two families may be less compelling (see Ref. [125]). For completeness, we also summarize the present status on the theoretical and experimental search of CLFV for the first two families.

The search for CLFV has received much dedication in the second half of the last century, followed by the first negative results to observe the expected $\mu \to e\gamma$ decay. Since then, many experiments have tried to observe this phenomenon, increasing their sensitivities and statistics, but only limits have been set so far (see Fig.3.1 taken from Ref [126]). The three canonical processes to study CLFV involving the first two families are the decays $\mu \to e\gamma$ and $\mu \to 3e$, and the μ–e conversion in nuclei. There are also several other channels to study CLFV processes like in rare meson decays, collider experiments or through more exotic channels as muonium-antimuonium oscillations $\mu^+ e^- \leftrightarrow \mu^- e^+$ [69], but we do not consider them in the following. A schematic list is presented in Fig. 3.2 taken from Ref. [127]. The former three golden channels pose the most stringent bounds up to date: $\mathrm{Br}(\mu^+ \to e^+\gamma) < 4.2 \times 10^{-13}$ by the MEG experiment [128], $\mathrm{Br}(\mu^+ \to e^+e^+e^-) < 1.0 \times 10^{-12}$ by
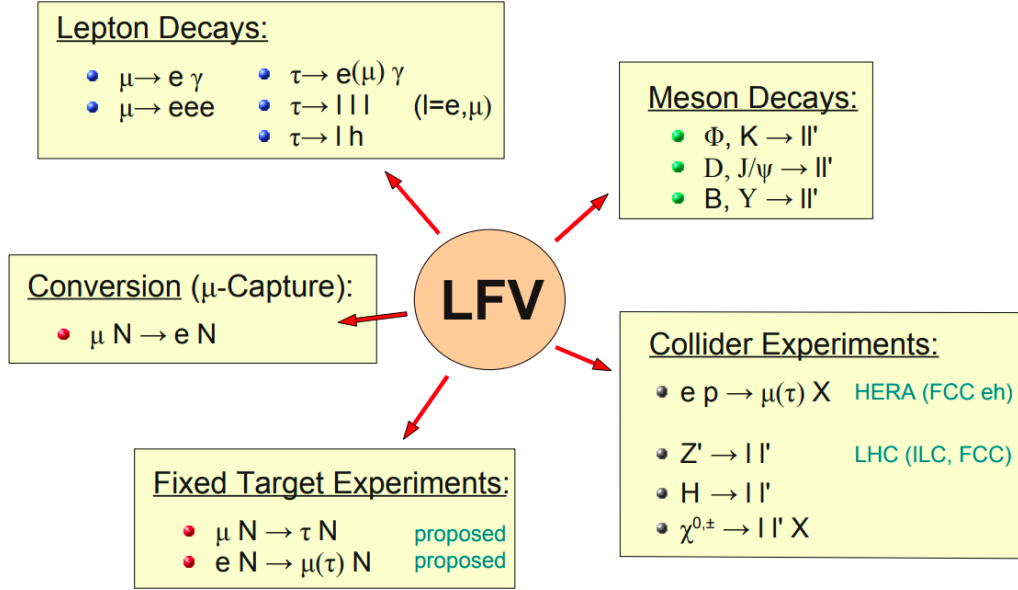
FIGURE 3.2: Different CLFV channels. Figure taken from Ref. [127].

the SINDRUM collaboration [129] and $\sigma(\mu^-\text{Au} \to e^-\text{Au})/\sigma(\mu^-\text{Au} \to \text{ capture}) <$ 7.0×10^{-13} by the SINDRUM II collaboration [130]. Along this decade, these bounds are expected to be improved by several orders of magnitude (see Ref. [131] for a short review) to reach a sensitivity of $\mathcal{O}(6 \times 10^{-14})$ for $\mu \to e\gamma$ by MEG II [132], $\mathcal{O}(10^{-16})$ for $\mu \to 3e$ by the Mu3e experiment at the Paul Scherrer Institute (PSI) [133] and $\mathcal{O}(3 \times 10^{-17})$ for μ–e conversion in nuclei by Mu2e [134] and COMET II in its second phase [135], potentially overpassing the $\mathcal{O}(10^{-18})$ frontier in the Mu2e II [136] and PRIME [137] experiments.

Focusing on the τ lepton, we can see in Fig.3.1 that the leptonic modes are several orders of magnitude less constrained as compared to the limits obtained for the first two families. This is indeed the case for $\tau \to \mu\gamma$ and $\tau \to 3\mu$. However, there is no experimental bound for the missing golden channel τ conversion in nuclei. In this sense, there is a proposal by the NA64 experiment at CERN [138] to study ℓ–τ conversion in the presence of nuclei: $\mu^-(e^-) + \mathcal{N}(A, Z) \to \tau^- X$, i.e. with a fixed-target of atomic and mass numbers Z and A respectively and an outgoing hadronic state X. This process has received minor attention due to the complexities of its experimental setting; see, however, Refs. [138–142] and references therein. Furthermore, future foreseen experiments such as the muon collider [143], the electron-ion collider [144,145], the ILC [146] or circular colliders as LHeC [147] could also consider to look for this conversion.

At the end of the previous section, we pointed out the interest of studying the tau lepton regarding also the rich phenomenology provided by its hadronic decays. Therefore, complementary to ℓ–τ conversion in nuclei, the B-meson factories with CLEO at the beginning followed later by the Belle and BaBar experiments, have searched for both the lepton and hadronic decays of the tau lepton (see Fig. 3.3
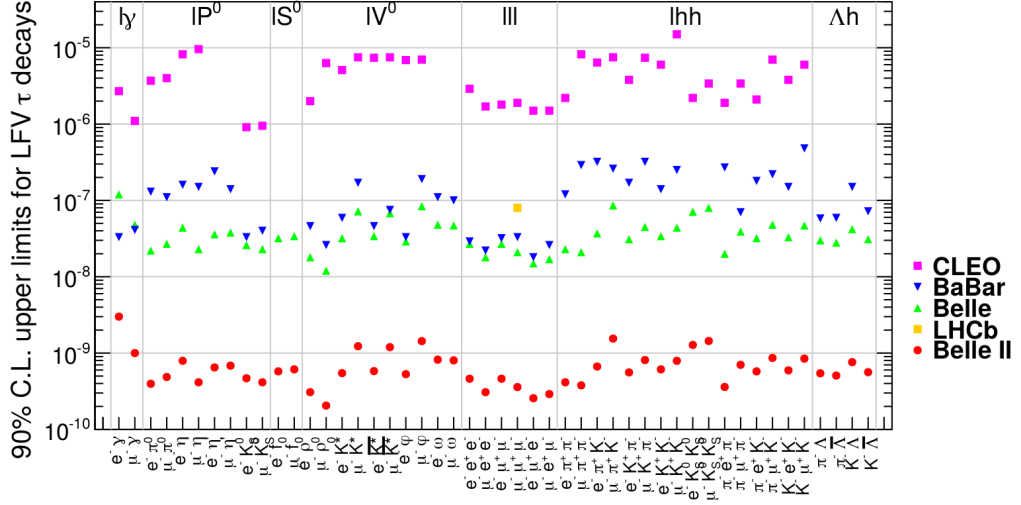
FIGURE 3.3: Limits on the branching ratios of CLFV tau decays, both for leptonic and hadronic modes, searched for by CLEO, BaBar, Belle, LHCb and the expected sensitivity on those by Belle II [71].

from Ref. [71]). Currently, Belle II is operating since 2019 and, by the end of the data acquisition period, it is expected to increase the sensitivity on these decays one order of magnitude over its predecessors. The past and expected limits on these processes are shown in Fig. 3.3.

On the theoretical side, the confirmation of lepton-flavor violation via neutrino oscillations — with the corresponding determination of oscillation parameters: the mixing angles and mass differences — does not unambiguously tell us the expected rates for the analogous charged phenomena. The evaluation of the latter strongly depends on the mechanism giving mass to neutrinos as well as lepton mixing, which may, but does not have to, be related. In this sense, as sketched above, there are models naturally inducing CLFV (see e.g. Chapter 4 four our analysis of CFLV within the most general leptoquark framework), but not necessarily providing mass to the neutrinos. On the other hand, different neutrino-mass-generating mechanisms provide distinct CLFV rates [148–152]. For instance, the simplest straightforward extension of the Standard Model with three families of right-handed Dirac neutrinos entails, for the process with usually (depending on the model) the largest rate $\mu \to e\gamma$, the tiny-unobservable branching ratio [70]

$$\mathcal{B}(\mu \to e\gamma) \simeq \frac{\Gamma(\mu \to e\gamma)}{\Gamma(\mu \to e\nu\bar{\nu})} = \frac{3\alpha}{32\pi} \left| \sum_{i=2,3} U_{\mu i}^* U_{ei} \frac{\delta m_{i1}^2}{M_W^2} \right|^2 < 10^{-54} , \qquad (3.2.4)$$

computed from the diagram in Fig. 3.4, with α the fine-structure constant, U the PMNS neutrino-mixing matrix, $\delta m_{ij}^2 = m_i^2 - m_j^2$ the neutrino mass-squared differences and M_W the W-boson mass. More involved extensions with extra heavier neutrinos, like the seesaw mechanisms, may even enhance these CLFV rates to current or expected sensitivities see, e.g. Ref. [153].
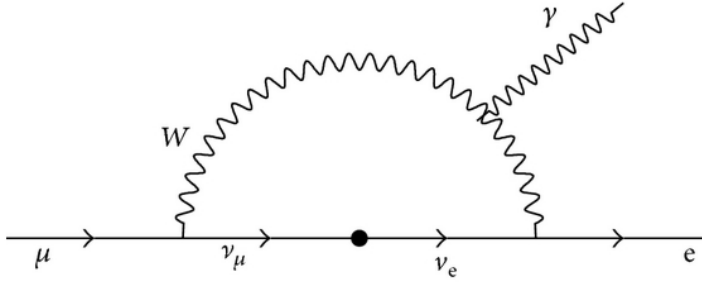
FIGURE 3.4: Diagram of the main contribution to the process $\mu \to e\gamma$, within the minimal extension of the SM with a right-handed Dirac neutrino for each family.

In the work of Ref. [74], we performed a model-independent analysis of CLFV tau processes that involve hadrons. A model-independent framework is provided by the Standard Model effective field theory (see Chapter 2 for a detailed explanation). The first contribution to CLFV processes can be generated by $d = 6$ operators, so we kept only those. For definiteness, we used the basis and notation consistent with Ref. [56]. As it was pointed out in Chapter 2, our procedure would not be valid if the origin of CLFV lied at $E \lesssim M_W$, in which case the SMEFT Lagrangian (see Eq. (2.5.63) in Section 2.5) does not serve as an appropriate framework. In this Lagrangian Λ represents the energy scale at which new physics appears. Accordingly, Λ depends on the new dynamics we want to describe, i.e. it does not need to be the same for LFV or violation of lepton number. In the following, we use Λ_{CLFV} to denote the scale of interest of the described analysis. In this work we focused, as already explained, on the third family of leptons. Therefore, our SMEFT operators are still invariant under global $\mathrm{U}(1)_e \times \mathrm{U}(1)_\mu$ rotations that do not involve the tau lepton anymore. The large mass of the tau lepton allows its CLFV decays into hadrons, opening a wide set of modes that can be looked for in dedicated experiments. Moreover, ℓ–τ conversion ($\ell = \mu, e$) in the presence of nuclei has been scarcely considered in the bibliography. The obvious relevance of studying both type of processes at the same time is that they involve, generically, the same SMEFT operators. In addition, we assumed that the Wilson coefficients involving the muon and the electron are the same, i.e. we presume universality in the two lighter lepton families. This seems endorsed, up to now, by the experimental results.

There is only one $d = 5$ operator in the SMEFT Lagrangian [57], but it violates lepton number and is of no interest for our research here. The list of $d = 6$ operators is rather large [58] and contains the first relevant operators that implement CLFV processes. We will limit our study to those, and we will use, essentially, the notation from Ref. [56]. The operators contributing to processes under consideration here are collected in Table 3.1.

3.3 Hadronic τ decays

We studied the CLFV decays $\tau^- \to \ell^- \{P, P_1 P_2, V\}$, with $\ell = \mu, e$, and P and V standing for pseudoscalar and vector mesons with light-quark content (namely u, d

$\Lambda^2 \times$ Coupling	Operator	$\Lambda^2 \times$ Coupling	Operator
$C_{LQ}^{(1)}$	$\left(\bar{L}_p\gamma_\mu L_r\right)\left(\bar{Q}_s\gamma^\mu Q_t\right)$	$C_{e\varphi}$	$\left(\varphi^\dagger\varphi\right)\left(\bar{L}_p e_r\varphi\right)$
$C_{LQ}^{(3)}$	$\left(\bar{L}_p\gamma_\mu\sigma^I L_r\right)\left(\bar{Q}_s\gamma^\mu\sigma^I Q_t\right)$	$C_{\varphi e}$	$\left(\varphi^\dagger i\overset{\leftrightarrow}{D}_\mu\varphi\right)(e_p\gamma^\mu e_r)$
C_{eu}	$(\bar{e}_p\gamma_\mu e_r)(\bar{u}_s\gamma^\mu u_t)$	$C_{\varphi L}^{(1)}$	$\left(\varphi^\dagger i\overset{\leftrightarrow}{D}_\mu\varphi\right)\left(\bar{L}_p\gamma^\mu L_r\right)$
C_{ed}	$(\bar{e}_p\gamma_\mu e_r)\left(\bar{d}_s\gamma^\mu d_t\right)$	$C_{\varphi L}^{(3)}$	$\left(\varphi^\dagger i\overset{\leftrightarrow}{D}_{I\mu}\varphi\right)\left(\bar{L}_p\sigma_I\gamma^\mu L_r\right)$
C_{Lu}	$\left(\bar{L}_p\gamma_\mu L_r\right)(\bar{u}_s\gamma^\mu u_t)$	C_{eW}	$\left(\bar{L}_p\sigma^{\mu\nu}e_r\right)\sigma_I\varphi W_{\mu\nu}^I$
C_{Ld}	$\left(\bar{L}_p\gamma_\mu L_r\right)\left(\bar{d}_s\gamma^\mu d_t\right)$	C_{eB}	$\left(\bar{L}_p\sigma^{\mu\nu}e_r\right)\varphi B_{\mu\nu}$
C_{Qe}	$\left(\bar{Q}_p\gamma_\mu Q_r\right)(\bar{e}_s\gamma^\mu e_t)$		
C_{LedQ}	$\left(\bar{L}_p^j e_r\right)\left(\bar{d}_s Q_t^j\right)$		
$C_{LeQu}^{(1)}$	$\left(\bar{L}_p^j e_r\right)\varepsilon_{jk}\left(\bar{Q}_s^k u_t\right)$		
$C_{LeQu}^{(3)}$	$\left(\bar{L}_p^j\sigma_{\mu\nu}e_r\right)\varepsilon_{jk}\left(\bar{Q}_s^k\sigma^{\mu\nu}u_t\right)$		

TABLE 3.1: $d=6$ operators appearing in the Lagrangian (2.5.63) and contributing to the CLFV processes that we study in this work. The four-fermion operators appear on the left-hand side, while those involving the Higgs doublet φ and the gauge bosons are on the right. The notation (up to small apparent changes), is the one from Ref. [56]. For the family indices we use p, r, s and t, while j and k are isospin indices. For $I=1,2,3$, σ_I are the Pauli matrices, with $\varepsilon=i\sigma_2$, and $\sigma^{\mu\nu}\equiv\frac{i}{2}[\gamma^\mu,\gamma^\nu]$. Λ is then the scale where the new dynamics arises. The operators share the same notation with the associated couplings, substituting simply $C\to\mathcal{O}$, i.e. $\mathcal{O}_{LQ}^{(1)}$ and so on.

and s), respectively. In order to determine the widths of the hadronic tau decays using the $d=6$ operators in Table 3.1, the procedure has two steps:

1) determine the perturbative amplitudes at parton level,

2) hadronize those partons into mesons.

The key role in the perturbative contribution has been customarily given to $\tau \to \ell q\bar{q}$ shown in Fig. 3.5. However, in Ref. [154] it was pointed out that the scalar contribution via the diagram shown in Fig. 3.6 should also be considered — as the hadronization of gluons into mesons is not small at these energies. In the second step, we proceed to hadronize the $\bar{q}\Gamma q$ currents (with $\Gamma=\{1,\gamma_5,\gamma_\mu,\gamma_\mu\gamma_5,\sigma_{\mu\nu},\sigma_{\mu\nu}\gamma_5\}$) into observable pseudoscalar and vector mesons, and analogously, for the gluons from Fig. 3.6. Let us now discuss separately the two points stated above.

3.3.1 Perturbative amplitudes

The SMEFT framework provides the processes $\tau \to (\ell + \text{hadrons})$ already at the tree level. Operators in Table 3.1 generate two kinds of contributions:

i) Those yielding a two-quark current $\tau \to \ell\bar{q}q$ (shown in Fig. 3.5), either provided by local vertices as in (a), or by gauge-boson (b) or Higgs (c) exchanges; in the latter case, we will consider massless up and down quarks, but $m_s \neq 0$, and, accordingly, the diagram (c) will only contribute to the production of $\bar{s}s$.
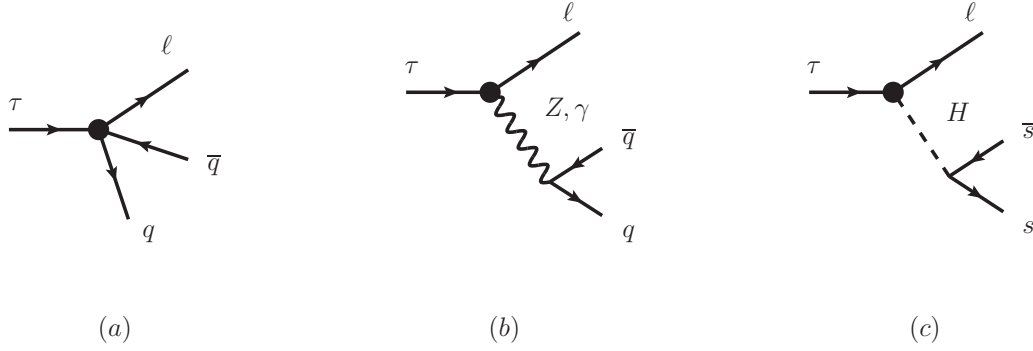
FIGURE 3.5:   Different contributions of the SMEFT Lagrangian to $\tau \to \ell\,\overline{q}q$, with $\ell = e, \mu$. The dot indicates the CLFV vertex. We consider $m_u = m_d = 0$, but $m_s \neq 0$: the contribution of the Higgs in (c) thus only exists for the production of $\overline{s}s$.
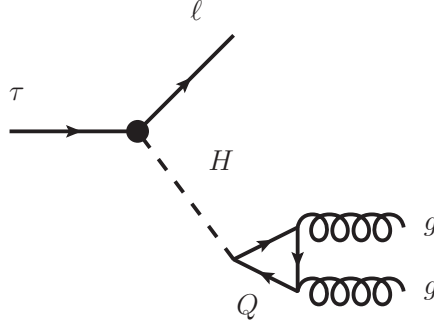
FIGURE 3.6:   Dominant scalar contribution [154] to $\tau \to \ell\overline{P}P$, with $\ell = e, \mu$ and $P = \pi, K$. The dot indicates the CLFV vertex. The Q in the loop stands for a heavy quark, namely $Q = c, b, t$.

ii) The scalar two-gluon contribution $\tau \to \ell gg$ (shown in Fig. 3.6), with heavy quarks in the finite fermion loop, that was also considered previously in Ref. [154]; here it was concluded that, in spite of the loop suppression, this is the dominant Higgs contribution to these processes.

The results of the tree-level amplitudes related to diagrams from Fig. 3.5 and generated by LFV operators from Table 3.1 are collected in Section C.1 of Appendix C; the loop contribution from Fig. 3.6 is given in Section C.2. In the latter amplitude, we have written (for hadronization purposes) the two-gluon final state in terms of the trace of the energy–momentum tensor [155], as explained in Section D.1 of Appendix D. Accordingly, the general perturbative amplitude that describes the CLFV tau decays into hadrons is given by

$$\mathcal{M}_\tau = \mathcal{M}_{\text{tree}} + \mathcal{M}_{\tau gg}\,, \tag{3.3.5}$$

with $\mathcal{M}_{\text{tree}}$ and $\mathcal{M}_{\tau gg}$ defined in Eqs. (C.1.1) and (C.2.7), respectively.

3.3.2 Hadronization

Our results for the tau decay amplitude $\mathcal{M}_\tau$ are given, for the tree-level contributions, in terms of light-quark bilinears, and, for the gluon case, by the energy–momentum tensor. The final states we take into account involve pseudoscalar mesons and vector resonances. Therefore, we need to hadronize the quark bilinears and the energy–momentum tensor. We have seen in Section 2.3 that Chiral Perturbation Theory [31, 32] provides a model-independent scheme for this procedure. Unfortunately, this framework only provides reliable results (typically) for $E \ll 1\,\mathrm{GeV}$, while the mass of the tau lepton is much larger: the energy region, that happens to be populated by hadron resonances, becomes kinematically available and relevant for the final state. A complementary tool to handle this scenario consistent with the constraints of the chiral symmetry was given in Section 2.4 by the name of Resonance Chiral Theory [41–43]. It provides us with a phenomenological Lagrangian, driven also by the chiral symmetry, that includes not only the light pseudoscalar mesons, but also the lightest U(3) nonets of resonances that remain in the large-number-of-colors framework (i.e. when $N_\mathrm{C} \to \infty$). We refer the reader to Section 2.4 for a detailed explanation. In addition, external currents with appropriate quantum numbers allow to hadronize the relevant quark bilinears. The specific procedure to perform the hadronization of the latter as well as to include the relevant resonances within the RχT framework is explained in Section 2.4.3. Let us sketch the main steps based on the results shown in those sections. From the equalities obtained in Eqs. (2.4.52) and (2.4.54) we are able to relate the quark bilinears (2.4.52) to the hadronized pseudoscalar mesons and vector resonances (2.4.54). However, these are not the final results of the hadronization. The resonance chiral Lagrangian provides additional interactions that allow us to introduce intermediate resonances contributing to the currents of Eq. (2.4.52). The mesonic final states will be two pseudoscalars $P_1 P_2$, one pseudoscalar P, or one vector resonance V. The final results are:

$$[\, i\, \overline{q}_i\, \gamma_5\, q_j \;\to\; P\,] \simeq 2\, B_0\, F\, \Omega_P^{(1)}(ij) \;+\; 2\, \frac{B_0}{F}\, \frac{d_m^2}{M_P^2}\, m_K^2\, \Omega_P^{(2)}(ij)\,,$$

$$[\, \overline{q}_i\, \gamma_\mu\, \gamma_5\, q_j \;\to\; P\,] \simeq -i\, 2\, F\, \Omega_A^{(1)}(ij)\, p_\mu\,,$$

$$[\, \overline{q}_i\, \gamma_\mu\, q_j \;\to\; V\,] \simeq -2\, F_V\, M_V\, \Omega_V^{(1)}(ij)\, \varepsilon_\mu\,,$$

$$[\, \overline{q}_i\, \sigma_{\mu\nu}\, q_j \;\to\; V\,] \simeq i\, 2\, \frac{T_V}{M_V}\, \Omega_T^{(1)}(ij)\, (\, p_\mu\, \varepsilon_\nu\; -\; p_\nu\, \varepsilon_\mu\,)\,,$$

$$[\, \overline{q}_i\, q_j \to P_1\, P_2\,] \simeq 2\, B_0\, \Omega_S^{(1)}(ij)\, \left[\, 1 + 4\, \frac{L_5^{\mathrm{SD}}}{F^2}\, \left(s - m_1^2 - m_2^2\right) \right] + 2\, \frac{B_0}{F^2}\, \frac{d_m^2}{M_P^2}\, m_K^2\, \Omega_S^{(2)}(ij)$$

$$+\frac{B_0}{F^2}\, c_m \sum_S \frac{\Omega_S^{(3)}(ij)}{s\, -\, M_S^2}\, \left[\, c_d\, \Omega_S^{(4)}\, \left(s\, -\, m_1^2\, -\, m_2^2\right) \;+\; 2\, c_m\, m_K^2\, \Omega_S^{(5)}\, \right]$$

$$+\frac{1}{3}\, \frac{B_0}{F^2}\, \gamma \sum_T \frac{\Omega_T^{(2)}(ij)}{M_T^4}\, \Big\{\, g_T\, \Omega_T^{(3)}\, \big[\, (m_1^2 - m_2^2)^2 \;+\; M_T^2\, (m_1^2 + m_2^2)$$

$$-s\, (M_T^2\, +s)\, \big] + 2\, (2M_T^2 + s)\, \left[\, \beta\, \Omega_T^{(4)}(m_1^2 + m_2^2 - s)\, -\, 2\, \gamma\, m_K^2\, \Omega_T^{(5)}\, \right] \Big\}\,,$$

$$[\,\bar{q}_i\,\gamma_\mu\,q_j \to P_1\,P_2\,] \simeq \left[\,2\,\Omega_V^{(2)}(ij) + \sqrt{2}\,\frac{F_V\,G_V}{F^2}\sum_V \frac{s}{M_V^2 - s}\,\Omega_V^{(1)}(ij)\,\Omega_V^{(3)}\right](\,p_1 - p_2\,)_\mu$$

$$+ \left[\,\sqrt{2}\,\frac{F_V\,G_V}{F^2}\,(m_2^2 - m_1^2)\sum_V \frac{\Omega_V^{(1)}(ij)\,\Omega_V^{(3)}}{M_V^2 - s}\right](\,p_1 + p_2\,)_\mu\,,$$

$$[\,\bar{q}_i\,\sigma^{\mu\nu}\,q_j \to P_1\,P_2\,] \simeq \frac{i}{F^2}\left[\,-\Lambda_2^{\rm SD}\,\Omega_T^{(6)}(ij) + 2\,\sqrt{2}\,G_V\,T_V\sum_V \frac{\Omega_T^{(1)}(ij)\,\Omega_V^{(3)}}{M_V^2 - s}\right](\,p_1^\mu\,p_2^\nu - p_1^\nu\,p_2^\mu\,)\,.$$

$$(3.3.6)$$

Note that the remaining currents in Eq (2.4.52) do not contribute to these final states. The dimensionless parameters Ω identify the different intermediate and final states and are listed in Appendix E.1. These results within the RχT correspond to a model of the Large-$N_{\rm C}$ limit, assuming that only the lightest multiplet of intermediate resonances (that survive in the $N_{\rm C} \to \infty$ limit) contribute to the dynamics. The widths of resonances appear at the subleading order ($\mathcal{O}(1/N_{\rm C})$), and are therefore not present in the expressions above. However, this is not satisfactory from the phenomenological point of view and we thus implemented the widths in the corresponding poles: $[M_R^2 - s] \to [M_R^2 - s - iM_R\Gamma_R]$. Moreover, a constant width reasonably represents only narrow resonances (typically when $\Gamma_R/M_R \lesssim 0.1$) and in such a case it is a good approximation. The analytical construction of momentum-dependent widths is only known for dominant two-body decays [156].

The hadronization of the vector current into two pseudoscalars of equal mass[4] is driven by the well-known vector form factor, that has been thoroughly studied in the literature. In fact, the expression in Eq. (3.3.6) is just the starting point of a more thorough model-independent construction based both on the RχT and the use of dispersion relations [157–159] or Padé approximants [160]. The vector form factor for the pseudoscalar P is defined as

$$\langle P(p_1)\overline{P}(p_2)|V_\mu^{\rm EM}|0\rangle = (p_1 - p_2)_\mu F_{\rm V}^P(q^2)\,, \tag{3.3.7}$$

where $q = p_1 + p_2$, and where the electromagnetic current is defined by

$$V_\mu^{\rm EM} = \sum_q Q_q\,\bar{q}\,\gamma_\mu\,q = V_\mu^3 + \frac{1}{\sqrt{3}}\,V_\mu^8\,, \tag{3.3.8}$$

with Q_q standing for the electric charge (in units of e) of the quark $q = u, d, s$. Hence, we notice that, for instance, we can hadronize the $\bar{u}\gamma_\mu u$ current through

$$\langle P(p_1)\overline{P}(p_2)|\bar{u}\gamma_\mu u|0\rangle = (p_1 - p_2)_\mu F_{\rm V}^P(q^2) + \frac{2}{\sqrt{6}}\,\langle P(p_1)\overline{P}(p_2)|V_\mu^0|0\rangle\,. \tag{3.3.9}$$

Analogous expressions could be obtained for the $\bar{d}\gamma_\mu d$ and $\bar{s}\gamma_\mu s$ currents, where the V_μ^3 current appears in addition on the r.h.s. We only applied this procedure to the hadronization of the u-quark current in order to point out the possibility for further improvements. The singlet vector current was determined using the RχT

---

[4]For two pseudoscalars of different mass the matrix element has, in addition, another form factor.

framework, giving

$$V_\mu^0 = F_V \left[\sin\theta_V \, \partial^\nu \phi_{\nu\mu} - \cos\theta_V \, \partial^\nu \omega_{\nu\mu} \right], \qquad (3.3.10)$$

which further contributes to the hadronization of two pseudoscalars. For our vector form factor $F_V^P(q^2)$, we employed the result from Appendix B of Ref. [161], modifying the hadronization for the final states $\pi^+\pi^-$, K^+K^- and $\overline{K}^0 K^0$.

We turn now to the hadronization of the two gluons from the diagram in Fig. 3.6. The amplitude represented by this diagram contributes only to two pseudoscalars in the final state, and is given in Eq. (C.2.7) of Appendix C.2 in terms of the matrix element $\theta_P(q^2)$ of the energy–momentum tensor (see Section D.1 in Appendix D). We could perform an evaluation of the matrix element within the RχT, but final-state interactions in the two-pseudoscalar final state are ruled by the $I = J = 0$ scattering phase shift. This implies that such interactions are important and have to be considered, for instance, using dispersion relations. This was already pointed out in Ref. [155] for $\pi\pi$ and $\overline{K}K$, and has been recently reevaluated for the two-pion case in Ref. [154]. We only considered the $\pi\pi$ final state and we used the results of the latter reference: incidentally, they have also improved the matrix element for the two-pion final state of the mass term $m_s \bar{s}s$ (see Eq. C.1.6), which we also used.

3.4 ℓ–τ conversion in nuclei

The conversion among flavors of charged leptons in the presence of a nucleus is a well-motivated scenario to study CLFV phenomena that has been pursued already in the past, namely for the μ–e conversion in nuclei with the strongest limit set by Sindrum II [162]:

$$\mathcal{B}_{\mu e}^{Au} = \frac{\Gamma(\mu^- \, Au \to e^- \, Au)}{\Gamma_{\text{capture}}(\mu^- \, Au)} < 7 \times 10^{-13}, \quad 90\% \, \text{C.L.} \qquad (3.4.11)$$

The μ–e experiments are of a different nature than those concerning the τ lepton: typically, these experiments are performed at low energy and the muon becomes bounded before decaying in orbit or being captured by the nucleus.

For ℓ–τ with $\ell = e, \mu$, the conversion is expected to occur by deep inelastic scattering of the lepton off the nucleus, thus these experiments are based on a fixed-target nucleus hit by an incoming lepton beam of a given flavor ℓ. If the energy of the beam is high enough, they will penetrate the hadronic structure of the nucleons within the nucleus and interact with its constituents, the partons, i.e. quarks and gluons. Due to the fact that lepton flavor is conserved within the SM (which also holds at the tree level for the charged-lepton sector in its minimally extended version), a change of the flavor of the incoming charged lepton as a result of the interaction with nuclei is forbidden. Therefore, any measurable signal of a process of this kind would suggest new physics.

Our aim here was to perform a model-independent analysis within the SMEFT framework of ℓ–τ conversion in nuclei ($\ell = \mu, e$). Regarding the product of the interaction, we consider a τ lepton plus any hadronic content of no particular relevance
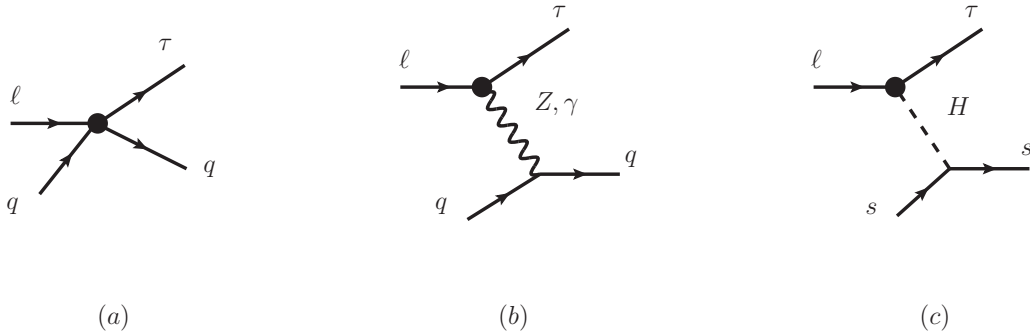
FIGURE 3.7:   Different contributions of the SMEFT Lagrangian to $\ell q \to \tau q$ for $\ell = e, \mu$ and $q = u, d, s$. The dot indicates the CLFV vertex. We consider $m_u = m_d = 0$ but $m_s \neq 0$. Hence, the contribution of the Higgs in (c) only exists for $q = s$.

to us, i.e. we are only interested in the inclusive process $\ell + \mathcal{N}(A, Z) \to \tau + X$, where we do not have any information about X.

Since the interacting parton lives in the hadronic environment of the nucleus, its dynamics is heavily influenced by low-energy non-perturbative QCD effects. However, we can make use of QCD factorization theorems to separate the non-perturbative behaviour — encoded in the so-called parton distribution functions (PDFs) — from the part that we can compute perturbatively. Once the perturbative calculation is done, we calculate the convolution of the result with the PDFs to obtain the total cross section of the process.

3.4.1   Perturbative amplitudes

The perturbative cross sections involved in this process are computed using the SMEFT operators listed in Table 3.1. These yield three different leading contributions:

i) The process $\ell q \to \tau q^{(\prime)}$ (see Fig. 3.7), represented in terms of local vertices (a), the gauge-boson (b), and Higgs (c) exchange. We consider massless up and down quarks, while $m_s \neq 0$: the diagram (c) thus only contributes to the production of $\bar{s}s$.

ii) The same process as i), but with antiquarks: $\ell \bar{q} \to \tau \bar{q}^{(\prime)}$. This leads to different cross sections of the process and also the non-perturbative behaviour of antiquarks inside the nucleons is not the same as of their opposite-charged partners.

iii) The process $\ell g \to \tau g$ (see Fig. 3.8), represented by the Higgs (a) or Z-gauge-boson (b) exchange, and a quark triangle loop.

Note that for the processes of type i) and ii), $\ell q(\bar{q}) \to \tau q^{(\prime)}(\bar{q}^{(\prime)})$, we may also allow for quark-flavor change. Therefore, we also take into account quark currents such as $\bar{c}u, \bar{b}s, \ldots$, which contribute to the total amplitude only via contact-interaction contribution, i.e. via the process depicted in Fig. 3.7(a). Nevertheless, we consider the same Wilson coefficients for all quark flavors, thus assuming minimal flavor
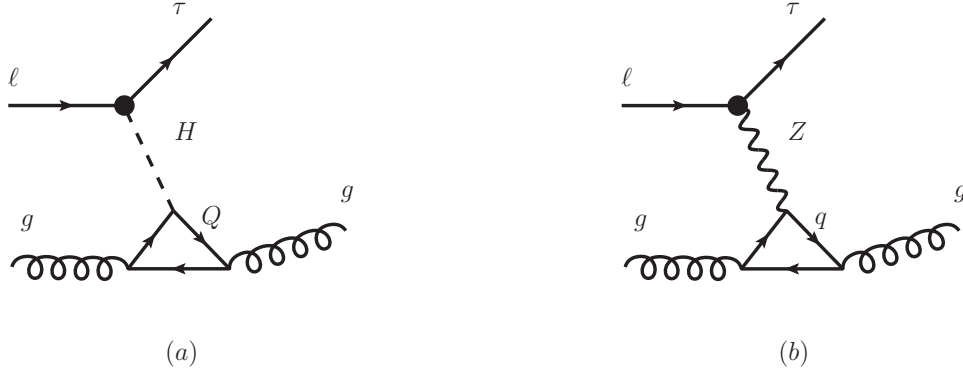
FIGURE 3.8: Higgs and Z contribution to $\ell g \to \tau g$, with $\ell = e, \mu$. The dot indicates the CLFV vertex. Q is a heavy quark, namely $Q = c, b, t$, and $q = u, d, c, s, t, b$.

violation in the quark sector (driven only by the CKM matrix). Allowing quarks to change flavor during the interaction allows us to consider a wider variety of final states for the hadronic τ decays, as well as it leads to an increased cross section of the process of ℓ–τ conversion in nuclei. This implies a richer phenomenology and stronger constraints on the Wilson coefficients. These flavor-changing neutral currents are forbidden at the tree level in the SM due to the GIM mechanism [6], while there is no reason to assume that such a mechanism is also relevant for the beyond-Standard Model physics at higher energy scales. We thus studied both cases: 1) CLFV with FCNC, and 2) CLFV only. However, for the first scenario, one could expect the CLFV and FCNC phenomena to be mediated by different type of new physics, since there might be no reason for both phenomena to be related to each other. Describing both interactions within the SMEFT framework, this would mean different energy scales Λ. In spite of these considerations, as we were studying both scenarios, we assumed throughout the whole work only one energy scale driving all new-physics interactions, and thus implicitly considering the same energy scale for both phenomena.

The results for the tree-level amplitudes shown in Fig. 3.7 and generated by LFV operators from Table 3.1 are given in Section C.1 of Appendix C. Regarding the contribution iii), for the Higgs exchange with heavy quarks in the finite fermion loop (as it happened in its hadronic τ decay counterpart; see Fig. 3.6) it was shown in Ref. [142] that (in spite of the loop suppression) this is the dominant Higgs contribution to the ℓ–τ conversion in nuclei. We also conclude that the diagram in Fig. 3.8 (b) is not negligible compared to the Higgs exchange: actually, they are of the same order of magnitude. All the relevant amplitudes for process iii) are collected in Section C.3 of Appendix C, while for a thorough discussion regarding the contribution shown in Fig. 3.8 (b), an interested reader is referred to Section D.2 of Appendix D. Accordingly, the general perturbative amplitudes that describe the CLFV $\mu(e)$–τ conversion in nuclei are given in terms of the amplitudes from Appendix C, using

i)

$$\mathcal{M}_{qq} = \mathcal{M}_{\mathrm{loc}} + \mathcal{M}_Z + \mathcal{M}_\gamma + \mathcal{M}_H \,, \tag{3.4.12}$$

ii)

$$\mathcal{M}_{\bar{q}\bar{q}} = \mathcal{M}'_{\mathrm{loc}} + \mathcal{M}'_Z + \mathcal{M}'_\gamma + \mathcal{M}'_H \,, \tag{3.4.13}$$

iii)

$$\mathcal{M}_{gg} = \mathcal{M}_{Hl} + \mathcal{M}_{Zl} \,, \tag{3.4.14}$$

where $\mathcal{M}'$s stand for the same amplitudes as those from Appendix C, but for anti-quarks.

3.4.2   Non-Perturbativity: Nuclear parton distribution functions

Nuclei are bound systems where the low-energy non-perturbative effects of QCD among their constituents are non-negligible. Therefore, to address this problem properly, we make use of quantities that describe these long-distance effects: the parton distribution functions. By means of the QCD factorization theorems, the total cross section can be computed as a convolution of the non-perturbative PDFs (f) and the perturbative cross sections ($\hat{\sigma}$) calculated using the amplitudes of the previous section (Section 3.4.1):

$$\sigma_{\ell-\tau} = \hat{\sigma} \otimes f \,. \tag{3.4.15}$$

The total cross section is an observable quantity. However, since the perturbative cross sections are computed within perturbation theory, our inability to calculate them at every order of the perturbative expansion generates a non-physical dependence on the energy scale which propagates into the PDFs; this also means that they depend on the renormalization scheme. The above-mentioned scale is usually taken as $Q^2 = -q^2$, with q^2 being the transferred momentum of the system; Q^2 is also often called the characteristic scale of the process. Furthermore, it is customary to characterize the PDFs through the Lorentz invariant quantity ξ, the fraction of the nucleus momentum carried by the interacting parton. Consequently, we express the perturbative cross section as well as the PDFs in terms of the two discussed invariant quantities

$$\sigma_{\ell-\tau} = \hat{\sigma}(\xi, Q^2) \otimes f(\xi, Q^2) \,, \tag{3.4.16}$$

where the total cross section still depends on the Wilson coefficients C_i and the BSM energy scale Λ_{CLFV}.

Whereas the dependence of the PDFs on the momentum fraction ξ is completely non-perturbative and has to be extracted from the data, their evolution in terms of Q^2 is achieved by using the DGLAP evolution equations: once the PDFs are determined at a given scale Q_0^2, we can calculate it at any other scale Q^2. There are several groups performing this global QCD analysis using state-of-the-art perturbative theoretical computations to obtain the best PDFs given the current data; for an overview of the field, see Ref. [163] and references therein. Since, in our case, we are dealing with heavy nuclei instead of free nucleons, nuclear binding effects alter significantly the non-perturbative behaviour of the constituents at different ξ

regimes, as it was first pointed out in Ref. [164]. All these effects are included in the nuclear parton distribution functions (nPDFs), which we find more suitable to describe the ℓ–τ conversion in nuclei: we use the nCTEQ15-np fit of the nPDFs provided by the group around the nCTEQ15 project [165], incorporated within the ManeParse Mathematica package [166].

3.4.3   Total cross section

The convolution of the perturbative and non-perturbative pieces is a rather complicated topic due to higher-order QCD corrections, target mass corrections, etc. However, when including next-to-leading-order QCD corrections, it can be shown within the QCD-improved parton model [167] that the modifications can be absorbed into the PDFs, while keeping the perturbative cross sections at tree level. This is the leading-order QCD formalism (or twist-2 factorization) which we follow in this work: our SMEFT perturbative cross sections are calculated at tree level, while the nCTEQ15 nPDFs that we use are computed at NLO [165]. We would like to point out that the twist-2 factorization is appropriate in the limit of massless partons [168]. This may be the case for the u, d and s quarks, however, note that larger uncertainties are expected when considering the quark currents of diagrams of type (a) in Fig. 3.7 of processes i) and ii) with massive c and b quarks. Notwithstanding, this is partially mitigated by the typical small value taken by the PDFs for the less-probable-to-find-in-nucleus c and b quarks.

The perturbative unpolarized differential cross sections for the processes from Section 3.4.1 (contributing to ℓ–τ conversion in nuclei) in terms of the invariants ξ and Q^2 and computed within the SMEFT framework (using the operators from Table 3.1) are

$$\frac{d\hat{\sigma}(\ell\, n_i(\xi P) \to \tau\, n_j)}{d\xi dQ^2} = \frac{1}{16\pi\lambda(s(\xi), m_\ell^2, (\xi M)^2)} \overline{|\mathcal{M}_n(\xi, Q^2)|^2}, \qquad (3.4.17)$$

with $n_i = q_i, \bar{q}_i, g$ and the momentum of the interacting parton $p_i = \xi P$ being a fraction of the nucleus total momentum P; thus, we have considered above $p_i^2(= m_i^2) = \xi^2 M^2$ since only the nucleus mass M is physical. $\lambda(a, b, c) \equiv (a + b - c)^2 - 4ab$ is the Källén's triangle function. Finally, using the LO QCD formalism, the total differential cross section reads

$$\sigma(\ell\,\mathcal{N}(P) \to \tau\,X) = \sum_{i,j} \int_{\xi_{\min}}^1 \int_{Q_-^2(\xi)}^{Q_+^2(\xi)} d\xi dQ^2 \left\{ \frac{d\hat{\sigma}(\ell\, q_i(\xi P) \to \tau\, q_j)}{d\xi dQ^2}\, f_{q_i}(\xi, Q^2) \right.$$

$$\left. + \frac{d\hat{\sigma}(\ell\, \bar{q}_i(\xi P) \to \tau\, \bar{q}_j)}{d\xi dQ^2}\, f_{\bar{q}_i}(\xi, Q^2) + \frac{d\hat{\sigma}(\ell\, g(\xi P) \to \tau\, g)}{d\xi dQ^2}\, f_g(\xi, Q^2) \right\}.$$

$$(3.4.18)$$

The integration limits are given in Appendix F.

3.5   Numerical results

In this section, we present the main features and results of our numerical analysis performed on the SMEFT $d = 6$ operators generating CLFV τ-involved processes: hadronic τ decays and ℓ–τ conversion in nuclei. In the first part, we introduce the HEPfit tool [169] employed in the analysis and its statistical framework. We also present the existing or expected experimental limits on these processes. In the second part, we present the results of the fits for each process class (tau decays or conversion in nuclei) individually as well as the combined analysis, making always the distinction between the 1) CLFV with FCNC, and 2) CLFV only cases.

3.5.1   Set-up

The effects of new physics on the physical observables are parametrized within the SMEFT framework by the Wilson coefficients C_i and the energy scale where the new degrees of freedom live; in our case we denote this scale as Λ_{CLFV}. In general, every observable with a specific experimental bound will depend on several WCs. Consequently, in our work, we have a set of observables related to CLFV phenomena, each depending on several WCs and Λ_{CLFV}. Our goal is to translate the available information on the former into relations and constraints for the latter. Actually, we got bounds on the ratios $C/\Lambda_{\mathrm{CLFV}}^2$.

HEPfit

To achieve the stated goal above, we made use of the open-source code HEPfit [169]. This program was born as a tool to combine several different experimental and theoretical data from various sources, aiming to optimize the sensitivity of current searches to new physics, e.g. by narrowing down regions of the parameter space that turn out to be excluded once several constraints are considered at the same time. The use-case of HEPfit is two-fold: on one hand it can be used as a library to compute a great deal of built-in observables (or to extend this list) calculated up to high orders in the corresponding theoretical expressions; on the other hand, HEPfit is embedded with a Bayesian statistical framework that uses a Markov chain Monte Carlo (MCMC) routine, which can be used to sample a large parameter space. We took profit of the latter and made use of HEPfit to sample our complete WC parameter space. As the output, we obtain bounds on the possible values for the WCs at different confidence levels, as well as the correlations among all of them.

Let us elaborate further on the statistical framework used by HEPfit. This follows the Bayesian statistical approach, whose posterior probability distribution — the probability distribution of the values of the parameters $\vec{\mathbf{C}}$ (in our case the ratio $C/\Lambda_{\mathrm{CLFV}}^2$) given the data D (in our case the bounds on hadronic tau decays and ℓ–τ conversion in nuclei) — takes the form

$$P(\vec{\mathbf{C}}|D) = \frac{P(D|\vec{\mathbf{C}})P_0(\vec{\mathbf{C}})}{\int P(D|\vec{\mathbf{C}})P_0(\vec{\mathbf{C}})d\vec{\mathbf{C}}} \, . \tag{3.5.19}$$

Above $P_0(\vec{C})$ is the prior distribution of the parameters, i.e. the knowledge we have in advance about the parameters expressed in terms of their initial probability distributions. The priors are of paramount importance within the Bayesian statistical framework and, as we have for instance checked, a different initial choice of those although providing similar results for the constraints on the parameters, it leads to different results for the sampled observables after the fit. In our case we used for the WCs flat distributions centered around zero, since we did not have any reason to favor some values over others. The other term in the numerator $P(D|\vec{C})$ is the likelihood: the probability of having the data (D) given some values of the parameters ($\vec{C}$), i.e. it encodes the theoretical relations among the $C/\Lambda^2_{\text{CLFV}}$ ratio and the observable data. The denominator is the so-called normalization, but a MCMC analysis with a large parameter space (as it is the case) provides unnormalized posterior distributions and then we forget about the normalization in the following.

Schematically, the MCMC routine makes use of the unnormalized posterior distribution (the numerator of Eq. (3.5.19)) to sample the parameter space: firstly, a random choice of the parameter vector $\vec{C}$ is made in each chain and the posterior is computed, then a Metropolis-Hasting algorithm consistently computes $P(D|\vec{C})P_0(\vec{C})$, for choices of the parameters with higher probabilities, until a stationary state is reached based on a targeted efficiency. For more details of the MCMC implementation we refer to Refs. [169–172]. All in all, we end up with an unnormalized posterior distribution of all the parameters $P(\vec{C}|D)$, from which the marginalized posterior distributions of the individual parameters are computed via

$$P(C_i|D) = \int P(\vec{C}|D) \prod_{j \neq i} dC_j \,, \tag{3.5.20}$$

so integrating the total posterior over all parameters except the one for which we are computing it.

Due to the fact that the studied CLFV processes depend on more than one WC, we could not know which WC (or WCs) is (are) behind one possible experimental signal. Measurements of other CLFV processes would be required in order to answer what kind of NP is responsible for these observations. This is where the main importance of our general (marginalized) numerical analysis lies. Without additional information, a naive analysis of the sensitivity of the observables on individual Wilson coefficients would lead to overestimated (too strong) bounds on the latter: if the actual new physics contributes through more than one operator, this sensitivity gets diluted due to the correlations among different WCs.

Experimental bounds

The best experimental results on CLFV hadronic τ decays (as upper limits on the widths) have been given mainly by Belle and BaBar (see Fig. 3.3) [173]. Possible final states considered in this work are

$$
\begin{aligned}
\tau \to \ell P : \qquad & P = \pi^0, K^0, \eta, \eta' \,, \\
\tau \to \ell P_1 P_2 : \qquad & P_1 P_2 = \pi^+\pi^-, K^0\bar{K}^0, K^+K^-, \pi^+K^-, K^+\pi^- \,,
\end{aligned}
\tag{3.5.21}
$$

$$\tau \to \ell V : \qquad\qquad V = \rho^0(770), \omega(782), \phi(1020), K^{*0}(892), \bar{K}^{*0}(892) \,,$$

with $\ell = e, \mu$. Note that in Appendix E.1 we give the RχT results for the hadronization of the quark currents into two pseudoscalars for more states than those listed here. This is because of the lack of experimental data on those decays; there are still many processes that have not been searched for. The expressions for the decay widths and our definition of the width of tau decays into hadron resonances are given in Appendix G. This analysis is expected to be improved when new data appear and better bounds are set, as it should be the case with Belle II [71]: they claim an improvement on the sensitivity by at least one order of magnitude. Hence, we also consider the Belle II expected limits.

Regarding ℓ–τ conversion in nuclei, there are no experimental limits yet. However, for the numerical analysis and intending to show the relevance of this process for CLFV searches, we consider the most conservative expected sensitivity of the NA64 experiment [138] (and for reasons that will become clear below, we also consider a potential improvement of two orders of magnitude). This can be further translated in terms of the limits on the physical observables of our interest as

$$R_{\ell\tau} = \frac{\sigma(\ell\,\mathcal{N} \to \tau\,X)}{\sigma(\ell\,\mathcal{N} \to \ell\,X)} \sim 10^{-13} - 10^{-12} \quad (\sim 10^{-15}) \,. \tag{3.5.22}$$

Here, the numerator is given by Eq. (3.4.18) and the denominator is the dominant contribution to the inclusive $\ell + \mathcal{N}$ process: the lepton bremsstrahlung on nuclei, that we take from Eq. (21) of Ref. [138]. We use two specific nuclei, namely Fe(56,26) and Pb(208,82). Following the prospects of this experiment, we consider for the energy of the incident lepton beam $E_e = 100\,\mathrm{GeV}$ and $E_\mu = 150\,\mathrm{GeV}$ for electrons and muons, respectively.

Wilson coefficients

In what follows, we slightly modify the basis of $d = 6$ operators contributing to CLFV shown in Table 3.1, so that it suits better our study. We comment on some (hopefully well-motivated) modifications of several WCs, as well as their running.

-Redefinitions

We find that the operators $\mathcal{O}_{\varphi L}^{(1)}$ and $\mathcal{O}_{\varphi L}^{(3)}$ lead to the same contribution to CLFV τ-involved processes. Therefore, our analysis is not sensitive to associated WCs separately, but only to their combination, namely

$$C_{\varphi L}^{(1)\prime} \equiv C_{\varphi L}^{(1)} + C_{\varphi L}^{(3)} \,. \tag{3.5.23}$$

Likewise, for the non-FCNC case, once the analysis is performed, it turns out that we cannot distinguish between this redefined $C_{\varphi L}^{(1)\prime}$ and $C_{LQ}^{(3)}$. This forces us to consider only the following combination as independent:

$$C_{LQ}^{(3)\prime} \equiv C_{LQ}^{(3)} + C_{\varphi L}^{(1)} + C_{\varphi L}^{(3)} \,. \tag{3.5.24}$$

Similarly, the contributions stemming from $\mathcal{O}_{eB}$ and $\mathcal{O}_{eW}$ are equal up to factors of $c_\mathrm{W} \equiv \cos\theta_\mathrm{W}$ and $s_\mathrm{W} \equiv \sin\theta_\mathrm{W}$, with θ_W being the weak angle (see Section 1.3).

We are thus again not sensitive to these two WCs, but only to their combination. Moreover, both operators contribute through a photon and Z exchange. Hence, to disentangle these contributions, we can do a 'rotation' of both WCs and define their particular combinations C_γ and C_Z as

$$\begin{pmatrix} C_\gamma \\ C_Z \end{pmatrix} = \begin{pmatrix} c_{\mathrm{W}} & -s_{\mathrm{W}} \\ s_{\mathrm{W}} & c_{\mathrm{W}} \end{pmatrix} \begin{pmatrix} C_{eB} \\ C_{eW} \end{pmatrix}. \tag{3.5.25}$$

We then put constrains on C_γ and C_Z instead of C_{eB} and C_{eW}.

-Running

As we discussed in Section 3.4.2, our inability to calculate the physical observables to all orders in the perturbation theory produces an artificial dependence of the WCs on the energy scale. Therefore, in order to compare the constraints set on the WCs coming from different processes at different energies, we should apply the renormalization-group equations to run all the WCs to the same energy scale. We only considered the QCD running since it is (by far) dominant, and performed the analysis at the scale of τ decays, i.e. the natural scale given by the mass of the tau[5].

Likewise, since, in effective field theories, the scale dependence of WCs is related to the scale dependence of associated currents of the fundamental theory, we should worry about them:

1. It is customary not to consider the QCD running of the vector current. On the one hand, the vector current is indeed always renormalized by effects that are isospin-breaking (in SU(2)) or SU(3)-breaking in the case of three flavors; see Sections 3.3.1 and 3.3.2 in Chapter 2 of Ref. [174], or Sections 8.1 and 8.2 in Chapter 8 of Ref. [175] or Ref. [176]. As a consequence, these effects are around 2% and 20% in the first and second cases respectively. In fact, it turns out that the corrections are even smaller because of, for instance, the Ademollo-Gatto theorem [177]. Hence, we understood, as it is usual in the literature, that they are small and not relevant in our case.

2. On the other hand, the axial-vector current is always renormalized by the breaking of the chiral symmerty, i.e. by terms proportional to the masses of the three lightest quarks (see the same references as for the vector-quark currents above). Accordingly, the corrections in this case are again 20% at most, and we thus neglect them since they are irrelevant for our analysis.

3. In the case of the scalar (pseudoscalar) quark currents, the running concerns the divergences of the vector (axial-vector) currents and quark masses. For instance [178],

$$\partial^\mu(\bar{s}\gamma_\mu u) = i(m_s - m_u)(\bar{s}u), \tag{3.5.26}$$

and, therefore, if we neglect the small running of the vector quark current (on the left), we conclude that the product of the quark masses times the scalar current has also a small QCD running that we, again, neglect. We applied

---

[5]We did not consider the running coming from electroweak (including electromagnetic) interactions, that are tiny (at these scales) in comparison to the one of QCD.

this idea both for $\bar{q}_i q_i$ and $\bar{q}_i q_j$, and we arrived at scale-independent C'_{LedQ} and $C^{(1)\prime}_{LeQu}$ using the following redefinitions:

$$C_{LedQ} = \frac{m_i}{m_\tau} C'_{LedQ}, \qquad\qquad C^{(1)}_{LeQu} = \frac{m_i}{m_\tau} C^{(1)\prime}_{LeQu}, \qquad (3.5.27)$$

where m_i stands for a quark mass stemming from the associated quark current. This allows us to remove the scale dependence of B_0 in τ decays through the χPT relation $2B_0 M_q \simeq M_p$, with $M_q = \text{diag}(m_u, m_d, m_s)$ being the diagonal matrix of the light quark masses and M_p the pseudoscalar physical-mass matrix defined in Eq. (2.4.55).

4. The running of the tensorial WC is given by

$$C^{(3)}_{LeQu}(m_\tau) = Z(m_\tau, \mu_{\ell-\tau}) \, C^{(3)}_{LeQu}(\mu_{\ell-\tau}), \qquad (3.5.28)$$

where $C^{(3)}_{LeQu}(m_\tau)$ is the WC at the scale of hadronic τ decays. The Z-factor is given by

$$Z(m_\tau, \mu_{\ell-\tau}) = \left[\frac{\alpha_s^4(m_\tau)}{\alpha_s^4(m_b)}\right]^{-\frac{12}{75}} \left[\frac{\alpha_s^5(m_b)}{\alpha_s^5(\mu_{\ell-\tau})}\right]^{-\frac{12}{69}}. \qquad (3.5.29)$$

Finally, the set of 15 independent WCs considered in our general (with FCNC) analysis reads

$$\left\{C^{(1)}_{LQ}, C^{(3)}_{LQ}, C_{eu}, C_{ed}, C_{Lu}, C_{Ld}, C_{Qe}, C'_{LedQ}, C^{(1)\prime}_{LeQu}, C^{(3)}_{LeQu}(m_\tau), C^{(1)\prime}_{\varphi L}, C_{\varphi e}, C_\gamma, C_Z, C_{e\varphi}\right\}. \qquad (3.5.30)$$

For the non-FCNC scenario, one needs to trade $C^{(1)\prime}_{\varphi L}$ and $C^{(3)}_{LQ}$ for their combination $C^{(3)\prime}_{LQ}$ from Eq. (3.5.24).

3.5.2   Results

Here, we present the main results obtained from the numerical analysis in several scenarios. First, we address the case of hadronic τ decays both for the existing Belle and expected Belle II limits. Second, we focus on ℓ–τ conversion in nuclei. Finally, we show the results of the combined analysis.

Hadronic τ decays

The observables used in this analysis are the branching ratios of τ decays into an electron or a muon and the hadronic final states given in Eq. (3.5.21). In total, there are 14 observables for each final-state-lepton flavor. Needless to mention, these observables are not equally sensitive to all WCs and the experimental limits are not equally strong either. This then leads to different constraints on the ratios $C/\Lambda^2_{\text{CLFV}}$ and correlations among them.

After using the current limits from Belle depicted in Fig 3.3, the corresponding results are shown in blue in Fig. 3.9. The least constrained WCs are — due to the small quark masses involved — the scalar (Higgs) $C_{e\varphi}$ and (up-type-quark)
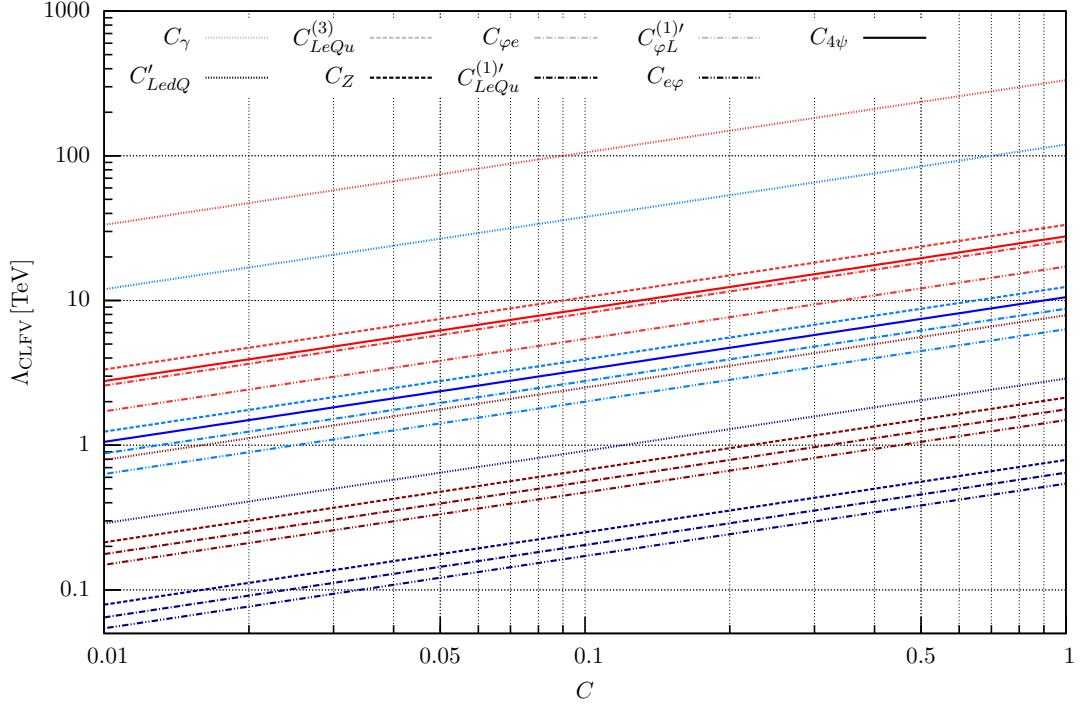
FIGURE 3.9: Constraints on Λ_{CLFV} with respect to the values of WCs, based on the current Belle (shades of blue) and expected Belle II (shades of red) limits, given at the 99.8 % confidence level. The four-fermion WCs are represented altogether as $C_{4\psi}$. For a given set of limits (distinguished by blue and red color shades), the lighter shades correspond to the WCs listed in the first row of the key (omitting now for a moment the common four-fermion WC $C_{4\psi}$) and the darker shades correspond to the WCs listed in the second row. To make the use of the plot even simpler, for a given set of bounds (red or blue lines), the WCs (again up to $C_{4\psi}$) are listed in the key in the same order as they appear in the plot, the light-shaded lines being always above the dark-shaded ones. Similarly, for a given WC, the red line appears always above the blue line, corresponding to stronger limits expected from Belle II.

$C_{LeQu}^{(1)\prime}$. These are followed by the 'rotated' C_Z and the other scalar $C_{LedQ}^{\prime}$. The $C_{\varphi L}^{(1)\prime}$ and $C_{\varphi e}$, both contributing via an intermediate-Z-exchange diagram, as well as the 4-fermion vectorial WCs are practically equally constrained: here, the down-type-quark WCs are constrained slightly stronger. The constraint on the tensorial $C_{LeQu}^{(3)}$ is then slightly stronger than on the 4-fermion ones. Finally, the strongest constraint is on the 'rotated' C_γ. Let us now comment on how the situation changes while including/excluding the FCNCs. First, the non-FCNC case results in an incapability of disentangling the contribution of $C_{LQ}^{(3)}$ and $C_{\varphi L}^{(1)\prime}$, i.e. a blind direction, so we are only sensitive to their combination (3.5.24). Second, FCNCs only happen through 4-fermion operators. One would then expect these to be less constrained in the non-FCNC case. However, the lost of sensitivity on $C_{LQ}^{(3)}$ and $C_{\varphi L}^{(1)\prime}$ separately results in lower correlations among the redefined $C_{LQ}^{(3)\prime}$, $C_{LQ}^{(1)}$ and C_{Lu}. As compared to the FCNC case, this in turn leads to a slightly stronger constraint on $C_{LQ}^{(3)\prime}$, equal constraints for both $C_{LQ}^{(1)}$ and C_{Lu}, and slightly weaker ones for the rest of the 4-fermion WCs. The later effect is enhanced even further for the cases of C_{eu}, C_{ed} and

C_{Qe} due to the increase of the correlations among these WCs. Note also that, due to the strong correlation between C'_{LedQ} and $C_{e\varphi}$, and the lower constraint on the former due to the previous argument, the constraint on the latter is also reduced in the non-FCNC case. Correlation matrices for the two aforementioned scenarios are presented in Figs. H.1 and H.2 of Appendix H. The stronger the correlation between two WCs, the more difficult is to disentangle each contribution separately, up to the point where a correlation $\rho = 1$ entails a blind direction such that we are only sensitive to a linear combination of the correlated WCs.

Considering WCs of $\mathcal{O}(1)$, the current Belle limits are probing energy scales up to ≈ 120 TeV: this holds for the best case related to C_γ, while the scale of 1 TeV is not reached for the least constrained WCs. This situation is expected to improve with Belle II by approximately a factor of 3. Examining the expected Belle II limits, depicted also in Fig 3.3, the analysis results in the same pattern of constraints as in the previous case of Belle limits, which are shown in red in Fig. 3.9 as well. In Table 3.2 we give (including FCNCs) the energy scales probed both by Belle and Belle II for WCs of order 1.

Bounds on Λ_{CLFV} [TeV]					
WC	Belle	Belle II	WC	Belle	Belle II
$C_{LQ}^{(1)}$	$\gtrsim 8.5$	$\gtrsim 26$	$C_{LeQu}^{(1)\prime}$	$\gtrsim 0.65$	$\gtrsim 1.8$
$C_{LQ}^{(3)}$	$\gtrsim 7.5$	$\gtrsim 21$	$C_{LeQu}^{(3)}$	$\gtrsim 12$	$\gtrsim 33$
C_{eu}	$\gtrsim 7.7$	$\gtrsim 22$	$C_{\varphi L}^{(1)\prime}$	$\gtrsim 6.3$	$\gtrsim 17$
C_{ed}, C_{Ld}	$\gtrsim 10$	$\gtrsim 26$	$C_{\varphi e}$	$\gtrsim 8.8$	$\gtrsim 26$
C_{Lu}	$\gtrsim 6.5$	$\gtrsim 20$	C_γ	$\gtrsim 120$	$\gtrsim 330$
C_{Qe}	$\gtrsim 11$	$\gtrsim 28$	C_Z	$\gtrsim 0.79$	$\gtrsim 2.1$
C'_{LedQ}	$\gtrsim 2.9$	$\gtrsim 7.9$	$C_{e\varphi}$	$\gtrsim 0.54$	$\gtrsim 1.5$

TABLE 3.2: Bounds on the new-physics energy scale mediating CLFV phenomena (Λ_{CLFV}) in tau decays. Here, we consider $C \approx 1$. The results are based on Belle and Belle II limits, given at the 99.8 % confidence level.

The results presented above were obtained from a marginalized analysis where all WCs are considered to be present at the same time. Let us now comment on another important result of the work presented here, i.e. the difference between marginalized and individual analyses. In order to present the results in dimensionless units, we consider the ratio $C/(G_\mathrm{F}\Lambda^2)$ instead. In Fig. 3.10 we compare the bounds on the Wilson coefficients from Belle and Belle II limits, obtained from an individual analysis, i.e. when only one of the operators and accompanying Wilson coefficients is considered to contribute to the observables at a time. The two τ-decay channels which restrict the given Wilson coefficient the most are shown. This scenario gives the most stringent bounds since correlations among the parameters are omitted. A more realistic scenario is given in Fig. 3.11, where we present the same bounds set on $C/(G_\mathrm{F}\Lambda^2)$ from a marginalized analysis, i.e. when all Wilson coefficients are varied simultaneously. This kind of analysis gives a more accurate picture since
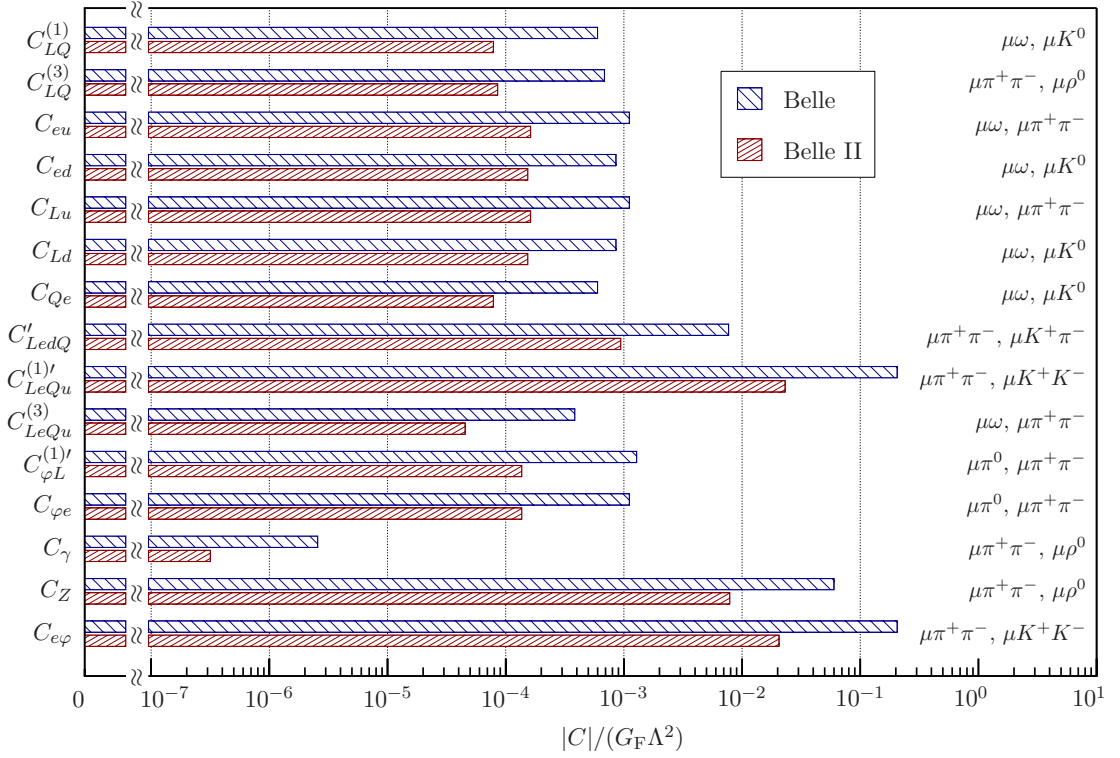
FIGURE 3.10: Allowed values for $C/(G_F \Lambda^2)$ based on the current Belle and expected Belle II limits, stemming from the *individual* analysis for hadronic tau decays, given at the 99% confidence level. The two most sensitive channels for the given WC are shown.

it also takes into account the possible correlations among the parameters, which in turn tend to relax the bounds set on them. The improvement entailed by the expected Belle II limits over current Belle data can be readily seen from this figure. It represents a more realistic description of nature since most of BSM theories provide us with several extra degrees of freedom, which in turn contribute to different Wilson coefficients. Finally, to directly compare how the correlations among the Wilson coefficients affect the imposed bounds, in Fig. 3.12 we show the results from both the individual and marginalized analyses based on Belle II expected data. The corresponding correlation matrices are given in Appendix H.

ℓ–τ conversion in nuclei

Considering ℓ–τ conversion in nuclei only, we performed the fit by taking into account four observables: two for each lepton (electron and muon) and other two for different nuclei, Fe(56,26) and Pb(208,82). The normalization channel (the bremsstrahlung cross section) in the observable under consideration (3.5.22) is much larger for electrons than for muons, as it is for lead compared to iron. This means that the results will be mainly driven by the μ–τ conversion in Fe(56,26) and to a lesser degree in Pb(208,82), as indeed, it turns out to be the case. Accordingly, this fit behaves as a single-parameter analysis. The correlation matrix (see Fig. H.3 of Appendix H) is thus almost diagonal, except for the $C_{LeQu}^{(1)\prime}$–$C_{LeQu}^{(3)}$ correlation of $\rho \approx 0.5$, and for
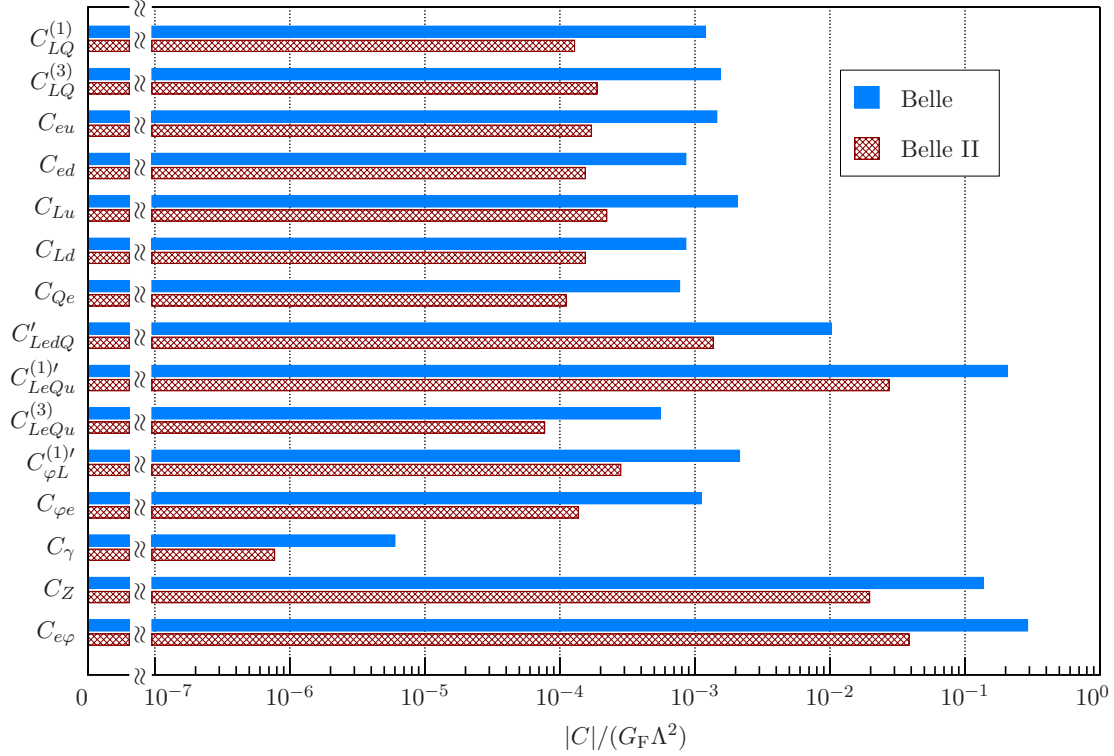
FIGURE 3.11: Allowed values for $C/(G_\mathrm{F}\Lambda^2)$ based on the current Belle and expected Belle II limits, stemming from the *marginalized* analysis for hadronic tau decays, given at the 99% confidence level.
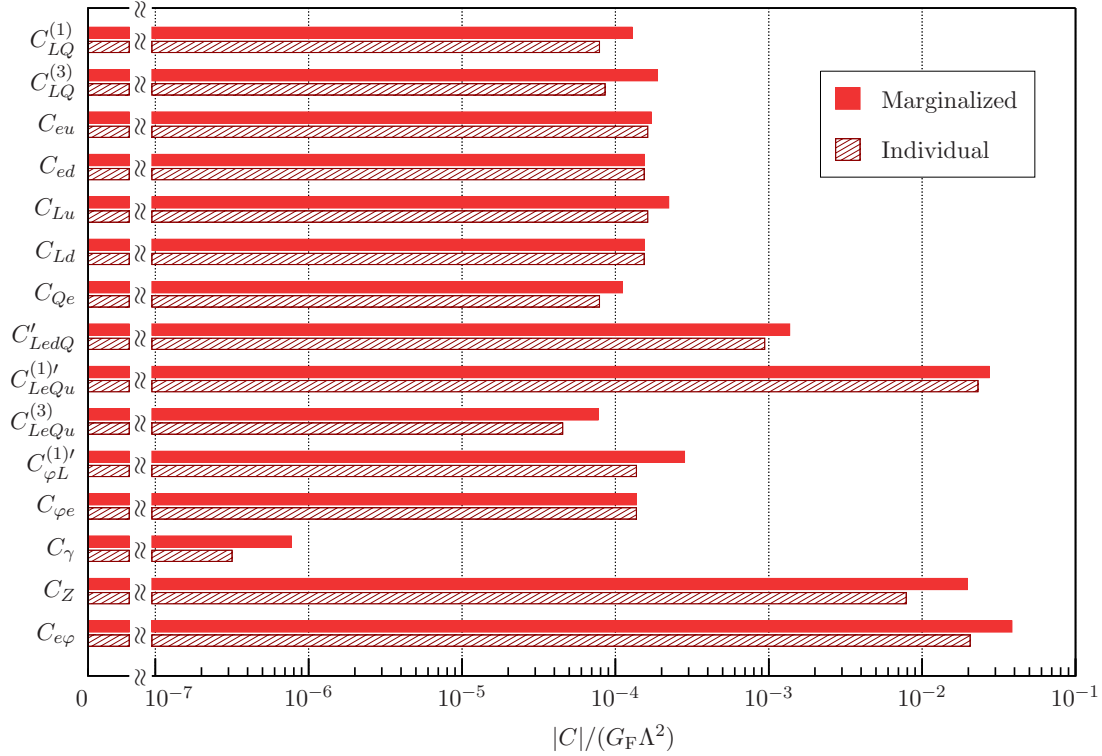
FIGURE 3.12: Allowed values for $C/(G_\mathrm{F}\Lambda^2)$ based on the expected Belle II limits, comparing the individual and marginalized analyses for hadronic tau decays, given at the 99% confidence level.
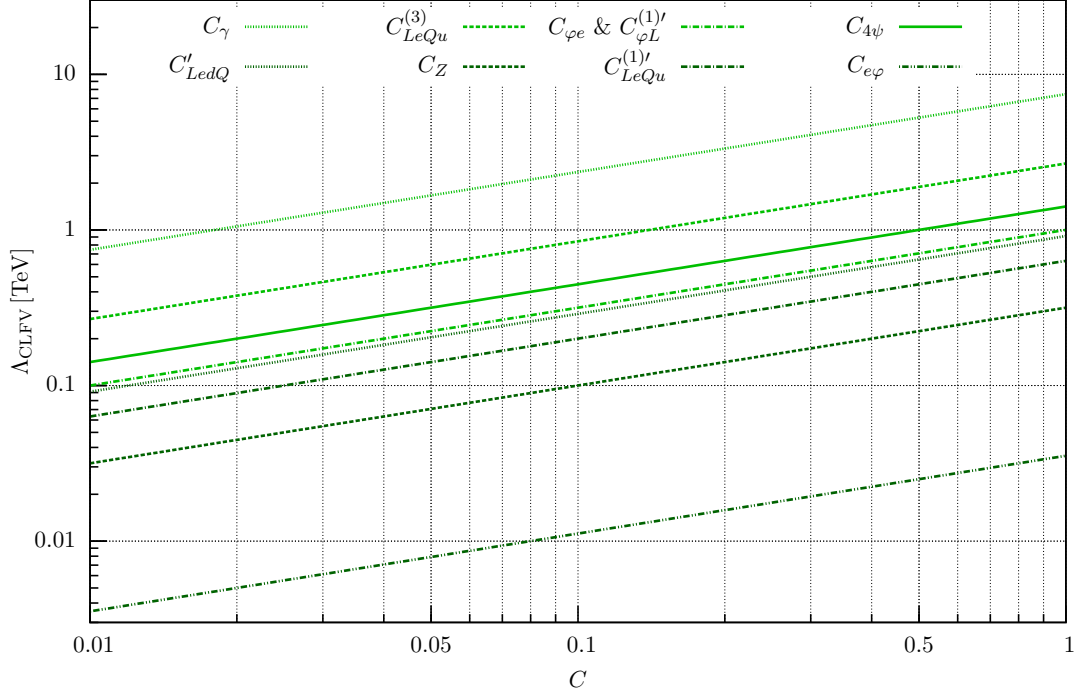
FIGURE 3.13: Constraints on Λ_{CLFV} with respect to the values of WCs from μ-τ conversion in Fe(56,26), based on the expected sensitivity of the NA64 experiment, given at the 99.8 % confidence level.

the case $C_{LQ}^{(3)}$–$C_{\varphi L}^{(1)\prime}$ for which we find $\rho \approx 0.66$: even though we are able to constrain the WCs from the latter pair separately (as opposed to the non-FCNC case), their correlation is still strong.

The pattern of constraints is shown in Fig. 3.13. The weakest constraints are again for the $C_{e\varphi}$, followed by the 'rotated' C_Z one order of magnitude away. After this comes the scalar $C_{LeQu}^{(1)\prime}$, and the remaining WCs then follow the same pattern as for hadronic τ decays. Note that the order of C_Z and $C_{LeQu}^{(1)\prime}$ has been inverted compared to the previous case. This is due to the fact (since we are considering FCNCs) that for ℓ–τ conversion it is possible to have an outgoing charm quark after the effective interaction has taken place. Hence, due to the redefinition of Eq. (3.5.27), the related matrix element is enhanced by the mass of the charm quark.

Based on the expected sensitivity of the NA64 experiment, it would be possible to probe energy scales from[6] $E \approx 30\,\text{GeV}$ for $C_{e\varphi}$ up to $E \approx 7.5\,\text{TeV}$ for C_γ, as it is shown in Table 3.3. There, we give also the numbers for the e–τ case separately. As we said above, the numerical analysis is dominated mainly by the μ–τ conversion, which means that the constraints obtained by considering the e–τ case only are much worse. This implies that the quantity $R_{\mu\tau}$ related to the μ–τ conversion in nuclei is the most sensitive to new physics in this case.

---

[6]Note that bounds on the energy scale below $E \sim 1\,\text{TeV}$ are not really informative, since the SMEFT is not valid in the absence of a mass gap between the electroweak and the higher-energy scale where we expect the new physics to live.

Bounds on Λ_{CLFV} [TeV]					
WC	e–τ	μ–τ	WC	e–τ	μ–τ
$C_{LQ}^{(1)}$	$\gtrsim 0.13$	$\gtrsim 1.7$	C_{LedQ}	$\gtrsim 0.06$	$\gtrsim 0.9$
$C_{LQ}^{(3)}$	$\gtrsim 0.11$	$\gtrsim 1.5$	$C_{LeQu}^{(1)}$	$\gtrsim 0.05$	$\gtrsim 0.6$
C_{eu}	$\gtrsim 0.11$	$\gtrsim 1.4$	$C_{LeQu}^{(3)}$	$\gtrsim 0.2$	$\gtrsim 2.7$
C_{ed}	$\gtrsim 0.11$	$\gtrsim 1.4$	$C_{\varphi e}, C_{\varphi L}^{(1)}$	$\gtrsim 0.08$	$\gtrsim 1$
C_{Lu}	$\gtrsim 0.09$	$\gtrsim 1.1$	C_{γ}	$\gtrsim 0.6$	$\gtrsim 7.5$
C_{Ld}	$\gtrsim 0.09$	$\gtrsim 1.2$	C_Z	$\gtrsim 0.02$	$\gtrsim 0.3$
C_{Qe}	$\gtrsim 0.1$	$\gtrsim 1.4$	$C_{e\varphi}$	$\gtrsim 0.003$	$\gtrsim 0.04$

TABLE 3.3:   Bounds on the new-physics energy scale mediating CLFV phenomena (Λ_{CLFV}), both for e–τ and μ–τ conversion in Fe(56,26). Here, we consider $C \approx 1$. The results are based on the expected sensitivity of the NA64 experiment, given at the 99.8 % confidence level.

Comparing the non-FCNC scenario with respect to the FCNC case for the ℓ–τ conversion, the main differences are as follows. First, the incapability to disentangle, as for τ decays, the contributions from $C_{LQ}^{(3)}$ and $C_{\varphi L}^{(1)\prime}$ (due to their strong correlation) forces us again to consider the redefinition (3.5.24): we can thus be sensitive to both operators independently only when FCNCs are included, i.e. FCNCs break the blind direction. Second, all 4-fermion WCs are less constrained, the largest difference occurring for C_{LedQ}' (two orders of magnitude weaker constraint regarding the ratio $C/\Lambda_{\text{CLFV}}^2$) and $C_{LeQu}^{(1)\prime}$ (for which this analysis is actually not sensitive at all). The previous correlation among the latter and $C_{LeQu}^{(3)}$ is trivially lost, because of the redefinition (3.5.27) together with the vanishing up-quark mass, which we consider throughout the work. The constraints on the remaining WCs stay practically the same and the correlation matrix is rather diagonal.

Combined analysis

From the discussion and results of the previous sections, it is straightforward to see that the results of the combined analysis — where we consider 28 hadronic τ decay channels and 4 cross sections of ℓ–τ conversion in nuclei — are dominated by the current Belle or expected Belle II limits. We may try different ratios (3.5.22) for ℓ–τ conversion in nuclei in order to see at which point these processes become competitive with the hadronic τ decays. We find that already with $R_{\ell\tau} \sim 10^{-13}$ the scalar $C_{LeQu}^{(1)\prime}$ receives a stronger constraint from the μ–τ conversion due to its large sensitivity to the charm-quark mass (when considering FCNCs and the redefinition of Eq. (3.5.27)). Nevertheless, it is not until we reach $R_{\ell\tau} \sim 10^{-15}$ that μ–τ plays a significant role in the analysis: most of the correlations among the WCs are then removed or diluted, which allows for slightly stronger constraints on the WCs compared to the ones Belle alone provides. This implies that, in case that several LFV hadronic τ decays would be observed by Belle II, μ–τ conversion in nuclei may

have the last word in unveiling what $d = 6$ operator(s) is/are behind the new-physics mechanism responsible for this manifestation of charged-lepton-flavor violation.

$\tau \to \mu\gamma$

In the work [74], the main focus was on the hadronic τ decays and the corresponding Wilson coefficients involved. Accordingly, the $\tau \to \mu\gamma$, a golden channel to study CLFV τ-involved processes, was not considered. However, this mode is usually enhanced close to observable rates in several BSM extensions and the current bound on $\tau \to \mu\gamma$ is stringent enough to be worthy of consideration. Therefore, to demonstrate the sensitivity of the golden channel $\tau \to \mu\gamma$ to new physics, let us compute here the (only) contribution from the SMEFT operators in Table 3.1 to this process, i.e. the contribution from $C_\gamma \mathcal{O}_\gamma$ (see Eq. (4.3.30)). The decay width is given by

$$\Gamma(\tau \to \mu\gamma) = \frac{v^2}{4\pi} m_\tau^3 \left(1 - \frac{m_\ell^2}{m_\tau^2}\right)^3 \frac{C_\gamma^2}{\Lambda^4} . \tag{3.5.31}$$

The bounds from Fig 3.3 (with 90% confidence level) then translate into (applying the individual-analysis approach)

$$\frac{|C_\gamma|}{G_{\rm F}\Lambda^2} \lesssim \begin{cases} 1.7 \times 10^{-7} \ [\text{Belle}] , \\ 6.6 \times 10^{-8} \ [\text{Belle II}] , \end{cases} \tag{3.5.32}$$

which entail the following bounds for the probed Λ once a natural value of order 1 is set for the Wilson coefficients:

$$\Lambda_{C_\gamma \approx 1} \gtrsim \begin{cases} 720\,\text{TeV} \ [\text{Belle}] , \\ 1100\,\text{TeV} \ [\text{Belle II}] . \end{cases} \tag{3.5.33}$$

Direct limits from the golden channel $\tau \to \mu\gamma$ thus provide the strongest bounds on the rotated dipole operator C_γ.

3.6 Conclusions

We have presented the model-independent numerical analysis of the SMEFT dimension-6 operators related to CLFV τ-involved processes of Ref [74]: we used the current Belle and the expected Belle II limits on hadronic τ decays, as well as a more exotic process, the ℓ–τ conversion in nuclei, still not tried but feasible at the NA64 experiment at CERN. We have used HEPfit to perform the statistical part of the analysis.

After BaBar and Belle experiments, tau decays started to be considered complementary to processes involving electrons and muons in the search for CLFV. That capability will be enforced even more with the expected results of the Belle II experiment. Here, we have studied the LFV decays of the tau lepton into hadrons by explaining in detail the procedure of hadronization. The wide range of possible final states provides 14 specific observables to include in our analysis. Our results show that the WC of the operator $\mathcal{O}_\gamma = c_{\rm W}\mathcal{O}_{eB} - s_{\rm W}\mathcal{O}_{eW}$ is the most constrained

one providing, for $C_\gamma \approx 1$, a bound of $\Lambda_{\mathrm{CLFV}} > 120\,\mathrm{TeV}$ (based on Belle data) or $\Lambda_{\mathrm{CLFV}} > 330\,\mathrm{TeV}$ (foreseen by Belle II).

In comparison with the μ–e conversion in nuclei widely studied in the bibliography, μ–τ conversion has not attracted much attention, mainly due to the fact that its possible experimental determination has non-trivial complexities. However, in our opinion, the μ–τ conversion is again a complementary tool in the endeavor of looking for CLFV since it obeys different dynamics compared to that of the μ–e conversion and, accordingly, it could provide an independent setting. In addition, its feasibility at NA64 at CERN should be strongly considered, although other fixed-target experiments (ILC, EIC, etc.) also offer good expectations. In our study, we have taken into account both the e–τ and μ–τ conversion in Fe(56,26) and Pb(208,82) and we have concluded that μ–τ conversion in Fe(56,26) imposes the strongest constraints. In the latter case, the $\mathcal{O}_\gamma$ operator is again the most constrained, but giving only $\Lambda_{\mathrm{CLFV}} > 7.5\,\mathrm{TeV}$ for $C_\gamma \approx 1$. We conclude that the current expected sensitivity, for instance, of the NA64 experiment cannot compete with Belle limits and it would need an improvement of at least two orders of magnitude in order to explore a slightly larger parameter space.

The outcomes of our analyses show that the experimental results on hadronic tau decays expected by Belle II could improve significantly the search for LFV in such processes. Although the search for ℓ–τ conversion in nuclei cannot compete, at present, with the information coming from tau decays, it could be used to unveil the relative weights of different dimension-6 operators. Finally, we have explicitly demonstrated the necessity to perform a marginalized numerical analysis of the parameters under consideration (see Fig. 3.12 for an explicit comparison): in this way, one can avoid naively deducing stronger estimates obtained when considering only one non-vanishing WC at a time.

This work sets a useful setting in the search for physics beyond the Standard Model — namely charged-lepton-flavor violation — through a systematic analysis within the framework of the Standard Model Effective Field Theory, taking into account all presently available information from experiments involving charged-lepton-flavor violation and the third family. Moreover, our tool will also be of use for analyzing results from upcoming experiments like Belle II.

Chapter 4

Leptoquarks in CLFV τ-involved processes

The Standard Model of particle physics as explained in Chapter 1, is a very successful quantum field theory, which describes the dynamics of the strong interaction as well as the unified electromagnetic and weak interactions — the electroweak theory. While the SM has passed a number of elaborate experimental tests over a broad range of energies, it is already believed for decades that it does not provide us with the final and complete picture of reality as expected from a fundamental theory. There are purely theoretical reasons to think like that: besides the fact that the SM contains many a priori unknown parameters, there are indications for the unification of the strong and EW forces and the common underlying structure of all fermions, which form the so-called families or generations. From the phenomenological point of view, there are several phenomena which cannot be explained within its framework. For instance, the SM does not provide a viable dark-matter candidate, fails to predict the observed matter–antimatter asymmetry in the Universe, and it does not strive to unambiguously incorporate the tiny (though nonzero) masses of neutrinos. Hence, one of the major goals of contemporary particle physics is to look beyond the SM for possible explanations of these and other shortcomings.

As explained in Chapter 2, the effects of BSM phenomena on the dynamics of SM particles, arising at energy scales higher than the EW scale ($\Lambda_{\mathrm{EW}} \sim v$), can be encoded in terms of the Standard Model Effective Field Theory [56,58], in particular in the Wilson coefficients — low-energy constants standing in front of the monomials in such an effective Lagrangian. These coefficients can be related to parameters of particular BSM models and could be also determined from experimental results.

Within the rich palette of BSM scenarios, a very well motivated class of theories predicts the existence of leptoquarks — electrically charged bosons (with spin $S = 0, 1$) which transform as triplets under $\mathrm{SU}(3)_{\mathrm{C}}$ and can turn quarks into leptons and vice versa. They naturally emerge in Grand Unification Theories, where strongly non-interacting leptons are accommodated into the same multiplets as quarks: they first appeared in the Pati–Salam model [179, 180], and right after in theories based on other symmetry groups, such as the simplest SU(5) in the case of the Georgi–Glashow model [181], SO(10) [182, 183], or further on in superstring-inspired E_6 models [184, 185]. They were as well predicted in technicolor and other related models based on the dynamically generated symmetry breaking [186–188], or in models with composite fermions [189–191] or extended scalar sectors [192, 193].

At the same time, the persisting existence of several anomalies — discrepancies between the SM theoretical predictions of observables and their experimental values — signals possible effects of new physics, and leptoquarks present themselves as relevant NP candidates, being able to address one or more of these deviations, depending on the chosen model. The discrepancies that have drawn more attention in the recent literature — as we also mentioned in Section 3.2 of the previous Chapter 3 — are $R_{D^{(*)}}$ [105–112], R_K [113–120] and the more recent $R_{K_S^0}$ and $R_{K^{*+}}$ [121], the so-called B anomalies [122], and the anomalous magnetic moment $(g - 2)$ of the muon [123, 124]. Effects of LQs in these and other processes are extensively studied and parametrized via effective field theory frameworks; see e.g. Ref. [194] and references therein. More recent updates on the role of leptoquarks in B anomalies and constraints on their couplings to ordinary matter can be found in Refs. [195–217], while the $(g - 2)_\mu$ discrepancy is addressed in Refs. [195–199, 212–214, 216–228]. A detailed analysis of low-energy signals of scalar leptoquarks is presented in Ref. [222]. Finally, for current and expected limits from collider searches see Refs. [201, 203, 204, 208, 217, 229–242].

Besides the notorious anomaly-related issues, leptoquarks have also been considered to address other BSM problems like the generation of neutrino masses through one [195, 210, 228, 243–245], two [195, 198, 213, 219, 246] and three loops [196]. Furthermore, their role as mediators between the SM sector and dark matter candidates is studied in Refs. [247, 248], their implications for baryogenesis are considered in Ref. [249], and the ANITA anomalous events are explained using particular leptoquark models in Refs. [246, 250]. Their existence might also offer a hint on why there are exactly three generations of matter or why there is the same number of quark and lepton species, the consequence of which is, as commented in the previous chapter, the fact that the currents associated with the SM gauge symmetries are non-anomalous — free of Adler–Bell–Jackiw axial anomalies [93–95].

Following the above reasoning, leptoquarks belong, at present, among the most promising NP contributions. However, despite the immense experimental effort, they have not been directly observed yet.

In the work of Ref. [251], upon which this chapter is based, we addressed another interesting BSM phenomenon, namely processes exhibiting charged-lepton-flavor violation. This effect, while absent in the SM, is expected to happen in presence of massive neutrinos. However, as we explained in Section 3.2 of the previous chapter, minimal extensions of the SM with light right-handed neutrinos predict tiny CLFV rates, inaccessible to current and mid-term foreseen experiments [148–152, 252] (see Eq. (3.2.4)). Within the leptoquark framework, CLFV processes can occur at tree level via the exchange of a LQ coupled to $(\bar{\ell}\,\Gamma\,q)$ and $(\bar{q}\,\Gamma\,\ell')$ currents (here, q is short for a quark field, ℓ for a lepton field, and Γ the relevant Dirac tensors), providing enhanced rates for these processes that could be measured at present or future experiments. We again focused on CLFV τ-involved processes since most of the work done in this area has been mainly related to the first and second families (see, for instance, the reviews [68–70]), and the persistence of some charged-current-driven B anomalies suggests an apparent violation of universality around the third family.

Hence, complementary to the bottom-up analysis presented in Chapter 3, here we follow a top-down approach (see Chapter 2) within the leptoquark framework, for

which we take the most general couplings of the 5 different types of both scalar and vector leptoquarks to the SM fermions (see, for instance, Ref. [194]); in the presence of a right-handed neutrino, that we do not consider, there is an additional type of scalar and vector LQs. In the spirit of the top-down approach, upon integration of those leptoquarks — assuming $M_{\mathrm{LQ}} \gg \Lambda_{\mathrm{EW}}$ — the four-fermion dimension-6 ($d = 6$) operators of the SMEFT [56, 58] are generated. As commented above, we break universality in the lepton sector by attaching different couplings to the tau lepton and those of the first two families. This is because some works [253, 254] point to the aforementioned particularity of the third family and, moreover, the implications related to the first two families in this regard are far less compelling [125]. Moreover, we have also taken into account the $\tau \to \ell \gamma$ decays (with $\ell = e, \mu$), although their leading contribution arises at one loop. Throughout this procedure, we get the WCs of the $d = 6$ SMEFT operators expressed in terms of products of a pair of unknown couplings of LQs to SM fermions. In addition, we identify the energy scale of the corresponding SMEFT with the masses of leptoquarks.

In Chapter 3, we have shown the model-independent analysis that we performed in Ref. [74], taking into account current and foreseen experimental data for lepton-flavor-violating hadronic τ decays (from Belle [255] and Belle II [71]) and ℓ–τ conversion in nuclei, $\ell = e, \mu$ (from the NA64 expected sensitivity [138]). From this analysis, we obtained tight bounds on the participating WCs that we can translate to the products of LQs couplings. Upon general assumptions on those couplings we can also arrive at estimates for the lower bounds on LQ masses. Based on our results, we would like to highlight the strong bounds on LQ masses and couplings that Belle II future results on the hadronic τ decays will be able to establish.

This chapter is organised in the following way. In Section 4.1, we present the most general CLFV leptoquark Lagrangian based on the SM symmetries accommodating scalars and vectors, and describe the important features of this framework. In Section 4.2, we recover the four-fermion $d = 6$ SMEFT operators that result from integrating out the LQ fields at tree level. There we also show the computation of the one-loop diagrams contributing to the largely bounded photon-dipole operator. Hence, we give the relations between the WCs and the leptoquark couplings, which we use to constrain the latter in Section 4.3 by using our results from Chapter 3. We point out our main conclusions in Section 4.4. Several technical appendices make easier the understanding of the present work.

4.1 Leptoquark Lagrangian

To systematically explore all possible options, leptoquarks may be classified with respect to their spin (scalar or vector) and the way they couple to matter (quarks and leptons) based on their transformation properties under the SM gauge group $\mathrm{SU}(3)_{\mathrm{C}} \times \mathrm{SU}(2)_{\mathrm{L}} \times \mathrm{U}(1)_{\mathrm{Y}}$. This classification is easily understood in group theoretical terms as follows.

The $\mathrm{SU}(3)_{\mathrm{C}}$ group

Under the symmetry group of the strong interactions, quarks transform as triplets while leptons do as singlets. Therefore, leptoquarks should necessarily

transform as 3-dimensional representations of $SU(3)_C$ as well, for quark-lepton-LQ interactions to be invariant under this symmetry transformation. More concretely, those interactions correspond to the singlet resulting of the quark-lepton-LQ decomposition: $\mathbf{3} \otimes \mathbf{1} \otimes \bar{\mathbf{3}} \equiv \mathbf{8} \oplus \mathbf{1}$. Likewise, this is shared by all leptoquarks, i.e. all LQs transform as triplets of $SU(3)_C$. Consequently, leptoquarks can couple as well with pairs of quarks — the so-called diquark couplings — what usually entails matter stability issues, we comment on them at the end of this section. Obviously, from the triplet dimensionality assignment under $SU(3)_C$, lepton-lepton-LQ interactions are not gauge invariant and are consequently forbidden.

The $SU(2)_L \times U(1)_Y$ group

The $SU(2)_L$ transformation properties of leptoquarks are a bit more involved than in the previous case. Both quarks and leptons transform under this symmetry group either as singlets $\mathbf{1}$ (right-handed fields) or doublets $\mathbf{2}$ (left-handed fields). Accordingly, one should consider all possible contractions among the representations of the matter fields to ascertain the LQ-dimensionality assignments under $SU(2)_L$. These are: singlet-singlet $\mathbf{1} \otimes \mathbf{1} \equiv \mathbf{1}$, resulting in singlet LQ representations; singlet-doublet $\mathbf{1} \otimes \mathbf{2} \equiv \mathbf{2}$, resulting in doublet LQ representations; and doublet-doublet $\mathbf{2} \otimes \mathbf{2} \equiv \mathbf{3} \oplus \mathbf{1}$, for which both 1 and 3-dimensional representations of LQs can build up gauge invariant terms. Therefore, under $SU(2)_L$, leptoquarks can be singlets, doublets or triplets. These assignments can be used to label and thus differentiate among the different leptoquark species. Accordingly, they correspond to the subindex given to each LQ in Table 4.1.

However, for singlet and doublet LQs (both scalar and vector), there turns out to be two multiplets with the same dimensionality. They are hence distinguished by their charges under $U(1)_Y$: their hypercharges, and one includes a tilde over the LQ symbol to differentiate them (see Table 4.1)[1]. The leptoquark hypercharges are easily computed from the quark-lepton-LQ interactions, since it is an additive quantity and gauge invariance forces these interactions to have a total vanishing hypercharge. The electric charge of the leptoquarks is then given, as usual, by $Q_{LQ} = I_3 + Y$, where I_3 stands for the $SU(2)_L$ generator and Y for the $U(1)_Y$ hypercharge operator.

Finally, leptoquarks have a well-defined fermion number $F = 3\,B + L$, with B and L being the baryon and lepton numbers, respectively. Based again on the lepton-quark-LQ possible interactions, all leptoquark fields are then categorized into two sets: $|F| = 0, 2$.

All in all, the most general renormalizable Lagrangian based on the SM symmetries that realizes interactions of leptoquarks with fermion pairs contains in total 10 types of leptoquark fields (which extends to 12 if right-handed neutrinos are brought into the picture): 5 scalar and 5 vector ones. We thus write our ultra-violet (UV) Lagrangian, at the leptoquark mass scale, as:

$$\mathcal{L}_{UV} = \mathcal{L}_{SM} + \mathcal{L}_{LQ\text{-}\psi} + \mathcal{L}_S + \mathcal{L}_V + \mathcal{L}_{LQ\text{-}H}. \tag{4.1.1}$$

---

[1] If right-handed neutrinos are added to the particle content, one should include another singlet leptoquark (both for scalar and vectors) that is usually distinguished from the other two by a bar over the LQ symbol.

LQ type	SM symmetries	Lagrangian
S_3	$(\bar{\mathbf{3}}, \mathbf{3}, 1/3)$	$Y_{3,ij}^{\mathrm{LL}}\, \bar{Q}_{\mathrm{L}}^{\mathrm{C}i,a}\, \varepsilon^{ab}\, (\tau_k S_3^k)^{bc}\, L_{\mathrm{L}}^{j,c} + \text{h.c.}$
R_2	$(\mathbf{3}, \mathbf{2}, 7/6)$	$-Y_{2,ij}^{\mathrm{RL}}\, \bar{u}_{\mathrm{R}}^i\, R_2^a\, \varepsilon^{ab}\, L_{\mathrm{L}}^{j,b} + Y_{2,ij}^{\mathrm{LR}}\, \bar{e}_{\mathrm{R}}^i\, R_2^{a\dagger}\, Q_{\mathrm{L}}^{j,a} + \text{h.c.}$
$\tilde{R}_2$	$(\mathbf{3}, \mathbf{2}, 1/6)$	$-\tilde{Y}_{2,ij}^{\mathrm{RL}}\, \bar{d}_{\mathrm{R}}^i\, \tilde{R}_2^a\, \varepsilon^{ab}\, L_{\mathrm{L}}^{j,b} + \text{h.c.}$
$\tilde{S}_1$	$(\bar{\mathbf{3}}, \mathbf{1}, 4/3)$	$\tilde{Y}_{1,ij}^{\mathrm{RR}}\, \bar{d}_{\mathrm{R}}^{\mathrm{C},i}\, \tilde{S}_1\, e_{\mathrm{R}}^j + \text{h.c.}$
S_1	$(\bar{\mathbf{3}}, \mathbf{1}, 1/3)$	$Y_{1,ij}^{\mathrm{LL}}\, \bar{Q}_{\mathrm{L}}^{\mathrm{C}i,a}\, S_1\, \varepsilon^{ab}\, L_{\mathrm{L}}^{j,b} + Y_{1,ij}^{\mathrm{RR}}\, \bar{u}_{\mathrm{R}}^{\mathrm{C}i}\, S_1\, e_{\mathrm{R}}^j + \text{h.c.}$
U_3	$(\mathbf{3}, \mathbf{3}, 2/3)$	$X_{3,ij}^{\mathrm{LL}}\, \bar{Q}_{\mathrm{L}}^{i,a}\, \gamma^\mu\, (\tau_k U_{3,\mu}^k)^{ab}\, L_{\mathrm{L}}^{j,b} + \text{h.c.}$
V_2	$(\bar{\mathbf{3}}, \mathbf{2}, 5/6)$	$X_{2,ij}^{\mathrm{RL}}\, \bar{d}_{\mathrm{R}}^{\mathrm{C}i}\, \gamma^\mu\, V_{2,\mu}^a\, \varepsilon^{ab}\, L_{\mathrm{L}}^{j,b} + X_{2,ij}^{\mathrm{LR}}\, \bar{Q}_{\mathrm{L}}^{\mathrm{C}i,a}\, \gamma^\mu\, \varepsilon^{ab}\, V_{2,\mu}^b\, e_{\mathrm{R}}^j + \text{h.c.}$
$\tilde{V}_2$	$(\bar{\mathbf{3}}, \mathbf{2}, -1/6)$	$-\tilde{X}_{2,ij}^{\mathrm{RL}}\, \bar{u}_{\mathrm{R}}^{\mathrm{C},i}\, \gamma^\mu\, \tilde{V}_{2,\mu}^a\, \varepsilon^{ab}\, L_{\mathrm{L}}^{j,b} + \text{h.c.}$
$\tilde{U}_1$	$(\mathbf{3}, \mathbf{1}, 5/3)$	$\tilde{X}_{1,ij}^{\mathrm{RR}}\, \bar{u}_{\mathrm{R}}^i\, \gamma^\mu\, \tilde{U}_{1,\mu}\, e_{\mathrm{R}}^j + \text{h.c.}$
U_1	$(\mathbf{3}, \mathbf{1}, 2/3)$	$X_{1,ij}^{\mathrm{LL}}\, \bar{Q}_{\mathrm{L}}^{i,a}\, \gamma^\mu\, U_{1,\mu}\, L_{\mathrm{L}}^{j,a} + X_{1,ij}^{\mathrm{RR}}\, \bar{d}_{\mathrm{R}}^i\, \gamma^\mu\, U_{1,\mu}\, e_{\mathrm{R}}^j + \text{h.c.}$

TABLE 4.1: Classification of leptoquarks based on the representations of matter fields under the SM gauge group $\mathrm{SU(3)_C} \times \mathrm{SU(2)_L} \times \mathrm{U(1)_Y}$, and related Lagrangians representing the interactions of leptoquarks with SM quarks and leptons. All these terms then constitute the $\mathcal{L}_{\mathrm{LQ}-\psi}$ Lagrangian and are potentially responsible for CLFV. The Yukawa-like couplings $Y_{d,ij}^{\chi_1\chi_2}$ and $X_{d,ij}^{\chi_1\chi_2}$, $d = 1, 2, 3$, are dimensionless. The hypercharge Y is related to the electric charge Q via $Q = I_3 + Y$, with I_3 staying for the third $\mathrm{SU(2)_L}$ generator, the specific realization of which, as mentioned in the main text, depends on the corresponding leptoquark representation. As is customary, Q_{L} and L_{L} stand for the left-handed quark and lepton $\mathrm{SU(2)}$ doublets, $u_{\mathrm{R}}(d_{\mathrm{R}})$ and e_{R} are the up(down)-type quark and lepton right-handed $\mathrm{SU(2)}$ singlets, respectively. Finally, τ_k are the Pauli matrices ($\{\tau_k, \tau_l\} = 2\delta_{kl}\mathbb{1}_2$) and ε stands for the Levi-Civita symbol in two dimensions ($\varepsilon = i\tau_2$). The letters $i, j = 1, 2, 3$ denote flavor indices, while $a, b, c = 1, 2$ are $\mathrm{SU(2)}$-gauge-group-related indices.

The first term $\mathcal{L}_{\mathrm{SM}}$ above, containing the SM interactions, is fully given in Chapter 1. Let us now comment on the other terms and point out the relevant pieces for our analysis.

4.1.1 Leptoquark couplings to the SM fermions

The second term on the r.h.s. of Eq. (4.1.1) $\mathcal{L}_{\mathrm{LQ}-\psi}$ collects the matter couplings of leptoquarks, which are given for each leptoquark species in Table 4.1. There and throughout the text, we use the same notation and conventions as in Ref. [194]. Note that, as written down in Table 4.1, we are not showing terms with right-handed neutrinos (which are not considered here) nor terms with two quark fields (irrelevant for our analysis as explained below).

For each leptoquark type, the terms potentially responsible for the ℓ–τ conversion and $\tau \to (\ell + \text{hadrons})$ decays (with $\ell = e, \mu$) are the same terms as presented in Table 4.1, where all possible flavor structures for the Yukawa-like couplings should be taken into account. However, as it was motivated in the previous chapter, we consider an egalitarian flavor structure in the quark sector: equal entries for all quark flavors in the Wilson coefficient matrices C_{ij} of the SMEFT, where i, j run over all quark flavors. Hence, our LQ Yukawas are quark-flavor-blind, whereas in the lepton sector we assume the particularity of the tau-lepton family Yukawas, but keep them

equal for the electron and muon families. This, despite the B anomalies regarding the first two lepton families, is partially motivated by the results of Ref. [125]. The LQ Yukawa couplings in Table 4.1, namely Y and X, will be assumed to be real.

Among various possible additional interactions, the so-called diquark couplings (i.e. when the LQ is coupled to a quark–antiquark pair) may appear at tree level in the Lagrangian (4.1.1) (although there are no analogous dilepton couplings to leptoquarks as explained above). This entails a possible danger to matter stability, or, in turn, strong bounds on LQ masses or couplings: after leptoquarks are integrated out, diquark operators provide baryon (and thus lepton)-number-violating processes. Therefore, to avoid dealing with the proton-decay issue and since, in any case, diquark couplings do not play any role at tree level in CLFV processes, without any loss of generality we do not consider these couplings in this work and we have not included them in Table 4.1. Although this precludes proton decay in the minimal scenario when assuming (besides the SM content) only one leptoquark species at a time, note that regardless of the presence or absence of diquark couplings, a richer scenario as the one treated here with all leptoquarks considered simultaneously is much more involved [194, 256]. Hence, since these kinds of interactions do not affect our CLFV analysis and in order not to dive into this issue any further here, we simply assume, in what follows, that the proton is stable.

4.1.2   Leptoquark covariant derivative and self interactions

The terms $\mathcal{L}_\mathrm{S}$ and $\mathcal{L}_\mathrm{V}$ in Eq. (4.1.1), consist of the leptoquark kinetic terms as well as the interactions among those and the SM gauge bosons, for which the relevant parts to our work are discussed here.

Generically, the kinetic and gauge couplings of leptoquarks are described by the Lagrangians

$$
\begin{aligned}
\mathcal{L}_\mathrm{S} &= \sum_{\text{scalars}} \left[(D_\mu S)^\dagger D^\mu S \,-\, M_S^2 \, S^\dagger S \right], \\
\mathcal{L}_\mathrm{V} &= \sum_{\text{vectors}} \left[-\frac{1}{2} V_{\mu\nu}^\dagger V^{\mu\nu} \,+\, M_V^2 \, V_\mu^\dagger V^\mu \,+\, \dots \right],
\end{aligned}
\tag{4.1.2}
$$

where the field-strength tensor for the vector leptoquarks is $V_{\mu\nu} = D_\mu V_\nu - D_\nu V_\mu$. The SM covariant derivative is given by

$$
D_\mu = \partial_\mu + i g_1 Y B_\mu + i g_2 I_k W_\mu^k + i g_3 \frac{\lambda^A}{2} G_\mu^A \,,
\tag{4.1.3}
$$

where the λ^A and I_k are the generators of the SU(3) and SU(2) symmetry groups, respectively, while Y is the LQ hypercharge operator. Note that the I^k depend on the leptoquark SU(2) representation, e.g. for a leptoquark doublet, $I_k = \tau_k/2$, with τ_k being the Pauli matrices, while for a triplet we have $I_k = (I_k)_{lm} = -i\varepsilon_{klm}$, with ε_{abc} being the three-dimensional Levi-Civita pseudotensor ($\varepsilon_{123} = 1$). In Eq. (4.1.2), the dots in the vector leptoquark Lagrangian correspond to other $d = 4$ terms that involve additional interactions of the SM gauge fields with the leptoquarks, and self-interactions among them (the latter are not relevant for our work and are not

considered from now on). These are allowed by the gauge symmetry (although their couplings are not determined by it) and facilitate the renormalizability of the vector Lagrangian (see Ref. [257]).

More concretely, we shall present here the photon-leptoquark interactions, since they proved to be relevant in our analysis, whereas the rest of gauge-boson interactions could be easily neglected based on the results of Chapter 3, i.e. the Wilson coefficients of the $d = 6$ operators of the SMEFT to which they would contribute upon leptoquark integration, turned out to be much less constrained by the CLFV τ processes than the photon-dipole operator. For instance, the LQ-(γ, Z) interactions provide the diagram (b) of Fig. 3.5 for hadronic tau decays and of Figs. 3.7 and 3.8 for ℓ-τ conversion in nuclei, once the leptoquark is integrated away.

Scalar leptoquarks For scalar leptoquarks, their interactions with photons arise directly from the SM covariant derivative of Eq. (4.1.3) and are unequivocally given by:

$$\mathcal{L}_{\rm S}^{\gamma} = ie \sum_{\rm scalars} Q_{\rm S} \left[\left(\partial_{\mu} S^{\dagger} \right) S - S^{\dagger} \left(\partial_{\mu} S \right) \right] A^{\mu} \,, \qquad (4.1.4)$$

where $Q_{\rm S}$ stands for the electric charge, in units of e, of the leptoquark under consideration and A^{μ} is the photon-vector field. Note that the strength of the interaction is completely determined by the leptoquark charge.

Vector leptoquarks For vector leptoquarks the situation is not that clear. As usual, one of the sources of the LQ-photon interactions stems from the field-strength tensor containing the SM covariant derivative. In addition to that, among the aforementioned omitted terms in Eq. (4.1.2) represented by dots and depending on the (gauge) nature of the vector leptoquarks, there can be present another source of this interaction: an anomalous magnetic moment coupling of the vector leptoquark to the photon (represented here by κ). Considering this term, the total vector leptoquark-photon interacting Lagrangian reads

$$\mathcal{L}_{\rm V}^{\gamma} = -ie \sum_{\rm vectors} Q_{\rm V} \left[\left(\mathcal{V}_{\mu\nu}^{\dagger} V^{\nu} - \mathcal{V}_{\mu\nu} V^{\nu\dagger} \right) A^{\mu} - (1 - \kappa) V_{\mu}^{\dagger} V_{\nu} F^{\mu\nu} \right] \,, \qquad (4.1.5)$$

where $F^{\mu\nu}$ is the usual photon field strength tensor and we have defined the field strength tensor of the vector leptoquark with only partial derivatives as

$$\mathcal{V}_{\mu\nu} \equiv \partial_{\mu} V_{\nu} - \partial_{\nu} V_{\mu} \,. \qquad (4.1.6)$$

In contrast to the scalar leptoquark case, for vector leptoquarks we cannot unambiguously ascertain their interactions with photons: if vector leptoquarks are not gauge bosons, then $\kappa \neq 0$ and we have an extra free parameter at play; on the contrary, if vector leptoquarks turn out to be (part of) the gauge bosons of a higher energy theory described by a larger symmetry group — as it is usually the case in Grand Unified Theories — then $\kappa = 0$ and the covariant derivative D_{μ} should be modified to include the gauge bosons of the enlarged gauge group.

However, the ambiguity present when considering vector leptoquarks does not only reside on the specific value of κ, but their propagators do also depend on their underlying origin. For gauge bosons, we can write their propagator (in the 't Hooft-Feynman gauge) as

$$\frac{-i g^{\mu\nu}}{k^2 - M_{\mathrm{V}}^2 + i\epsilon}, \qquad (4.1.7)$$

on the other hand, for not-gauge-boson vector LQs, their propagator reads

$$\frac{-i}{k^2 - M_{\mathrm{V}}^2 + i\epsilon}\left(g^{\mu\nu} - \frac{k^\mu k^\nu}{M_{\mathrm{V}}^2}\right). \qquad (4.1.8)$$

Our aim by considering the leptoquark-photon couplings is firstly to compute the LQ contribution to the photon-dipole operator, whose bound we translate into constraints on the LQ Lagrangian parameters, and then compare the latter against the bounds obtained directly from the limit on the branching ratio of $\tau \to e\gamma$. For both calculations we need to compute the diagrams of Fig. 4.1 below. However, while for scalar leptoquarks this is achieved as presented in Section 4.2.2, for (not-gauge) vector LQs the $k^\mu k^\nu / M_{\mathrm{V}}^2$ term in Eq. (4.1.8) introduces extra divergences in the calculation of those diagrams that remain after all contributing diagrams are considered [258], as opposed to the scalar LQ case. On the other hand, if we assume the vector leptoquarks to be gauge bosons of a higher-energy theory, one could argue the presence of other massive degrees of freedom in the extended gauge group that could potentially contribute to those diagrams for $\tau \to e\gamma$. All in all, we conclude that the gauge interactions of vector leptoquarks cannot be unambiguously defined due to their uncertain gauge nature (so neither their contributions to $\tau \to e\gamma$ can be ascertained), and an ultraviolet completion might be needed. Accordingly, we do not consider the gauge couplings of vector leptoquarks in the following.

4.1.3   Leptoquark couplings to the Higgs

Let us now focus on the coupling of leptoquarks to the SM Higgs doublet and study their role in our CLFV analysis. The complete form of these interactions is given in Refs. [217, 259] and is contained in the term $\mathcal{L}_{\mathrm{LQ-H}}$ of Eq. (4.1.1). The diagonal couplings contribute, together with the mass parameters in the Lagrangian, to the total LQ mass after the spontaneous symmetry breaking has taken place and the Higgs acquired a vacuum expectation value. Therefore, they do not contribute to any of the $d = 6$ operators considered in Chapter 3. On the other hand, the off-diagonal couplings translate into a mixing of leptoquarks in Table 4.1 when diagonalizing the total LQ mass matrix and working in the mass basis. However, and as a consequence of the fact that gauge symmetry requires these couplings to always involve two leptoquark fields, the corresponding mixing components behave as $\mathcal{O}(1/M_{\mathrm{LQ}}^2)$(see Eq. (2.13) of Ref. [217]). Hence, upon integration, the effects of the induced mixing to the four-fermion operators present in our analysis are $\mathcal{O}(1/M_{\mathrm{LQ}}^4)$, and are thus of higher order in the SMEFT (they will generate effective $d = 8$ operators) than the ones we consider in our work. Finally, even though tree-level contributions to the CLFV-τ observables studied in Chapter 3 are not possible via LQ-Higgs couplings as

we have already seen, one could argue that similar loop-level contributions as those of Fig. 4.1 below — by exchanging the photon by a Higgs field — are allowed within the most general leptoquark framework. This is also the case for the Z boson but, as stated above, besides the loop suppression for both bosons, the bounds obtained in the matched Wilson coefficients were the weakest of the previous work of Chapter 3. All in all, we find that the extra couplings introduced by the LQ-Higgs interactions can be safely neglected when considering low-energy CLFV-τ processes.

4.2 The integration of leptoquarks

The aim of this work is to translate the bounds on the ratio $C/\Lambda_{\mathrm{CLFV}}^2$ (containing the Wilson coefficients of the $d = 6$ operators in the SMEFT and the high-energy scale Λ_{CLFV}) obtained by analyzing charged-lepton-flavor-violating τ processes in Chapter 3, into constraints on the couplings and mass scales of the leptoquark Lagrangian described in Section 4.1.

Direct searches of leptoquarks have been extensively carried out at the LHC [48]. Lower bounds on their masses depend crucially on their spin (scalar or vector), their weak charges and generations involved, and the supposedly dominant decay products. Generically, we can say that the present status requires $M_{\mathrm{LQ}} > 1$–2 TeV, with a slight preference for the higher value [260, 261]. Meanwhile, indirect determinations from the B anomalies or lepton-number-violating processes [48] require heavier LQs with masses of at least few TeVs (for $\mathcal{O}(1)$ LQ couplings). Hence, it is rather fair to say that $M_{\mathrm{LQ}} \gg \Lambda_{\mathrm{EW}}$ and that their contribution to $d = 6$ SMEFT monomials is hidden into the Wilson coefficients we denote C (or, more generally, into C/Λ^2). Assuming, in consequence, that there is such a mass gap between the SM particles and leptoquarks, the requirements explained in Chapter 2 to perform a top-down analysis of leptoquarks are fullfilled and we can integrate out the (heavy) leptoquark fields to recover the associated $d = 6$ operators that contribute to the CLFV processes we study.

In the work presented in Chapter 3, we concluded that the strongest bounds from CLFV processes involving the tau lepton, namely hadronic tau decays, were imposed on the four-fermion operators and the operator responsible for the radiative decay $\tau \to \ell\gamma$; see Table 4.2 for a detailed list of these operators. Indeed, it was the $\mathcal{O}_\gamma = c_{\mathrm{W}}\mathcal{O}_{eB} - s_{\mathrm{W}}\mathcal{O}_{eW}$ operator (recall that $c_{\mathrm{W}} = \cos\theta_{\mathrm{W}}$ and $s_{\mathrm{W}} \equiv \sin\theta_{\mathrm{W}}$; see also Section 4.3.1) which was getting the strongest bound. It has two relevant features. Firstly, it incorporates a Higgs field (as can be seen in Table 4.2). Secondly, it is generated at the one-loop level upon leptoquark integration once the spontaneous symmetry breaking of the electroweak symmetry has taken place.

In this chapter, we consider the leptoquark contributions to both the four-fermion and $\mathcal{O}_\gamma$ operators at leading order. We thus perform the low-energy matching ($M_{\mathrm{LQ}} \gg \Lambda_{\mathrm{EW}}$) of the leptoquark Lagrangian $\mathcal{L}_{\mathrm{UV}}$ from Eq. (4.1.1) with the SM extended by the $d = 6$ operators (i.e. with the SMEFT Lagrangian) and obtain the relation among the Wilson coefficients and the couplings of the leptoquark framework — after their running with the scale is taken into account.

WC	Operator	WC	Operator
$C_{LQ}^{(1)}$	$\left(\bar{L}_p\gamma_\mu L_r\right)\left(\bar{Q}_s\gamma^\mu Q_t\right)$	$C_{LQ}^{(3)}$	$\left(\bar{L}_p\gamma_\mu\tau^I L_r\right)\left(\bar{Q}_s\gamma^\mu\tau^I Q_t\right)$
C_{eu}	$\left(\bar{e}_p\gamma_\mu e_r\right)\left(\bar{u}_s\gamma^\mu u_t\right)$	C_{ed}	$\left(\bar{e}_p\gamma_\mu e_r\right)\left(\bar{d}_s\gamma^\mu d_t\right)$
C_{Lu}	$\left(\bar{L}_p\gamma_\mu L_r\right)\left(\bar{u}_s\gamma^\mu u_t\right)$	C_{Ld}	$\left(\bar{L}_p\gamma_\mu L_r\right)\left(\bar{d}_s\gamma^\mu d_t\right)$
C_{Qe}	$\left(\bar{Q}_p\gamma_\mu Q_r\right)\left(\bar{e}_s\gamma^\mu e_t\right)$	C_{LedQ}	$\left(\bar{L}_p^j e_r\right)\left(\bar{d}_s Q_t^j\right)$
$C_{LeQu}^{(1)}$	$\left(\bar{L}_p^j e_r\right)\varepsilon_{jk}\left(\bar{Q}_s^k u_t\right)$	$C_{LeQu}^{(3)}$	$\left(\bar{L}_p^j\sigma_{\mu\nu}e_r\right)\varepsilon_{jk}\left(\bar{Q}_s^k\sigma^{\mu\nu}u_t\right)$
C_{eW}	$\left(\bar{L}_p\sigma^{\mu\nu}e_r\right)\tau_I\varphi W_{\mu\nu}^I$	C_{eB}	$\left(\bar{L}_p\sigma^{\mu\nu}e_r\right)\varphi B_{\mu\nu}$

TABLE 4.2: Dominant $d=6$ SMEFT operators contributing to the CLFV processes generated by leptoquarks. The notation (up to small apparent changes) is the one from Ref. [56]. For the family indices, we use p, r, s and t, while j and k are weak isospin indices. For $I=1,2,3$, τ_I are the Pauli matrices, with $\varepsilon=i\tau_2$, and $\sigma^{\mu\nu}\equiv\frac{i}{2}[\gamma^\mu,\gamma^\nu]$. In the first row, Λ denotes the scale where the new dynamics arises. The operators share the same notation with the associated couplings, substituting simply $C\to\mathcal{O}$, i.e. $\mathcal{O}_{LQ}^{(1)}$ and so on. Four-fermion operators are obtained by integrating out, at the leading tree-level contribution, the leptoquark Lagrangian that we described in Section 4.1. The last two operators in the table generate $\mathcal{O}_\gamma=c_W\mathcal{O}_{eB}-s_W\mathcal{O}_{eW}$, which is obtained by integrating out the leptoquarks at the leading one-loop contribution.

4.2.1 Four-fermion operators

We start first with the matching giving the four-fermion CLFV operators. In the classical limit (tree level) this can be achieved by using the equations of motion of the integrated fields, as follows from the application of the steepest descent method to determine the path integral of the effective action [262,263]. This procedure gives a non-local Lagrangian. Assuming that these scalars (mass M_S) and vectors (mass M_V) are very heavy, in comparison with the energy scale of the effective action, we can make an expansion in momenta in the corresponding solutions for scalars S and vectors V, producing a local action. Sticking to the first order, we have, in a generic notation,

$$S_d \simeq \frac{Y_{d,rs}^{\chi_1\chi_2}}{M_S^2}\bar{\psi}'^s_{\chi_1}\psi^r_{\chi_2}, \qquad\qquad S_d^\dagger \simeq \frac{Y_{d,rs}^{\chi_1\chi_2}}{M_S^2}\bar{\psi}^r_{\chi_1}\psi'^s_{\chi_2}, \qquad (4.2.9)$$

$$V_d^\mu \simeq -\frac{X_{d,rs}^{\chi_1\chi_2}}{M_V^2}\bar{\psi}'^s_{\chi_1}\gamma^\mu\psi^r_{\chi_2}, \qquad\qquad V_d^{\mu\dagger} \simeq -\frac{X_{d,rs}^{\chi_1\chi_2}}{M_V^2}\bar{\psi}^r_{\chi_1}\gamma^\mu\psi'^s_{\chi_2}, \qquad (4.2.10)$$

where d refers to the SU(2) representation (dimensionality) of the LQ field, and repeated indices (chiralities χ_k and flavors r,s) are summed over. We will assume, in the following, that all the scalar leptoquarks, independently of their SU(2) quantum numbers, have the same mass M_S, and analogously for vector leptoquarks (having mass M_V). Inserting these relations back into Eq. (4.1.1) and introducing the notation of Table 4.1 used in the rest of the chapter, we obtain contributions to the effective Lagrangians accounting for effects stemming from the interactions of the

scalar and vector LQ fields:

$$
\begin{aligned}
\mathcal{L}_{\mathrm{S}}^{\mathrm{eff}} &\supset \frac{Y_{d,ij}^{\chi_1\chi_2} Y_{d,mn}^{\chi_3\chi_4}}{M_{\mathrm{S}}^2} \, (\bar{\psi}_{\chi_1}^i \psi_{\chi_2}'^{\,j})(\bar{\psi}_{\chi_4}'^{\,n} \psi_{\chi_3}^m)\,, \\
\mathcal{L}_{\mathrm{V}}^{\mathrm{eff}} &\supset \frac{X_{d,ij}^{\chi_1\chi_2} X_{d,mn}^{\chi_3\chi_4}}{M_{\mathrm{V}}^2} \, (\bar{\psi}_{\chi_1}^i \gamma_\mu \psi_{\chi_2}'^{\,j})(\bar{\psi}_{\chi_4}'^{\,n} \gamma^\mu \psi_{\chi_3}^m)\,.
\end{aligned}
\tag{4.2.11}
$$

Using the above prescription and restoring the SU(2) gauge structures, we end up with a list of effective $d = 6$ four-fermion operators. In order to recognize the couplings of the SMEFT Lagrangian in Table 4.2 (or the modified basis suitable for the numerical analysis from Chapter 3), we have employed Fierz reordering and several relations and identities, as detailed in the Appendix I. Hence, considering generically $\Lambda = M_{\mathrm{LQ}}$ for every leptoquark type,[2] we can identify products of two LQ couplings with the Wilson coefficients. The results are collected in Table I.1.

Leptoquarks can mediate lepton-flavor violation even when all Yukawa couplings are considered equal. However, since we have motivated and assumed an enhancement of this phenomenon for the third lepton family, we consider the τ-related Yukawas different (potentially larger) than those for the other two charged leptons, so that the (potentially stronger) limits imposed (from other works) on the first- or second-family-related Yukawas do not apply to our case. This fact, together with the flavor considerations (quark-flavor-blind Yukawas) discussed in the previous section, entail a rather simple flavor structure for the Yukawa matrices. In general,

$$
Y_{d,rs}^{\chi_1\chi_2} = \begin{pmatrix} y_d^{\chi_1\chi_2} & y_d^{\chi_1\chi_2} & y_{d\tau}^{\chi_1\chi_2} \\ y_d^{\chi_1\chi_2} & y_d^{\chi_1\chi_2} & y_{d\tau}^{\chi_1\chi_2} \\ y_d^{\chi_1\chi_2} & y_d^{\chi_1\chi_2} & y_{d\tau}^{\chi_1\chi_2} \end{pmatrix}_{rs}, \qquad y_d^{\chi_1\chi_2} \neq y_{d\tau}^{\chi_1\chi_2}\,.
\tag{4.2.12}
$$

The only exception to this prescription is, by definition, for Y_2^{LR}, the structure of which would be the $Y_d^{\chi_1\chi_2}$ from above transposed. For vector leptoquarks, we proceed analogously taking $Y \to X$.

4.2.2 Dipole operator and C_γ

Among all the $d = 6$ operators present in the relevant CLFV basis of Ref. [56], we concluded that the dominant contribution to the processes that we analyzed in the previous chapter, stemmed from dipole operators via the exchange of a photon, namely $\mathcal{O}_\gamma = c_{\mathrm{W}}\mathcal{O}_{eB} - s_{\mathrm{W}}\mathcal{O}_{eW}$ as written in terms of the operators from Table 4.2. However, within the leptoquark framework, the leading-order contribution to this operator occurs at one loop. In spite of that, and given the relevance of the strong bound on the corresponding WC, we think that it is pertinent that we also consider the leptoquark contribution to this coupling.

We consider the process $\ell_1 \to \ell_2\gamma$, with $\ell_1 = \tau$ and $\ell_2 = e, \mu$ at the leading one-loop order and driven by scalar leptoquarks (see Table 4.1). Before entering the calculation some comments are in order. Note that for the CLFV processes under

---

[2]As it will be clear further below, we consider two separate cases taking $\Lambda = M_{\mathrm{S}}$ ($\Lambda = M_{\mathrm{V}}$) for scalar (vector) leptoquarks.

consideration, a leptoquark and a quark enter necessarily in the loop. The relevant leptoquarks are thus $S_3^{1/3}$, $R_2^{5/3}$ and $S_1^{1/3}$ (with the superscripts identifying the respective electric charges) but only the last two provide a dominant contribution. Indeed, the main contribution to these amplitudes comes from chirality-enhanced effects. The triplet scalar LQ only couples to fermion doublets — hence to two fields of the same (left) chirality (see Table 4.1) — and their amplitudes are thus suppressed by the mass of either *lepton* in the process [264]. Meanwhile, the singlet and doublet LQs couple to both chiralities, and their amplitudes are hence proportional to the mass of the *quark* in the loop. Accordingly, the dominant amplitudes will be those which include the exchange of a LQ and a top quark. As a consequence, we will only consider the third-family quark. In addition — and this is also further motivated from the Yukawa flavor structure of Eq. (4.2.12) — all quarks couple with the same strength to leptoquarks and leptons, the difference among the latter then stemming from the specific lepton flavor only. Related to the dipole operator, we will thus only present the bounds for these singlet and doublet LQs, assuming that — as it also happens for the other LQs — the Yukawas of $S_3^{1/3}$ are more strongly constrained from the four-fermion operators (as it turns out to be the case). Note that the rest of the leptoquarks would also contribute through their couplings to other quark flavors, e.g. to bottom and charm quarks. Accordingly, their Yukawas would also be constrained by the C_γ bound. However, similar arguments as for $S_3^{1/3}$ apply.

Finally, since we are considering the $\ell_1 \to \ell_2\gamma$ process to perform the aforementioned matching, we can take into account also the bounds provided by direct searches for $\tau \to \ell\gamma$, with $\ell = e, \mu$ [71, 255]. For this we use the results from Ref. [264] and compare both types of constraints in Section 4.3.2; see also Ref. [265] for a complete matching of the scalar leptoquarks at the one-loop level to operators up to $d = 6$.

Matching the leading one-loop contribution from leptoquarks to C_γ

In this section we study, within the leptoquark framework, the leading one-loop order contribution to the $\ell_1 \to \ell_2\gamma$ process. Then, by integrating out the LQs we match our UV theory with the corresponding operators in the SMEFT [56]. This integration is performed following the so-called "integration by regions" method [266–269]. We thus sketch here the crucial steps to perform the matching via this method. This procedure will allow us to identify the leptoquark Lagrangian parameters with the C_γ Wilson coefficient (defined by Eq. (4.3.30)). Once the matching is performed, we will be able to translate the bounds on the later WC obtained in Chapter 3 over the relevant leptoquark parameters. The SMEFT operator, after spontaneous symmetry breaking, reads

$$\mathcal{L} \supset \frac{C_\gamma v}{\sqrt{2}\Lambda_{\mathrm{CLFV}}^2}\Big[\bar{\ell}_2\sigma^{\mu\nu}P_R\ell_1 + \bar{\ell}_2\sigma^{\mu\nu}P_L\ell_1\Big]F_{\mu\nu}\,, \qquad (4.2.13)$$

where $v = \langle 0|\varphi|0\rangle = (\sqrt{2}G_{\mathrm{F}})^{-1/2}$ and $F_{\mu\nu}$ is the photon field-strength tensor.

We write the effective Lagrangian generated by scalar leptoquarks giving the $\ell_1 \to \ell_2 \gamma$ process as

$$\mathcal{L}_{\text{eff}}^{\ell_1 \to \ell_2 \gamma} = \frac{e}{2} \bar{\ell}_2 \, i\sigma^{\mu\nu} \Big(\sigma_{\text{R}}^{\ell_1 \ell_2} P_{\text{R}} + \sigma_{\text{L}}^{\ell_1 \ell_2} P_{\text{L}} \Big) \ell_1 F_{\mu\nu} \,, \qquad (4.2.14)$$

where $\sigma_{\text{R}}^{\ell_1 \ell_2}$ and $\sigma_{\text{L}}^{\ell_1 \ell_2}$ are different loop functions given, in the most general case, by Ref. [264] and recast here below in terms of the parameters of our LQ framework (once the integration has taken place). Note that in the work of Chapter 3 no distinction between left and right polarizations was considered — hence the factorization of C_γ in Eq. (4.2.13) — which in turn meant working with symmetric WC flavor matrices in lepton flavor space, e.g. $C_\gamma^{\mu\tau} = C_\gamma^{\tau\mu}$ (omitting quark-flavor indices). However, within the leptoquark framework this is not always the case as it can be seen in the distinction between ℓ–τ conversion and hadronic τ decay processes for some of the Yukawa pairs (see Sections 4.3.2 and 4.3.3 below). This also happens in this loop computation entailing a distinction between $C_\gamma^{\tau h}$ and $C_\gamma^{\ell-\tau}$. Therefore, we made use of the amplitude squared of the $\ell_1 \to \ell_2 \gamma$ process to relate both frameworks since no direct matching at the Lagrangian level is possible. We find the relation

$$\left(\frac{C_\gamma^{\ell_1 \ell_2}}{\Lambda_{\text{CLFV}}^2} \right)^2 = \frac{e^2}{\sqrt{2}v^2} \left[\left(\sum_i \sigma_{\text{L},i}^{\ell_1 \ell_2} \right)^2 + \left(\sum_i \sigma_{\text{R},i}^{\ell_1 \ell_2} \right)^2 \right], \qquad (4.2.15)$$

with i running over all contributing leptoquarks, i.e. $S_3^{1/3}$, $R_2^{5/3}$ and $S_1^{1/3}$. The superscripts on C_γ label the specific process for which the matching is computed — either $\ell_1 = \ell$, $\ell_2 = \tau$ for ℓ–τ conversion in nuclei, or $\ell_1 = \tau$, $\ell_2 = \ell$ for the hadronic τ decays, with $\ell = e, \mu$. As explained above, the $S_3^{1/3}$ leptoquark does not provide a chirality enhancement effect and so its σ loop functions depend only on the lepton masses and not on the top-quark mass. From now on, we will consider the limit of massless leptons and neglect thus the $S_3^{1/3}$ contribution.

Equation (4.2.15) gives us the relation between our (bounded) Wilson coefficient C_γ and the σ functions which shall be matched to the parameters of the leptoquark framework. This matching consists of two parts.

First, the amplitude of the $\ell_1 \to \ell_2 \gamma$ is given from Eq. (4.2.14), in the following form [264]

$$\mathcal{A} = e \epsilon_\mu^*(q) \mathcal{M}^\mu \,. \qquad (4.2.16)$$

Due to Gauge invariance $\mathcal{M}^\mu$ may be expressed as

$$\mathcal{M}^\mu = \bar{u}_{\ell_2} (\sigma_L \Sigma_L^\mu + \sigma_R \Sigma_R^\mu + \dots) u_{\ell_1} \,, \qquad (4.2.17)$$

where

$$\Sigma_{L(R)}^\mu = (p_1^\mu + p_2^\mu) P_{L(R)} + \dots \,, \qquad (4.2.18)$$

with $\epsilon_\mu^*(q)$ the polarization vector of the outgoing photon with momentum q^μ and $p_{1(2)}^\mu$ the momentum of the lepton $\ell_{1(2)}$. Above we have omitted (in the dots) terms that are not relevant for the matching.

Second, the leading-order leptoquark contribution to this process is given by the four diagrams depicted in Fig. 4.1. Note that diagrams (B) and (D) do not contribute
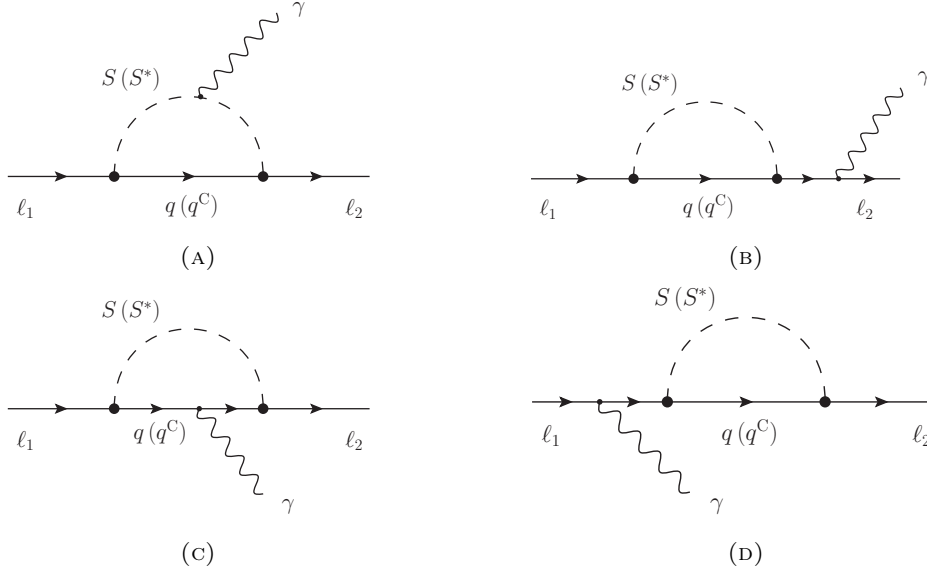
FIGURE 4.1: Feynman diagrams of the leading-order contribution to the $\ell_1 \to \ell_2\gamma$ process from scalar leptoquarks.

to the matching, but are necessary in the full calculation to properly account for the divergences. We thus consider only diagrams (A) and (C). The "integration by regions"[3] method consists in separating the "hard" (high energy) and "soft" (low energy) contributions and perform the matching via the hard part. Let us illustrate in the following the main steps this method involves. We focus here on the $R_2^{5/3}$ leptoquark, the procedure for $S_1^{1/3}$ is analog up to trivial changes. The amplitude of diagram (A) is (with $S \equiv R_2^{5/3}$ and $q \equiv t$)

$$\mathcal{A}_A = -N_{\rm C} e Q_{R_2^{5/3}} V_{tb} y_2^{LR} y_{2\tau}^{RL} \epsilon^{\mu*}(q) \times$$

$$\bar{u}_{\ell_2}(p_2) P_L \int \frac{d\ell^4}{(2\pi)^4} \frac{(2\ell - p_1 - p_2)_\mu (\slashed{\ell} + m_t)}{[\ell^2 - m_t^2][(\ell - p_2)^2 - M_S^2][(\ell - p_1)^2 - M_S^2]} P_L u_{\ell_1}(p_1) \,, \tag{4.2.19}$$

where we use the standard notation $\slashed{\ell} \equiv \ell_\nu \gamma^\nu$, $N_{\rm C}$ is the number of colors of the quark within the loop, M_S stands for the generic mass of the (scalar) leptoquarks and V_{tb} is the top–bottom entry of the CKM matrix (1.4.82) arising when working with the operators of Table 4.1 in the mass basis. In order to perform the integral over the high energy region, we should expand the integrand over the large momenta in the loop ℓ. Note that, even though ℓ is here the momentum of the quark, and we aim, on the contrary, to integrate out the leptoquarks, actually since $k_{1,2} = \ell - p_{1,2}$, where $k_{1,2}$ are the momenta of both leptoquarks within the loop, large ℓ entails large $k_{1,2}$ and viceversa. The expansion over $\ell \gg p_1, p_2, m_t$ then reads

$$\frac{1}{[\ell^2 - m_t^2][(\ell - p_2)^2 - M_S^2][(l - p_1)^2 - M_S^2]} \approx$$

---

[3]The procedure describe in the main text should be done in dimensional regularization.

$$\frac{1}{\ell^2[\ell^2 - M_S^2]^2}\left(1 + \frac{m_t^2}{\ell^2}\right)\left(1 - \frac{p_2^2 - 2(\ell \cdot p_2)}{\ell^2 - M_S^2}\right)\left(1 - \frac{p_1^2 - 2(\ell \cdot p_1)}{\ell^2 - M_S^2}\right).$$
(4.2.20)

The integral of Eq. (4.2.19) can be then computed — with the expansion of Eq. (4.2.20) — via the Passarino-Veltman reduction in terms of scalar n-point functions. In the massless-lepton limit and keeping only the finite and leading terms in the expansion, i.e. terms of $\mathcal{O}(1/M^2)$, we obtain

$$\mathcal{A}_A = -N_C e Q_{R_2^{5/3}} V_{tb} y_2^{LR} y_{2\tau}^{RL} \epsilon^{\mu*}(q) \bar{u}_{\ell_2}(p_2) P_L \left[\frac{i}{16\pi^2} \frac{m_t}{2M_S^2}\left((p_1 + p_2)_\mu - m_t \gamma_\mu\right)\right] P_L u_{\ell_1}(p_1),$$
(4.2.21)

note that the γ_μ term gets canceled by the sandwich $P_L \gamma_\mu P_L = 0$.

For diagram (C) we find

$$\mathcal{A}_C = -N_C e Q_t V_{tb} y_2^{LR} y_{2\tau}^{RL} \epsilon^{\mu*}(q) \times$$

$$\bar{u}_{\ell_2}(p_2) P_L \int \frac{d\ell^4}{(2\pi)^4} \frac{(\slashed{\ell} - \slashed{p}_2 + m_t)\gamma_\mu(\slashed{\ell} - \slashed{p}_1 + m_t)}{[\ell^2 - M_S^2][(\ell - p_2)^2 - m_t^2][(\ell - p_1)^2 - m_t^2]} P_L u_{\ell_1}(p_1), \quad (4.2.22)$$

with Q_t the charge of the top quark in the loop. The expansion of the integrand looks now like

$$\frac{1}{[\ell^2 - M_S^2][(\ell - p_2)^2 - m_t^2][(\ell - p_1)^2 - m_t^2]} \approx$$

$$\frac{1}{\ell^4[\ell^2 - M_S^2]}\left(1 - \frac{p_2^2 - 2(\ell \cdot p_2) - m_t^2}{\ell^2}\right)\left(1 - \frac{p_1^2 - 2(\ell \cdot p_1) - m_t^2}{\ell^2}\right). \quad (4.2.23)$$

The integral of Eq. (4.2.22) — under the same assumptions as for the previous case — thus provides

$$\mathcal{A}_C = -N_C e Q_t V_{tb} y_2^{LR} y_{2\tau}^{RL} \epsilon^{\mu*}(q) \bar{u}_{\ell_2}(p_2) \left[\frac{-i}{16\pi^2} \frac{3m_t}{2M_S^2}(p_1 + p_2)_\mu\right] P_L u_{\ell_1}(p_1). \quad (4.2.24)$$

Note that the results of the amplitudes in Eqs. (4.2.21) and (4.2.24) now have the same shape as Eqs. (4.2.17) and (4.2.18). Therefore, the matching of the σ functions is straightforward, giving for $R_2^{5/3}$ and $S_1^{1/3}$

- $R_2^{5/3}$

$$\sigma_{L, R_2^{5/3}}^{\tau h} = \sigma_{R, R_2^{5/3}}^{\ell-\tau} = \frac{iN_C}{16\pi^2}\frac{m_t}{M_S^2} y_{2\tau}^{RL} y_2^{LR} V_{tb}\left(\frac{3}{2}Q_t - \frac{1}{2}Q_{R_2^{5/3}}\right),$$

$$\sigma_{R, R_2^{5/3}}^{\tau h} = \sigma_{L, R_2^{5/3}}^{\ell-\tau} = \frac{iN_C}{16\pi^2}\frac{m_t}{M_S^2} y_{2\tau}^{LR} y_2^{RL} V_{tb}\left(\frac{3}{2}Q_t - \frac{1}{2}Q_{R_2^{5/3}}\right),$$
(4.2.25)

- $S_1^{1/3}$

$$\sigma_{L, S_1^{1/3}}^{\tau h} = \sigma_{R, S_1^{1/3}}^{\ell-\tau} = -\frac{iN_C}{16\pi^2}\frac{m_t}{M_S^2} y_{1\tau}^{LL} y_1^{RR} V_{tb}\left(\frac{3}{2}Q_{\bar{t}} - Q_{S_1^{1/3}}\right),$$

$$\sigma_{R, S_1^{1/3}}^{\tau h} = \sigma_{L, S_1^{1/3}}^{\ell-\tau} = -\frac{iN_C}{16\pi^2}\frac{m_t}{M_S^2} y_{1\tau}^{RR} y_1^{LL} V_{tb}\left(\frac{3}{2}Q_{\bar{t}} - Q_{S_1^{1/3}}\right).$$
(4.2.26)

This coincides — in the limit of massless leptons — with the results from Ref. [264], once the logarithms (stemming from the low-energy behaviour and, hence, not contributing to the matching) are removed. Above, $Q_t = 2/3$ ($Q_{\bar{t}} = -2/3$) is the charge of the top (anti-top) quark and $Q_{R_2^{5/3}} = 5/3$ and $Q_{S_1^{1/3}} = 1/3$ are the charges of the $R_2^{5/3}$ and $S_1^{1/3}$ leptoquarks, respectively. Note that $\sigma_{\mathrm{L},i}^{\tau h} = \sigma_{\mathrm{R},i}^{\ell-\tau}$ holds true only in the case of massless leptons.

The total result for the matching, including the contribution from both leptoquarks, is thus (see Eq. (4.2.15))

$$
\left(\frac{C_\gamma}{\Lambda_{\mathrm{CLFV}}^2}\right)^2 = \frac{e^2 N_C^2 m_t^2 V_{tb}^2}{2^{11}\pi^4 v^2 M_{\mathrm{S}}^4}
$$

$$
\times \left[\left((y_{2\tau}^{\mathrm{RL}}y_2^{\mathrm{LR}})^2 + (y_{2\tau}^{\mathrm{LR}}y_2^{\mathrm{RL}})^2\right)\left(Q_{R_2^{5/3}} - 3Q_t\right)^2 + \left((y_{1\tau}^{\mathrm{LL}}y_1^{\mathrm{RR}})^2 + (y_{1\tau}^{\mathrm{RR}}y_1^{\mathrm{LL}})^2\right)\left(Q_{S_1^{1/3}} - 3Q_{\bar{t}}\right)^2 \right.
$$

$$
\left. - 2\left((y_{2\tau}^{\mathrm{RL}}y_2^{\mathrm{LR}})(y_{1\tau}^{\mathrm{LL}}y_1^{\mathrm{RR}}) + (y_{2\tau}^{\mathrm{LR}}y_2^{\mathrm{RL}})(y_{1\tau}^{\mathrm{RR}}y_1^{\mathrm{LL}})\right)\left(Q_{R_2^{5/3}} - 3Q_t\right)\left(Q_{S_1^{1/3}} - 3Q_{\bar{t}}\right) \right].
$$

$$(4.2.27)$$

Above, we have omitted the superscripts $\ell_1\ell_2$ of C_γ since in the limit of massless leptons we obtain the same matching for hadronic τ decays and ℓ–τ conversion in nuclei. Consequently, the bounds from both processes can be applied to the same combination of Yukawa couplings.

One may wonder, once we have introduced this loop calculation and due to the strong bound provided either from hadronic τ decays or the $\tau \to (e, \mu)\gamma$ process, wether running effects on C_γ may help constraining other operators. The one-loop RGE for C_γ indeed relates several Wilson coefficients:

$$
\frac{dC_\gamma}{d\ln\mu} = \gamma_{\gamma j} C_j = f(C_\gamma, C_Z, C_{LeQu}^{(3)}) \tag{4.2.28}
$$

where μ is the renormalization-group energy scale, $\gamma_{\gamma j}$ is the anomalous-dimension matrix defined in Chapter 2 and for which the subindex γ corresponds to C_γ while j runs over all WCs. According to Eq. (4.2.28), the only non-zero $\gamma_{\gamma j}$ terms are those regarding C_γ, C_Z and $C_{LeQu}^{(3)}$, which are given in Ref. [63]. However, these RGEs contain only electroweak (not QCD) effects which we are neglecting in accordance to the work of Chapter 3. Therefore, in order to keep the consistency with the previous work and since the RGE usually involves loop-suppressed relations for the non-diagonal anomalous-dimension matrices, we do not consider the RGE of C_γ.

4.3 Results

We address now the results of our analyses. The constraints for the SMEFT $d = 6$ Wilson coefficients presented in the previous chapter were obtained considering the expected sensitivity of the NA64 experiment at CERN [138] (for ℓ–τ conversion in nuclei), and the current and expected results of Belle [255] and Belle II [71] experiments (for hadronic τ decays). We arrived at the final numerical values for

the bounds by means of the open-source tool `HEPfit` [270]. These have to be now translated to the leptoquark-associated ratios $yy'/M_{\rm S}^2$ and $xx'/M_{\rm V}^2$. Let us list some important aspects of relating the SMEFT and leptoquark frameworks.

In Chapter 3, all $d = 6$ operators contributing to CLFV processes were considered simultaneously, and it was shown that a naive single-operator analysis would result in overestimated (stronger) constraints on the corresponding WCs, simply due to the lack of correlations among the operators. On a similar basis, we think that it is more natural to consider a scenario in which not only one type of scalar or vector LQ drives the CLFV dynamics. Furthermore, the limits extracted by reviewing the results on the processes involving the CLFV phenomena in our previous work assumed only one energy scale $\Lambda_{\rm CLFV}$. On the other hand, within the leptoquark framework we have many possible scales: LQ masses. The nature of different LQs (scalar and vector) can, in principle, be completely unrelated, and stem from a very different origin and/or scale. Hence, we divide our analysis into two separate parts: We consider first the simultaneous contribution of all different types of scalar leptoquarks (described by a common mass $M_{\rm S}$) and then of all vector leptoquarks (common mass $M_{\rm V}$), with $M_{\rm S} \neq M_{\rm V}$ in general. Note that one could alternatively perform a single-LQ analysis with non-degenerated (scalar or vector) leptoquarks. In the literature, it is indeed customary to consider one or (less often) two LQs at a time. However, it seems to us that this assumption is much more restrictive than simply suggesting that LQs might arise at the same or similar scale and, as stated above, it is an approach that necessarily misses the relevant correlations among leptoquark contributions.

In the work of Ref. [74] presented in the previous chapter, we extracted bounds on the aforementioned $d = 6$ SMEFT Wilson coefficients from CLFV τ-involved processes within two distinct scenarios:

(i) we considered new physics driving only CLFV in the τ sector,

(ii) on top of these phenomena, we also allowed for flavor-changing neutral currents in the quark sector — transitions $(\bar{c}u)$, $(\bar{b}s)$, $(\bar{s}d)$, etc. However, for the second scenario, we made the assumption that the energy scales $\Lambda_{\rm CLFV}$ and $\Lambda_{\rm FCNC}$ driving these phenomena were the same.

Within the leptoquark framework, due to the nature of the LQ–lepton–quark interactions, this hypothesis is much better motivated, e.g. leptoquarks readily mediate some FCNC processes even in the presence of negligible off-diagonal Yukawa couplings. Hence, we present all the bounds obtained in the (second) FCNC case.

Finally, since the constraints are obtained from CLFV τ-involved processes, we performed the running of all the Wilson coefficients to the scale given by the τ mass; see Chapter 3 for more details. Accordingly, the bounds on the pairs of Yukawa couplings are presented at this scale.

4.3.1 Dictionary for the CLFV effective basis

In Table I.1, we collect the results for the matching of the leptoquark framework to the SMEFT operators listed in Table 4.2 upon tree-level integration of the leptoquarks. However, the basis of $d = 6$ operators presented in Table 4.2 does not

exactly match the basis constrained from the CLFV processes studied in Chapter 3. A short dictionary is given here to ease the transition.

Consistently with Chapter 3, we only consider the QCD running of the SMEFT operators. On top of that, we do not consider the (very suppressed) QCD running of the vector and axial-vector currents, while the running of the scalar densities is related to the divergences of the vector currents through, for instance, $\partial^\mu(\bar{s}\gamma_\mu u) = i(m_s - m_u)(\bar{s}u)$. Hence, the scalar Wilson coefficients were redefined into scale-invariant C'_{LedQ} and $C^{(1)\prime}_{LeQu}$, such that

$$C^{(1)}_{LeQu} = \frac{m_i}{m_\tau} C^{(1)\prime}_{LeQu}\,, \qquad\qquad C_{LedQ} = \frac{m_i}{m_\tau} C'_{LedQ}\,, \qquad\qquad (4.3.29)$$

with m_i being the mass of the quark involved in the process. For the related bound, this just entails a change by a factor proportional to m_i. For u-processes ($C^{(1)}_{LeQu}$) in ℓ–τ conversion, since we considered $m_u = 0$, the overall factor becomes m_c; in hadronic τ decays though, despite having taken into account the χPT scale-independent combination $2B_0 M_q \simeq M_p$ (with M_q being the diagonal matrix of the light-quark masses and M_p the physical-mass matrix of the pseudoscalar Goldstone bosons defined in Eq. (2.4.55)), we will consider the mass of the up quark at the energy scale of the τ mass. For d-processes (C_{LedQ}), the situation is slightly more involved: For the lightest quark in ℓ–τ conversion, it holds accordingly $m_d = 0$. However, for s and b quarks, even though different masses were considered, only a single bound was obtained, introducing an ambiguity when translating the constraints on the primed WCs into the non-primed. This is solved for vector leptoquarks[4] by considering the most conservative bound, i.e. taking $m_i = m_b$. For hadronic τ decays, related accordingly to the most conservative bound, m_s at the scale of m_τ is used.

Considering now the γ dipole case, the C_{eB} and C_{eW} (see Table 4.2) were rotated into C_γ and C_Z, parametrizing the γ- and Z-mediated contributions separately, i.e.

$$\begin{pmatrix} C_\gamma \\ C_Z \end{pmatrix} = \begin{pmatrix} c_W & -s_W \\ s_W & c_W \end{pmatrix} \begin{pmatrix} C_{eB} \\ C_{eW} \end{pmatrix}. \qquad\qquad (4.3.30)$$

However, neither the C_Z nor the rest of Z-mediated contributions (provided by the coupling of the Z to leptoquarks) will be considered in our analyses, since the related leading LQ contribution appears at one loop and the resulting constraints would thus not be competitive.

The absence of some operators within each leptoquark scenario poses another caveat related to the correlations between the present and absent (or numerically negligible) operators. The correlations found in the analysis of Chapter 3 and presented in Appendix H tend to relax the bounds set on individual Wilson coefficients: A loss of any correlation would turn into stronger constraints for the specific WC. In this study, when the results are presented below, in case there is some significant correlation between present and absent WCs, we will adopt the most conservative view and assume that, somehow, the correlated operators could be present and the weakest constraint is used. To explain this point better, let us provide an example. We found that, for instance, $C^{(1)\prime}_{\varphi L}$ (that is absent) correlates strongly with $C^{(1)}_{LQ}$,

---

[4]Note that scalars do not contribute at tree level to C_{LedQ}, as can be seen in Table I.1.

$C_{LQ}^{(3)}$ and C_{Lu} (see Fig. H.1), and that the limits on the three latter mentioned stem from the global analysis where these correlations are taken into account. The same happens for the correlation of the rotated C_Z with $C_{LeQu}^{(3)}$ and C_γ, the latter of which further translates into C_{eB} and C_{eW}. To be more specific, let us discuss other examples within the vector LQ scenario: C_{LedQ} is strongly correlated with $C_{e\varphi}$, although the latter is omitted here; $C_{LeQu}^{(1)}$ and $C_{LeQu}^{(3)}$ are completely absent and, while the first is practically uncorrelated, the second correlates significantly with the (rotated) C_γ (not considered here) and C_Z (not taken into account).

The previous paragraph refers to the case of τ decays; for $\ell-\tau$ conversion in nuclei, the only Wilson coefficients used here are either correlated among each other ($C_{LeQu}^{(1)\,\ell-\tau}$ and $C_{LeQu}^{(3)\,\ell-\tau}$) or not correlated with other WCs ($C_{LedQ}^{\ell-\tau}$).

In summary, the correlations between the Wilson coefficients of the SMEFT are transferred into the corresponding constraints on the products of LQ Yukawa-like couplings. As commented above, we have taken into account this feature in our analysis and we consider the bounds we present conservative.

4.3.2 Scalar leptoquarks

We have considered the contribution of all scalar leptoquarks to both the four-fermion and the dipole operators.

Four-fermion constraints

For scalar leptoquarks, assuming a common energy scale $\Lambda_{\mathrm{CLFV}} = M_{\mathrm{S}}$, one can unambiguously relate pairs of Yukawa LQ couplings with distinct linear combinations of Wilson coefficients. We find

$$
\begin{aligned}
y_3^{\mathrm{LL}} y_{3\,\tau}^{\mathrm{LL}} &= C_{LQ}^{(1)} + C_{LQ}^{(3)}\,, \\
y_2^{\mathrm{RL}} y_{2\,\tau}^{\mathrm{RL}} &= -2C_{Lu}\,, & y_2^{\mathrm{LR}} y_{2\,\tau}^{\mathrm{LR}} &= -2C_{Qe}\,, \\
y_1^{\mathrm{LL}} y_{1\,\tau}^{\mathrm{LL}} &= C_{LQ}^{(1)} - 3C_{LQ}^{(3)}\,, & y_1^{\mathrm{RR}} y_{1\,\tau}^{\mathrm{RR}} &= 2C_{eu}\,, \\
\tilde{y}_2^{\mathrm{RL}} \tilde{y}_{2\,\tau}^{\mathrm{RL}} &= -2C_{Ld}\,, & \tilde{y}_1^{\mathrm{RR}} \tilde{y}_{1\,\tau}^{\mathrm{RR}} &= 2C_{ed}\,, & (4.3.31) \\
y_{2\,\tau}^{\mathrm{RL}} y_2^{\mathrm{LR}} &= -C_{LeQu}^{(1)\,\ell-\tau} - 4C_{LeQu}^{(3)\,\ell-\tau}\,, & y_2^{\mathrm{RL}} y_{2\,\tau}^{\mathrm{LR}} &= -C_{LeQu}^{(1)\,\tau h} - 4C_{LeQu}^{(3)\,\tau h}\,, \\
y_{1\,\tau}^{\mathrm{LL}} y_1^{\mathrm{RR}} &= C_{LeQu}^{(1)\,\ell-\tau} - 4C_{LeQu}^{(3)\,\ell-\tau}\,, & y_1^{\mathrm{LL}} y_{1\,\tau}^{\mathrm{RR}} &= C_{LeQu}^{(1)\,\tau h} - 4C_{LeQu}^{(3)\,\tau h}\,.
\end{aligned}
$$

Here, the superscripts '$\ell-\tau$' and 'τh' stand for the respective processes ($\ell-\tau$ conversion in nuclei and hadronic τ decays), from which the bounds on WCs stem, given that the corresponding pairs of Yukawa couplings (which we simply refer to as 'Yukawa pairs' further on) contribute only to one of those processes.

The numerical results are presented in Table 4.3, which shows constraints for two different aspects of the leptoquark framework: *lower* bounds for the masses of scalar leptoquarks assuming the product of LQ Yukawa couplings being of $\mathcal{O}(1)$, and, in turn, *upper* bounds for the Yukawa pairs, taking $M_{\mathrm{S}} = 1\,\mathrm{TeV}$. Note that the two Yukawa pairs $y_{2\,\tau}^{\mathrm{RL}} y_2^{\mathrm{LR}}$ and $y_{1\,\tau}^{\mathrm{LL}} y_1^{\mathrm{RR}}$ are unconstrained by τ decays. Thus, the $\ell-\tau$ conversion limits are considered instead. Regarding these last couple of

τ decays	Upper bounds on $\frac{|yy'|}{M_S^2}$ [10^{-3} TeV^{-2}]		Lower bounds on M_S [TeV]	
Yukawa pair	Belle	Belle II	Belle	Belle II
$|y_3^{LL} y_{3\,\tau}^{LL}|$	12	1.9	9.1	23
$|y_2^{RL} y_{2\,\tau}^{RL}|$	47	5.0	4.6	14
$|y_2^{LR} y_{2\,\tau}^{LR}|$	17	2.6	7.8	20
$|y_2^{RL} y_{2\,\tau}^{LR}|$	28	3.7	6.0	16
$|\tilde{y}_2^{RL} \tilde{y}_{2\,\tau}^{RL}|,\ |\tilde{y}_1^{RR} \tilde{y}_{1\,\tau}^{RR}|$	20	3.0	7.1	18
$|y_1^{LL} y_{1\,\tau}^{LL}|$	64	7.7	3.9	11
$|y_1^{RR} y_{1\,\tau}^{RR}|$	34	4.1	5.4	16
$|y_1^{LL} y_{1\,\tau}^{RR}|$	28	3.7	6.0	16

ℓ–τ conversion	Upper bounds on $\frac{|yy'|}{M_S^2}$ [10^{0} TeV^{-2}]		Lower bounds on M_S [TeV]	
Yukawa pair	e–τ	μ–τ	e–τ	μ–τ
$|y_{2\,\tau}^{RL} y_2^{LR}|$	350	2.3	0.054	0.66
$|y_{1\,\tau}^{LL} y_1^{RR}|$	250	1.8	0.063	0.75

TABLE 4.3: Obtained bounds for the scalar leptoquark case from the results presented in Chapter 3. In the left-hand part of the table, we present *upper* bounds on the ratio $|yy'|/M_S^2$; these numbers, of course, also correspond to (with appropriate power of 10) *upper* bounds on the Yukawa pairs $|yy'|$, assuming $M_S = 1$ TeV. On the right, there are *lower* bounds on the probed energy scale of the scalar leptoquarks mediating CLFV phenomena ($\Lambda_{CLFV} = M_S$), considering $|yy'| \approx 1$. The strongest bounds found are shown, most of which are stemming from the τ decays analysis (Belle and Belle II results), the exception being the last couple of rows dedicated to Yukawas contributing only to ℓ–τ conversion. The values are given at the 99.8 % confidence level.

bounds, the allowed values for the Yukawa pairs from e–τ conversion exceed by far the limits suggested by perturbativity considerations; on the other hand, the bounds on the probed mass (with $|yy'| \approx 1$) just indicate that the expected experimental constraints from ℓ–τ conversion in nuclei could not yet compete with those stemming from the τ decays.

Dipole operator and C_γ constraints

In order to translate the constraint on the dipole C_γ shown in Chapter 3 (see Fig. 3.9 and Table 3.2) into the most general leptoquark framework considered in this work, we have evaluated the (leading) one-loop contribution to the $\ell_1 \to \ell_2 \gamma$ process within the leptoquark UV theory (4.1.1) and, upon integrating out the leptoquark fields, performed the matching of the result with the one obtained within SMEFT; for details, see Section 4.2.2. As explained there, only two LQ fields contribute to this process, namely $S_1^{1/3}$ and $R_2^{5/3}$.

For completeness, we also consider the most stringent bounds stemming from the $\tau \to \ell\gamma$ direct searches (with $\ell = e, \mu$) by Belle and BaBar [255], and compare them with the constraints obtained from C_γ, in the same way as it is explained for

$C_\gamma/\Lambda_{\mathrm{CLFV}}^2$	Upper bounds on $\frac{|yy'|}{M_{\mathrm{S}}^2}$ $[10^{-3}\,\mathrm{TeV}^{-2}]$		Lower bounds on M_{S} [TeV]	
Yukawa pair	Belle	Belle II	Belle	Belle II
$|y_{2\tau}^{\mathrm{RL}}y_2^{\mathrm{LR}}|$	150	19	3.1	8.6
$|y_{1\tau}^{\mathrm{LL}}y_1^{\mathrm{RR}}|$	21	2.7	8.2	23

$\tau \to \ell\gamma$	Upper bounds on $\frac{|yy'|}{M_{\mathrm{S}}^2}$ $[10^{-3}\,\mathrm{TeV}^{-2}]$		Lower bounds on M_{S} [TeV]	
Yukawa pair	$\tau \to e\gamma$	$\tau \to \mu\gamma$	$\tau \to e\gamma$	$\tau \to \mu\gamma$
$|y_{2\tau}^{\mathrm{RL}}y_2^{\mathrm{LR}}|$	0.66	0.79	83	75
$|y_{1\tau}^{\mathrm{LL}}y_1^{\mathrm{RR}}|$	1.4	1.7	71	64

TABLE 4.4: Obtained bounds for the $R_2^{5/3}$ (first row) and $S_1^{1/3}$ (second row) single-scalar-leptoquark cases (only one scalar leptoquark considered at a time). The values in the top part of the table stem from the bounds on $C_\gamma/\Lambda_{\mathrm{CLFV}}^2$ (once the four-fermion constraints are applied) based on the results from Chapter 3. The bottom part shows bounds obtained from direct searches for $\tau \to \ell\gamma$ by Belle and BaBar experiments [255]. In the left-hand part of the table, we present *upper* bounds on the ratio $|yy'|/M_{\mathrm{S}}^2$; these numbers also correspond to *upper* bounds on the Yukawa pairs $|yy'|$, assuming $M_{\mathrm{S}} = 1\,\mathrm{TeV}$. On the right, there are *lower* bounds on the probed energy scale of the scalar leptoquarks mediating CLFV phenomena ($\Lambda_{\mathrm{CLFV}} = M_{\mathrm{S}}$), considering $|yy'| \approx 1$. The strongest bounds found on C_γ are shown and are stemming from the τ decays analysis (i.e. from the Belle and Belle II results). The values from C_γ are given at the 99.8 % confidence level while bounds from direct searches are given at the 90 % confidence level.

the single leptoquark scenarios below. Since these processes provide bounds on the same ratios yy'/M_{S}^2 as the C_γ constraint, we compare all of them in Table 4.4.

In the following, we explain the different cases that we analyze:

Leptoquark $R_2^{5/3}$

In a framework with only the $R_2^{5/3}$ leptoquark, the main contribution to the process $\ell_1 \to \ell_2\gamma$ — once the LQ is integrated out — provides the following matching between the SMEFT γ dipole operator and the UV theory (see Section 4.2.2):

$$\left(\frac{C_\gamma}{\Lambda_{\mathrm{CLFV}}^2}\right)^2 = \frac{e^2 N_C^2 m_t^2 V_{tb}^2}{2^{11}\pi^4 v^2 M_{\mathrm{S}}^4}\left(Q_{R_2^{5/3}} - 3Q_t\right)^2\left[(y_{2\tau}^{\mathrm{RL}}y_2^{\mathrm{LR}})^2 + (y_{2\tau}^{\mathrm{LR}}y_2^{\mathrm{RL}})^2\right]. \qquad (4.3.32)$$

The main bounds coming from the four-fermion operators on the above-appearing Yukawa pairs are $\left|y_{2\tau}^{\mathrm{RL}}y_2^{\mathrm{LR}}\right| = 8\,C_{LeQu}^{(3)\,\ell-\tau} \lesssim 1.1\left(\frac{\Lambda_{\mathrm{CLFV}}}{\mathrm{TeV}}\right)^2$ and $\left|y_{2\tau}^{\mathrm{LR}}y_2^{\mathrm{RL}}\right| = 2\,C_{LeQu}^{(1)\,\tau h} \lesssim 5.8 \times 10^{-3}\left(\frac{\Lambda_{\mathrm{CLFV}}}{\mathrm{TeV}}\right)^2$ (Belle). Since the bound from τ decays constrains the value of $\left|y_{2\tau}^{\mathrm{LR}}y_2^{\mathrm{RL}}\right|$ by about 3 orders of magnitude stronger than the bound from $\ell-\tau$ conversion does for $\left|y_{2\tau}^{\mathrm{RL}}y_2^{\mathrm{LR}}\right|$, we can, in Eq. (4.3.32), neglect the contribution from the former and use the limits from Belle and Belle II for $C_\gamma/\Lambda_{\mathrm{CLFV}}^2$ to constrain $\left|y_{2\tau}^{\mathrm{RL}}y_2^{\mathrm{LR}}\right|/M_{\mathrm{S}}^2$. The results are presented in Table 4.4. As we can see, the Yukawa pair $\left|y_{2\tau}^{\mathrm{RL}}y_2^{\mathrm{LR}}\right|$ as well as the corresponding probed scale M_{S} both receive a stronger constraint than in the previous case (cf. Table 4.3) where this pair was only sensitive to the limits from $\ell-\tau$ conversion in nuclei, and was, accordingly, bounded rather weakly.

Leptoquark $S_1^{1/3}$

In this case, we end up with the following matching (see Section 4.2.2):

$$\left(\frac{C_\gamma}{\Lambda_{\mathrm{CLFV}}^2}\right)^2 = \frac{e^2 N_C^2 m_t^2 V_{tb}^2}{2^{11}\pi^4 v^2 M_{\mathrm{S}}^4}\left(Q_{S_1^{1/3}} - 3Q_{\bar{t}}\right)^2\left[(y_{1\tau}^{\mathrm{LL}}y_1^{\mathrm{RR}})^2 + (y_{1\tau}^{\mathrm{RR}}y_1^{\mathrm{LL}})^2\right]. \qquad (4.3.33)$$

The main bounds coming from the four-fermion operators on the Yukawa pairs involved are $\left|y_{1\tau}^{\mathrm{LL}}y_1^{\mathrm{RR}}\right| = 8\,C_{LeQu}^{(3)\,\ell-\tau} \lesssim 1.1\left(\frac{\Lambda_{\mathrm{CLFV}}}{\mathrm{TeV}}\right)^2$ and $\left|y_{1\tau}^{\mathrm{RR}}y_1^{\mathrm{LL}}\right| = 2\,C_{LeQu}^{(1)\,\tau h} \lesssim 5.8 \times 10^{-3}\left(\frac{\Lambda_{\mathrm{CLFV}}}{\mathrm{TeV}}\right)^2$ (Belle). As before, in Eq. (4.3.33), we can thus neglect the contribution of $\left|y_{1\tau}^{\mathrm{RR}}y_1^{\mathrm{LL}}\right|$ (which receives stronger bounds), and use the limits from Belle and Belle II on $C_\gamma/\Lambda_{\mathrm{CLFV}}^2$ to constrain $\left|y_{1\tau}^{\mathrm{LL}}y_1^{\mathrm{RR}}\right|/M_{\mathrm{S}}^2$. The results are presented in Table 4.4. Again the bound on the dipole operator helps to constrain the otherwise weakly-bounded (cf. Table 4.3) Yukawa pair $\left|y_{1\tau}^{\mathrm{LL}}y_1^{\mathrm{RR}}\right|$.

Finally, note that in both single-leptoquark cases — even though the Yukawa pairs are more constrained from the bound on C_γ stemming from τ decays than from ℓ–τ conversion limits — the probed energy scale (when assuming $|yy'| \approx 1$) is still smaller than the value obtained from the four-fermion bound of 13 TeV and 36 TeV from Belle and Belle II limits, respectively, on $\left|y_{2\tau}^{\mathrm{LR}}y_2^{\mathrm{RL}}\right|/M_{\mathrm{S}}^2$ (for $R_2^{5/3}$) and $\left|y_{1\tau}^{\mathrm{RR}}y_1^{\mathrm{LL}}\right|/M_{\mathrm{S}}^2$ (for $S_1^{1/3}$). This is due to the fact that the same mass enters for all WCs (operators).

Leptoquarks $R_2^{5/3} + S_1^{1/3}$

When both contributing leptoquarks $R_2^{5/3}$ and $S_1^{1/3}$ are considered at the same time, the corresponding matching given in Eq. (4.2.27) — for natural values of the Yukawa pairs $|yy'| \approx 1$ — is probing $M_{\mathrm{S}} \gtrsim 4.7\,\mathrm{TeV}$ stemming from the Belle τ decay limits (using $C_\gamma/\Lambda_{\mathrm{CLFV}}^2 \lesssim 7 \times 10^{-5}\,\mathrm{TeV}^{-2}$) or $M_{\mathrm{S}} \gtrsim 13\,\mathrm{TeV}$ stemming from the Belle II limits (using $C_\gamma/\Lambda_{\mathrm{CLFV}}^2 \lesssim 9 \times 10^{-6}\,\mathrm{TeV}^{-2}$). However, it does not provide relevant bounds on the Yukawa pairs.

4.3.3   Vector leptoquarks

We consider the contribution of vector leptoquarks to the four-fermion operators only, since, as explained in Section 4.1, the interactions of vector leptoquarks with gauge bosons cannot be unambiguously ascertained. Upon their integration, with $\Lambda_{\mathrm{CLFV}} = M_{\mathrm{V}}$, we end up with 11 distinct Yukawa pairs contributing to 8 Wilson coefficients (see Table I.1). Due to the flavor structure of the Yukawas and the integration of the LQs themselves, most of the Yukawa pairs contribute equally to both the ℓ–τ conversion and τ decays. However, there are two pairs (stemming from the last column in Table I.1) which are not symmetric (built from two same matrices) and produce couplings in combinations relevant only to one type of process at a time, thus adding an extra effective bound. These relate only to C_{LedQ} through the following relations:

$$\frac{1}{2}\,C_{LedQ}^{\ell-\tau} = x_{1\tau}^{\mathrm{LL}}x_1^{\mathrm{RR}} - x_{2\tau}^{\mathrm{RL}}x_2^{\mathrm{LR}}, \qquad\qquad \frac{1}{2}\,C_{LedQ}^{\tau h} = x_1^{\mathrm{LL}}x_{1\tau}^{\mathrm{RR}} - x_2^{\mathrm{RL}}x_{2\tau}^{\mathrm{LR}}. \qquad (4.3.34)$$

Hence, we can take the two linear combinations of Yukawa pairs present in Eq. (4.3.34) and define new independent pairs of couplings, $x_{1,2}^{\ell-\tau} \equiv x_{1\tau}^{\mathrm{LL}} x_1^{\mathrm{RR}} - x_{2\tau}^{\mathrm{RL}} x_2^{\mathrm{LR}}$ and $x_{1,2}^{\tau h} \equiv x_1^{\mathrm{LL}} x_{1\tau}^{\mathrm{RR}} - x_2^{\mathrm{RL}} x_{2\tau}^{\mathrm{LR}}$, and set bounds on them instead. The relations among the Yukawa pairs and the WCs are then straightforward:

$$
\begin{aligned}
x_3^{\mathrm{LL}} x_{3\tau}^{\mathrm{LL}} &= \frac{1}{2}(C_{LQ}^{(3)} - C_{LQ}^{(1)}), & x_2^{\mathrm{RL}} x_{2\tau}^{\mathrm{RL}} &= C_{Ld}, & x_2^{\mathrm{LR}} x_{2\tau}^{\mathrm{LR}} &= C_{Qe}, \\
\tilde{x}_2^{\mathrm{RL}} \tilde{x}_{2\tau}^{\mathrm{RL}} &= C_{Lu}, & x_1^{\mathrm{LL}} x_{1\tau}^{\mathrm{LL}} &= -\frac{1}{2}(C_{LQ}^{(1)} + 3C_{LQ}^{(3)}), & x_1^{\mathrm{RR}} x_{1\tau}^{\mathrm{RR}} &= -C_{ed}, \\
\tilde{x}_1^{\mathrm{RR}} \tilde{x}_{1\tau}^{\mathrm{RR}} &= -C_{eu}, & x_{1,2}^{\tau h} &= \frac{1}{2} C_{LedQ}^{\tau h}, & x_{1,2}^{\ell-\tau} &= \frac{1}{2} C_{LedQ}^{\ell-\tau}.
\end{aligned}
\tag{4.3.35}
$$

Therefore, even though we have 11 Yukawa pairs restricted by 9 effective bounds — which implies that not all Yukawa pairs can be constrained independently from bounds on the WCs — by introducing $x_{1,2}^{process}$, this budget is effectively changed to 9 Yukawa pairs only. Moreover, the constraints coming from ℓ–τ conversion are not competitive compared to those stemming from the τ decays, which implies a softer bound on $x_{1,2}^{\ell-\tau}$, exceeding (as in the scalar LQ scenario) for e–τ conversion the limits suggested by perturbativity considerations; the bounds for the probed mass (with $|xx'| \approx 1$) indicate again that the experimental constraints expected at present from the ℓ–τ conversion in nuclei are rather weak.

The numerical results are given in Table 4.5 and follow the same pattern as in the scalar scenario. Note that the main differences arise for the $x_3^{\mathrm{LL}} x_{3\tau}^{\mathrm{LL}}$, $x_2^{\mathrm{RL}} x_{2\tau}^{\mathrm{RL}}$ and $x_1^{\mathrm{RR}} x_{1\tau}^{\mathrm{RR}}$ pairs, which are constrained stronger than their scalar analogues. The combination of Yukawa pairs $x_{1,2}^{\tau h}$ is also strongly constrained. Alternatively, we can try to get information on single Yukawa couplings. Under the flavor structure established in Eq. (4.2.12), we have 14 couplings in total. The 4 wearing a tilde contribute in pairs in a unique way (i.e. not to other WCs or in combination with other Yukawas) to C_{Lu} and C_{eu} (see Eq. (4.3.35)), and thus the resulting relations among the single Yukawa couplings and Wilson coefficients necessarily depend on other Yukawas. However, the 10 remaining Yukawas contribute in different ways to the rest of Wilson coefficients: there are in total 7 effective WCs once the bounds from ℓ–τ conversion and τ decays are distinguished. Thus, one can express 7 out of these 10 single Yukawas in terms of WCs and 3 remaining unconstrained (free) Yukawas. The corresponding relations are given in Appendix J, with $\tilde{x}_2^{\mathrm{RL}}$ and $\tilde{x}_1^{\mathrm{RR}}$ in the former case and x_3^{LL}, x_1^{LL} and x_2^{LR} in the latter chosen to be free. In light of possible non-zero values of these WCs, the (usually stronger) bounds on the e- and μ-involved Yukawas (chosen to be free in this setting) can be used to constrain the remaining 7.

Finally, limits on single Yukawas can also be obtained with the help of the perturbativity bounds. Taking the upper bounds on $|yy'|$ obtained above, it can be assumed that the bound on the absolute value of the target Yukawa (say y) can be obtained by assuming that $|y'|$ equals the value given by the perturbative limit.

τ decays	Upper bounds on $\dfrac{\|xx'\|}{M_V^2}$ [10^{-3} TeV^{-2}]		Lower bounds on M_V [TeV]	
Yukawa pair	Belle	Belle II	Belle	Belle II
$\|x_3^{\mathrm{LL}} x_{3\,\tau}^{\mathrm{LL}}\|$	15	1.7	8.2	25
$\|x_2^{\mathrm{RL}} x_{2\,\tau}^{\mathrm{RL}}\|,\ \|x_1^{\mathrm{RR}} x_{1\,\tau}^{\mathrm{RR}}\|$	10	1.5	10	26
$\|x_2^{\mathrm{LR}} x_{2\,\tau}^{\mathrm{LR}}\|$	8.3	1.3	11	28
$\|\tilde{x}_2^{\mathrm{RL}} \tilde{x}_{2\,\tau}^{\mathrm{RL}}\|$	24	2.5	6.5	20
$\|x_1^{\mathrm{LL}} x_{1\,\tau}^{\mathrm{LL}}\|$	22	3.1	6.7	18
$\|\tilde{x}_1^{\mathrm{RR}} \tilde{x}_{1\,\tau}^{\mathrm{RR}}\|$	17	2.1	7.7	22
$\|x_{1,2}^{\tau h}\|$	3.1	0.42	18	49

$\ell\text{--}\tau$ conversion	Upper bounds on $\dfrac{\|xx'\|}{M_V^2}$ [10^{0} TeV^{-2}]		Lower bounds on M_V [TeV]	
Yukawa pair	$e\text{--}\tau$	$\mu\text{--}\tau$	$e\text{--}\tau$	$\mu\text{--}\tau$
$\|x_{1,2}^{\ell-\tau}\|$	330	1.5	0.055	0.83

TABLE 4.5: Obtained bounds for the vector leptoquark case from the bounds determined in Chapter 3. In the left-hand part of the table, we present *upper* bounds on the ratio $\|xx'\|/M_V^2$; these numbers also correspond to *upper* bounds on the Yukawa pairs $\|xx'\|$, assuming $M_V = 1$ TeV. On the right, there are *lower* bounds on the probed energy scale of the scalar leptoquarks mediating CLFV phenomena ($\Lambda_{\mathrm{CLFV}} = M_V$), considering $\|xx'\| \approx 1$. Again, the strongest bounds found are shown, stemming mostly from the τ decay constraints, except for the last row related solely to $\ell\text{--}\tau$ conversion. The values are given at the 99.8 % confidence level.

4.4 Conclusions

Leptoquarks are omnipresent in the recent literature that brings up extensions of the Standard Model of particle physics. Although their concept comes from the period where the construction of Grand Unified Theories was at its high spot [179,180], they have been reborn in the last ten years as a possible explanation to the LHCb [122] and muon $(g-2)$ anomalies [123,124,271]. To play this role they should have a mass of few to tens TeVs. At present, there is no experimental evidence of their existence and present bounds by LHC indicate $M_{\mathrm{LQ}} \gtrsim 1$ TeV.

Learning that nature allows for neutrino mixing, the immediate rationale suggests that lepton flavor violation should be also present in processes with charged leptons. In Chapter 3, we carried out a phenomenological model-independent analysis of charged-lepton-flavor-violating processes involving the tau lepton, namely its hadronic decays and $\ell\text{--}\tau$ conversion in the presence of nuclei ($\ell = e, \mu$), and established bounds on the Wilson coefficients of the corresponding $d = 6$ SMEFT operators.

In this chapter, we have merged both lines from above. We have considered that leptoquarks (both scalar and vectors) should be driving the dynamics of charged-lepton-flavor-violating processes and, in addition, we consider an extra input: There is a breaking of universality related to the third lepton family with respect to the

two lighter ones. Upon the integration of the heavy LQs, we get most of CLFV $d = 6$ SMEFT operators and, accordingly, we can relate the couplings of LQs to fermions with the Wilson coefficients of the SMEFT. We can then combine these relations with our results from Chapter 3, providing relevant information (in terms of bounds) on those couplings and LQs masses.

Our main results are collected in Tables 4.3, 4.4 and 4.5. They all show bounds on the LQ masses and the Yukawa-like couplings of LQs to SM fermions. The first two tables correspond to scalar leptoquarks and the last one to vector leptoquarks. In addition, Table 4.3 shows the couplings of four-fermion operators, while Table 4.4 shows the results related to C_γ. In our analyses on the latter-mentioned WC, we have included the bounds on the processes $\tau \to \ell\gamma$ for $\ell = e, \mu$ and its leptoquark generated leading contribution that appears at the one-loop level in the perturbative expansion. As already commented in Chapter 3, we notice the significant improvement arriving with the foreseen bounds from the expected Belle II results in the hadronic decays of the tau lepton.

Considering the Belle II prospects, our results show that the bounds on scalar leptoquarks are weaker ($M_{\rm S} \gtrsim 10\,{\rm TeV}$) than those on vector leptoquarks ($M_{\rm V} \gtrsim 20\,{\rm TeV}$). The numerical values of these bounds are in the expected region where LQs could help to explain the aforementioned phenomenological anomalies.

Part III

Constraining neutrino physics

Chapter 5

Effective field theory description of the COHERENT experiment

One of the main motivations for the CLFV-τ analyses performed in the previous chapters were the oscillatory phenomena displayed by the neutrino flavors in their propagation. As we saw in Chapter 1, there are no right-handed neutrinos (and corresponding left-handed antineutrinos) in the Standard Model and hence, the Higgs mechanism fails to provide mass to (Dirac) neutrinos. Accordingly, the flavor eigenstates that enter in weak interactions may be directly identified with the mass eigenstates. However, in analogy to the quark sector, the addition of a neutrino mass term would directly induce a mixing between flavor eigenstates and thus give rise to an oscillation pattern, as a consequence of a missmatch between flavor and mass eigenstates, being the latter the relevant states for the space-time propagation.

While the actual origin and nature of the neutrino mass term is still an open question, oscillation experiments have unambiguously proved the aforementioned phenomenon and subsequently, the existence of neutrino masses and LFV.

The possible consequences of non-trivial flavor dynamics onto the charged-lepton sector were, indeed, the departure point of the previous chapters. There, we focused mainly on low-energy observables to probe and constrain — in an essentially model-independent way — the underlying fundamental interactions driving these phenomena. However, a complementary approach to study deviations from the SM flavor paradigm are neutrino oscillations themselves: apart from neutrino masses and mixings, these oscillations are as well sensitive to potential NP contributions to low-energy interactions between quarks and leptons.

The main idea behind neutrino oscillation experiments is to probe the characteristic oscillatory pattern of neutrinos from the neutrino detection rate at a given experiment, which depends on the neutrino energy and distance to the source. The standard parameters entering oscillations — mass squared differences as well as parameters of the mixing PMNS matrix — have already been measured using oscillations experiments with good accuracy [48]. Therefore, our good understanding gained on this matter, allows us already to use the observables involved in experiments where the oscillatory behaviour plays some role, to constrain BSM physics affecting them.

The deviations from the canonical SM predictions for neutrino-involved observables are typically parametrized in the literature by the so-called non-standard interactions (NSI). For neutral-current NSI these correspond to effective operators added

to the SM Lagrangian that affect neutrino production, propagation and detection and hence, as stated above, may modify the oscillatory pattern. However, neutrino oscillations are often described in a simple quantum mechanical setting, where flavor states are linear combinations of the mass eigenstates, in this case charged-current NSI are defined from the mismatch between the pure flavor eigenstates and the actual states produced at the source and detected at the target [272]. Such a formalism may hinder the comparison and implementation of those bounds in a more general EFT framework. Accordingly, in Ref. [273] an appropriate EFT description of neutrino oscillation experiments involving charged-current interactions was developed within the QFT formalism. The matching between the effective NSI parameters was computed and the consistency between the QM and QFT frameworks was studied.

In the same spirit as in Ref. [273], in the work of Ref. [274] upon which this chapter is based, we complement the previous work on charged-current interactions by working out the EFT description of the coherent elastic neutrino-nucleus scattering in the presence of charged-current NSI at production and neutral-current NSI at detection. We then use it to extract bounds on the EFT parameters of the low-energy effective field theory (see Chapter 2) from experimental data on this process.

The first theoretical determination of CEνNS was accomplished by D.Z. Freedman [275] in 1974 but, due to the very low energies involved, it was not until 2017 that the first measurement of this process was achieved by the COHERENT experiment [276] (see Section 5.3), forty years later. The detection process at COHERENT takes place via CEνNS, which is a purely neutral-current interaction between the arriving neutrinos and the nucleus of the detector, thus providing a perfect environment to apply our QFT formalism of neutrino oscillations in the presence of neutral-current NSI.

Therefore, in Section 5.1 we present the QFT formalism to treat neutrino oscillation involved processes. In the following Section 5.2, we sketch the importance of the coherent elastic neutrino-nucleus scattering process in several branches of high-energy physics and describe the theoretical underpinnings of CEνNS and the experimental efforts to observe and study it. Then, in Section 5.3 we explain in more detail the COHERENT experiment and in subsequent subsections provide its full EFT description, which results in the theoretical expression of the CEνNS number of events measured at COHERENT. The experimental effects to translate the theoretical prediction into the actual observed data are presented in Section 5.4. We finish this section outlining some preliminary results of the work presented in this chapter. We conclude in Section 5.5.

5.1   Quantum field theory description of neutrino oscillations: the event rate R_α

In order to use data from neutrino oscillation experiments to constrain new physics interactions, we need the appropriate theory description of the relevant observables in those experiments, in terms of the fundamental BSM parameters (in our case parametrized in a model-independent way through an EFT framework). In

Ref. [273] the corresponding map between the parameters of the low-energy effective field theory and several observables involving charged-current interactions was provided. Such a map allows us to understand the NP implications of a given neutrino measurement. In our case we are interested in the corresponding map between the LEFT (see Section 2.6) and the observable of the CEνNS: the measured number of events[1].

For the configuration we are interested in this work: production and detection are driven by charged- and neutral-current interactions respectively, the neutrinos are produced by a source S through the process $S \to X_\alpha \nu_k$, where X_α may be one or more body final states that contain a charged lepton ℓ_α, with $\alpha = e, \mu, \tau$ (a flavor index), and ν_k, with $k = 1, 2, 3$, a neutrino-mass eigenstate denoted by latin subindices. These neutrinos propagate a distance L — conserving its mass index k — and are detected via the process $\nu_k T \to \nu_j Y$, where $j = 1, 2, 3$ is again a mass index and T and Y are again one or more body final states with no charged leptons in this case. The corresponding QFT amplitudes are then given by $\mathcal{M}^{\mathrm{P}}_{\alpha k} \equiv \mathcal{M} (S \to X_\alpha \nu_k)$ and $\mathcal{M}^{\mathrm{D}}_{jk} \equiv \mathcal{M} (\nu_k T \to \nu_j Y)$, as a function of the LEFT parameters. These should then be connected to the observable of interest.

At COHERENT this observable is the differential number of events per time t, incident neutrino energy E_ν and recoil energy T, which is given as

$$\frac{dN_\alpha}{dt \, dE_\nu \, dT} = N_T R_\alpha \,, \tag{5.1.1}$$

where R_α is the differential rate of detected events per target particle and N_T stands for the number of target particles.

A slightly different version of the event rate R_α was derived within the QFT formalism for the case of charged-current interactions both at production and detection in Ref. [273]. The main idea behind such derivation was, instead of taking the usual approach where neutrino production and detection are considered separately, to treat both interactions as a single process [277]. In our CC-NC configuration, that translates into the following process

$$ST \to X_\alpha Y \nu_j \,, \tag{5.1.2}$$

where the neutrino is considered just as an intermediate particle in the amplitude.

We can adapt the rate found in Ref [273] to describe the CEνNS observed at COHERENT in a simple way. The fact that there is a neutral-current interaction at detection means we have no information about the neutrino final mass eigenstate and hence, we should sum over the corresponding mass index j. Furthermore, at COHERENT they observe the differential number of events per recoil energy, so that we should express the rate accordingly. Recalling the result from Eq. (2.1) in Ref. [273] and including the statements above, we thus obtain (for neutrinos emitted isotropically from a source at rest)

$$R_\alpha = \frac{N_S}{32\pi L^2 m_S m_T E_\nu} \sum_j \sum_{k,l} e^{-i\frac{L\Delta m^2_{kl}}{2E_\nu}} \int d\Pi_{P'} \mathcal{M}^P_{\alpha k} \bar{\mathcal{M}}^P_{\alpha l} \int d\Pi_{D'} \mathcal{M}^D_{jk} \bar{\mathcal{M}}^D_{jl}, \tag{5.1.3}$$

---

[1]Depending on the available experimental information we may be rather interested in the total number of events or, if we have access to the energy distribution of the events, in the differential number of events per recoil energy of the nucleus, as it is the case of the COHERENT experiment. In some cases we will also have access to the time distribution of the events, which we will use as well when possible.

where we have explicitly separated the sum over j. From now on, we will refer to Eq. (5.1.3) above as the master formula for neutrino oscillations. The list of the terms appearing in that equation is as follows. First, N_S is the number of source particles, and $m_{S,T}$ are the corresponding masses of the source and target particles respectively. Then, $\Delta m_{kl}^2 \equiv m_k^2 - m_l^2$ is the mass squared difference between neutrino (mass) eigenstates. The phase space elements for the production and detection processes $d\Pi_P$ and $d\Pi_D$, are defined as usual

$$d\Pi \equiv \frac{d^3 k_1}{(2\pi)^3 2E_1} \cdots \frac{d^3 k_n}{(2\pi)^3 2E_n} (2\pi)^4 \delta^4 \left(p - \sum_i k_i \right) , \qquad (5.1.4)$$

with p the total 4-momentum of the initial states and k_i the 4-momentum of the final state i. However, in order to obtain the observable of interest at COHERENT, we are using a slight modification of the production and detection phase spaces where $d\Pi_P \equiv d\Pi_{P'} dE_\nu$ and $d\Pi_D \equiv d\Pi_{D'} dT$, such that R then provides the differential number of events per incident neutrino energy E_ν and recoil energy T via Eq. (5.1.1). As it is customary, the integral sign involves both integration as well as sum and averaging over all unobserved degrees of freedom as spins. The amplitudes $\mathcal{M}^{P,D}$ describe the neutrino production and detection respectively and will encapsulate the BSM interactions parametrized by the Wilson coefficients of the LEFT; the complex conjugate amplitudes are denoted as usual with a bar. Finally, Eq. (5.1.3) presents the oscillatory behavior via the $e^{-i \frac{L \Delta m_{kl}^2}{2 E_\nu}}$ factor.

5.2   Coherent elastic neutrino-nucleus scattering

When a neutrino interacts elastically with a nucleus (Z, N), under certain conditions regarding the neutrino energy and size of the nucleus, the corresponding cross section suffers an enhancement due purely to the basic quantum-mechanical principle of coherence. Under such circumstances (described below in more detail), the neutrino interacts with the nucleus as a whole and the corresponding coherent scattering receives the name of CEνNS[2]. This effect was first described by D.Z. Freedman [275], following the first observation of neutral-current interactions by the Gargamelle experiment [278, 279].

CEνNS turns out to be of paramount importance for its many potential applications not only in high-energy physics, but also in astrophysics, nuclear physics and beyond [280]. For instance, in the particle physics domain, CEνNS can serve both to provide extra tests of SM physics as: extract information about the weak mixing angle, from what represents a complementary source at low momentum transfer [281, 282], study the nuclear structure factors of the target nuclei [282–291] or probe the distribution of neutrons in nuclei [292, 293] (what complements the proton densities obtained from elastic electron scattering [294, 295]); or to constrain BSM

---

[2]To be pronounced as "sevens".

physics in different ways as: setting bounds on NSI [296–310], on neutrino electro-magnetic properties[3], the most typical one being a magnetic moment of the neutrino [303, 305, 309–314], searching for sterile neutrinos [314–318] or even searching for weakly-interacting particles in hidden sectors [319, 320] like light vector mediators [291, 300, 304, 311, 321–328] and another BSM scenarios [303, 308, 309, 329] like leptoquarks [325, 330].

Let us now address, in a simple form, the basic principles of the coherence scattering of the neutrino off a nucleus. The CEνNS process occurs when the neutrino scatters (elastically) off a composite system, which consists of a number A of individual constituents (in this case the nucleons). The superposition principle of quantum mechanics tells us that the total amplitude $\mathcal{M}(\vec{k}', \vec{k})$ of the scattering of an incoming neutrino with momentum $\vec{k}$, resulting in an outgoing neutrino of momentum $\vec{k}'$, can be written as the sum of the contributions from each constituent[4] j:

$$\mathcal{M}(\vec{k}', \vec{k}) = \sum_{j=1}^{A} f_j(\vec{k}', \vec{k}) \exp\left\{ i(\vec{k}' - \vec{k}) \cdot \vec{x}_j \right\}, \qquad (5.2.5)$$

where the nucleons are considered to be distributed at positions $\vec{x}_j$, with $j = 1, 2, \ldots A$, and the individual amplitudes for each constituent $f_j(\vec{k}', \vec{k})$ are added with a phase factor to take into account the relative phases of the wave scattering at $\vec{x}_j$.

According to Eq. (5.2.5), the corresponding cross section $\sigma \propto |\mathcal{M}(\vec{k}', \vec{k})|^2$ will depend on the resulting behaviour stemming from the relative phases. Therefore, it will depend on both the momentum transfer $\vec{q} = \vec{k}' - \vec{k}$ ($q \equiv |\vec{q}|$) and the size of the nucleus, given by the maximum distance between the positions of its constituents $R = \max_{ij} |\vec{x}_i - \vec{x}_j|$:

- If $q \gtrsim 1/R$, the relative phase factors become important and the individual contributions tend to cancel. The coherence is then lost and the corresponding cross section is expected to be small. This is analogous to the case where we want to observe a (composite) object of size L with light of wavelength $\lambda < L$: the energy of the light is too high that, instead of observing the object as a whole, we are actually able to resolve shorter distances within it and see its constituents.

- If the transferred momentum is small compared to the inverse target size, i.e. $q \ll 1/R$ (for most nuclei the typical inverse sizes are in the range from 25 to 150 MeV), the relative phases are such that individual contributions add up coherently, thus providing for the total cross section the aforementioned enhancement $\sigma \sim A^2 |\bar{f}(\vec{k}', \vec{k})|^2$, where we have defined the averaged amplitude over the constituents as $\bar{f}(\vec{k}', \vec{k}) = \frac{1}{A} \sum_j f_j(\vec{k}', \vec{k})$. The CE$\nu$NS cross section becomes $A^2 \sigma_j$, with σ_j the cross section of the single constituent, as expected from the coherence phenomenon.

---

[3]Non-trivial EM properties require a spin flip, what implies the lost of the coherence effect, and should consequently be added incoherently (see below).

[4]It is important to note that such expression is only valid when individual amplitudes are small enough to neglect multiple scattering, what is indeed the case for the weakly interacting neutrinos.

For the second case described above ($q \ll 1/R$), in the nucleus we have two different constituents: protons and neutrons. Therefore, since the weak interactions involved in CEνNS treat both nucleons in a different way, it turns out that in the SM the CEνNS is protophobic and the cross section scales as the number of neutrons squared N^2 instead of the atomic mass number A^2. Needless to say, new physics interactions may modify this behaviour and change the associated weak charges (see Section 5.3.1). Furthermore, the coherence is as well lost for interactions that change the quantum states, e.g. interactions that change the chirality of the particles or for charged-current interactions that change the charge. This is why scalar, pseudoscalar and tensor interactions, that may arise when introducing to the SM spectrum right-handed and Majorana neutrinos, should be added incoherently to the total cross section. This is also the case for an electric or magnetic dipole moment of the neutrino.

Despite the enhancement of the CEνNS cross section, which is amplified up to become even large by neutrino standards [280], the only single observable from this interaction is the recoil of the whole nucleus with very little kinetic energy (of the order of keV). This is the reason why it took forty-three years to measure the CEνNS, in spite of the potential great physics insight we can gain from it.

From the experimental side, as we have already stated, the first observation of the CEνNS was performed by the COHERENT collaboration [276] with a detector material made of cesium (Cs) and iodine (I), followed by a subsequent detection in liquid argon (LAr) [331,332] and an improvement on CsI again [333]. COHERENT makes use of one of the largest terrestrial sources of neutrinos: stopped-pion beams from spallation sources (see next section). Beyond the one used by COHERENT, several others spallation sources plan to study CEνNS in the future [280] as the Coherent CAPTAIN-Mills (CCM) liquid argon detector at Los Alamos National Laboratory, the J-PARC Sterile Neutrino Search experiment at the Japan Spallation Neutron Source of J-PARC or the European Spallation Source (ESS), which will provide the largest pulsed neutrino flux for CEνNS detection [334].

However, in addition to spallation sources, CEνNS is, and will be, searched for by several experiments using the electron antineutrinos emitted from nuclear reactors. For a review of the (long) list of nuclear reactor experiments see Ref. [280]. Such experiments provide very intense fluxes of low-energy antineutrinos ($E_\nu < 10$ MeV), thus being able to explore the kinematic regime where complete quantum-mechanical coherence is expected [335]; but suffer from a larger background that cannot be removed exploiting the pulsed feature characteristic of the spallation sources. Among them, only the NCC-1701 experiment at Dresden-II nuclear reactor reported to have observed a CEνNS signal [336,337].

Other experiments focusing on direct searches of dark matter, more concretely of WIMPs, will also be sensitive to CEνNS from astrophysical sources like the Sun, supernovae or atmospheric cosmic-ray-showers. The CEνNS driven by neutrinos from those sources presents an unshieldable irreducible background in dark matter detectors that should be well under control in order to improve their sensitivity. For a review on the upcoming dark matter experiments that will be able to study CEνNS as well, we refer again to Ref. [280].

5.3 EFT description of COHERENT

The COHERENT collaboration makes use of the currently most intense Spallation Neutron Source (SNS), located at the Oak Ridge National Laboratory in the US, which is also known to provide a large yield of neutrinos. The production mechanism of these neutrino fluxes in the SM is depicted in Fig. 5.1. At this facility high-energy
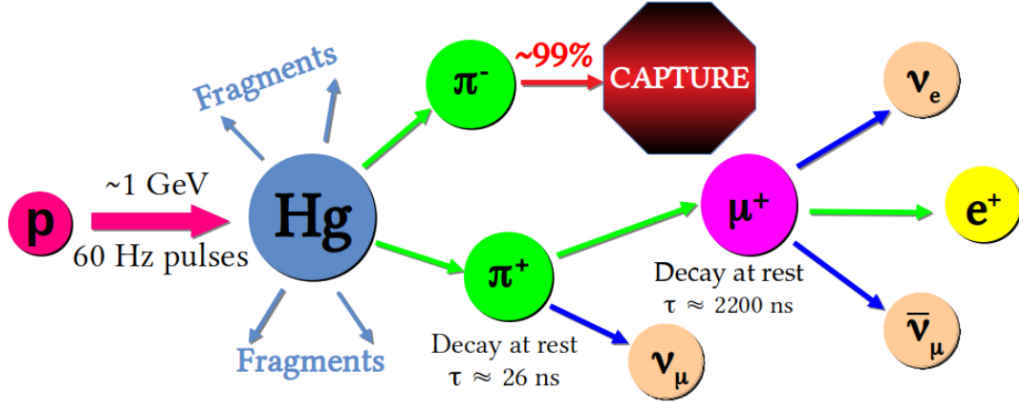
FIGURE 5.1: Diagram of the production mechanism of neutrinos at the SNS used by the COHERENT collaboration, taken from Ref. [338].

protons with $E \sim 1$ GeV hit a mercury (Hg) target producing the most intense pulsed neutron beams in the world. At the same time, as a by-product of those proton interactions in the Hg target, positive and negative pions are produced. Both kinds of pions are quickly stopped within the target with a negligible probability of decay-in-flight. The negatively charged pions are subsequently captured on target nuclei. The π^+ on the other hand experience decay-at-rest (DAR), into mono-energetic muon neutrinos ν_μ with $E_{\nu_\mu} = \frac{m_\pi^2 - m_\mu^2}{2m_\pi} \simeq 29.7$ MeV, which are referred to as *prompt* neutrinos, and into antimuons μ^+. The μ^+ then travels around $\tau \sim 2200$ ns and decays at rest producing a positron e^+, an electron neutrino ν_e and a muon antineutrino $\bar{\nu}_\mu$, both with a continuous energy spectrum up to their maximum energy $E_{\nu_e, \bar{\nu}_\mu}^{\max} = m_\mu/2 \simeq 52.8$ MeV. These last two neutrinos receive the name of *delayed* neutrinos. Since the two production mechanisms from pion and muon decays happen at rest, both prompt and delayed neutrinos are emitted isotropically, thus fulfilling the requirement to apply Eq. (5.1.3) to compute the number of events measured at COHERENT. Note as well that the three neutrino fluxes contribute to the total number of events, whose only experimental distinction stems from their arrival time and energy distributions.

In order to study the CEνNS process, the COHERENT collaboration placed three detectors around the aforementioned source of neutrinos. They were intended to provide a CEνNS observation in CsI, Ar and sodium-iodine (NaI) [339]. The CsI detector is located at a distance of $L_{\mathrm{CsI}} = 19.3$ meters from the neutrino source, with a detector active mass of $M_{\mathrm{det}}^{\mathrm{CsI}} = 24.4$ kg. On the other hand, the CENNS-10 detector using LAr was situated at $L_{\mathrm{Ar}} = 27.5$ meters, and had an active mass of $M_{\mathrm{det}}^{\mathrm{Ar}} = 14.6$ kg. The detector active masses allow us to compute the number of

target atoms (particles, see Section 5.1) in the detector via $N_T = N_A M_{\rm det}/M_{\rm mol}$, where $N_A = 6.022 \times 10^{23} \, {\rm mol}^{-1}$ is the Avogadro number and $M_{\rm mol}$ stands for the molar mass of each of the detector materials: $M_{\rm mol}^{\rm CsI} = 259.8$ g/mol and $M_{\rm mol}^{\rm Ar} = 39.96$ g/mol. These are the two detectors that have been able to measure the CEνNS signal, with the following exposure to the neutrino flux:

- First measurement on CsI or $({\rm CsI})_1$ [276]: it was achieved after 308.1 live days of neutrino production. This translates into a total of $n_{\rm POT} = 1.76 \times 10^{23}$ protons delivered to the mercury target (protons on target), where each proton provides a pion (π^+) yield of $0.0848 \pm 10\% \, \pi^+$/POT. These pions decay totally by DAR into the interesting neutrinos, thus providing an (equal) neutrino yield of $r_{\nu/p}^{\rm CsI} = 0.0848 \pm 0.0085$ [340] neutrinos per flavor emitted isotropically.

- Second measurement on CsI or $({\rm CsI})_2$ [333]: it presents an improvement over the first measurement using the final CsI dataset, the total number of protons on target increased to $n_{\rm POT} = 3.2 \times 10^{23}$, so almost twice the neutrino flux (with the same $r_{\nu/p}^{\rm CsI}$ as in the previous case).

- First measurement on LAr [331]: in this case, the data used for CEνNS detection corresponds to $n_{\rm POT} = 13.7 \times 10^{22}$, where in this case the experimental prescription tells us to use $r_{\nu/p}^{\rm Ar} = 0.090 \pm 0.009$.

The aim of this work is to provide a complete EFT description of the COHERENT experiment, where new physics interactions may affect both stages of the process: the production and detection, and oscillation effects are well characterized within the QFT formalism. Therefore, in the following sections we compute the detection and production amplitudes within the LEFT formalism and obtain the differential number of events expected at COHERENT in the presence of NSI, via the QFT prescription for the rate of events in Eq. (5.1.3).

5.3.1   Detection at COHERENT: CEνNS

The detection process at COHERENT occurs via the interesting neutral-current driven CEνNS. In Section 2.6, we provided the relevant neutral-current Lagrangian containing the Standard Model contributions to this process, which we properly extended to include NSI between neutrinos and quarks parametrized within the LEFT via the Wilson coefficients (see Eq. (2.6.79)). However, as shown in Section 5.2, in CEνNS neutrinos interact coherently with the nucleons conforming the nuclei and hence, the relevant degrees of freedom are the nucleons. We thus modified our EFT to describe neutral-current interactions between neutrinos and nucleus (see Eq. (2.6.84)) and, further on, took the non-relativistic limit to better describe the low energies involved in the recoil of the nucleus. Therefore, we arrived at the Lagrangian of Eq. (2.6.88) describing low-energy neutral-current interactions between neutrinos and nucleons with negligible recoil energy.

From the aforementioned resulting Lagrangian (2.6.88), the scattering amplitude of a neutrino off a nucleus $\mathcal{N}$ is given in terms of the nuclear matrix elements as:

$$\mathcal{M}(\nu_\beta \mathcal{N} \to \nu_\alpha \mathcal{N}) = \sum_{N=n,p} \left\{ - [C_V^N]_{\alpha\beta} \langle \mathcal{N}(k_4, J_z') | \psi_N^\dagger \psi_N | \mathcal{N}(p_2, J_z) \rangle (\bar{x}_3 \bar{\sigma}^0 x_1) \right.$$

$$+ [C_A^N]_{\alpha\beta} \langle \mathcal{N}(k_4, J_z') | \psi_N^\dagger \sigma^k \psi_N | \mathcal{N}(p_2, J_z) \rangle (\bar{x}_3 \bar{\sigma}^k x_1) \bigg\} , \quad (5.3.6)$$

where $x_{1,3}$ are the 2-component spinor wave functions of the incoming and outgoing neutrinos, p_2 and k_4 are the momenta of the incoming and outgoing nucleus, and J_z, J_z' their polarizations. Note that in the COHERENT experiment the nuclear spin is zero and accordingly $\langle \mathcal{N}(k) | \psi_N^\dagger \sigma^k \psi_N | \mathcal{N}(p_2) \rangle = 0$. Therefore, experiments using spinless nuclei are blind to axial-current interactions.

Since we are neglecting $\mathcal{O}(\nabla)$ terms in the Lagrangian, for consistency we should take the matrix element in the zero-recoil limit, i.e. $k_4 \to p_2$. In this limit, for a nucleus of spin J, rotational symmetry requires the nuclear matrix elements to have the following form

$$\begin{aligned}
\langle \mathcal{N}(k, J_z') | \psi_N^\dagger \psi_N | \mathcal{N}(k, J_z) \rangle &= 2\sqrt{E_\mathcal{N} E_\mathcal{N}'} M_V^N \delta_{J_z' J_z} , \\
\langle \mathcal{N}(k, J_z') | \psi_N^\dagger \sigma^k \psi_N | \mathcal{N}(k, J_z) \rangle &= 2 E_\mathcal{N} M_A^N [\mathcal{T}_J^k]_{J_z' J_z} ,
\end{aligned} \quad (5.3.7)$$

where we keep for convenience (see below) distinct $E_\mathcal{N}$ and $E_\mathcal{N}'$: the initial and final energy respectively of the target nucleus, and $\mathcal{T}_J^k$ are the spin-J generator, in particular $\mathcal{T}_0^k = 0$ (which recovers the aforementioned result showing the insensitivity of spinless nuclei to axial currents) and $\mathcal{T}_{1/2}^k = \sigma^k/2$. As usual M_A^N is a strongly coupled parameter that would have to be taken from the experiment or the lattice. On the other hand M_V^N can be calculated from isospin symmetry to give

$$M_V^p = Z, \qquad M_V^n = A - Z = N . \quad (5.3.8)$$

All in all, the neutrino scattering amplitude on nuclei reads

$$\mathcal{M}(\nu_\beta \mathcal{N} \to \nu_\alpha \mathcal{N}) = -\frac{2\sqrt{E_\mathcal{N} E_\mathcal{N}'}}{v^2} [\mathcal{Q}]_{\alpha\beta} (\bar{x}_3 \bar{\sigma}^0 x_1) , \quad (5.3.9)$$

where we have already taken to zero the axial piece, and we have introduced a factor $1/v^2$ in order to define the weak charge as

$$[\mathcal{Q}]_{\alpha\beta} = v^2 \bigg(Z [C_V^p]_{\alpha\beta} + N [C_V^n]_{\alpha\beta} \bigg) , \quad (5.3.10)$$

with the normalization factor v^2 chosen from the definitions of $[C_V^p]_{\alpha\beta}$ and $[C_V^n]_{\alpha\beta}$ in Eq. (2.6.85), such that we recover the usual SM weak charge in the flavor diagonal case with no new physics (see Eq. (2.6.86) as well):

$$[\mathcal{Q}]_{\alpha\beta}^{\text{SM}} = \left[\left(\frac{1}{2} - 2\sin^2\theta_W \right) Z - \frac{1}{2} N \right] \delta_{\alpha\beta} \equiv \mathcal{Q}^{\text{SM}} \delta_{\alpha\beta} . \quad (5.3.11)$$

Note that from the SM result on the weak charge (5.3.11) we obtained the expected enhancement, where all nucleons add up coherently to the total amplitude. However, instead of the naive $\mathcal{M} \propto A$, since in the SM $\sin^2\theta_W \sim 1/4$ and then $[C_V^p]^{\text{SM}}$ is suppressed, such accidental cancellation reduces the effect to $\mathcal{M} \propto A - Z = N$. Accordingly, the scattering rate will be proportional to N^2. On the other hand, NP interactions modify the weak charge via Eq. (5.3.10).

We can now rotate to neutrino mass eigenstates, entailing for the amplitude

$$\mathcal{M}(\nu_k\,\mathcal{N} \to \nu_\gamma\,\mathcal{N}) = -\frac{2\sqrt{E_\mathcal{N}E'_\mathcal{N}}}{v^2}U_{\alpha k}[\mathcal{Q}]_{\gamma\alpha}(\bar{x}_3\bar{\sigma}^0 x_1)\,, \tag{5.3.12}$$

where $U_{\alpha k}$ is the PMNS matrix (see Section 1.4.3) and we can keep the flavor index of the outgoing neutrino since we do not detect it and then, we sum over it (otherwise, we would end up with a sum over PMNS matrices which would, by unitarity conditions, disappear). From this amplitude (5.3.12), we can compute the detection part entering the master formula for neutrino oscillations in Eq. (5.1.3):

$$\sum_\gamma \int d\Pi_{D'}\mathcal{M}(\nu_k\,\mathcal{N} \to \nu_\gamma\,\mathcal{N})\mathcal{M}(\nu_l\,\mathcal{N} \to \nu_\gamma\,\mathcal{N})^*$$
$$= \frac{2M_\mathcal{N}(M_\mathcal{N}+T)E_\nu}{\pi v^4}\left(1-\frac{(M_\mathcal{N}+2E_\nu)T}{2E_\nu^2}\right)[U^\dagger\mathcal{Q}^\dagger\mathcal{Q}U]_{lk}\,, \tag{5.3.13}$$

where we have introduced the recoil energy $T = E'_\mathcal{N} - M_\mathcal{N}$, kinematically restricted to the interval $T \in [0, T_{\max} \equiv 2E_\nu^2/(M_\mathcal{N}+2E_\nu)]$, and we have integrated over the modified phase space $d\Pi_{D'}$. From Eq. (5.3.13) we can easily compute the usual cross section of the process:

$$\sum_{\gamma,k}\frac{d\sigma\,(\nu_k N \to \nu_\gamma N)}{dT} = \frac{1}{4M_\mathcal{N}E_\nu}\sum_{\gamma,k,l}\delta_{kl}\int d\Pi_{D'}\mathcal{M}(\nu_k\,\mathcal{N} \to \nu_\gamma\,\mathcal{N})\mathcal{M}(\nu_l\,\mathcal{N} \to \nu_\gamma\,\mathcal{N})^*$$
$$= \frac{M_\mathcal{N}G_F^2}{\pi}\left(1-\frac{M_\mathcal{N}T}{2E_\nu^2}-\frac{T}{E_\nu}\right)\mathrm{Tr}[\mathcal{Q}^\dagger\mathcal{Q}]\,, \tag{5.3.14}$$

where in the last step we approximated $M_\mathcal{N} + T \approx M_\mathcal{N}$ and we used the relation $v = (\sqrt{2}G_F)^{-1/2}$. Therefore, departing from our QFT formalism we have been able to retrieve the standard result for the CEνNS cross section as a function of the recoil energy T [309,310,330]. Note that at COHERENT there are three fluxes contributing to CEνNS: two consisting of neutrinos and one of antineutrinos. Therefore, we should compute as well the detection piece for the coherent scattering of an antineutrino off a nucleus. This is given by the same expression in Eq. (5.3.13) but modifying the part of the weak charges by

$$[U^\dagger\mathcal{Q}^\dagger\mathcal{Q}U]_{lk} \qquad \longrightarrow \qquad [U^\dagger\mathcal{Q}\mathcal{Q}^\dagger U]_{kl}\,. \tag{5.3.15}$$

In the derivation of the detection piece (5.3.13), we have made use of the non-relativistic Lagrangian (2.6.88) describing neutrino-nucleon low-energy interactions. This effective Lagrangian allowed us to easily obtain the appropriate CEνNS cross section. However, in the procedure we followed to obtain such Lagrangian (which we named as cascade of EFTs) in Section 2.6, we made an important assumption, i.e. we worked in the zero recoil limit, $q = p_2 - k = 0$. This in turn led us to neglect $\mathcal{O}(\nabla)$ terms in the non-relativistic expansion of Eq. (2.6.87). We can qualitatively understand all these approximations as being translated — in the usual derivation of the CEνNS cross section — into the characterization of the non-perturbative behaviour of the hadronic part of the process: the form factors $\mathcal{F}(q^2)$ of the nucleons[5].

---

[5]Form factors are the Fourier transform of the spatial density distribution of the nucleons: the scatterers in CEνNS in our case.

Therefore, the assumptions stated above translate into considering the usual low-energy behaviour of the form factors $\mathcal{F}(0) = 1$ — what obviously entails equal form factors for both protons and neutrons within the nucleus, c.f. [307, 310]. Although it seems a good approximation due to the low energies involved in CEνNS, it has been shown [310] that they are not low enough and the actual choice of the form factors is a key ingredient in the analysis of COHERENT data and consequently, the naive choice $\mathcal{F}(q^2) = 1$ provides inaccurate results.

In view of these concerns, we include as well momentum-dependent form factors for both protons and neutrons, inserting them into the weak charge via [306]

$$[\tilde{\mathcal{Q}}]_{\alpha\beta} = v^2 \left(Z[C_V^p]_{\alpha\beta}\mathcal{F}_p(q^2) + N[C_V^n]_{\alpha\beta}\mathcal{F}_n(q^2) \right), \tag{5.3.16}$$

where $\mathcal{F}_p$ and $\mathcal{F}_n$ correspond to the form factors of the proton and neutron respectively, which depend on the squared three-momentum transfer $q^2 \simeq 2M_\mathcal{N}T$. Concretely, we follow Refs. [292] and [310] and use the Helm parametrization of the form factor [341]

$$\mathcal{F}_{(p,n)}(q^2) = 3\frac{j_1(qR_0^{(p,n)})}{qR_0^{(p,n)}}e^{-q^2s^2/2}, \tag{5.3.17}$$

where j_1 is the first order spherical Bessel function, $s = 0.9$ fm [342] and

$$(R_0^{(p,n)})^2 \equiv \frac{5}{3}R_{(p,n)}^2 - 5s \tag{5.3.18}$$

with R_p and R_n the root-mean-square (rms) radius of the proton and neutron distributions respectively. Obviously, these are nucleus dependent quantities [310]:

$$R_p(Cs) = 4.821 \text{ fm}, \qquad R_p(I) = 4.766 \text{ fm}, \qquad R_p(Ar) = 3.448 \text{ fm}, \tag{5.3.19}$$

and

$$R_n(Cs) = 5.09 \text{ fm}, \qquad R_n(I) = 5.03 \text{ fm}, \qquad R_n(Ar) = 3.55 \text{ fm}. \tag{5.3.20}$$

Since the differences between the proton and neutron rms radius are that small, for convenience we consider them to be equal and take the average between the numbers given above. Accordingly, both proton and neutron form factors become $\mathcal{F}(q^2) \equiv \mathcal{F}_p(q^2) = \mathcal{F}_n(q^2)$, and we factorize them out of the weak charges: $[\tilde{\mathcal{Q}}]_{\alpha\beta} = [\mathcal{Q}]_{\alpha\beta}\mathcal{F}(q^2)$. Hence, the detection piece in Eq. (5.3.13) above (and consequently Eq. (5.3.14)), is modified by a factor of $(\mathcal{F}(q^2))^2$.

5.3.2 Production at COHERENT: π^+ and μ^+ decay at rest

The two production mechanisms at play, for the three flavor neutrino fluxes, in the COHERENT experiment are pion (π^+) and muon (μ^+) decays at rest:

$$\pi^+ \rightarrow \mu^+ \nu_\mu \rightarrow \nu_\mu \bar{\nu}_\mu \nu_e e^+. \tag{5.3.21}$$

Standard Model fluxes are computed from the decay width of the parent particles, which represents the probability per unit time that the particle will decay. At

COHERENT, the parent particles producing the neutrino fluxes are the charged pions π^+. For each POT a $r_{\nu/p}$ number of pions are created, as provided by the Geant4 simulation [340] of the neutrino production process at the SNS used by COHERENT. However, we expect that for sufficiently large times, all pions will decay into a muon and a neutrino and the former, subsequently, into two neutrinos and a positron, both processes with a probability of one. This is why in the literature the three neutrino fluxes are given normalized to each proton collision on the target by [307]:

$$
\begin{aligned}
\frac{d\Phi_{\nu_\mu}}{dE_\nu} &= \frac{1}{4\pi L^2}\delta\left(E_\nu - \frac{m_{\pi^\pm}^2 - m_\mu^2}{2m_{\pi^\pm}}\right), \\
\frac{d\Phi_{\bar\nu_\mu}}{dE_\nu} &= \frac{1}{4\pi L^2}\frac{64}{m_\mu}\left[\left(\frac{E_\nu}{m_\mu}\right)^2\left(\frac{3}{4} - \frac{E_\nu}{m_\mu}\right)\right], \\
\frac{d\Phi_{\nu_e}}{dE_\nu} &= \frac{1}{4\pi L^2}\frac{192}{m_\mu}\left[\left(\frac{E_\nu}{m_\mu}\right)^2\left(\frac{1}{2} - \frac{E_\nu}{m_\mu}\right)\right],
\end{aligned}
\tag{5.3.22}
$$

where, by construction, the integral over the whole energy range $E_\nu \in [0, m_\mu/2]$ gives 1 (in units of $1/(4\pi L^2)$). Above, the first term corresponds to pion decay, thus the delta term on the r.h.s. take care of the fact that the produced neutrino is mono-energetic, and the second and third terms are the neutrino fluxes generated by muon decay.

   The normalization of the flux entails that the constant factors stemming from the computation of the production processes are canceled out. In our formalism we do not work with fluxes or cross sections, but instead we should compute the rate of events via Eq. (5.1.3), for which the (similar) consequences of the discussion above about normalization are treated at the beginning of Section 5.3.3. Therefore, in the derivation of the production pieces in the next two sections, we will not pay attention to those irrelevant factors — although we do indeed recover (as expected) the energy spectrum of each neutrino flux — but will just focus on the characterization of the NP contributions to the production pieces. The relevant charged-current interactions — both within and beyond the Standard Model — driving those production processes above are parametrized within $\mathcal{L}_{\text{LEFT}}^{\text{CC}}$ in Eqs. (2.6.77) for pion decay and (2.6.78) for muon decay, and, together with our rate of events (5.1.3), allow us to extend the production mechanism to include NSI as well as to properly treat the neutrino oscillatory behavior between production and detection. Then, we will use these results in a following section to compute the total differential number of events for each neutrino type.

Pion decay

From the Lagrangian in Eq. (2.6.77), we can simply write the amplitude for pion decay into a lepton ℓ_α of flavor α and a (mass eigenstate) neutrino ν_k as

$$
\mathcal{M}(\pi^+ \to \ell_\alpha^+ \nu_k) = \mathcal{A}^{\pi^+} U_{\beta k}^* [\mathcal{P}]_{\alpha\beta}^*,
\tag{5.3.23}
$$

where sum over repeated indices is understood. Above $\mathcal{A}^{\pi^+}$ contains the spinor wave functions of the fields and other factors and we have defined

$$[\mathcal{P}]_{\alpha\beta} = \delta_{\alpha\beta} + [\epsilon_L]_{\alpha\beta} - [\epsilon_R]_{\alpha\beta} - [\epsilon_P]_{\alpha\beta}\frac{m_{\pi^\pm}^2}{m_{\ell_\alpha}(m_u + m_d)}\,. \tag{5.3.24}$$

Particularizing to the case of the muon $\alpha = \mu$, the amplitude (5.3.23) leads, for the production piece by pion decay in the master formula (5.1.3), to

$$\int d\Pi_{P'}\mathcal{M}(\pi^+ \to \mu^+\nu_k)\mathcal{M}(\pi^+ \to \mu^+\nu_l)^* = $$
$$\mathcal{B}^{\nu_\mu}[\mathcal{P}U]_{\mu l}[U^\dagger\mathcal{P}^\dagger]_{k\mu}\delta\left(E_\nu - \frac{m_{\pi^\pm}^2 - m_\mu^2}{2m_{\pi^\pm}}\right), \tag{5.3.25}$$

where on the r.h.s. we have already integrated over the phase space, such that $\mathcal{B}^{\nu_\mu}$ contains only constant factors.

Muon decay

In this case, the amplitude of the decay $\ell_a^+ \to \bar{\nu}_\alpha\ell_b^+\nu_\beta$ is given by the Lagrangian (2.6.78) as

$$\mathcal{M}(\ell_a^+ \to \bar{\nu}_\alpha\ell_b^+\nu_\beta) = A_L^{\ell_a}[\mathcal{P}_L]_{a\alpha\beta b} + A_R^{\ell_a}[\mathcal{P}_R]_{a\alpha\beta b}\,, \tag{5.3.26}$$

where A_L and A_R contains the spinor wave functions and depend as well on the parameters of the Lagrangian. Above we have defined

$$[\mathcal{P}_L]_{a\alpha\beta b} = \delta_{\alpha a}\delta_{\beta b} + [\rho_L]_{a\alpha\beta b}\,, \tag{5.3.27}$$
$$[\mathcal{P}_R]_{a\alpha\beta b} = [\rho_R]_{a\alpha\beta b}\,. \tag{5.3.28}$$

For muon decay ($a = \mu$ and $b = e$), in terms of the neutrino mass eigenstates we have

$$\mathcal{M}(\mu^+ \to \bar{\nu}_j e^+\nu_k) = A_L^{\mu^+}[\mathcal{P}_L]_{\mu\alpha\beta e}U_{\alpha j}U_{\beta k}^* + A_R^{\mu^+}[\mathcal{P}_R]_{\mu\alpha\beta e}U_{\alpha j}U_{\beta k}^*\,, \tag{5.3.29}$$

where again summation over repeated indices is assumed. From the amplitude above we can compute the production pieces for both neutrinos and antineutrinos:

- Neutrinos

The production term for neutrinos is obtained from the amplitude (5.3.29) by summing over all possible antineutrino mass eigenstates

$$\int d\Pi_{P'}\sum_j \mathcal{M}(\mu^+ \to \bar{\nu}_j e^+\nu_k)\mathcal{M}(\mu^+ \to \bar{\nu}_j e^+\nu_l)^* = $$
$$\mathcal{B}_L^{\nu_e}[\mathcal{P}_L]_{\mu\alpha\beta e}U_{\beta k}^*[\mathcal{P}_L]_{\mu\alpha\sigma e}^* U_{\sigma l}^* + L \leftrightarrow R = \mathcal{B}_L^{\nu_e}[\mathcal{P}_L^* U]_{\alpha l}[U^\dagger P_L^T]_{k\alpha} + L \leftrightarrow R\,, \tag{5.3.30}$$

where we have neglected the crossed terms RL and LR since they behave as m_e/m_μ. In the last step above, we introduced the more suitable 2×2 matrix notation $[\mathcal{P}_X]_{\mu\alpha\beta e} \equiv [\mathcal{P}_X]_{\alpha\beta}$ because muon decay (hence the COHERENT experiment) is only sensitive to that particular combination of μ and e indices. However, we should be cautious when taking the transpose of the $\mathcal{P}$ matrices in flavor space, since transposing only those two free flavor indices (α and β) entails assuming the more general $3 \times 3 \times 3 \times 3$ matrix to be symmetric in the two other fixed indices.

- Antineutrinos

For antineutrinos we should sum now over all possible neutrino mass eigenstates, thus giving

$$\int d\Pi_{P'} \sum_j \mathcal{M}(\mu^+ \to \bar{\nu}_k e^+ \nu_j)\mathcal{M}(\mu^+ \to \bar{\nu}_l e^+ \nu_j)^* = \mathcal{B}_L^{\bar{\nu}_\mu}[\mathcal{P}_L^T U]_{\alpha k}[U^\dagger P_L^*]_{l\alpha} + L \leftrightarrow R\,,$$

(5.3.31)

where we have again neglected the RL, LR terms since they go as m_e/m_μ.

Finally, note that in Eqs. (5.3.25), (5.3.30) and (5.3.31), the mass indices k and l remain (as expected) free to be later summed over when computing the total number of events together with the detection piece.

5.3.3 Differential number of events at COHERENT

The three neutrino fluxes produced at the SNS contribute to the total number of events detected at COHERENT, as expected from the neutral-current-driven CEνNS. However, this experiment measures the (differential) number of events as a function of the recoil energy T, which they provide distributed in energy bins. Therefore, since each neutrino flux has a different T dependence, in principle we may use the recoil energy distributions provided by the collaboration to extract better constraints in the LEFT parameter space. Accordingly, we provide here the differential number of events as a function of the recoil energy computed within our formalism, for the three neutrino fluxes.

As explained above, once we have both production (see Eqs. (5.3.25), (5.3.30) and (5.3.31)) and detection (see Eqs. (5.3.13) and (5.3.15)) pieces, the differential number of events (5.1.1) is computed by inserting them into Eq. (5.1.3) and summing over the neutrino-mass indices k, l and j. This is given in terms of the recoil energy T via

$$\frac{dN_\alpha}{dT} = \int dt \int dE_\nu \frac{dN_\alpha}{dt\, dE_{\nu_\alpha}\, dT}\,,$$

(5.3.32)

where the time dependence of the rate (5.1.3) enters the (two) number of sources producing the neutrinos, i.e. after a given time t following the production of the neutrino sources (pions and muons), the actual number of sources that will have decayed (thus counting for neutrino production) will be just a fraction of the total production. For a large enough period of time, all pions and muons decay into neutrinos and then the integral over time becomes

$$\int_0^\infty dt\, N_S(t) = N_{S_0}\tau_S\,,$$

(5.3.33)

where $\tau_S = \Gamma_S^{-1}$ is the mean lifetime of the source — which is given by the inverse of its decay width — and at COHERENT we may identify[6] $N_{S_0} \equiv n_{\mathrm{POT}} r_{\nu/p}$.

---

[6]Note that the pulsed feature of the SNS beam entails that the source particles as well as the neutrinos are produced in bunches. The identification $N_{S_0} \equiv n_{\mathrm{POT}} r_{\nu/p}$ entails already the factorization of the (equal) time dependences of each bunch, and the sum over them reaching the total number of produced sources provided by the experiment.

Pion decay

The differential number of events from pion decay is given by

$$
\frac{dN_{\nu_\mu}}{dT} = n_{\text{POT}} r_{\nu/p} \frac{N_T M_\mathcal{N} G_F^2}{4\pi L^2} \mathcal{F}^2 \left(1 - \frac{M_\mathcal{N} T}{2(E_\nu^\pi)^2} - \frac{T}{E_\nu^\pi} \right) \times
$$
$$
\sum_{k,l} e^{-i \frac{L \Delta m_{kl}^2}{2 E_\nu^\pi}} [\mathcal{P} U]_{\mu l} [U^\dagger \mathcal{Q}^\dagger \mathcal{Q} U]_{lk} [U^\dagger \mathcal{P}^\dagger]_{k\mu} , \tag{5.3.34}
$$

where we do not show explicitly the q^2 dependence of $\mathcal{F}(q^2)$, and $E_\nu^\pi = (m_{\pi^\pm}^2 - m_\mu^2)/(2m_{\pi^\pm})$ is the discrete energy at which the neutrino is produced. Note that most of the factors related to the production mechanism are canceled out by the introduction[7] of Γ_π^{-1} from the discussion above.

The characteristic short baseline at COHERENT allows us to further neglect the exponential factor. Assuming $L\Delta m_{kl}^2/E_\nu^\pi \sim 0$, which from now on we will refer to as the no-oscillation limit, the expression above reduces to

$$
\frac{dN_{\nu_\mu}}{dT} = n_{\text{POT}} r_{\nu/p} \frac{N_T M_\mathcal{N} G_F^2}{4\pi L^2} \mathcal{F}^2 \left(1 - \frac{M_N T}{2(E_\nu^\pi)^2} - \frac{T}{E_\nu^\pi} \right) \sum_{\beta,\beta'} [\mathcal{P}]_{\mu\beta} \left[\mathcal{Q}^\dagger \mathcal{Q} \right]_{\beta\beta'} \left[\mathcal{P}^\dagger \right]_{\beta'\mu} , \tag{5.3.35}
$$

where the PMNS matrices drop out from the unitarity condition $U^\dagger U = 1$ and we observe that production and detection (charges) NP flavor matrices mix. The last term can also be expressed as $\left[\mathcal{P} \mathcal{Q}^\dagger \mathcal{Q} \mathcal{P}^\dagger \right]_{\mu\mu}$.

It is illustrative to compare our result (in the no-oscillation limit) with a "factorization" approach, where we would compute the number of events via

$$
\frac{dN_{\nu_\mu}}{dT} = \sum_{\beta,\gamma} \int dE_\nu \frac{d\Phi(\pi^+ \to \mu^+ \nu_\beta)}{dE_\nu} \frac{d\sigma(\nu_\beta \mathcal{N} \to \nu_\gamma \mathcal{N})}{dT} , \tag{5.3.36}
$$

where we have factorized the flux and cross section (see Eq. (5.3.14)) and summed over neutrino flavors. The flux is defined from the decay width by $\frac{d\Phi}{dE_\nu} \equiv \frac{N_S}{4\pi L^2} \frac{d\Gamma}{dE_\nu}$. The corresponding result for pion decay looks like

$$
\frac{dN_{\nu_\mu}}{dT} = n_{\text{POT}} r_{\nu/p} \frac{N_T M_\mathcal{N} G_F^2}{4\pi L^2} \mathcal{F}^2 \left(1 - \frac{M_N T}{2(E_\nu^\pi)^2} - \frac{T}{E_\nu^\pi} \right) \sum_{\beta,\beta'} [\mathcal{P}]_{\mu\beta} \left[\mathcal{Q}^\dagger \mathcal{Q} \right]_{\beta\beta'} \left[\mathcal{P}^\dagger \right]_{\beta'\mu} \delta_{\beta\beta'} , \tag{5.3.37}
$$

that is, obviously, different from Eq. (5.3.35). The sum in Eq. (5.3.35) contains additional terms with $\beta \neq \beta'$, which are projected out by $\delta_{\beta\beta'}$ in Eq. (5.3.37). More concretely, at linear order in the WCs both results match. At second order but only flavor-diagonal WCs, we recover the same results from both equations again. However, if flavor off-diagonal WCs are considered, at second order the factorization approach fails to provide the correct results for those terms.

---

[7]Here we have assumed $\Gamma_S \equiv \Gamma_S^{\text{SM}}$, for the EFT case at hand see Section 5.3.3 below.

Muon decay

The differential number of events for neutrinos is given by

$$\frac{dN_{\nu_e}}{dT} = n_{\text{POT}} r_{\nu/p} \frac{N_T M_{\mathcal{N}} G_F^2}{4\pi L^2} \mathcal{F}^2 \int_{E_\nu^{\min}}^{m_\mu/2} dE_\nu \frac{192}{m_\mu} \left(\frac{E_\nu}{m_\mu}\right)^2 \left(\frac{1}{2} - \frac{E_\nu}{m_\mu}\right) \left(1 - \frac{M_{\mathcal{N}} T}{2E_\nu^2} - \frac{T}{E_\nu}\right)$$

$$\times \sum_{k,l} \exp^{-i\frac{L\Delta m_{kl}^2}{2E_\nu}} \sum_{\alpha} \left\{ [\mathcal{P}_L^* U]_{\alpha l} [U^\dagger \mathcal{Q}^\dagger \mathcal{Q} U]_{lk} [U^\dagger P_L^T]_{k\alpha} p_{LL} + L \leftrightarrow R \right\}, \quad (5.3.38)$$

where as in the previous case, most of the production-related factors are canceled out by Γ_μ^{-1}. Taking again the no-oscillation limit we arrive at

$$\frac{dN_{\nu_e}}{dT} = n_{\text{POT}} r_{\nu/p} \frac{N_T M_{\mathcal{N}} G_F^2}{4\pi L^2} \mathcal{F}^2 \int_{E_\nu^{\min}}^{m_\mu/2} dE_\nu \frac{192}{m_\mu} \left(\frac{E_\nu}{m_\mu}\right)^2 \left(\frac{1}{2} - \frac{E_\nu}{m_\mu}\right) \left(1 - \frac{M_{\mathcal{N}} T}{2E_\nu^2} - \frac{T}{E_\nu}\right)$$

$$\times \sum_{\alpha} \left\{ [\mathcal{P}_L^* \mathcal{Q}^\dagger \mathcal{Q} P_L^T]_{\alpha\alpha} p_{LL} + [\mathcal{P}_R^* \mathcal{Q}^\dagger \mathcal{Q} P_R^T]_{\alpha\alpha} p_{RR} \right\}. \quad (5.3.39)$$

In the factorization scheme provided by Eq. (5.3.36) above, we obtain

$$\frac{dN_{\nu_e}}{dT} = g_{\nu_e}(T, E_\nu) \sum_{\alpha} \sum_{\beta,\beta'} \left\{ [\mathcal{P}_L^*]_{\alpha\beta} [\mathcal{Q}^\dagger \mathcal{Q}]_{\beta\beta'} [P_L^T]_{\beta'\alpha} \, p_{LL} + [\mathcal{P}_R^*]_{\alpha\beta} [\mathcal{Q}^\dagger \mathcal{Q}]_{\beta\beta'} [P_R^T]_{\beta'\alpha} \, p_{RR} \right\} \delta_{\beta\beta'},$$

$$(5.3.40)$$

where we have just collected all terms remaining equal in both approaches in $g_{\nu_e}(T, E_\nu)$. Same consequences as for the pion decay case are observed (see above).

The computation for antineutrinos leads to (recalling that the change in Eq. (5.3.15) should be applied)

$$\frac{dN_{\bar{\nu}_\mu}}{dT} = n_{\text{POT}} r_{\nu/p} \frac{N_T M_{\mathcal{N}} G_F^2}{4\pi L^2} \mathcal{F}^2 \int_{E_\nu^{\min}}^{m_\mu/2} dE_\nu \frac{64}{m_\mu} \left(\frac{E_\nu}{m_\mu}\right)^2 \left(\frac{3}{4} - \frac{E_\nu}{m_\mu}\right) \left(1 - \frac{M_{\mathcal{N}} T}{2E_\nu^2} - \frac{T}{E_\nu}\right)$$

$$\times \sum_{k,l} \exp^{-i\frac{L\Delta m_{kl}^2}{2E_\nu}} \sum_{\alpha} \left\{ [\mathcal{P}_L^T U]_{\alpha k} [U^\dagger \mathcal{Q} \mathcal{Q}^\dagger U]_{kl} [U^\dagger P_L^*]_{l\alpha} \bar{p}_{LL} + L \leftrightarrow R \right\}, \quad (5.3.41)$$

where the no-oscillation limit now provides

$$\frac{dN_{\bar{\nu}_\mu}}{dT} = n_{\text{POT}} r_{\nu/p} \frac{N_T M_{\mathcal{N}} G_F^2}{4\pi L^2} \mathcal{F}^2 \int_{E_\nu^{\min}}^{m_\mu/2} dE_\nu \frac{64}{m_\mu} \left(\frac{E_\nu}{m_\mu}\right)^2 \left(\frac{3}{4} - \frac{E_\nu}{m_\mu}\right) \left(1 - \frac{M_{\mathcal{N}} T}{2E_\nu^2} - \frac{T}{E_\nu}\right)$$

$$\times \sum_{\alpha} \left\{ [\mathcal{P}_L^T \mathcal{Q} \mathcal{Q}^\dagger P_L^*]_{\alpha\alpha} \bar{p}_{LL} + [\mathcal{P}_R^T \mathcal{Q} \mathcal{Q}^\dagger P_R^*]_{\alpha\alpha} \bar{p}_{RR} \right\}. \quad (5.3.42)$$

In the following we will always work in the no-oscillation limit.

The factorization approach (5.3.36) now provides

$$\frac{dN_{\bar{\nu}_\mu}}{dT} = g_{\bar{\nu}_\mu}(T, E_\nu) \sum_{\alpha} \sum_{\beta,\beta'} \left\{ [\mathcal{P}_L^T]_{\alpha\beta} [\mathcal{Q} \mathcal{Q}^\dagger]_{\beta\beta'} [P_L^*]_{\beta'\alpha} \, \bar{p}_{LL} + [\mathcal{P}_R^T]_{\alpha\beta} [\mathcal{Q} \mathcal{Q}^\dagger]_{\beta\beta'} [P_R^*]_{\beta'\alpha} \, \bar{p}_{RR} \right\} \delta_{\beta\beta'},$$

$$(5.3.43)$$

with the same differences as compared to our formalism as in the other two cases.

In the equations above we have introduced the minimum neutrino energy to produce an event with a recoil energy T as

$$E_\nu^{\min} = \frac{T}{2}\left(1 + \sqrt{1 + 2\frac{M_\mathcal{N}}{T}}\right),\tag{5.3.44}$$

and we have also defined [273]

$$
\begin{aligned}
p_{LL} &= 1, & p_{RR} &= \frac{3m_\mu - 4E_\nu}{6m_\mu - 12E_\nu} + \mathcal{O}(m_e), \\
\bar{p}_{LL} &= 1, & \bar{p}_{RR} &= \frac{6m_\mu - 12E_\nu}{3m_\mu - 4E_\nu} + \mathcal{O}(m_e).
\end{aligned}
\tag{5.3.45}
$$

Modified weak charges

The new-physics contributions — both at production and detection — parametrized in the LEFT Lagrangian, can be thought of as modifying the SM weak charge. Accordingly, and due to the fact that the only observable of CEνNS is the recoil energy of the nucleus, we will have access only to particular combinations of WCs, which we will collect in modified weak charges Q.

However, before addressing the corresponding expressions, there is an important caveat to point out. This is related to the discussion we made in Section 2.5.2 about the input scheme in particular. As explained in more length there, when working within the EFT framework we introduce a set of new parameters (the WCs), which will inevitably affect other observables as well. Accordingly, the numerical values extracted from the experiments for those observables should be understood as being contaminated by NP interactions, which should be correspondingly taken into account. For the case at hand, this effect enters both at production and detection.

At production the total decay widths of the source particles have been introduced via the time integral in Eq. (5.3.33). Within our EFT framework their dependence on the NP coefficients is the following:

$$\hat{\Gamma}_\pi = \Gamma_\pi^{\mathrm{SM}}\left[\mathcal{P}\mathcal{P}^\dagger\right]_{\mu\mu},\tag{5.3.46}$$

$$\hat{\Gamma}_\mu = \Gamma_\mu^{\mathrm{SM}}\sum_\alpha\left\{\left[\mathcal{P}_L\mathcal{P}_L^\dagger\right]_{\alpha\alpha} + \left[\mathcal{P}_R\mathcal{P}_R^\dagger\right]_{\alpha\alpha}\right\},\tag{5.3.47}$$

where we have made explicit that Γ_X^{SM} is the decay width computed within the SM (with the corresponding SM parameters) and $\hat{\Gamma}_X$ is the actual physical quantity measured in experiments (and then potentially contaminated by new physics interactions). Therefore, in our calculation of the differential number of events within the EFT formalism above, the actual total decay widths introduced by Eq. (5.3.33) are $\hat{\Gamma}_\pi$ and $\hat{\Gamma}_\mu$. Expressing them as Eqs. (5.3.46) and (5.3.47) removes, as before, most of the production-related factors (via Γ^{SM}), but necessarily introduces the NP coefficients contaminating the decay widths.

At detection, the NP contamination enters the Fermi constant, such that we should express the SM value used until now G_F (see Eqs. (5.3.35), (5.3.39) and (5.3.42)), in terms of the experimentally measured $\hat{G}_F$ and the NP coefficients via

$$\hat{G}_F^2 = G_F^2 \sum_\alpha \left\{ \left[\mathcal{P}_L \mathcal{P}_L^\dagger \right]_{\alpha\alpha} + \left[\mathcal{P}_R \mathcal{P}_R^\dagger \right]_{\alpha\alpha} \right\}. \tag{5.3.48}$$

All in all, we obtain for the (differential) number of events, in terms of the aforementioned modified weak charges,

$$\frac{dN_{\nu_\mu}}{dT} = n_{\text{POT}} r_{\nu/p} \frac{N_T M_\mathcal{N} \hat{G}_F^2}{4\pi L^2} \mathcal{F}^2 f_{LL}^{\nu_\mu}(T) \left(Q_{LL}^{\nu_\mu} \right)^2, \tag{5.3.49}$$

$$\frac{dN_{\nu_e}}{dT} = n_{\text{POT}} r_{\nu/p} \frac{N_T M_\mathcal{N} \hat{G}_F^2}{4\pi L^2} \mathcal{F}^2 \left[f_{LL}^{\nu_e}(T) \left(Q_{LL}^{\nu_e} \right)^2 + f_{RR}^{\nu_e}(T) \left(Q_{RR}^{\nu_e} \right)^2 \right], \tag{5.3.50}$$

$$\frac{dN_{\bar{\nu}_\mu}}{dT} = n_{\text{POT}} r_{\nu/p} \frac{N_T M_\mathcal{N} \hat{G}_F^2}{4\pi L^2} \mathcal{F}^2 \left[f_{LL}^{\bar{\nu}_\mu}(T) \left(Q_{LL}^{\bar{\nu}_\mu} \right)^2 + f_{RR}^{\bar{\nu}_\mu}(T) \left(Q_{RR}^{\bar{\nu}_\mu} \right)^2 \right], \tag{5.3.51}$$

where we have already integrated over the incoming neutrino energy E_ν and whose results are collected in the $f(T)$ functions, these satisfy the following equalities: $f_{LL}^{\nu_e}(T) = f_{RR}^{\bar{\nu}_\mu}(T)$ and $f_{RR}^{\nu_e}(T) = f_{LL}^{\bar{\nu}_\mu}(T)$. Notice that these also depend on the recoil energy T.

The modified weak charges are given by

$$\left(Q_{LL}^{\nu_\mu} \right)^2 = \frac{\left[\mathcal{P}\mathcal{Q}^\dagger \mathcal{Q}\mathcal{P} \right]_{\mu\mu}}{\left[\mathcal{P}\mathcal{P}^\dagger \right]_{\mu\mu} \times \sum_\alpha \left\{ \left[\mathcal{P}_L \mathcal{P}_L^\dagger \right]_{\alpha\alpha} + \left[\mathcal{P}_R \mathcal{P}_R^\dagger \right]_{\alpha\alpha} \right\}}, \tag{5.3.52}$$

$$\left(Q_{LL\,(RR)}^{\nu_e} \right)^2 = \frac{\sum_\alpha [\mathcal{P}_{L(R)}^* \mathcal{Q}^\dagger \mathcal{Q} P_{L(R)}^T]_{\alpha\alpha}}{\left(\sum_\alpha \left\{ \left[\mathcal{P}_L \mathcal{P}_L^\dagger \right]_{\alpha\alpha} + \left[\mathcal{P}_R \mathcal{P}_R^\dagger \right]_{\alpha\alpha} \right\} \right)^2}, \tag{5.3.53}$$

$$\left(Q_{LL\,(RR)}^{\bar{\nu}_\mu} \right)^2 = \frac{\sum_\alpha [\mathcal{P}_{L(R)}^T \mathcal{Q}^\dagger \mathcal{Q} P_{L(R)}^*]_{\alpha\alpha}}{\left(\sum_\alpha \left\{ \left[\mathcal{P}_L \mathcal{P}_L^\dagger \right]_{\alpha\alpha} + \left[\mathcal{P}_R \mathcal{P}_R^\dagger \right]_{\alpha\alpha} \right\} \right)^2}. \tag{5.3.54}$$

The fact that, as a result from the new-physics contamination of the decay widths discussed above (and consequently of the experimental determination of G_F) the NP in production enter the denominator, the part of the contamination coming from the decay widths of the production pieces will cancel (almost exactly) the production WCs in the numerator, but the part stemming from G_F in the detection piece will remain in the denominator. Accordingly, the COHERENT experiment is (partially) sensitive to the CC NSI in production but in a different way as one may expect from a naive identification of the experimentally measured parameters.

The recoil-energy dependent functions $f(T)$ above characterize the energy sensitivity of the number of events to the modified weak charges. The equalities found among the f's entails that, even though we have access at COHERENT to the energy distribution of the events, we will not be able to distinguish the contributions from those modified charges whose accompanying f's are equal, i.e. we cannot constrain them separately, but only their combination.

5.4 Data analysis and results

We have already repeated several times throughout this chapter that the only observable effects after a CEνNS event takes place, is the low-energy recoil of the nucleus and the time distribution of the events. The theoretical expectation for such an event to happen at COHERENT is given in Eqs. (5.3.49), (5.3.50) and (5.3.51), for each of the three neutrino fluxes produced at the SNS, parametrized within the low-energy effective field theory framework and computed within our QFT-oscillation formalism. However, from the recoil of the nucleus until the actual experimental determination of the corresponding energy, as well as the number of events given in each recoil-energy bin, the experimental analysis involves yet several steps. In general they are summarized as follows.

Regarding the characterization of the signal, first, the COHERENT experiment does not measure directly the recoil energy of the scattered nucleus, but the experimental data is provided either in number of photoelectrons (PE), produced by an event with a certain nuclear recoil, or directly in electron-equivalent recoil energy T_{ee} (see below). These three quantities are related by the Quenching Factor (QF). On top of that, in order to account for the probability that the detector measures a different number of PE than what would be expected, in average, from a given event, we have to take into account the energy resolution of the detector $\mathcal{R}$. This entails moving from T_{ee} to a reconstructed electron-equivalent recoil energy T_{rec}: $\mathcal{R}(T_{\text{rec}}, T_{ee})$. Then, the efficiency of the detector in terms of T_{rec} should also be applied $\epsilon(T_{\text{rec}})$.

In general, all these considerations can be collected in the following modified expression for the number of events in each reconstructed recoil-energy bin i [309,310]

$$N_i = \int_{T_{\text{rec}}^i}^{T_{\text{rec}}^{i+1}} dT_{\text{rec}} \, \epsilon(T_{\text{rec}}) \int_{T_{\min}}^{T_{\max}} dT \, \mathcal{R}(T_{\text{rec}}, T_{ee}(T)) \sum_{\nu=\nu_\mu, \nu_e, \bar{\nu}_\mu} \frac{dN_\nu}{dT}(T) \, , \qquad (5.4.55)$$

where the (differential) number of events is given in terms of the true recoil energy T (as provided in the preceding section). We have expressed the energy resolution $\mathcal{R}(T_{\text{rec}}, T_{ee})$ in terms of T instead of T_{ee} by means of the QF and, together with the number of events, should be integrated between $T_{\min} = \{0, 19.5\}$ eV for CsI and Ar respectively (the former will become clear below while the latter is given by the average energy to produce a scintillation photon [309]) and $T_{\max} = 2E_\nu^2/(2E_\nu + M_{\mathcal{N}})$ to shift to the reconstructed energy T_{rec}. Finally, the efficiency for each energy bin is applied as a function of the reconstructed recoil energy. Needless to say, each of the three analyses entails different QF, energy resolution, efficiencies and even the way final data is provided and as such, the expression above will differ. We provide how Eq. (5.4.55) should be adapted for each analysis below.

On the other hand, the background should be properly characterized as well. This is mostly achieved at COHERENT thanks to the characteristic pulsed beam provided by the SNS. We give below the main backgrounds present at COHERENT.

In addition to the recoil-energy distribution of the events, to which all the effects described above apply, the collaboration provides as well the arrival-time distribution. Since we can distinguish between two kinds of neutrino fluxes in terms of

their arrival time, i.e. prompt and delayed neutrinos, we can use this information to strengthen the data analysis by combining both distributions.

We follow closely the work of Refs. [307, 309] and [310], based on the three data releases of the collaboration [343–345], to include the aforementioned experimental effects in our analysis and thus be able to use the data provided by COHERENT. First, let us address those effects in more detail.

5.4.1 Quenching Factor

Once the CEνNS event takes place, the nuclear recoil energy is dissipated in a combination of ionization (electron recoils, also called scintillation) and secondary nuclear recoils. The latter are the characteristic signal of a nuclear recoil. However, the corresponding signal is smaller than that provided by electron recoils. This is why COHERENT measures the events in terms of electron-equivalent recoil energy T_{ee} or PE, which have to be translated into the true nuclear recoil energy. The relation between the true recoil energy T and T_{ee} is given by the Quenching Factor as

$$T_{ee} = \mathrm{QF}(T) \times T \,, \tag{5.4.56}$$

where we have made explicit that, besides being a detector dependent quantity, QF is also a function of the recoil-energy. The number of PE can be extracted from the relation above by introducing the light (or signal) yield LY, as the number of PE produced by an electron recoil of one keV:

$$\mathrm{PE} = \mathrm{QF}(T) \times \mathrm{LY} \times T \,. \tag{5.4.57}$$

The Quenching Factor is actually a way to parametrize the quenching of the signal, what should be understood as the ratio between the light yields from a nuclear and an electron recoil of the same energy. Accordingly, it allows to translate from the true recoil energy to the measured electron-equivalent energy (or PE). Let us now address the QF of the three COHERENT measurements.

(CsI)$_1$: The first measurement on CsI used a energy-independent QF in the whole energy range considered for the analysis, between 6 and 30 PE [276]. They adopted such an unphysical QF with large error bars due to a tension existing at that time between several calibration measurements. However, in Ref. [346] the Chicago-3 group found the origin of that tension and, when corrected, a better agreement among the various data sets was obtained. They concluded that the physics-based model favored by the data for the QF, was a modification of the semi-empirical approach by Birks [347]:

$$\mathrm{QF}(T) = \frac{1 - e^{-T/E_0}}{kB \frac{dE}{dR}(T)} \,, \tag{5.4.58}$$

where E_0 and kB are two free parameters to be extracted from the experiment and for which the best fit by the Chicago-3 group [346] provides $kB = 3.311 \times 10^{-3}$ g·cm^2/MeV and $E_0 = 12.97$ keV. The factor in the denominator $\frac{dE}{dR}(T)$ is the energy loss per unit length of the ions. Following Ref. [307] we

use the average between Cs and I that can be obtained from SRIM-2013. The differences in both the SM prediction as well as in some NSI constraints from COHERENT data, between the energy-independent QF used in the first analysis by the collaboration and the QF in Eq. (5.4.58) with the Chicago-3 fit, are shown in Ref. [307]. Finally, the number of PE is given by a light yield of LY= 13.848 PE/keV.

(CsI)$_2$: For this second measurement [333], the energy distribution of the number of events is again given in PE, and the collaboration data release provides for the QF an empirically parametrized degree 3 polynomial

$$QF(T) = a + bT + cT^2 + dT^3 \, , \qquad (5.4.59)$$

with $a = 0.0555$, $b = 4.31$ MeV^{-1}, $c = -112$ MeV^{-2} and $d = 840$ MeV^{-3}.

LAr: In this case the data is provided in the reconstructed electron-equivalent recoil energy. The data release provides in this case [344]

$$QF(T) = a + bT \, , \qquad (5.4.60)$$

where $a = 0.246$ and $b = 0.00078$ keV^{-1}.

5.4.2   Energy resolution of the detector

Following the discussion on the QF above, once a nuclear-recoil event takes place, the corresponding (true) recoil energy is converted to the measurable T_{ee} or number of PE (depending on the analysis: CsI or Ar), via the relation provided by the QF ((5.4.57) or (5.4.56)). Accordingly, the collaboration ascribes such an event to the corresponding T_{ee} or PE bin. However, since no experimental apparatus is perfect, due to the resolution of the detector it can happen that, instead of measuring the real number of PE associated to the underlying nuclear-recoil event, a different value is observed by the detector. As a consequence, the corresponding energy bin of the event may be misidentified. These are the aforementioned energy smearing effects.

Therefore, the actual implications of the effect of the resolution of the detector are mainly twofold: on one hand, it has an impact on the energy distribution of the events and, on the other, it can affect the number of events at the tails of the bin distribution, i.e. the first and last bin can have an unreal number of events, thus affecting the total observed number of events. From this discussion it follows that, the thinner the energy bin, the more important the energy resolution of the detector becomes in the characterization of the recoil-energy distribution of the number of events.

The collaboration corrects for this effect via an energy resolution function $\mathcal{R}(T_{\rm rec}, T_{ee})$, which "reconstructs" the electron-equivalent recoil energy, thus accounting for this effect. For each analysis the collaboration modelize $\mathcal{R}(T_{\rm rec}, T_{ee})$ in the following ways:

(CsI)$_1$: For this first measurement, in their data release [343] the collaboration does not mention the associated effects of the energy resolution. Furthermore, in Ref. [306] it is claimed that such effects are negligible. Then, following

Ref. [306], we do not consider smearing effects for the data of this first CEνNS measurement. Accordingly, we do not have to reconstruct T_{ee} and we work — as it is provided by the collaboration — directly with PE.

(CsI)$_2$: In this case, in the supplemental material [345] they explain that the smearing is better modeled with a gamma function than a Gaussian model, via

$$\mathcal{R}(\text{PE}, T_{ee}) = \frac{(a\,(1+b))^{1+b}}{\Gamma(1+b)} \text{PE}^b e^{-a(1+b)\text{PE}}, \qquad (5.4.61)$$

with the parameters a and b fitted to $a = 0.0749\,\text{keV}/T_{ee}$ and $b = 9.56\,\text{keV}^{-1}T_{ee}$. Note that, in this case, the energy-resolution function (5.4.61) translates directly from T_{ee} to the reconstructed number of PE. Following Eq. (5.4.55), once we have, for example, expressed a and b in terms of the true recoil energy T via the QF (and thus the energy resolution as $\mathcal{R}(\text{PE}, T)$) and integrated over 0 and $T_{\max}$ (we have explicitly checked that the inclusion of a minimum energy to produce scintillation in CsI has negligible effects, so we take directly 0), we obtain the number of events in terms of the actual measured reconstructed number of PE, for which the data is given.

LAr: The data release [344] now prescribes to use a Gaussian modelization of the energy resolution

$$R(T_{\text{rec}}, T_{ee}; \sigma_{ee}) = \frac{1}{\sqrt{2\pi}\sigma_{ee}} e^{-\frac{(T_{\text{rec}} - T_{ee})^2}{2\sigma_{ee}^2}}, \qquad (5.4.62)$$

with the Gaussian standard deviation given in terms of the electron-equivalent recoil energy by $\sigma_{ee} \equiv \sigma(T_{ee}) = (0.58\ \text{keV})\sqrt{T_{ee}/\text{keV}}$. Following, e.g. the same procedures mentioned above, once we integrate this Gaussian distribution convoluted with the number of events, we obtain the latter as a function of T_{rec}.

5.4.3   Eficiency of the detector

In contrast to the energy resolution of the detector, its efficiency characterizes how probable is that the detector misses an event. The COHERENT collaboration provides the efficiencies in energy bins, so a (constant) efficiency of, let's say, $\epsilon = 0.9$ in an energy bin of $T \in [15, 20]$ keV, tells you that the detector misses 1 out of ten events with a recoil energy comprised between 15 and 20 keV. The efficiencies are energy-dependent quantities, so that for each bin the efficiency varies. Following the resulting energy or PE dependences after the energy resolution of the detector is taken into account as shown above, the efficiencies for each measurement by COHERENT are provided as follows:

(CsI)$_1$: The data release [343] provides the following efficiency function in terms of number of photoelectrons

$$\epsilon(\text{PE}) = \frac{a}{1 + e^{-k(\text{PE}-\text{PE}_0)}} \Theta(\text{PE} - 5), \qquad (5.4.63)$$

where $a = 0.6655$, $k = 0.4942$, $PE_0 = 10.8507$ and $\Theta(PE)$ is a modified Heaviside step function given by

$$\Theta = \begin{cases} 0 & PE < 5 \,, \\ 0.5 & 5 \leq PE < 6 \,, \\ 1 & PE \geq 6 \,. \end{cases} \qquad (5.4.64)$$

$(CsI)_2$: For the second measurement on CsI the collaboration provides [345] the following modified efficiency (now in terms of reconstructed PE)

$$\epsilon(PE) = \frac{a}{1 + e^{-b(PE-c)}} + d \,, \qquad (5.4.65)$$

whose parameter values are $a = 1.32$, $b = 0.286$, $c = 10.9$ and $d = -0.333$, and it is restricted to be evaluated at $PE > 0$.

LAr: The collaboration provides in their data release [344] for the Ar measurement, a text file with the efficiency values corresponding to the reconstructed electron-recoil energy bin central values. We implement this efficiency by performing an interpolation in the whole energy range considered in the analysis.

5.4.4 Backgrounds at COHERENT

Once we have implemented all the aforementioned experimental effects, we have in Eq. (5.4.55) the theoretical prediction for the CEνNS signal measured at COHERENT: the recoil-energy distribution of the observed number of events. However, as an interaction mediated by the weak force, the corresponding rates are low and, in order to observe such a signal, the background that populates the signal region of interest (ROI) should be well characterized. For instance, the actual CEνNS measurement by COHERENT suffers from three main background sources:

(i) The steady-state backgrounds, being by far the largest kind of background at COHERENT, corresponds to cosmic rays or their by-products that arrive to the detector.

(ii) The prompt neutron or beam-related neutron (BRN) background corresponds to neutrons produced in the mercury target at the SNS, which then travel to the detector and may mimic the CEνNS signal.

(iii) The neutrino-induced neutron (NIN) background, a characteristic background of the SNS consisting of neutrons produced by neutrino interactions near the detector that, as for BRNs, can provide a false CEνNS signal.

Due to the nature of the backgrounds above, these can be further classified into beam-related or beam-uncorrelated. While the SS is completely beam-uncorrelated, the other two neutron-related backgrounds arise as a by-product of the beam itself. Moreover, one of the most attractive features of the beam provided by the SNS is its pulsed nature. This allows to separate the measured data by COHERENT into two regions called *coincident* (after the POT trigger onset, so the beam is producing

pions and the subsequent neutrino fluxes) and *anti-coincident* (just before the POT trigger onset). Since the largest background is by far the beam-uncorrelated steady-state, the coincidence (C) region is also called signal region and the anti-coincident (AC) is called background region.

Accordingly, at COHERENT, besides applying several techniques to mitigate the steady-state background [339], this is fully characterized by the measured AC data that the collaboration provides, for the three analyses, in their data releases. There, they give both energy and time distributions[8].

With respect to the prompt-neutron background, the (low energy) neutrons arriving at the detector entail a severe problem, since the energy deposition of CEνNS and the elastic neutron scattering off nucleus happen both in terms of nuclear recoils and their signal cannot be distinguished. In addition, the specific shielding for BRN background is not able to reduce it to negligible levels and then, it has to be modelized and included it in the analysis of CEνNS data. The collaboration provides the energy and time distributions of the BRN events for the three analyses.

Finally, the SNS is currently the most intense (pulsed) neutrino source and as such, it shows unique source of backgrounds as the production of neutrino-induced neutrons close to the detector which, as for BRNs, can mimic the CEνNS signal. NINs were considered negligible in the first analysis on CsI by COHERENT, and was found to be also the case for Ar (less than 1 event in the data set). However, the collaboration provides for its second measurement on CsI the energy (PE) and time distributions of NIN events (but time efficiency should be applied for the latter [345]).

5.4.5   Analysis and results

Once we have implemented all the aforementioned experimental effects, we have from Eq. (5.4.55) the theoretical prediction for the signal measured at COHERENT: the recoil-energy distribution of the observed number of events.

However, the collaboration provides as well the arrival-time distribution of neutrinos. Accordingly, we can express the probability distribution function (pdf) of the number of events (5.4.55) as a 2D distribution in energy and time: N_{ij}, where now i corresponds to the ith energy bin and j to the jth time bin. In order to obtain the corresponding expression, we should first come back to Eq. (5.3.32). There, we integrated the time dependence of $N_S(t)$ over an infinite time to ensure that all source particles decay into neutrinos. If we want to obtain the theoretical time distribution of the events, we should instead integrate over the time intervals defined by the time bins provided by the collaboration:

$$\int_{t_j}^{t_{j+1}} dt \, N_S(t) \,. \tag{5.4.66}$$

However, the time efficiency of the detector $\epsilon_t(t)$ should be considered as well. Accordingly, the 2D distribution in energy and time of the number of events can be

---

[8]Note that, since the provided data is the actual measured AC distribution, we do not have to apply further experimental corrections as, e.g. efficiencies and so on.

expressed as

$$N_{ij} = N_i \times \left[\int_{t_j}^{t_{j+1}} g(t)\epsilon_t(t)dt \right] , \qquad (5.4.67)$$

where $g(t)$ characterizes the time dependence of the production and decay of the neutrino sources (pions and muons), and we have already factorized out the time-independent $N_{S_0}\hat{\tau}_S$ (see Eq. (5.3.33)), which is included in N_i defined in Eq. (5.4.55). The time convolution on the r.h.s. of Eq. (5.4.67) is provided by the collaboration. For more details on those distributions as well as the experimental effects and backgrounds discussed above, we refer to the data releases of the collaboration and the references we have been citing throughout this section.

With the theoretical distribution of signal events N_{ij}, the rest of 2D pdfs of the backgrounds and the actual experimental distribution of coincidence C data N_{ij}^{exp}, following Ref. [310] we can perform a statistical analysis of the COHERENT data by means of the Poissonian χ^2. For this we use the same time and energy ranges as the collaboration, $(\text{CsI})_1$: $6 \leq \text{PE} < 30$ and $t_{\text{rec}} < 6$ μs [276]; $(\text{CsI})_2$: $\text{PE} < 60$ and $t_{\text{rec}} < 6$ μs [333]; and Ar: $T_{ee} < 120$ keV and $t_{\text{rec}} < 4.9$ μs [344]. This is still an ongoing work so we will not delve much into it here, but let us just point out several features of the analysis and the results.

If we were to consider how NSI affect the total number of CEνNS events measured at COHERENT, even though this is sensitive to many Wilson coefficients, one observable can only constrain the particular combination of WCs entering its computation. However, COHERENT provides as well the energy and time distributions of CEνNS events. We collected the NP effects to the number of events in five modified weak charges, for which the three different contributions related to the production mechanism of neutrinos (see Eqs (5.3.49), (5.3.50) and (5.3.51)) had different energy sensitivities parametrized by the $f(T)$ functions defined in the previous section. Hence, in principle the energy distribution of the events allows to break the existing degeneracy on the sensitivity to new physics when considering a single observable and constrain more directions in the parameter space, more concretely the 3 combinations provided by

$$\left\{ (Q_{LL}^{\nu_\mu})^2, (Q_{LR}^{\nu_e \bar{\nu}_\mu})^2, (Q_{RL}^{\nu_e \bar{\nu}_\mu})^2 \right\} \equiv \left\{ (Q_{LL}^{\nu_\mu})^2, (Q_{LL}^{\nu_e})^2 + (Q_{RR}^{\bar{\nu}_\mu})^2, (Q_{RR}^{\nu_e})^2 + (Q_{LL}^{\bar{\nu}_\mu})^2 \right\},$$
$$(5.4.68)$$

since $f_{LL}^{\nu_e}(T) = f_{RR}^{\bar{\nu}_\mu}(T)$ and $f_{RR}^{\nu_e}(T) = f_{LL}^{\bar{\nu}_\mu}(T)$. Nonetheless, it turns out that the $f(T)$ functions are not really much sensitive (i.e. do not vary much) for the energy range in the ROI of CEνNS and therefore, large correlations among the three Qs are found. For instance, using only the energy distribution of the second measurement on CsI we find the preliminary bounds

$$\begin{pmatrix} (Q_{LL}^\mu)^2/Q_{\text{SM}}^2 \\ (Q_{LR}^{\nu_e \bar{\nu}_\mu})^2/Q_{\text{SM}}^2 \\ (Q_{RL}^{\nu_e \bar{\nu}_\mu})^2/Q_{\text{SM}}^2 \end{pmatrix} = \begin{pmatrix} 3.3 \pm 2.1 \\ -2.5 \pm 5.7 \\ 2.5 \pm 3.2 \end{pmatrix} , \quad \rho = \begin{pmatrix} 1 & -0.91 & 0.88 \\ -0.91 & 1 & -0.99 \\ 0.88 & -0.99 & 1 \end{pmatrix} , \quad (5.4.69)$$

where we have normalized the results to the SM weak charge Q_{SM}^2. As can be seen from the correlation matrix ρ, from the energy distribution of CEνNS events

provided by COHERENT on $(CsI)_2$, we can just slightly disentangle the contributions from the three charges, i.e. all charges are strongly correlated with correlations greater than ~ 0.9. In turn this occurs because similar combinations of the three Qs enter each energy bin.

Luckily, the time distribution provided by the collaboration on prompt and delayed neutrino fluxes can help to break the above correlations. In particular, to help disentangle between the $(Q_{LL}^{\mu})^2$ contribution to prompt neutrinos and the other two combination of charges affecting the delayed neutrinos produced at the SNS. In order to exemplify this effect, let us consider now the time distribution of $(CsI)_1$ CEνNS events as well as both energy distributions for the CsI measurements. Such a configuration leads to the following preliminary results

$$
\begin{pmatrix} (Q_{LL}^{\mu})^2/Q_{SM}^2 \\ (Q_{LR}^{\nu_e\bar{\nu}_\mu})^2/Q_{SM}^2 \\ (Q_{RL}^{\nu_e\bar{\nu}_\mu})^2/Q_{SM}^2 \end{pmatrix} = \begin{pmatrix} 1.60 \pm 0.45 \\ 0.7 \pm 2.2 \\ 0.8 \pm 1.4 \end{pmatrix}, \quad \rho = \begin{pmatrix} 1 & -0.42 & 0.39 \\ -0.42 & 1 & -0.99 \\ 0.39 & -0.99 & 1 \end{pmatrix}, \quad (5.4.70)
$$

where we can explicitly see in the ρ matrix, that the correlations between $(Q_{LL}^{\mu})^2$ and the other two charges $(Q_{LR}^{\nu_e\bar{\nu}_\mu})^2$ and $(Q_{RL}^{\nu_e\bar{\nu}_\mu})^2$ have been substantially reduced.

The above constraints on the charges Q, subsequently translate into constraints on the LEFT Wilson coefficients presented in Section 2.6: the different $[\epsilon]_{\alpha\beta}$ (2.6.77) and $[\rho]_{\alpha\beta}$ (2.6.78) entering the neutrino production mechanisms and the $[g]_{\alpha\beta}$ (2.6.79) (or $[C]_{\alpha\beta}$ (2.6.84)) affecting the CEνNS detection. Regarding the constraints on the detection BSM parameters, we (preliminarily) recover the banana-shape allowed regions for the NP part of the $[g]_{\alpha\beta}$ parameters, as presented in Refs. [307, 309].

As a final remark, let us point out that CEνNS measurements in different nuclei are highly motivated since, due to the dependence on the number of neutrons N (and to a much lesser extent on Z) of the different modified weak charges, they allow in turn to constrain different directions in the parameter space of the LEFT and, after the appropriate matching, also of the SMEFT.

5.5   Conclusions and steps forward

The COHERENT experiment, beyond measuring for the first time in history the low-energy neutral-current coherent elastic neutrino-nucleus scattering [276], has also opened up a new way to look for physics beyond the SM in a neutrino experiment, with the particularity of being of a much smaller size as compared to its companions. The feasibility of the CEνNS measurement is important in several branches of high-energy physics as particle physics and astrophysics, and more concretely also for searches of dark matter as it entails nowadays an irreducible background for WIMP searches.

In this chapter we have provided the full EFT description of the COHERENT experiment. In this experimental setup, neutrinos are produced at the SNS and propagate to the detector where they interact with its atoms via CEνNS. Therefore, we should properly characterize within the low-energy EFT the three stages of the experiment: neutrino production, propagation (oscillation) and detection. We

achieve this by using the QFT formalism described in Ref. [273], which differs from the usual quantum mechanical formalism employed in neutrino oscillations.

Within this formalism we described the detection process, computed in a different way as it is usual in the literature. Since this is a low-energy process the relevant degrees of freedom are, apart from the low-energy neutrinos, the nucleons conforming the nucleus with which the former interact coherently. Hence, we considered it was more consistent to work with a Lagrangian describing the interactions of the relevant degrees of freedom at the energies at play. With such an approach we computed the detection piece (5.3.13) to which we later add the relevant form factors that were shown in the literature to have a non-negligible effect, in spite of the low energies involved in the process.

Then, we computed the three production pieces of the neutrinos produced at the SNS and, together with the detection piece above, provided the expected number of events at COHERENT via Eqs. (5.1.3) and (5.1.1) in Section 5.3.3. There, one of the main results of this work is presented, namely the difference between our formalism and a naive calculation of the number of events via the (usual) factorization of the flux and the cross section. We show that the difference between the two approaches appears at the quadratic order in the Wilson coefficients if flavor off-diagonal NP interactions are allowed, when both production and detection are simultaneously considered. Despite the realization above, the NP contamination of the decay widths of the source particles (pions and muons) and $\hat{G}_F$ appearing at detection, introduces within the LEFT framework an extra combination of NP production parameters (see discussion in Section 5.3.3). However, even though as a consequence of this effect some partial cancellations occur, the COHERENT experiment is still sensitive to new-physics in production.

Finally, we provide the relevant steps and considerations to translate from our theoretical expression for the (differential) number of events, to the actual quantities measured at COHERENT: the energy distributions of the events in terms of photoelectrons (or electron-equivalent recoil energy) and their time distributions. We have summarized the relevant backgrounds suffered by a CEνNS measurement at this facility, and we have sketched some results to expect when the actual work is completed. For instance, the importance of considering both energy and time distributions to break blind directions in the parameter space of the LEFT.

A natural continuation of the work described in this chapter that we are planning to implement as well, is to translate the constraints set on the LEFT WCs into constraints onto its higher-energy version, the SMEFT. Then, we plan to include those in the global fit of low-energy observables performed in Ref. [348] to study the effects of COHERENT data. Even though current experimental data on CEνNS cannot compete with other precision probes, we expect it may potentially help to break some blind directions.

Chapter 6

Quasi-Dirac neutrinos in the linear seesaw model and its phenomenology

Neutrinos are unique in the Standard Model (see Chapter 1). They are the only fermion fields not carrying electric charge and thus do not experience electromagnetic interactions. They are blind as well to the strong force and consequently, only interact via the weak interactions. This is the reason why, experimentally, they have been historically more difficult to detect. In the SM, they come in three flavors, each associated to a generation of their charged partners (see discussion in Chapter 3): $(\nu_e, \nu_\mu, \nu_\tau)$. Since they are electrically neutral, a right-handed Dirac neutrino transforms as a total singlet under the SM gauge group (1,1,0) and it is thus not included. Accordingly, the absence of one of the chiralities precludes the Higgs mechanism in the neutrino sector. Therefore, neutrinos are massless in the Standard Model.

However, neutrino oscillation experiments have found overwhelming evidence for the existence of non vanishing — albeit small — neutrino masses [349–351], thus entailing one of the most compelling evidence of Physics Beyond the Standard Model. Despite the accuracy of the experiments, fundamental theoretical questions still remain, for instance the specific mechanism providing their masses or the related question regarding the Dirac vs. Majorana nature of the neutrinos, among others. Therefore, the SM has to be extended to address these unknowns. We have seen in Chapter 2 that there are two ways to extend the SM: one either chooses a particular BSM model solving those questions, and works with it, or treat the SM as an EFT to approach those questions from a model-independent perspective. Within the neutrino scheme, one can do even better and merge both approaches.

Following the second path, it is notorious that the first (and dominant) extension of the SM contains only one $d = 5$ local operator, which violates lepton number by two units and provide mass to the SM (Majorana) neutrinos after spontaneous symmetry breaking takes place. As we will see below, the structure of this operator may be used to work out all possible simplest BSM realizations. This procedure leads to the celebrated seesaw models [352–355], which has become the most widely accepted mechanism to generate small neutrino masses. Some of these seesaw mechanisms involve extra heavy neutral fermions, denoted here as N_i ($i = 1, 2, \ldots, n$, depending on the model). In most of these scenarios, the heavy neutrinos are Majorana fermions. However, there are seesaw scenarios where pairs of these Majorana neutrinos approach smoothly their mass degeneracy limit, $\Delta M_N \to 0$. In the exact

degeneracy limit ($\Delta M_N = 0$) these neutrinos become Dirac fermions and the lepton number violating (LNV) processes they induce cancel exactly. Instead, in the approximate degeneracy case, when ΔM_N is small but still finite (comparable to Γ_N), the LNV processes they induce cancel only partially. These almost degenerate Majorana neutrinos are usually called *Quasi-Dirac* neutrinos. These could appear at scales not far below the electroweak scale in some extensions, such as in the inverse seesaw [356–363] and in the linear seesaw [364–366]. In this chapter based on the work of Ref. [367], we will work within the framework of the minimal linear seesaw model, which naturally yields pairs of Quasi-Dirac right-handed neutrinos N and N' in a regime of masses below M_W.

While lepton number conserving (LNC) processes are mediated by either Dirac or Majorana neutrinos, lepton number violating processes are induced by Majorana neutrinos only. This feature is used in experimental searches to discriminate the nature of the hypothetical heavy neutrinos. At hadron colliders, a clear signal of Majorana neutrinos would come from the same-sign (SS) dileptons produced via LNV processes $pp \to W \to \ell^\pm N \to \ell^\pm \ell^\pm jj$. These modes involve two jets and no missing transverse energy. Similar events with opposite-sign (OS) lepton pairs could also be produced through $pp \to W \to \ell^\pm N \to \ell^\mp \ell^\pm jj$ [368]; however, these are LNC processes, and so can be mediated by both Dirac and Majorana neutrinos. Searches of these $\ell\ell jj$ events, for heavy neutrinos with mass above M_W, have been done at ATLAS and CMS [369–371].

For masses below M_W, the jets may not be energetic enough to be separated from the background, so searches of trileptons events $\ell^\pm \ell^\pm \ell'^\mp \nu$ could provide a more favorable signal [372–377]. However, here the lepton charges cannot tell us about the Dirac or Majorana nature of the intermediate neutrinos. Several ways to distinguish between Dirac or Majorana neutrinos using these pure leptonic modes at the LHC have been proposed [378–381]. An alternative for distinguishing Dirac from Majorana neutrinos at the LHC, with masses in the range 5 GeV $< M_N <$ 20 GeV, have also been proposed [382, 383], now using the exclusive semileptonic processes $W \to \ell(N \to \ell\pi, \ell2\pi, \ell3\pi)$, which again have no missing energy. Other ways to resolve the nature of neutrinos are given in Refs. [384–386].

Going back to the $\ell\ell jj$ modes, the ratio of SS to OS events, which we call $R_{\ell\ell}$, will indicate the Majorana/Dirac nature of the intermediate neutrinos that induce these events [387]. As mentioned above, Majorana neutrinos induce SS and OS in equal amount, thus $R_{\ell\ell} = 1$ in that case. In contrast, Dirac neutrinos only induce OS events, thus $R_{\ell\ell} = 0$.

A measurement of $R_{\ell\ell}$ different from zero or unity provides then valuable information about the Dirac/Majorana character of the heavy neutrinos, and thus about the mechanism underlying the neutrino mass generation. Indeed, in an inverse seesaw scenario with Quasi-Dirac neutrinos [362, 388], it was pointed out that dilepton states will exhibit $R_{\ell\ell} \neq 0, 1$, where the precise value $0 < R_{\ell\ell} < 1$ is controlled by the heavy neutrino mass splitting and the neutrino decay width. In Ref. [363], it is also pointed out that values $0 < R_{\ell\ell} < 1$ are possible as long as there exists a CP violating phase.

Similar to the inverse seesaw scenario, in the linear seesaw another softly-breaking lepton-number mass parameter, denoted here as M_ϵ, also allows to naturally fit small

masses for the light neutrinos, without requiring GUT scale masses for the heavy states. However, in the linear seesaw the mass splitting of the heavy states equals m_ν (the light neutrino mass), unlike the inverse seesaw where the splitting is given by a softly-breaking lepton number parameter μ_R. This feature will imply a different mass range for the Quasi-Dirac regime: in the linear seesaw scenario, which we study here for a mass range of the heavy neutrinos $M_N \in [10^{-1}, 10^3]$ GeV, $R_{\ell\ell}$ takes values different from 0 or 1 at lower M_N, including a few GeV. Therefore, sterile neutrino searches at current and near-future experiments such as SHiP, ANUBIS, MATUSHLA and DUNE [389–391], set interesting constraints on the parameter space of the linear seesaw scenario. It is worth to highlight that a measurement of $R_{\ell\ell}$ requires both leptons to be detected and their charge to be identified. Such low mass experiments can not detect these signals. However, ATLAS and CMS can probe this scenario by displaced vertex searches, covering neutral lepton masses roughly within 10-30 GeV [392–395]. Some experimental prospects for testing Quasi-Dirac neutrinos in the linear seesaw model, coming from displaced vertex searches, are also briefly discussed in this chapter.

It is important to note that, since values of $M_N \lesssim 2.5$ GeV enter our analysis, an appropriate treatment of non-perturbative QCD has to be considered for the heavy neutrino decay calculations. In this work we use the formulation of the *Resonance Chiral Theory* [41–43] presented in detail in Chapter 2. Also, a special and convenient parametrization of seesaw scenarios, described in [396], is used here in order to fit the light-neutrino data and also to properly relate input parameters with Quasi-Dirac and experimental constraints.

The chapter is organized as follows. In Section 6.1 we present the EFT extension of the SM via the $d = 5$ Weinberg operator and use it to obtain the simplest seesaw scenarios. Then, in Section 6.2, we recall the main features of the linear seesaw and discuss some relations on the neutrino masses appearing in linear seesaw scenarios. In Section 6.3, we show the $R_{\ell\ell}$ definition in the limit where the decay widths of both Quasi-Dirac neutrinos are of the same order. A detailed description of the total decay width of the heavy neutrino, including the hadronic decays calculated in the non-perturbative QCD regime $M_N \lesssim 2.5$ GeV, is given in Section 6.4. In Section 6.5.1, we describe the Yukawa parametrization based on two simple and convenient ansatzes for the input matrices. The relevant results concerning the constraints on the parameter space coming from the Quasi-Dirac condition $0 < R_{\ell\ell} < 1$ are presented in Section 6.5.2. Restrictions on the M_N values, coming from the low-mass experimental bounds and also from the sensitivity of the displaced vertex searching at the LHC, are depicted in Section 6.5.3. We close with a short summary and conclusions in Section 6.6.

6.1 Mass-generating neutrino extensions

Once the Standard Model is assumed to be just the effective low-energy realization of a more complete higher-energy theory, an infinite tower of operators in increasing dimension should be considered together with the $d = 4$ SM Lagrangian (see Eq. (2.5.63)). As explained in Chapter 2, the first terms of this expansion dominate

at low energies. Besides, it turns out that the very first term, the only $d = 5$ operator, is capable of inducing neutrino masses. Let us recall this operator, given as well in Eq. (2.5.64),

$$\frac{C_{\nu\nu}^{pr}}{\Lambda} \mathcal{O}_{\nu\nu}^{pr} = \frac{C_{\nu\nu}^{pr}}{\Lambda} \left(\tilde{\varphi}^\dagger L_p \right)^T C \left(\tilde{\varphi}^\dagger L_r \right) + \text{h.c.} \tag{6.1.1}$$

After the SSB takes place and the Higgs field, above denoted as φ, acquires a vev $\varphi_0 = v$, the operator in Eq. (6.1.1) gives rise to Majorana masses

$$m_\nu \sim \frac{C_{\nu\nu} v^2}{\Lambda} \,. \tag{6.1.2}$$

Note that the neutrino masses are of $\mathcal{O}(v^2/\Lambda)$, in contrast to the usual $\mathcal{O}(v)$ characteristic of fermion masses provided by the Higgs mechanism.

One of the premises of the EFT formalism, is the existence of a sufficiently large energy gap between the long- and short-distance theories. The Weinberg operator $\mathcal{O}_{\nu\nu}^{pr}$ violates lepton number by two units, i.e. $\Delta L = 2$; however, all experimental observations point to the conservation of lepton number up to a very good precision. Accordingly, the parameter Λ should be very large[1], since it parametrizes the scale of the high-energy theory. This means that for $C_{\nu\nu} \sim 1$, the ratio $v^2/\Lambda \ll v$, what entails small neutrino masses as it is observed. For instance, one can do the inverse exercise and, by inserting a neutrino mass $m_\nu \sim 5 \times 10^{-2}$, a $\Lambda \sim 10^{15}$GeV is recovered. The simple expression of Eq. (6.1.2) thus points to the origin of neutrino masses residing at the GUT scale. However, the previous discussion is only valid when the Weinberg operator in Eq. (6.1.1) is realized in the BSM theory via tree level exchange of the heavy degrees of freedom. Therefore, in full generality, we do not know the mechanism producing this EFT operator, the flavor structure of $C_{\nu\nu}$ or the mass scale Λ. There are many SM extensions providing mass to the light neutrinos via radiative mechanisms, so that the suppression does not come from a very high-energy scale but from the loops themselves (for a review on radiative models see Ref. [397]), or by adding extra heavy-neutral leptons, not necessarily much heavier than the electroweak scale, e.g. the inverse and linear seesaw models.

From a simplicity perspective, the $d = 5$ Weinberg operator realized in the higher-energy theory via tree-level exchanges, corresponds to the minimal extension and thus is one of the most appealing scenarios. Furthermore, it turns out that there are only three minimal realizations of this effective operator if we assume only tree-level exchanges. These are the well-known Type-I,-II and -III seesaws. In group theoretical terms, the Weinberg operator is made out of four doublets under $\mathrm{SU}(2)_\mathrm{L}$, two L and two φ. This structure is obtained upon the integration of some heavy degrees of freedom. Therefore, we should study all possible combinations to build gauge $\mathrm{SU}(2)_\mathrm{L}$ invariant terms out of L, φ and the heavy degrees of freedom. Since L and φ are both doublets, the possible combinations are either triplets or singlets of $\mathrm{SU}(2)_\mathrm{L}$: $\mathbf{2} \otimes \mathbf{2} \equiv \mathbf{3} \oplus \mathbf{1}$. The resulting combinations sum up to four [398]:

(i) L and φ are contracted into a singlet. A right-handed singlet $(1, 1, 0)$ fermion N is then needed to build an invariant term. This is the Type-I seesaw.

---

[1]It is also possible that the coupling constants of the high-energy theory embedded into the Wilson coefficient $C_{\nu\nu}$ are small enough to provide the needed suppression.

(ii) The contraction occurs between the two lepton doublets and the two Higgs doublets separately, into a triplet. A triplet scalar $(1, 3, 1)$ multiplet, usually denoted as Δ, is then needed. This configuration receives the name of Type-II seesaw.

(iii) L and φ are contracted into a triplet. Then, a right-handed fermionic triplet $(1, 3, 0)$ is introduced to make invariant terms. This constitutes the Type-III seesaw.

(iv) The last possible configuration comes from the contraction between both the two lepton fields and separately the two Higgs fields into singlets. A scalar singlet field is then needed to build $\text{SU}(2)_\text{L}$ invariant terms. This last combination provides terms of the form $\bar{\nu}_L^\text{C} e_L$, which cannot generate neutrino masses.

The procedure described above to match the EFT and short-distance physics, is usually called as "opening up the operator" and can be generalized to include more than just the tree-level realizations of the Weinberg operator (see Ref. [397] for a detailed review on this procedure).

6.2 The linear seesaw model

In this section we discuss the main aspects of the linear seesaw mechanism (LSM). Up to the SM, the minimal version of the LSM contains two different types of neutral $\text{SU}(2)$ singlet fermions (N, S) per generation. In addition to the kinetic sector, the Lagrangian contains the following terms:

$$\mathcal{L}_Y = Y_D \overline{L} H^\text{C} N + Y_\epsilon \overline{L} H^\text{C} S + M_R \overline{N^\text{C}} S + \text{h.c.}, \tag{6.2.3}$$

where L is the SM left-handed lepton doublet (see Eq. (1.1.5)).

We have omitted flavor indices to simplify the notation. In three generations, Y_D and Y_ϵ are 3×3 Yukawa matrices, with $Y_D \neq Y_\epsilon$, and M_R is a 3×3 complex matrix. In SM-seesaw extensions one can always perform a change of basis, in this case on N and S, such that M_R becomes diagonal. Here we take $M_R = \text{diag}(M_{R_1}, M_{R_2}, M_{R_3})$.

Considering the basis in Eq. (6.2.3), namely (ν_L^c, N, S), the texture of the neutrino mass (9×9) matrix, given in a 3×3 block notation, reads:

$$M_\nu = \begin{pmatrix} 0 & m_D & M_\epsilon \\ m_D^T & 0 & M_R \\ M_\epsilon^T & M_R^T & 0 \end{pmatrix}, \tag{6.2.4}$$

where $m_D = v Y_D / \sqrt{2}$ and $M_\epsilon = v Y_\epsilon / \sqrt{2}$. Bringing this 3×3 matrix into a block-diagonal form — through a diagonalization-like procedure considering $M_\epsilon \ll m_D < M_R$ — the non-diagonal mass matrix of the light neutrinos is given by

$$m_\nu = m_D M_R^{-1} M_\epsilon^T + M_\epsilon M_R^{T-1} m_D^T = \frac{v^2}{2} (Y_D M_R^{-1} Y_\epsilon^T + Y_\epsilon M_R^{T-1} Y_D^T). \tag{6.2.5}$$

The analogous expressions for the two 3×3 mass matrices of the heavy neutrinos are

$$M_{N_a, N_b} \simeq \frac{M_R}{2} + \frac{m_D^2 M_R^{-1}}{4} \mp \frac{m_D M_R^{-1} M_\epsilon^T}{2} + \text{h.c.} \qquad (6.2.6)$$

From Eq. (6.2.5), the effective ν mass is roughly directly proportional to m_D, also proportional to M_ϵ, and inversely proportional to M_R. The smallness of the lepton-number violating term M_ϵ, together with the linearity on m_D, gives this model the name *low-scale linear seesaw*, and generates small m_ν masses for the light neutrinos, without requiring M_R to be extremely large, beyond the reach of any foreseeable experiment. This is why we can deal with heavy neutrinos states in the region of masses of the few GeV's. Note that although N_a and N_b are not in general the heavy-neutrino mass eigenstates, which are really obtained from the diagonalization of the full 9×9 matrix in Eq. (6.2.4), due to the large mass gap between the light and heavy neutrinos one can identify Eq. (6.2.6) as the actual heavy-neutrino mass matrix in the region of interest of the parameter space of the model.

The Lagrangian, extended with the heavy neutral leptons of Eq. (6.2.3), turns the SM-flavor neutrinos (i.e. those that couple in the charged lepton currents) into a mixture of the light and heavy mass eigenstates. For a given flavor ℓ,

$$\nu_\ell = \sum_{k=1}^{3} U_{\ell \nu_k} \nu_k + \sum_{k=1}^{3} U_{\ell N_k} N_k + \sum_{k=1}^{3} U_{\ell N'_k} N'_k, \qquad (6.2.7)$$

where ν_k are the three light neutrino mass eigenstates, $U_{\ell \nu_k}$ is the Pontecorvo-Maki-Nakagawa-Sakata matrix and N and N' stand now for the two heavy-neutrino mass eigenstates for each generation (with $k = 1, 2, 3$ denoting the generation). Note that the PMNS matrix is not unitary anymore: unitarity is only preserved for the more general 9×9 mixing matrix U. However, current data excludes large departures from unitarity of the PMNS matrix, which entails small mixings among active and heavy neutrinos, $U_{\ell N}$.

An important feature of the LSM is that the mass splitting between the two heavy neutrinos within each generation is very small:

$$\Delta M_i \sim m_{\nu_i}, \qquad (6.2.8)$$

as it can be easily seen from (6.2.5) and (6.2.6). This is crucial in order to study the Quasi-Dirac behaviour of pairs of heavy neutrinos in the linear seesaw model, as it is thoroughly described in the next section.

6.3   Quasi-Dirac Neutrinos

The usual Dirac-Majorana dichotomy regarding the nature of neutrinos is somehow misleading, since the Dirac case can be considered as a limiting case of a more general Majorana scenario with twice the neutrino content. Indeed, a single Dirac neutrino corresponds to a pair of Majorana neutrinos exactly degenerate in mass, so from a scenario of $2n$ Majorana neutrinos one reaches a scenario of n Dirac neutrinos if the Majorana masses become degenerate in pairs. At that point, all sources of lepton number violation in the model vanish. Now, when this Dirac limit is reached in a

continuous way — by gradually switching off the LNV mass terms — one crosses an interesting, albeit narrow regime, usually called *Quasi-Dirac*.

An observable that is commonly used at the LHC to look for Majorana neutrinos is the same-sign to opposite-sign dilepton ratio in $\ell\ell jj$ events with no missing p_T, which we have called $R_{\ell\ell}$. The production of these events with a pair of leptons of the same sign, are expected to occur only through lepton number violating processes mediated by Majorana neutrinos, namely $\overline{q}q \to W^{\pm} \to \ell_{\alpha}^{\pm} N^{(\prime)} \to \ell_{\alpha}^{\pm} l_{\beta}^{\pm} W^{\prime\mp}$, where $\overline{q}$ and q denote the partons inside the colliding protons, while $N^{(\prime)}$ denotes the two heavy-neutrino mass eigenstates [2]. On the other hand, opposite-sign pairs of leptons are produced via lepton number conserving processes mediated by both Dirac and Majorana neutrinos, as $\overline{q}q \to W^{\pm} \to \ell_{\alpha}^{\pm} N^{(\prime)} \to \ell_{\alpha}^{\pm} \ell_{\beta}^{\mp} W^{\prime\pm}$. The virtual W' gauge boson then turns either into $q\overline{q}'$ producing the final state $\ell\ell jj$ or into $\ell\nu$ producing a trilepton plus missing energy. For $M_N \gtrsim 5$ GeV only around the 40% of the total number of events are into $\ell\ell jj$, which are those used for measuring the SS to OS dilepton ratio $R_{\ell\ell}$.

It is important to highlight the fact that prompt searches of such charged leptonic signals are background dominated, while the displaced vertex (DV) events are background free. Therefore, a more favorable measurement of $R_{\ell\ell}$ through $\ell\ell jj$ signals involves the detection of "displaced dileptons" plus jets. The region of parameters sensitive to such DV searches is described in the next sections.

The ratio of SS over OS events between times t_a and t_b, after heavy-neutrino production, is given by the ratio of the time-integrated amplitudes squared as [362, 363, 399]:

$$R(t_a, t_b) = \frac{\int_{t_a}^{t_b} |g_-(t)|^2 dt}{\int_{t_a}^{t_b} |g_+(t)|^2 dt}, \qquad (6.3.9)$$

where $g_-(t) \sim -ie^{-iMt}e^{-\frac{\Gamma}{2}t}\sin(\frac{\Delta M}{2}t)$ and $g_+(t) \sim -ie^{-iMt}e^{-\frac{\Gamma}{2}t}\cos(\frac{\Delta M}{2}t)$ are the oscillating amplitudes, with $M = \frac{1}{2}(M_N + M_{N'})$ and $\Delta M = M_N - M_{N'}$, and Γ is the total decay width of both heavy neutrino states ($\Gamma = \Gamma_N \sim \Gamma_{N'}$).

Oscillations between two quantum mechanical states can occur whenever these states can be distinguished by some quantum number (which is not conserved, hence the oscillation); however, their mass eigenstates are admixtures of them. In the present case the mass eigenstates N and N' are admixtures of N and S, which can be assigned opposite lepton number. Then $|g_-(t)|^2$ describes the probability of a lepton number conversion in the time interval $\Delta t \equiv t - 0$, while $|g_+(t)|^2$ denotes the probability that lepton number is not converted in that time interval. Sometimes this oscillation is described as between neutrino and antineutrino, however this denomination may lead to confusion, since a Majorana neutrino is its own antiparticle; the essential point is that there are two (or more) neutrinos with different mass and that there is a non-conserved quantum number that characterizes the states that oscillate, which are different than the mass states.

The approximations used for the probabilities are only valid in the limit where the decay widths of both Quasi-Dirac neutrinos are approximately equal, i.e. $\Delta\Gamma =$

---

[2]The ℓ-flavor N_ℓ heavy state and its conjugate ($N_{\overline{\ell}}$) produced in the decays $W^+ \to \overline{\ell} N_\ell$, ($W^- \to \ell N_{\overline{\ell}}$) can be written in terms of the QD mass eigenstates as: $N_\ell = (N - iN')/\sqrt{2}$, $N_{\overline{\ell}} = (N + iN')/\sqrt{2}$.
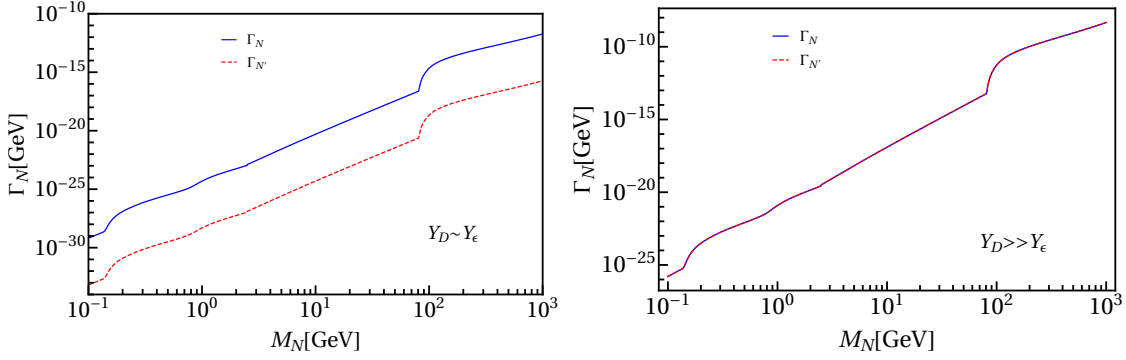
FIGURE 6.1: $\Gamma_{N^{(\prime)}}$ vs $M_{N^{(\prime)}}$. Left and right panels correspond to the cases where $Y_\epsilon \sim Y_D$ and $Y_\epsilon \ll Y_D$ respectively. Both are shown within *Scenario b* for $g = 1$ (left) and $g = 10^2$ (right), see Section 6.5 for more details.

$\Gamma_N - \Gamma_{N'} \to 0$ [399]. In terms of the Yukawa couplings of our model, $\Gamma_N \sim \Gamma_{N'}$ as long as $Y_\epsilon \ll Y_D$. In an attempt to scrutinize this aspect, we show in Fig. 6.1 the $\Gamma_{N^{(\prime)}}$ decay widths versus $M_{N^{(\prime)}}$ for the case where $Y_\epsilon = Y_D$ (left panel) and $Y_\epsilon = 10^{-4}Y_D$ (right panel). It is clearly appreciated that the larger the hierarchy among the Yukawas, the more accurate is the relation $\Gamma_N \sim \Gamma_{N'}$ and then, the better the approximations of the probabilities $g_\pm(t)$ used here. In the next sections, we highlight the impact of the hierarchy of the Yukawa couplings in our numerical results.

For our analysis, we consider the ratio $R_{\ell\ell} \equiv R(0, \infty)$, which can be expressed as:

$$R_{\ell\ell} = \frac{\Delta M^2}{2\Gamma^2 + \Delta M^2} . \tag{6.3.10}$$

Note that $R_{\ell\ell} \to 1$ if $\Gamma \ll \Delta M$, while $R_{\ell\ell} \to 0$ if $\Delta M \ll \Gamma$. These two scenarios correspond to the limiting Majorana and Dirac cases, respectively. In models with Quasi-Dirac neutrinos, the ratio $R_{\ell\ell}$ can take any value between 0 and 1; as we approach $R_{\ell\ell} \to 0$, the LNV effects are more and more suppressed. From Eq. (6.3.10), the QD condition $R_{\ell\ell} \neq 0, 1$ is ensured as long as $\Gamma(N) \sim \Delta M$. Using the estimate for the mass splitting from Eq. (6.2.8), it follows that

$$\Gamma(N) \sim m_\nu . \tag{6.3.11}$$

Therefore, the window of $R_{\ell\ell}$ values compatible with QD neutrinos is determined, in the linear seesaw model, by the light-neutrino masses and the heavy-neutrino decay width. In the next sections, we present first the decay modes of the heavy neutrinos, focusing on the hadronization of the final-state quark currents within the non-perturbative QCD regime below $E \sim 2.5$ GeV, and second, we explore in detail the parameter space provided by the above conditions and its phenomenological implications.

6.4 Heavy-neutrino decay rates

In order to characterize the Quasi-Dirac regime in the linear seesaw model, one needs to compute the total decay width of the heavy neutrino, Γ, that appears in Eq. (6.3.10). The mixture of the SM-flavor neutrinos in Eq. (6.2.7) provides the interactions of the –otherwise sterile– heavy neutrinos with the SM fields, i.e.

$$\mathcal{L}_{\text{int}} = \frac{g}{2\sqrt{2}} W_\mu^\dagger \bar{N}^{\text{C}} \sum_\alpha U_\alpha^* \gamma^\mu (1 - \gamma_5) \ell_\alpha^- + \frac{g}{4\cos\theta_{\text{W}}} Z_\mu \bar{N}^{\text{C}} \sum_\alpha U_\alpha^* \gamma^\mu (1 - \gamma_5) \nu_\alpha + \text{h.c.}.$$

$$(6.4.12)$$

Hence, all the decays of the heavy neutrinos proceed via charged and neutral-current interactions. We will follow the usual considerations and assume that the three families of the heavy neutrinos are not degenerate in mass, so that each leaves a different footprint in the experiment. We will assume only one pair of heavy neutrinos to be relatively light, while the other two pairs to be much heavier, namely $M_{N_1^{(\prime)}} \ll M_{N_2^{(\prime)}} \lesssim M_{N_3^{(\prime)}}$. Thus, we will focus on the lightest heavy neutrino pair, which for some mass range can be within the expected sensitivities of several experiments, compute their decay width and set constraints on the parameter space.

We are interested in the regime where $\Gamma_{N_1} \sim \Gamma_{N_1'}$, so we just need to calculate one of these decay widths for the $R_{\ell\ell}$ ratio of Eq. (6.3.10). The width necessarily depends on the HNL mass, since larger masses open more decay modes. We will separate these modes into four categories based on the nature of the final states [400–403]:

Leptonic decays	Semileptonic decays	Decays into gauge bosons	Decay into the Higgs boson
• $N \to \ell^- \ell'^+ \nu_{\ell'}$	• $N \to \ell^- u\bar{d}$	• $N \to \ell^- W_L^+$	• $N \to \nu_\ell H$
• $N \to \nu_\ell \ell'^- \ell'^+$	• $N \to \nu_\ell q\bar{q}$	• $N \to \ell^- W_T^+$	
• $N \to \nu_\ell \nu\nu$		• $N \to \nu_\ell Z_L$	
		• $N \to \nu_\ell Z_T$	

Here, L and T denote the longitudinal and transverse polarizations of the gauge bosons. The u and d stand for the up and down-type quarks respectively, while q includes all the quark types that are kinematically accessible in the decays[3]. The first three columns come from the interaction Lagrangian of Eq. (6.4.12), either from charged-current or neutral-current interactions, whereas the Higgs decay is directly driven by the Yukawa Lagrangian in Eq. (6.2.3). Note that for Majorana neutrinos, one should also consider the charge conjugate mode of the charged-current interacting processes, thus summing twice to the total widths.

The treatment of the decay modes of the heavy neutrino into quarks entails an inherent difficulty due to the non-perturbativity of QCD for $M_{N_1} \lesssim 2.5$ GeV. While perturbation theory works properly for larger masses of the heavy neutrino and, consequently, the usual computation of partial decays into quarks is appropriate to consider in the inclusive decays, in the non-perturbative regime below $E \sim 2.5$ GeV we are forced to consider the hadronization of the final quark currents into exclusive hadrons, which are the relevant degrees of freedom at those energies. For this purpose, a model-independent scheme is provided by Chiral Perturbation Theory.

---

[3]The contributions from the different channels into top quarks are not considered here, since they are negligible as compared to the decay into bosons.

This allows us to handle the hadronization procedure of quark currents into mesons. However, this framework alone is not enough to describe the whole non-perturbative energy regime, since it gives reliable results only for $E \ll 1$ GeV. The intermediate region is populated by hadron resonances, and therefore, a complementary scenario that encompasses these resonances as well as all the features of χPT, is given by the Resonance Chiral Theory. Both frameworks are explained in detail in Chapter 2.

Accordingly, we will consider the hadronization of the quark bilinears into one pseudoscalar (P), two pseudoscalars (PP) or a vectorial resonance (V) — considering all possible intermediate states provided by RχT — with only light-quark content, i.e. u, d and s. The list of final states, as resulting either from a neutral- or charged-current interaction, are shown in Table 6.1. A last remark before presenting the results is in order: due to the fast decay of hadron resonances, these are not proper asymptotic states, as it is required in quantum field theory, and consequently, the decay width of the heavy neutrino into a vectorial resonance as an external state is not well defined. In order to compute these decays we use the method employed in Appendix G in the context of tau decays (see as well Refs. [74, 161, 404]), based on the decay of these resonances into two pseudoscalars (see the parentheses in the third column of Table 6.1), i.e.

$$\mathcal{B}(N \to \ell(\nu)V) = \sum_{P_1 P_2} \mathcal{B}(N \to \ell(\nu)P_1 P_2)\Big|_V . \tag{6.4.13}$$

This treatment applies to the resonances that decay mainly into two pseudoscalars and whose decay width is large as compared to their mass. The $\omega(782)$ is not of this kind: it is a narrow resonance, and is thus treated as a well-behaved external state.

For the hadronization of the neutral quark currents, we take the results directly from Eq. (3.3.6). However, in that work the hadronization of the charged quark currents was not performed, hence we provide it here. Since the HNL decays into quarks via SM-like interactions (see Eq. (6.4.12)), we are left with the hadronization of the following charged quark bilinears:

$$
\begin{aligned}
\left[\, \overline{q}_i \, \gamma_\mu \, \gamma_5 \, q_j \to P \,\right] &\simeq -i \, 2 \, F \, \Omega^{(1)}_{A-C}(ij) \, p_\mu \,, \\
\left[\, \overline{q}_i \, \gamma_\mu \, q_j \to P_1 \, P_2 \,\right] &\simeq \left[\, 2\,\Omega^{(2)}_{V-C}(ij) + \sqrt{2}\,\frac{F_V \, G_V}{F^2} \sum_V \frac{s}{M_V^2 - s}\,\Omega^{(1)}_{V-C}(ij)\,\Omega^{(3)}_{V-C} \,\right] (p_1 - p_2)_\mu \\
&\quad + \left[\, \sqrt{2}\,\frac{F_V \, G_V}{F^2}\,(m_2^2 - m_1^2) \sum_V \frac{\Omega^{(1)}_{V-C}(ij)\,\Omega^{(3)}_{V-C}}{M_V^2 - s} \,\right] (p_1 + p_2)_\mu \,.
\end{aligned}
\tag{6.4.14}
$$

Here, the Ω coefficients are just numerical factors, which depend on the process considered; these are given in Appendix E.2. The information from QCD lies within the F, F_V and G_V factors. Note finally that, due to the larger uncertainties coming from other sources in this work, possible improvements in the hadronization resulting from the use of dispersive methods are not relevant and then, are not considered here.

	PP		P		V
Neutral-current interactions ($N \to \nu$ hadron(s))	$\pi^+\pi^-$		π^0	η	$\rho^0\,(\pi^+\pi^-)$
	$K^0\overline{K}^0$		K^0		$\phi\,(K^0\overline{K}^0 + K^+K^-)$
	K^+K^-		$\overline{K}^0$	η'	ω
Charged-current interactions ($N \to \ell^\pm$ hadron(s))	$\pi^-\pi^0$	$\overline{K}^0\pi^-$	π^-		$\rho^-\,(\pi^-\pi^0)$
	K^0K^-	$K^-\eta$	K^-		$K^{*-}\,(K^-\pi^0 + \overline{K}^0\pi^-)$
	$K^-\pi^0$	$K^-\eta'$			
	$\pi^0\pi^+$	π^+K^0	π^+		$\rho^+\,(\pi^0\pi^+)$
	$K^+\overline{K}^0$	ηK^+			
	π^0K^+	$\eta'K^+$	K^+		$K^{*+}\,(\pi^0K^+ + \pi^+K^0)$

TABLE 6.1: Final states considered in this work for the hadronic decays of the heavy neutrino in the regime $M_{N_1} \lesssim 2.5$ GeV. For the vectorial resonances, as explained in the main text, we show (when needed) the dominant decay channels used to calculate their widths.

6.5 Analysis and results

Current knowledge of the neutrino sector allows to probe models that address the origin of neutrino masses and related features of this sector. This is generically achieved by translating the information provided by the current neutrino experimental data into constraints on the parameters of the model under study. In this work we intend to cover in the most general way the parameter space of the linear seesaw, focusing on the regions where current and near-future experiments aim to explore.

6.5.1 Master parametrization

For the purpose stated above, we take the master parametrization described in Refs. [396, 405], which allows to fit any Majorana neutrino mass model and automatically reproduce current experimental data.

The departure point is the fact that any Majorana neutrino mass model leads for the light neutrino masses, to the general expression

$$m_\nu = f \cdot \left(Y_1^T M Y_2 + Y_2^T M^T Y_1\right), \qquad (6.5.15)$$

where m_ν is in general the complex symmetric light-neutrino mass matrix (to be compared with Eq. (6.2.5) for the linear seesaw model). For the case of three generations of light neutrinos, m_ν is a 3×3 matrix. We can bring it to a diagonal form via

$$\hat{m}_\nu = \text{diag}(m_1, m_2, m_3) = U_{\ell\nu}^T m_\nu U_{\ell\nu}, \qquad (6.5.16)$$

where $U_{\ell\nu}$ is the 3×3 neutrino PMNS mixing matrix. As explained in Section 6.2, in extended scenarios as the linear seesaw, this matrix is not unitary anymore but the whole (9×9 in the case at hand) mixing matrix of the model preserves the unitarity.

The Eq. (6.5.15) is usually called the master formula and, considered as an input from experimental data, we can use it to fit the parameters of the model via a general parametrizaton of the Yukawas, the so–called master parametrization. For the case of the linear seesaw, the Yukawa couplings of Eq. (6.2.5) are parametrized as:

$$
\begin{aligned}
Y_D^T &= \left(\frac{M_R}{v}\right)^{1/2} W T \left(\frac{\hat{m}_\nu}{v}\right)^{1/2} U_{\ell\nu}^\dagger, \\
Y_\epsilon^T &= \left(\frac{M_R}{v}\right)^{1/2} W^* B \left(\frac{\hat{m}_\nu}{v}\right)^{1/2} U_{\ell\nu}^\dagger,
\end{aligned}
\qquad (6.5.17)
$$

where v is the Higgs vacuum expectation value, $B = (T^T)^{-1}(I - K)$, with I the identity matrix, and

$$\hat{m}_\nu = \text{diag}(m_{\nu_1}, \sqrt{\Delta m_{\text{sol}}^2 + m_{\nu_1}^2}, \sqrt{\Delta m_{\text{atm}}^2 + m_{\nu_1}^2}).$$

The master parametrization calculates the two Yukawa matrices as functions of the input parameters m_{ν_1}, $U_{\ell\nu}$ and M_R and three arbitrary matrices W, T and K, which are unitary, upper triangular and antisymmetric, respectively. The role of these matrices can be viewed as follows: W encloses all possible rotations in the Yukawa parameter space, while T and K contain the scaling of the different components of the Yukawa couplings. For our analysis we consider two special cases:

Scenario a: we set $W = U_{\ell\nu}$, $T = f \times (v/\hat{m}_\nu)^{1/2}$ and $K = 0$, in such a way that one of the Yukawa matrices becomes diagonal. Here f is just a scale factor parametrizing the magnitude of the Yukawas. However, we conveniently redefine $f = \alpha 10^{-1}/f'$ with $\alpha = (246)^{-1/2}$. All results in the next subsections are given in terms of f'. Notice that f' is such that Y_ϵ and Y_D are proportional and inversely proportional to f', respectively.

Scenario b: we take a specially simple choice $W = I$, $T = g \times I$ and $K = 0$, such that $Y_D = g^2 Y_\epsilon$. Note that this parametrization leaves $Y_D Y_\epsilon^T$ constant and, in consequence, the neutrino mass unchanged for any value of g. For $g = 1$, both Yukawa matrices become equal $Y_D = Y_\epsilon$ and the traditional seesaw scenario is recovered.

Both ansatzes are particularly interesting, because they provide a parameter space that, for some specific values of f' and g, is not only allowed by the current experimental bounds, but it is also inside the measurable region of future experiments. A different choice in the parametrization structure either explores the same region or falls into non-testable or excluded regions. For all the calculations, we set the best fit point (b.f.p.) values of $U_{\ell\nu}$, $\Delta m_{\rm sol}$, $\Delta m_{\rm atm}$ and mixing angles, from neutrino oscillation experiments [351, 406].

6.5.2 Same-sign to opposite-sign dilepton ratio in the LSM

From Eq. (6.3.10), we can appreciate that there are two limiting cases corresponding to $R_{\ell\ell} = 1, 0$. If $\Delta M \sim m_\nu \gg \Gamma$, the decays proceed as in the usual Majorana case and probabilities for SS and OS dilepton events are the same, i.e. $R_{\ell\ell} = 1$. If $\Delta M \sim m_\nu \ll \Gamma$, the pure Dirac case is approached and then $R_{\ell\ell} = 0$. The Quasi-Dirac regime $0 < R_{\ell\ell} < 1$ occurs when $\Delta M \sim \Gamma$. Since $\Delta M \sim m_\nu$ and $\Gamma(M_N)$ grows quite fast with M_N, for smaller values of m_{ν_1}, smaller values of M_N are needed. This is illustrated in Fig. 6.2, which shows $R_{\ell\ell}$ versus M_{N_1} for different values of m_{ν_1}. For this calculation, we have chosen *Scenario a*, with a fixed value of $f' = 100$. As expected, for each specific m_{ν_1}, there is a relatively narrow window of M_{N_1} values such that $0 < R_{\ell\ell} < 1$. For example, if $m_{\nu_1} = 10^{-5}$ eV, then values of 10 GeV $\lesssim M_{N_1} \lesssim 20$ GeV are needed in order to obtain a $R_{\ell\ell}$ value within the QD regime. Unlike the inverse seesaw model [362], where values of $R_{\ell\ell} < 1$ are still obtained for larger values of M_{N_1}, here the current upper bound for the light neutrino mass $m_{\nu_1} \lesssim 0.1$ eV and a $f' = 100$ sets $R_{\ell\ell} = 0$ for values of $M_{N_1} \gtrsim 100$ GeV. This is why our analysis focuses on the regime of small M_{N_1} values.
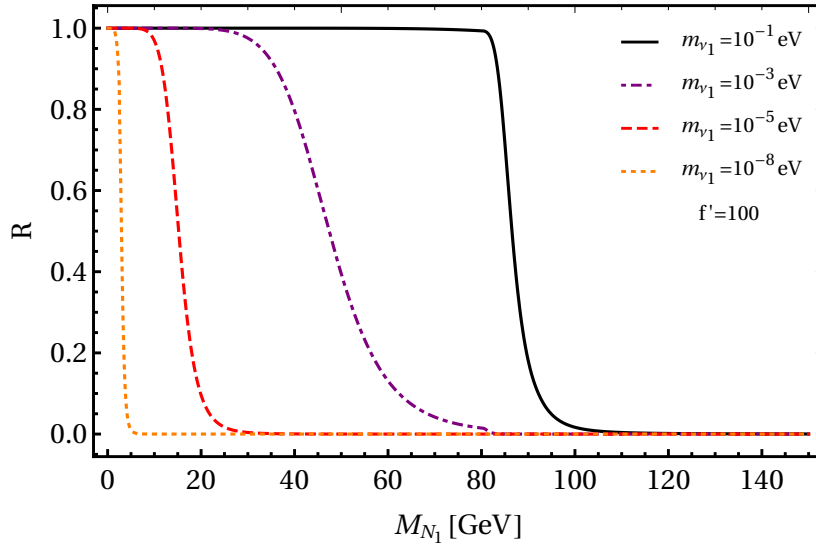
FIGURE 6.2: $R_{\ell\ell}$ vs M_{N1} for different values of m_{ν_1}.

Another interesting plot is Fig. 6.3, which shows the regions in the m_{ν_1}–M_{N_1} plane that belong to the QD regime (i.e. $0 < R_{\ell\ell} < 1$) in the linear seesaw model. This is done within *Scenario a* for some specific values of f'. The different colors

magenta, brown, red and blue correspond to values of $f' = 1$, 10, 10^2, and 10^3, respectively (recall that Y_ϵ grows with f'). In this Figure, for each f' there are three lines corresponding to values of $R_{\ell\ell} = 0.9$, 0.5 and 0.1, from left to right. Therefore, for a specific m_{ν_1}, each colored band roughly provides a range of M_{N_1} values for which $0 < R_{\ell\ell} < 1$. Note though that this QD regime is a continuum: the upper-left corner represents the Majorana case, while the lower-right corner approaches the Dirac limit. This QD–M_{N_1} window of values moves to the left as m_{ν_1} becomes smaller. For example, for $f' = 10$ and $m_{\nu_1} = 10^{-3}$ eV, the heavy neutrinos become Quasi-Dirac for values of 10 GeV $\lesssim M_{N_1} \lesssim 20$ GeV, while if $m_{\nu_1} = 10^{-6}$ eV, then the QD behaviour occurs for 2 GeV $\lesssim M_{N_1} \lesssim 4$ GeV. These specific ranges can be additionally constrained from the current and expected experimental bounds on the mixing $U_{N_1 e}$. Fig 6.3 allows us to directly translate those constraints into the QD regime, as we study in the next section.
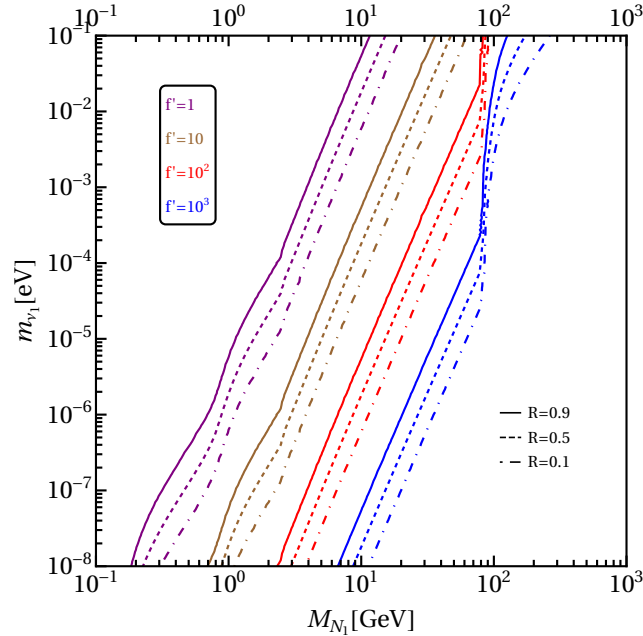
FIGURE 6.3: m_{ν_1}–M_{N_1} lines corresponding to a specific value of $R_{\ell\ell}$ and f'. For each color, the three lines correspond to values of $R_{\ell\ell} = 0.9$, 0.5 and 0.1 from left to right.

6.5.3   Heavy to light neutrino mixing $U_{N\ell}$

Here, we analyze the $|U_{N_1\ell}|^2$–M_{N_1} region and identify the zones in the parameter space where some current experiments could have sensitivity; the prospects of future experiments are also considered. The numerical analysis is based on the systematic diagonalization of the 9×9 mass matrix of the neutral states M_ν (see Eq. (6.2.4))

$$M_\nu = U \hat{M}_\nu U^T \,, \tag{6.5.18}$$

with U containing the PMNS mixing matrix and the heavy-light neutrino mixing elements $U_{N_1\ell}$ as well. For the U calculation, we parametrize the Yukawa couplings as in Eq. (6.5.17). Therefore, after fixing the neutrino oscillation parameters to the

best fit point, we obtain numerical expressions of the mixings $U_{N_1\ell}$ as a function of M_{N_1} and f' or g, depending on the specific scenario. As we sketched in Section 6.4, for the sake of simplicity we considered a large decoupling on the masses of the second and third generation of the heavy neutrinos with respect to $M_{N_1^{(\prime)}}$, i.e. $M_{N_1^{(\prime)}} \ll M_{N_2^{(\prime)}}, M_{N_3^{(\prime)}}$.[4] However, for completeness, at the end of this section we briefly comment on the phenomenologically different inverted-hierarchical case, where the mass of the third-generation heavy neutrino pair is lighter than the other two pairs.

Figure 6.4 shows $|U_{N_1e}|^2$ versus the heavy neutrino mass M_{N_1}, for different values of f' and g: solid and dashed gray straight lines correspond to scenarios a and b respectively. In *Scenario a* all light neutrino masses m_{ν_i} enter all Y_ϵ entries, while Y_D is independent of the light neutrino masses. Obviously, because $m_{\nu_3} \gg m_{\nu_2} \gg m_{\nu_1}$, the mixings $U_{N_1\ell}$ will not depend on m_{ν_1}. Otherwise, in *Scenario b*, each M_{R_i} is responsible for each m_{ν_i}, therefore an explicit dependence on m_{ν_1} is expected. For our calculations on *Scenario b*, we set $m_{\nu_1} = 10^{-3}$ eV. The current constraints and some future projections on the mixing are shown by the shaded region and the colored dashed lines. We can appreciate that for small (large) values of f' (g), the mixing U_{N_1e} becomes strongly constrained by the experimental bounds in a wide range of M_{N_1} values. This means that, if there is some appreciable hierarchy between the Yukawa couplings Y_D and Y_ϵ (see the description of both scenarios above), the predicted mixing falls into the range testable by present and near-future experiments. For some values of $g \lesssim 20$ the model remains unconstrained by the low-energy experimental bounds. A value of $g = 1$, where $Y_D = Y_\epsilon$, corresponds to the traditional seesaw mechanism [353, 354, 407] where the heavy-light neutrino mixing is given by $U_{N_1e} \simeq \sqrt{m_{\nu_1}/M_{N_1}}$. It is interesting to note that the traditional seesaw represented by the red line (for which we set $m_{\nu_1} = 10^{-3}$) is not sensitive to any experimental bound, while our model could be strongly constrained in a large part of the parameter space. The projected sensitivities for ANUBIS (purple dashed line), MATHUSLA (cyan dashed line), SHiP (green dashed line), DUNE (orange dashed line), FASER2 (blue dashed line), FCC-ee (brown dashed line) and AL3X (pink dashed line) are taken from Refs. [390, 391, 408, 409], while the already excluded values (grey shaded region) are taken from Ref. [389, 409]. There is in addition a region in the $|U_{N_1e}|^2$–M_{N_1} plane where a displaced vertex search could have sensitivity: the region limited by the darker red dashed line represents a 95 % CL reach at $\sqrt{s} = 13$ TeV of a multitrack displaced vertex strategy described in Ref. [392]. As depicted in this figure, for values of f' around $10 \lesssim f' \lesssim 10^2$ and a specific window of M_{N_1} values, a discovery of a displaced vertex signal in the model would be possible at the high-luminosity ($\mathcal{L} = 3000\,fb^{-1}$) LHC. A detailed study of displaced vertex signals for QD neutrinos in the linear seesaw model goes beyond the scope of this work, but it could be worth pursuing. Note finally that both scenarios a and b present a symmetry axis of U_{N_1e}, in powers of the parametrization factor, for $f' \sim 10^{4.5}$ and $g = 10^0$, respectively.

The characterization of the QD regime through the $R_{\ell\ell}$ observable implies a possibility for the experiments to measure the charge of the two final leptons (see

---

[4] Due $M_{N_1} \sim M_{N_1'}$, the results and figures involving M_{N_1} apply also for $M_{N_1'}$.
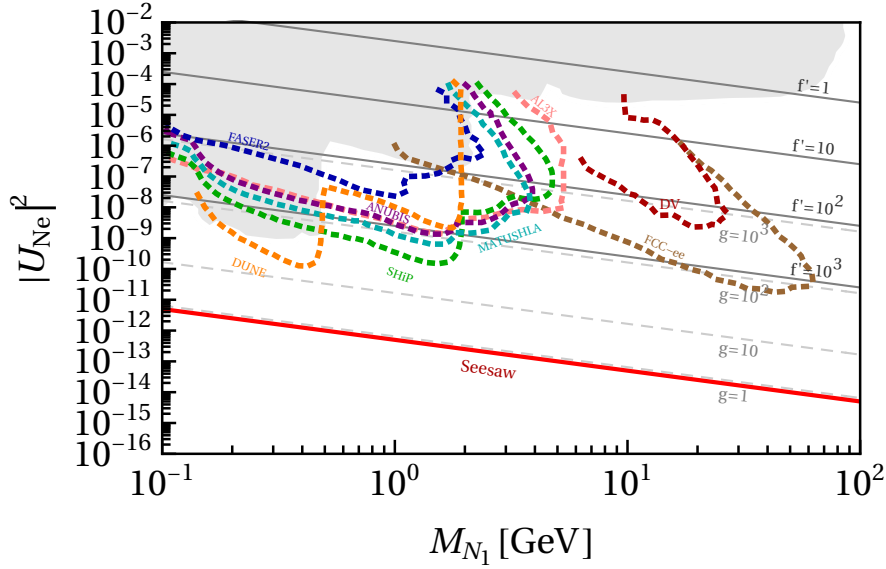
FIGURE 6.4: Active-sterile neutrino mixing $|U_{N_1 e}|^2$ versus the neutrino mass M_{N_1}, for different values of the parameters f' and g. Dashed lines correspond to the projected sensitivities of future experiments, while the gray shaded area indicates the regions already excluded from current searches as depicted in Ref. [409]. The dashed dark red line limits the zone of the sensitivity of DV searches. The solid red line represents the vanilla seesaw model.

Section 6.3). Nevertheless, some of the aforementioned low-energy scale experiments, except the ones concerning to LHC-displaced vertex searches, will not be able to differentiate the charge and then will be blind to this observable. However, the bounds on the mixing themselves can place already stringent constraints into the Quasi-Dirac regime, which can be found by studying the interplay between Fig. 6.3 and 6.4. According to Fig. 6.3, in *Scenario a* each value of m_{ν_1} leads to a specific M_{N_1} range where $0 < R_{\ell\ell} < 1$. At the same time, each M_{N_1}–QD range gets extra constraints by the experimental bounds shown in Fig. 6.4. For instance, with $f' = 10$ and $m_{\nu_1} = 10^{-3}$ eV, the corresponding QD masses 10 GeV $\lesssim M_{N_1} \lesssim$ 20 GeV (see Fig. 6.3) fall into the region where displaced vertex searches could have sensitivity, whereas for a value of $m_{\nu_1} = 10^{-6}$ eV, some region of the QD masses could be excluded by some of the low mass experiments. On the other hand, for $f' = 10^3$, the FCC-ee will be probing masses between 20 GeV $\lesssim M_{N_1} \lesssim$ 60 GeV, so it will be sensitive to QD neutrinos for 10^{-7} eV $\lesssim m_{\nu_1} \lesssim 10^{-4}$ eV, but it is not until one reaches very low values of m_{ν_1} that any foreseen low-energy experiment could be sensitive to QD neutrinos. These observations allow us to conclude that, for a specific value of f', the QD regime gets stronger constraints as the light neutrino mass becomes smaller. For *Scenario b*, since in this case the mixing depends on both the heavy and the light neutrino masses (and then also on the decay width), instead of the fixed-value $R_{\ell\ell}$ lines depicted in Fig. 6.3, we find straight vertical lines [from Eq. (6.3.10)]. This means that for a given g and M_{N_1}, all values of m_{ν_1} give an approximately equal $R_{\ell\ell}$, i.e. $R_{\ell\ell}$ is independent of the lightest neutrino mass. Therefore, there is more freedom when translating the bounds on the mixing to the Quasi-Dirac regimes, and in consequence the model becomes less constrained.

The inverted hierarchical case, with the third-generation heavy neutrino being the lightest of its kind, i.e. $M_{N_3^{(\prime)}} \ll M_{N_1^{(\prime)}}, M_{N_2^{(\prime)}}$, exhibits some different features, which we comment here briefly. First, it mixes predominantly into the τ neutrino, then we should compare $U_{N_3\tau}$ against the previous $U_{N_1 e}$. For *Scenario a*, no relevant difference is observed, but *Scenario b* is more interesting: now $U_{N_3\tau}$ is m_{ν_1}–independent, but m_{ν_3}–dependent. Similar to the $g = 1$ traditional seesaw scenario, where $U_{N_3\tau} \sim \sqrt{m_{\nu_3}/M_{N_3}}$, all dashed gray curves in Fig. 6.4 move upwards with respect to the previous case. All this leads for $R_{\ell\ell}$ to a similar QD behaviour as presented in Fig. 6.3, thus allowing for stronger constraints on the QD regime.

Let us now briefly mention the effects of current lepton-flavor violating (LFV) bounds in our model. We want to add that we have calculated the branching ratio of the $\mu \to e\gamma$ process in both scenarios. Taking into account that our model does not have extra charged scalars, the only contribution to this LFV process comes from the loop mediated by the W boson (see Fig. 3.4). We have found that $Br(\mu \to e\gamma)$ can provide additional relevant constraints only for extreme values of the f' and g, which lie on the already excluded area by the experimental searches depicted in Fig. 6.4.

Finally, regarding neutrinoless double beta decay ($0\nu\beta\beta$) searches, following Ref. [409] one can see that the corresponding bounds get worse as the mass splitting between the pair of heavy neutrinos becomes smaller — as it is expected since $0\nu\beta\beta$ is a LNV process that vanishes away for $\Delta M = 0$, i.e. in the Dirac case. In the linear seesaw model ($\Delta M_i = m_{\nu_i}$) we deal with values of $\Delta r \equiv \Delta M_1/M_{N_1} \in [10^{-11}, 10^{-19}]$, which are farther above the worst upper-bound $\Delta r = 10^{-6}$ depicted in Figs. 9 and 10 of Ref. [409]. Therefore, we conclude that the constraints coming from $0\nu\beta\beta$ are not competitive in the QD region of interest for our work.

6.6 Conclusions

We studied the Quasi-Dirac nature of the heavy neutrinos in the most minimal version of the linear seesaw. This model contains two extra heavy neutrinos, each replicated in three generations. The mass splitting of the heavy neutrino pair in each generation is shown to be of the order of the light-neutrino masses, as shown in Eq. (6.2.8). An interesting way to study the nature of these additional neutrinos is through the ratio $R_{\ell\ell}$, which relates the number of same-sign to opposite-sign dilepton final states (in $\ell\ell jj$ events at hadron colliders) when a heavy neutrino is involved, and may take any value from 0 (Dirac) to 1 (Majorana), with the intermediate region displaying the QD behaviour. We showed that in the LSM this observable is controlled by both the masses of the light neutrinos and the decay widths of their heavy partners (see Eq. (6.3.10)). Therefore, focusing on the first generation and decoupling it from the other two, we computed its decay width, paying special attention to the quark modes within the non-perturbative regime of $E \lesssim 2.5$ GeV. In order to properly hadronize these quark currents, we employed chiral perturbation theory and its higher energy extension the resonance chiral theory, which allowed us to include all features of QCD and systematically calculate all the variety of final hadronic channels.

We performed a numerical analysis based on the systematic diagonalization of the full mass matrix of the neutral states (see Eq. (6.2.4)). Due to the richness of the model, we implemented the master parametrization, that allowed us to scan the parameter space of the model, while automatically fit the current data of the neutrino sector in the most general way. Within this general framework, we chose two simplified realizations of the Yukawas (scenarios a and b) that, nonetheless, embraced the most interesting region of the model.

Unlike other seesaw models with QD regimes, in the linear seesaw the pair of heavy neutrinos exhibits a Quasi-Dirac behavior for relatively low masses.

For each scenario we found the regions of heavy neutrino masses which exhibit the QD regime, i.e. $0 < R_{\ell\ell} < 1$, and which at the same time are consistent with the current bounds for the light neutrino mass:

Scenario a showed a dependence on m_{ν_1}, such that lower light-neutrino masses entailed lower masses for the QD heavy neutrinos as well, in the range of a few GeV's; these QD regions in *Scenario b* on the other hand, happen to be m_{ν_1}-independent.

A phenomenological analysis using experimental data on current and near-future experiments was also carried out to constraint — within both scenarios — the heavy-light neutrino mixing $U_{N_1 e}$ as a function of the heavy-neutrino mass M_{N_1} (see Fig. 6.4). We found that low-energy experiments such as SHiP, MATUSHLA, ANUBIS, DUNE, FASER2 and AL3X together with displaced vertex searches and prospects for the FCC-ee, will explore a large part of the parameter space for both scenarios, either discovering or placing stringent bounds on the parameter space of the LSM, which is still far from reach for the ordinary seesaw. Therefore, we concluded that current and near-future experiments are actually probing hierarchical Yukawas, with the equal-Yukawa case remaining unbounded.

Despite the stated difficulty in measuring directly $R_{\ell\ell}$, we could translate the previous mixing constraints into bounds on the Quasi-Dirac nature of the heavy neutrinos through this observable, what was achieved by comparing Figs. 6.3 and 6.4. By doing so, we found that the QD regime is more strongly constrained in *Scenario a* than in *Scenario b*. In the former, the lower the light-neutrino mass, the lower the mass range yielding $R \neq 0, 1$ and then, the more constrained the QD regime turns out to be. Accordingly, this would lead to a Dirac behavior for these heavy neutrinos. Instead, *Scenario b* was shown to be less constrained: the QD mass regime was shifted to larger masses and the m_{ν_1} dependence of the mixing allowed to take it away of the exclusion area. The inverted hierarchical case was also considered and some of its main features were briefly discussed.

Finally, the most up-to-date stringent bounds on the neutrinoless double beta decay process as well as the lepton-flavor violating process $\mu \to e\gamma$ were also addressed. We concluded that the current experimental upper limits on these processes do not yield competitive constraints as compared to the ones shown in Fig. 6.4.

Chapter 7

Resum

Des de l'inici de les ciències formals, arrel de la revolució científica viscuda als segles XVI i XVII i que va establir les bases de la ciència moderna, la història de la física s'ha desenvolupat en paral·lel a la de les matemàtiques. Sorprenentment, cada nou fenomen físic que era descobert resultava poder ser descrit correctament amb alguna ferramenta matemàtica (la qual, de normal, no havia sigut desenvolupada amb eixa finalitat). Per tant, les matemàtiques es van convertir ràpidament en el llenguatge de la física. Un dels exemples paradigmàtics d'aquesta simbiosi entre física i matemàtiques són les lleis de la mecànica de Newton, que descriuen la cinemàtica i dinàmica dels objectes macroscòpics, i la seua reformulació més potent en termes de la mecànica lagrangiana (o hamiltoniana), que hui en dia encara és emprada diàriament en moltes branques de la ciència, entre elles la física de partícules.

L'àmbit de física de partícules sobre el que versa aquesta tesi, s'allunya molt del món macroscòpic descrit per Newton o Lagrange i els seus coetanis " clàssics" i per tant, les ferramentes matemàtiques necessàries per descriu-re-la s'han d'adaptar. Més concretament, en física de partícules estudiem els fenòmens físics en situacions extremes: a distàncies molt petites i a velocitats o energies molt grans. Els fenòmens poc intuitius que apareixen en estos règims van ser objecte d'estudi al llarg del segle passat. Dos teories es van desenvolupar de forma separada: la Mecànica Quàntica (que explicava com tractar amb el món a escala molt xicoteta, el món quàntic) i la Relativitat Especial, que adreçava els efectes que sorgien a energies i velocitats molt elevades. La posterior combinació dels dos marcs de treball va donar lloc a la teoria quàntica de camps (QFT per les seus sigles en anglés). Aquesta proporciona la millor comprensió que té la humanitat actualment del funcionament de la natura a nivell més elemental. La teoria quàntica de camps descriu les partícules com a excitacions (quàntiques) sobre l'estat fonamental (anomenat buit) d'un objecte que impregna tot l'espai-temps Minkowskià de 4 dimensions: un camp quàntic.

En física de partícules, el formalisme de QFT proporciona els fonaments per adreçar el seu objecte d'estudi: les partícules elementals que composen l'univers i les seues interaccions. En aquesta línia, la segona meitat del segle passat va resultar una època daurada que va culminar amb el desenvolupament del Model Estàndard (SM) de la física de partícules. El corresponent formalisme teòric (explicat en la Metodologia en la secció 7.2.1) on les simetries juguen un paper principal, amb el contingut de partícules observat experimentalment i les seues interaccions, ha resultat ser la teoria més precisa mai creada per l'ésser humà. Ha pogut descriure resultats com el moment magnètic anomal de l'electró amb una precisió mai vista

abans. I encara que és continuament posat a prova a nombrosos experiments de partícules al llarg del món, com per exemple al LHC, les seues prediccions per als resultats d'eixos experiments continuen coincidint amb l'observació.

Tot i el gran èxit del Model Estàndard, encara hi ha qüestions obertes tant de tipus observacional com teòric. Entre les primeres, hi ha diversos fenòmens observats que no tenen explicació dins del marc del SM. Per exemple, la massa dels neutrins (absent en el SM) observada a través de les oscil·lacions dels seus estats propis de sabor en processos febles; la falta d'una gran fracció de la massa total de l'univers, que el paradigma dominant actual tendeix a explicar a través de l'anomenada matèria fosca; o el domini de la matèria sobre l'antimatèria en l'univers, per al qual el SM només pot explicar-ne una xicoteta part, entre altres. Les qüestions teòriques, encara que no necessàriament comporten incoherències dins del propi marc de treball, no tenen una comprensió fonamental en el SM. L'exemple habitual és el problema de la naturalitat, relacionat amb un aparent ajust fi que s'ha de fer en alguns paràmetres. A part de la naturalitat, altra qüestió que no explica el SM és la seua estructura de sabor: per què tres copies de cada família, per què la jerarquia que s'observa dels Yukawes (les seues masses) i del patró de mescles entre estats propis de sabor i no qualsevols altres? A estes qüestions se les coneix pel nom del problema o puzle del sabor del SM. A més, hi ha altres indicis teòrics que apunten a una física més rica a altes escales energètiques, com la possible unificació de les interaccions del SM en una sola. En menor mesura, un altre exemple ve donat pel requisit de renormalizabilitat del SM. Aquesta restricció porta a l'aparició de simetries globals accidentals com la conservació global del número de leptons i barions. La inclusió de termes no renormalitzables en una teoria més general pot trencar naturalment aquesta simetria. Tot i que les dades experimentals (fins a la precissió actual) confirmen el marc del SM també en aquest assumpte, l'existència de simetries accidentals no té una explicació més profunda.

7.1   Objectius

En aquesta tesi hem tractat d'abordar parcialment alguns dels problemes mencionats abans i d'estudiar de forma més genèrica possibles contribucions de física més enllà del Model Estàndard (BSM).

Al capítol 3, basat en el treball publicat en la Ref. [74], estudiem la possible violació del sabor leptònic dels leptons carregats (CLFV), més en concret centrant-nos en la tercera família, i.e. violació del sabor del leptó tau. Mentre que aquest fenomen és possible en el sector dels quarks, l'absència d'un neutrí dretà en el SM empedeix la violació del sabor leptònic en general. No obstant, el fet que els neutrins tinguen realment massa (com indiquen les oscil·lacions de neutrins) apunta a una dinàmica més complexa en el sector dels leptons. Si la violació del sabor tauònic està estrictament lligada al mecanisme més simple de generacció de massa dels neutrins, aleshores els efectes predits de CLFV són tan petits que no es podrien mesurar amb les tècniques de hui en dia. No obstant, això mostra la importància d'estudiar aquests processos: si es mesura algun procés amb CLFV, seria un senyal directe de nova física. De fet, moltes extensions del SM prediuen contribucions mesurables de CLFV. Aquest efecte

s'ha estudiat molt en la literatura en relació a les dos primeres famílies, l'electró i el muó. En canvi, les complicacions experimentals associades amb tractar amb el tau han fet que no se li parara molta atenció: costa produir-los en molta quantitat i a més decauen molt ràpid. Tot i això, processos de CLFV que involucren al τ han sigut estudiats tant en LEP com en les anomenades factories de Bs com Belle i BaBar. A més, en la pròxima dècada les futures generacions d'experiments com Belle II, l'experiment NA64 al CERN, el col·lisionador electró-ió (EIC) o TeraZ al FCC-ee milloraran les restriccions en estos processos. Per consegüent, al capítol 3 fem una anàlisi genèrica per constrenyir possibles contribucions de nova física a processos de CLFV. Aquestes contribucions les parametritzem mitjançant la teoria efectiva del Model Estàndard (SMEFT), la qual ens permet considerar tots el possibles efectes provinents de nova física a altes energies d'una forma gènerica, i.e. sense dependre d'un model en particular. En concret, estudiem els decaïments hadronics del tau i la possible conversió de tau a muó o electró en presència d'un nucli. El primer procés el caracteritzem mitjançant la Teoria Quiral de Pertorbacions (χPT) i la Teoria Quiral de Resonàncies (RχT), les dues explicades a la Metodologia. Per al segon, utilitzem les funcions de distribucions dels partons en el nucli. Per dur a terme l'anàlisi emprem els resultats actuals dels experiments Belle [103] i BaBar [102] i dels resultats esperats de Belle II [410] en decaïments del tau en hadrons, i dels resultats esperats de l'experiment NA64 [138] en conversió en nucli del tau en altre sabor leptònic. D'aquesta forma, constrenyim l'espai de paràmetres de la SMEFT.

Dins de la rica paleta d'escenaris amb física més enllà del Model Estàndard, una classe molt ben motivada de teories prediu l'existència de leptoquarks (LQs): bosons carregats elèctricament (amb espí S = 0, 1) que a més, tenen càrrega de color i es transformen en triplets sota $SU(3)_C$ i poden convertir quarks en leptons i viceversa. Aquestes partícules emergeixen naturalment en les teories de Gran Unificació, on els leptons s'acomoden als mateixos múltiples que els quarks: van aparèixer per primera vegada en el model de Pati-Salam [179, 180], i han continuat apareixent en nombroses teories de nova física. Al mateix temps, l'existència persistent de diverses anomalies (discrepàncies entre les prediccions teòriques dels observables del SM i els seus valors experimentals) apunta a possibles efectes de nova física, i els leptoquarks es presenten com a candidats rellevants, sent capaços d'abordar una o més d'aquestes desviacions, depenent del model escollit. Les discrepàncies que han cridat més l'atenció en la literatura recent són $R_{D^{(*)}}$ [105–112], R_K [113–120] i la més recent $R_{K_S^0}$ i $R_{K^{*+}}$ [121], les anomenades anomalies B [122], i per altra banda, el moment magnètic anomal $(g - 2)$ del muó [123, 124]. A banda d'aquestes anomalies, els leptoquarks també han sigut considerats com a possibles solucions d'altres problemes del SM com els que hem comentat abans: s'ha estudiat la seua possible implicació en la generació de massa dels neutrins i també s'han considerat com a candidats de matèria fosca, entre altres. Inclús la seua existència podria donar pistes sobre el problema del sabor del SM, per què n'hi ha tres generacions de partícules elementals al SM. Aquestes partícules tan interessants, a més, donen contribucions d'ordre dominant als processos de violació de sabor leptònic estudiats en el capítol 3. Per tant, al capítol 4 basat en el treball de Ref. [251], considerem el model més genèric de leptoquarks. Aquest inclou un total de 10 leptoquarks, 5 escalars i 5 vectorials, els quals s'acoblen als fermions del SM, als bosons gauge

(dels quals ens interessen el γ i Z, ja que els processos estudiats de CLFV es donen a través de corrents neutres) i al Higgs. Aquest model ha de ser integrat (com s'explica en la metodologia) per a fer la identificació entre els paràmetres dels leptoquarks: acoblaments i masses, i els coeficients de la SMEFT que hem constrenyit al capítol 3. Finalment, traslladem les restriccions obtingudes a aquest capítol, en restriccions sobre la massa dels leptoquarks i els acoblaments d'estos a la matèria.

Al capítol 5 ens centrem de nou en posar restriccions als paràmetres de les teories efectives de camps, en aquest cas la teoria efectiva de camps de baixes energies (LEFT). D'aquesta manera, busquem restringir de la forma més general possible, les contribucions de nova física als processos que observem experimentalment. El procés en concret estudiat a aquest capítol involucra, a més, oscil·lacions de neutrins. La caracterització d'aquestes oscil·lacions es fa de normal en la literatura emprant el formalisme de Mecànica Quàntica, però, com es va demostrar al cas on n'hi ha interaccions amb corrents carregades [273], aquest formalisme pot fallar. Per tant, nosaltres utilitzem el formalisme desenvolupat en la Ref. [273] sobre la teoria quàntica de camps, per caracteritzar aquestes oscil·lacions de neutrins en presència, a més, d'interaccions de nova física que proporciona la LEFT. Al capítol 5, donem una descripció total de l'experiment COHERENT en aquest formalisme. L'objectiu de l'experiment va ser demostrar l'existència d'un procés descrit teòricament a l'any 1974, la dispersió elàstica i coherent de neutrins incidint sobre nuclis (CEνNS), però que encara no s'havia mesurat experimentalment. Finalment, a l'any 2017 l'experiment COHERENT va mesurar per primera vegada aquest procés que, dins d'un error no menyspreable, estava d'acord amb la predicció feta pel SM [276]. Aquesta mesura, i les següents fetes pel mateix experiment en diferents nuclis, a banda de demostrar l'existència d'aquest procés purament quàntic, ens serveix per a constrenyir els paràmetres de nova física introduïts per la LEFT, que podrien afectar a CEνNS. La corresponent caracterització de l'experiment COHERENT en el nostre formalisme d'oscil·lacions de neutrins dins del marc de QFT i la posterior extracció de restriccions sobre els paràmetres de la LEFT en base als resultats experimentals, constituixen l'objectiu del capítol 5.

Finalment, al capítol 6 basat en el treball de la Ref. [367], ens interessem per un mecanisme específic de generació de masses de neutrins: el model lineal de balancí. Aquest model introdueix a sobre de l'espectre de partícules del SM dos tipus de neutrins pesats amb tres families cadascú, és a dir, 6 neutrins nous, amb uns acoblaments amb els leptons del SM característics del model. El resultat és que, una volta és diagonalitza la matriu de massa dels neutrins, els neutrins actius del SM reben una massa molt xicoteta (com s'espera). No obstant, a diferència dels models típics de balancí, això no ocorre a costa del neutrins pesats que acaben tenint una massa sobre els 10^{15} GeV (impossible de mesurar al nostre període de vida), sinó que degut a la textura de masses característica d'aquest model, els neutrins pesats que hem afegit poden viure al voltant dels GeV (detectables en les noves generacions d'experiments). En general, els neutrins extra afegits són neutrins de Majorana i, per tant, violen el número leptònic. No obstant, en el límit d'igual massa, els dos neutrins es troben degenerats i (cada família) conjuntament formen un neutrí de Dirac, i.e. aquest es pot vore com un par de neutrins de Majorana degenerats en massa. És interessant estudiar el cas intermig, on ambdós neutrins s'apropen a la

degeneració i presenten una fenomenologia particular que es pot observar als experiments. El par de neutrins Majorana que es troben quasi-degenerats reben usualment el nom de neutrins Quasi-Dirac (QD). En el model lineal de balancí aquest règim depén de diversos paràmetres del model. En aquest capítol 6, caracteritzem els neutrins Quasi-Dirac del model lineal de balancí en termes dels seus paràmetres i fem una anàlisi fenomenològic per constrenyir tant els neutrins Quasi-Dirac com els mateixos paràmetres.

7.2 Metodologia

La metodologia de la tesi es recull principalment als capítols 1 i 2 i la resta es va introduïnt segons es necessita en cada capítol. En aquesta secció, fem un resum dels models teòrics, les tècniques i ferramentes que utilitzem al llarg de la tesi.

7.2.1 Model Estàndard

El Model Estàndard descrit al capítol 1 és una teoria quàntica de camps renormalitzable que descriu tres de les quatre interaccions que observem a la natura: la interacció electromagnètica, la dèbil i la forta (la inclusió en aquest marc de la gravetat és encara un problema obert objecte de molta investigació). En aquesta teoria, les interaccions fonamentals sorgeixen d'imposar unes determinades simetries locals (també anomenades gauge) sobre el Lagrangià que descriu les lleis bàsiques dels camps. En concret, el Lagrangià del SM és invariant baix la simetria local

$$G \equiv \mathrm{SU}(3)_{\mathrm{C}} \times \mathrm{SU}(2)_{\mathrm{L}} \times \mathrm{U}(1)_{\mathrm{Y}}, \qquad (7.2.1)$$

on $\mathrm{SU}(3)_{\mathrm{C}}$ correspon a la simetria de la interacció forta [4, 5] i $\mathrm{SU}(2)_{\mathrm{L}} \times \mathrm{U}(1)_{\mathrm{Y}}$ a la de la interacció electrofeble, la unificació de l'electromagnetisme amb la interacció feble [8–10] (altre èxit del SM). Cada interacció té una càrrega associada, e.g. l'electromagnètica té la càrrega elèctrica o la interacció forta la càrrega de color, per això la teoria que descriu les interaccions amb càrrega de color rep el nom de Cromodinàmica Quàntica (QCD).

Com es pot contemplar a la discussió de dalt, en la descripció més encertada que tenim hui en dia del món subatòmic, les simetries juguen un paper central. De fet, els camps quàntics associats a les partícules elementals corresponen a representacions irreduïbles del grup de simetria Lorentz. En aquest marc teòric, les partícules elementals es dividixen en dos grups en base al seu espí: fermions (espí semi-enter) i bosons (espí-enter). Per una banda, els fermions conformen la matèria ordinària i es divideixen de nou en dos grups: quarks i leptons. Els primers són les úniques partícules que senteixen les tres interaccions fonamentals, mentre que els leptons no tenen càrrega de color i no pateixen la interacció forta. Finalment, tant quarks com leptons es divideixen en dos subgrups: quarks tipus u o tipus d i leptons carregats (elèctricament) o leptons neutres. Estos quatre tipus de fermions són, doncs, les partícules de matèria més elementals que coneixem. De fet, el leptó carregat, també anomenat electró, junt amb les combinacions adequades de quarks u i d que donen lloc als protons i neutrons, conformen tota la matèria que veiem al nostre dia

a dia. No obstant, el SM inclou tres còpies més massives de cadascuna d'aquestes partícules. Estes reben el nom de *famílies* o *generacions* i es poden representar com:

$$1^{\text{ra}} : \begin{bmatrix} \nu_e & u \\ e^- & d' \end{bmatrix}, \qquad 2^{\text{a}} : \begin{bmatrix} \nu_\mu & c \\ \mu^- & s' \end{bmatrix}, \qquad 3^{\text{ra}} : \begin{bmatrix} \nu_\tau & t \\ \tau^- & b' \end{bmatrix}. \tag{7.2.2}$$

Aleshores, en total el SM conté 12 fermions, 4 per cada família. I cadascú d'aquests fermions té un sabor que el distingueix de la resta, e.g. el sabor de l'electró és el sabor electrónic, el del muó sabor muónic o el del quark u sabor u.

Per altra banda, en el SM els bosons amb espí 1 (bosons vectorials) adquireixen el paper de mediadors de les interaccions. Per això, també reben el nom de bosons de gauge. Així, el fotó sense massa seria el mediador de la interacció electromagnètica, els bosons massius $W^\pm$ i Z de la interacció feble i els huit bosons sense massa però amb càrrega de color anomenats gluons, serien els responsables de la interacció forta. De la discussió de dalt s'ha d'entendre doncs, que estos bosons de gauge ixen d'imposar la invariància sota la simetria gauge $\text{SU}(3)_{\text{C}} \times \text{SU}(2)_{\text{L}} \times \text{U}(1)_{\text{Y}}$ del SM.

Finalment, la simetria gauge que permet explicar les interaccions fonamentals, prohibeix, al mateix temps, que els fermions i els bosons $W^\pm$ i Z adquireixen massa. En altres paraules, els mecanismes que donen massa a estes partícules violen la simetria gauge. Per tant, es necessita algun mecanisme pel qual aquesta simetria es viole, i puga donar massa a les partícules, però que al mateix temps deixe les lleis que descriuen les partícules i les seues interaccions, i.e. el Lagrangià, invariant. La solució està al fenomen conegut com *ruptura espontània de simetria* (SSB) i que té com a resultat observable l'existència del bosó de Higgs [12–14]. En concret, en el SM el patró de ruptura de simetria és el següent:

$$\text{SU}(2)_{\text{L}} \times \text{U}(1)_{\text{Y}} \xrightarrow{\text{SSB}} \text{U}(1)_{\text{QED}}, \tag{7.2.3}$$

on el grup de simetria de la interacció electrofeble es trenca, i només el grup que descriu l'electromagnetisme (el qual ve descrit per l'electrodinàmica quàntica o QED) segueix sent una bona simetria. Per altra banda, el patró de SSB manté la simetria de color invariant.

La ruptura espontània de simetria es dona quan les lleis que descriuen els estats físics, les seues *lleis de moviment*, no comparteixen les mateixes simetries que els propis estats físics. En el cas que ens pertoca, el Lagrangià del Model Estàndard és invariant baix G (vore Eq. (7.2.1)), però el buit de la teoria sobre el que es construeixen els estats, sols és invariant sota el grup reduït $H \equiv \text{SU}(3)_{\text{C}} \times \text{U}(1)_{\text{QED}}$. Aixo s'aconsegueix en el SM incloent un potencial escalar amb un camp escalar que descriu quatre graus de llibertat i s'acobla tant als bosons $W^\pm$ i Z com als fermions. Aquest potencial també és invariant sota el grup de simetria del SM i, com a tal, el camp escalar té infinites configuracions per a les que el potencial té un mínim, i.e. la teoria presenta infinits estats degenerats de buit. El procés de SSB es dona quan el camp "decideix" un d'estos estats, i no qualsevol altre, com el buit físic i adquireix un valor esperat al buit (vev). És aquesta elecció entre les infinites possibilitats de buit, la que trenca la simetria i fa que, degut a l'acoblament del camp escalar als bosons $W^\pm$ i Z i als fermions, els done massa (excepte als neutrins). Tres dels quatre graus de llibertat que descriu el camp escalar són "menjats" pels bosons $W^\pm$ i

Z donant-los massa. El quart grau de llibertat és el bosó de Higgs que va ser trobat finalment a l'any 2012 a l'accelerador de partícules més gran del món, l'LHC [17,18].

Al sector dels fermions, l'acoblament amb el camp escalar es coneix com interacció de Yukawa. El fet que els quarks en el SM puguen tindre dos quiralitats diferents, dretans (R) o esquerrans (L), relacionades amb tindre espí $+1/2$ o espí $-1/2$, fa que els estats de massa de la teoria (amb una massa ben definida) no siguen els mateixos als estas de sabor (amb un sabor ben definit). Això dona lloc a una dinàmica de sabor molt complexa i variada, com es veu en la jungla d'hadrons (combinacions de quarks) observada als experiments. Respecte als leptons, mentre que els carregats també existeixen amb les dos quiralitats en el SM, els neutrins només apareixen amb quiralitat L (i els antineutrins amb R). Aquest fet fa que, primer els neutrins no reben massa per mitjà d'aquest mecanisme i segon, que la dinàmica de sabor al sector leptònic del SM siga molt més pobra.

7.2.2 Teories efectives de camps

En vista de les incògnites mostrades a la introducció que envolten el Model Estàndard, i degut també a la visió més profunda guanyada sobre el formalisme de teoria quàntica de camps, en els últims anys s'ha arribat a un consens sobre la interpretació del SM com una realització a baixes energies d'una teoria completa d'altes energies, habitualment coneguda com la seua completitud ultravioleta (UV). A més, les búsquedes directes de nous graus de llibertat i la nova dinàmica associada a aquests, com la supersimetria, no han trobat res fins a l'actualitat. Això ha dut a la comunitat a centrar-se més en les búsquedes indirectes: estudiar els efectes (quàntics) que la dinàmica de nova física pot tindre en els observables (ja estiguen permesos o prohibits) del SM. En aquest sentit, una forma sistemàtica que no depén de les prediccions de cap model particular, i que permet adaptar els resultats a qualsevol completitud UV, ve donada per les teories efectives de camps (EFT). Al capítol 2 presentem els fonaments teòrics de les EFTs i expliquem aquelles que utilitzem al llarg de la tesi. Les EFTs en general es construïxen sobre el contingut de partícules i simetries conegudes a baixes energies, les quals comporten els efectes més importants dels observables mesurats als experiments, i incorporen de forma consistent els possibles efectes de física desconeguda a altes energies. En general, qualsevol teoria efectiva es pot expressar de la següent forma

$$\mathcal{L}_{\text{EFT}} = \sum_{d=2}^{\infty} \left(\sum_i \frac{C_i^{(d)}}{\Lambda^{d-4}} \mathcal{O}_i^{(d)} \right) , \qquad (7.2.4)$$

on els $C_i^{(d)}$ són paràmetres adimensionals que reben el nom de coeficients de Wilson (WC). Per a cada valor de l'índex que marca la dimensió d, hi ha un subconjunt finit d'operadors construïts en base al contingut de camps de la teoria de baixa energia, els quals venen donats pels $\mathcal{O}_i^{(d)}$ de l'Eq. (7.2.4). A nivell dimensional, s'ha de compensar les dimensions dels operadors introduïnt un terme de massa Λ. Aquest terme correspon a l'escala d'energia característica de la nova física i ha de ser necessàriament major tant a l'escala dels camps i simetries sobre els que es

construeix la teoria efectiva com a l'energia E característica del procés que estem estudiant, per a que la EFT siga consistent.

Com es pot extraure de l'Eq. (7.2.4), el càlcul d'observables físics en una teoria efectiva involucra calcular infinits terms. No obstant, les contribucions dels operadors de dimensió major que $d = 4$ estan suprimides per factors $\mathcal{O}\left((E/\Lambda)^{(d-4)}\right)$, on E és l'energia característica de l'observable que estem estudiant. Per tant, a l'hora de calcular dins de la EFT les contribucions d'aquests operadors a un determinat procés, no fa falta realment utilitzar tota la torre infinita d'operadors en l'Eq. (7.2.4). Sinó que, degut a que necessàriament $E \ll \Lambda$, els terms amb dimensió cada volta més major contribuixen menys i menys i podem truncar aquesta suma infinita fins a un determinat valor n del paràmetre d, de tal fora que assumim un error en el càlcul de $\mathcal{O}\left((E/\Lambda)^{(n-4)}\right)$.

La construcció d'una EFT sobre els operadors renormalitzables (en el sentit vell de la paraula) amb $d = 4$ d'una teoria a baixes energies mitjançant l'expansió infinita sobre el terme de massa Λ a l'Eq. (7.2.4), rep el nom d'*apropament de baix a dalt*. Aquest és el que utilitzem al capítol 3, per a estudiar els processos de CLFV amb taus i constrenyir els WCs de la teoria efectiva del Model Estàndard que podrien intervindre a aquests processos. En canvi, si volem obtindre la teoria efectiva corresponent a una determinada completitud ultravioleta, amb uns camps molt massius i altres més lleugers, deuriem integrar els camps massius del generador funcional de la teoria. D'esta forma obtindríem la identificació dels paràmetres que acompanyen als camps massius (els seus acoblaments als camps lleugers i les seues masses) amb els coeficients de Wilson de l'Eq. (7.2.4). Aquest mètode és conegut com *de dalt a baix* i és el que emprem al capítol 4, per aplicar les restriccions obtingudes al capítol 3 sobre el model més genèric de leptoquarks: primer integrem els leptoquarks, obtenim la teoria efectiva corresponent amb la identificació dels paràmetres dels leptoquarks i els WCs i trasladem les constriccions sobre els últims a restriccions sobre els primers.

Teoria Quiral de Pertorbacions i Teoria Quiral de Resonàncies

Per a l'anàlisi de processos que violen sabor leptònic dut a terme al capítol 3, hem de calcular els decaïments del τ en hadrons. El càlcul consisteix d'una part pertorbativa, donada per la teoria efectiva del Model Estàndard, i d'una part no pertorbativa relacionada amb QCD. Aquesta última entra en joc degut a que, a l'energia característica del decaïment del τ en quarks ($E \sim m_\tau$), la constant d'acoblament de les interaccions fortes és molt gran i els quarks no es troben lliures, sinó confinats en hadrons, i.e. hadronitzen. En aquests règims, QCD és no pertorbativa i els mètodes usuals de càlcul amb diagrames de Feynman, i.e. els mètodes pertorbatius, no donen els resultats correctes. A estes energies, els quarks no són els graus de llibertat rellevants de la teoria, sinó que ho són els hadrons. Hi ha varies formes de calcular el decaïment del tau a hadrons, al capítol 3 nosaltres utilitzem la teoria dual (o efectiva) de QCD a baixes energies: La Teoria Quiral de Pertorbacions [31, 32], i la seua versió estesa que inclou també les resonàncies hadròniques que poblen la regió energètica d'interés: La Teoria Quiral de Resonàncies [41–43].

La Teoria Quiral de Pertorbacions és la teoria efectiva de QCD on, en compte de trebllar amb quarks, treballem amb els graus de llibertat rellevants a les energies on QCD no és pertorbativa $E \lesssim 2.5$ GeV, els hadrons. L'argument principal per construir aquesta teoria efectiva és que existeix un salt energètic entre els estats més lleugers observats experimentalment i la resta de l'espectre hadrònic. χPT descriu, doncs, les interaccions dels estats més lleugers de l'espectre. Per entendre χPT hem d'escomençar pel Lagrangià de QCD amb quarks sense massa. Aquest, a banda de la simetria de color SU(3)$_{\text{C}}$ (que no juga un paper en esta discussió) és invariant sota la simetria global en l'espai de sabor $G \equiv \text{SU}(n)_{\text{L}} \times \text{SU}(n)_{\text{R}}$, la qual transforma de forma independent els quarks amb quiralitat L i R. En la natura trobem tres quarks lleugers (u, d, s) per als quals s'espera que aquesta simetria aplique correctament, i d'igual forma a l'espectre hadrònic que sorgeix d'aquests tres quarks. No obstant, quan observem aquest als experiments, en compte de trobar els dos multiplets d'hadrons $(\vec{\pi}, \vec{K}_{S=1}, \vec{K}_{S=-1}, \eta_8)_{L+R}$ i $(\vec{\pi}, \vec{K}_{S=1}, \vec{K}_{S=-1}, \eta_8)_{L-R}$ que esperaríem del grup de simetria G, trobem, tan sols, un multiplet amb números quàntics axials: $L - R$. Aquest fet, junt a l'observació de la "gran" diferència en massa entre els estats hadrònics lleugers i la resta de l'espectre, mostren que hi ha una ruptura de simetria amb el següent patró

$$G \equiv \text{SU}(3)_{\text{L}} \times \text{SU}(3)_{\text{R}} \longrightarrow H \equiv SU(3)_{\text{L+R}} \,, \tag{7.2.5}$$

en analogia a la SSB del camp del Higgs en el SM. En aquest cas, la ruptura ve de la no invariància del buit de QCD baix la simetria quiral G. Pel teorema de Nambu-Goldstone [15, 16], el patró de ruptura de simetria de l'Eq. (7.2.5) significa l'existència de 8 bosons de Goldstone sense massa. aquests són identificats amb els estats hadrònics lleugers. El fet que en la realitat tinguen una massa (encara que xicoteta) ve donat per la ruptura (feble) explícita de la simetria quiral H, per les masses dels quarks lleugers.

En base al patró de ruptura de simetria (7.2.5) i de la conservació de la paritat en les interaccions fortes, és desenvolupa el Lagrangià de χPT amb una realització dels camps hadrònics no lineal. A més, com a tota teoria efectiva, aquest Lagrangià presenta una expansió infinita sobre un terme que, a cada ordre de l'expansió es fa més xicotet: el moment de les partícules involucrades (xicotet per construcció) i les masses de les partícules (lleugeres com hem vist). En la línia de χPT, es pot desenvolupar una teoria amb tints efectius que incloga, a més dels bosons de Goldstone, les resonàncies hadròniques més lleugeres. Aquest marc teòric es coneix com RχT i es basa en la simetria quiral de QCD i el límit d'infinit nombre de colors $N_{\text{C}} \to \infty$. En ambdós marcs teòrics, les interaccions d'aquests camps (bosons de Goldstone i resonàncies hadròniques) amb la resta del Model Estàndard s'inclouen afegint corrents externs als Lagrangians corresponents que venen purament de QCD. Una volta es té el Lagrangià sencer, l'hadronització dels corrents de quarks ve donada per la identificació dels funcionals generadors de les dos teories (QCD + corrents externs i χPT o RχT + corrents externs). Aquest és el mètode emprat al capítol 3 per hadronitzar (amb RχT) els corrents de quarks procedents del decaïment del tau.

La SMEFT i la LEFT

La teoria efectiva del Model Estàndard és la que s'obté partint dels camps del SM i incorporant les simetries d'aquest als possibles operadors efectius. El Lagrangià corresponent ve donat per

$$\mathcal{L}_{\text{SMEFT}} = \mathcal{L}_{\text{SM}}^{(4)} + \frac{1}{\Lambda}\sum_i C_i^{(5)}\mathcal{O}_i^{(5)} + \frac{1}{\Lambda^2}\sum_i C_i^{(6)}\mathcal{O}_i^{(6)} + \mathcal{O}\left(\frac{1}{\Lambda^3}\right). \tag{7.2.6}$$

La base d'operadors de $d = 5$ conté només l'operador de Weinberg que, quan es dona la ruptura espontània de simetria, genera massa als neutrins. Les conseqüencies d'aquest operador en els diferents models de balancí que generen massa als neutrins del SM s'expliquen al capítol 6. Per als operadors de $d = 6$ nosaltres emprem la base de la Ref. [56]. Aquesta conté un total de 59 operadors independents (si el número bariònic es conserva, o 64 si no). Al capítol 2 presentem aquesta base i descrivim unes bones pràctiques a l'hora de treballar amb la SMEFT (i qualsevol teoria efectiva). Una de les peces clau per a l'analis del capítol 5 és l'elecció de l'esquema de dades d'entrada i les seues conseqüencies en qualsevol anàlisi amb teories efectives. Resumidament, la importància que té aquesta elecció radica en el fet que dins d'un marc de EFTs els paràmetres que mesurem als experiments no són els del SM, sinó que estan contaminats de paràmetres de nova física. Aleshores, quan calculem un observable físic amb els paràmetres del SM i de la nova física, al utilitzar el valor mesurat per l'experiment dels primers, hem de corregir la contaminació de nova física que puguen tindre. Al capítol 5, aquest procediment de correcció dona lloc a una cancel·lació quasi total de la dependència dels paràmetres de nova física en els observables d'estudi.

Finalment, la teoria efectiva que emprem al capítol 5 no és la SMEFT, sinó la seua versió de baixa energia, la WEFT o LEFT [64]. En aquesta EFT, les partícules pesades del SM han sigut integrades i els graus de llibertat que queden són $(e, \mu, \nu_\alpha, u, d, g, \gamma)$, amb $\alpha = e, \mu, \tau$. Per l'energia característica del fenomen estudiat al capítol 5: CEνNS, al capítol 2 obtenim la descripció de la LEFT en termes de nucleons (els graus de llibertat rellevants en CEνNS) i a més, càlculem el seu límit no relativista en una cascada de teories efectives.

7.2.3   Model lineal de balancí i la parametrització màster

Al capítol 6, estudiem un model de generació de massa dels neutrins conegut com: model lineal de balancí [364–366]. Aquest introdueix dos tipus de neutrins extra N i S (amb tres generacions cadascú), de forma que, en la base (ν_L^{C}, N, S), la textura de la matriu de masses (9×9) del model ve donada per

$$M_\nu = \begin{pmatrix} 0 & m_D & M_\epsilon \\ m_D^T & 0 & M_R \\ M_\epsilon^T & M_R^T & 0 \end{pmatrix}. \tag{7.2.7}$$

Al diagonalitzar la matriu de dalt com a una matriu 3×3, la massa dels neutrins lleugers ve donada per

$$m_\nu = m_D M_R^{-1} M_\epsilon^T + M_\epsilon M_R^{T^{-1}} m_D^T, \tag{7.2.8}$$

on es pot vore que la petitesa de la massa dels nuetrins lleugers del SM vindria donada, per una banda, per la grandària de la massa dels neutrins pesats introduïts (M_R) i, per l'altra, per un valor petit del paràmetre de violació de número leptònic M_ϵ. D'aquesta forma, els neutrins pesats podrien tindre una massa no molt allunyada de la sensibilitat experimental actual.

Amb l'objectiu d'estudiar l'espai de paràmetres del model lineal de balancí de la forma més general possible, al capítol 6 presentem la parametrització màster dels acoblaments de Yukawa dels models de neutrins [396, 405]. Aquesta permet ajustar qualsevol model de masses de neutrins de Majorana de forma que reproduisca les dades experimentals actuals. La parametrització màster ens permet relacionar de la forma més genèrica possible els acoblaments de Yukawa del model lineal de balancí amb la resta de paràmetres del model, les dades experimentals com les masses dels neutrins lleugers i la matriu PMNS i altres paràmetres lliures, els quals s'ajusten amb les dades experimentals.

7.3 Resultats i conclusions

Aquesta secció es dedica a mostrar els resultats i les conclusions a les que arribem en les diverses anàlisis que duem a terme al llarg de la tesi.

7.3.1 Violació del sabor leptònic del τ

En l'anàlisi de CLFV amb leptons tau que fem al capítol 3 estudiem un total de 32 observables: 14 decaïments del tau a hadrons i un muó, 14 més a hadrons i un electró, 2 conversions de tau a muó en nuclis de Fe(56,26) i Pb(208,82) i 2 més de tau a electró en els mateixos nuclis. A més, considerem dos escenaris, un en que la nova física, parametritzada per la SMEFT, conserva el sabor en el sector dels quarks (no-FCNC) i altre on la nova física s'acobla d'igual forma a tots els sabors de quarks i per tant no conserva el seu sabor en les interaccions. El segon escenari és el més general i, per tant, presentem els resultats per aquest.

Un dels primers resultats és que l'anàlisi està dominat per les restriccions que estableixen els límits de Belle (i els esperats de Belle II) sobre els decaïments del tau a hadrons i un leptó. En comparació, els límits que venen de la sensibilitat esperada de l'experiment NA64 al CERN a conversió en nuclis de ℓ-τ no serien encara competitius. Les restriccions obtingudes sobre la nova física que podria contribuir a aquests processos, parametritzada pels paràmetres de la teoria efectiva del Model Estàndard, i.e. pel ratio C/Λ^2, es mostren en la Fig. 7.1.

Un dels altres resultats principals a extraure d'aquest treball és la importància de fer anàlisis *marginalitzades*, considerant tots els coeficients de Wilson al mateix temps, sobre les *individuals*, on a soles considerem un WC cada volta. La rellevància del primer és la inclusió de les possibles correlacions entre els WCs que poden tindre un impacte no menyspreable en els resultats finals (com resulta ser el cas en aquesta anàlisi). En el cas on es considera tan sols un coeficient de Wilson cada volta, aquestes correlacions es perden, el que resulta en restriccions més fortes que les que realment es poden extraure de les dades experimentals. Una comparació entre les dos tipus d'anàlisis es dona en la Fig. 7.2.
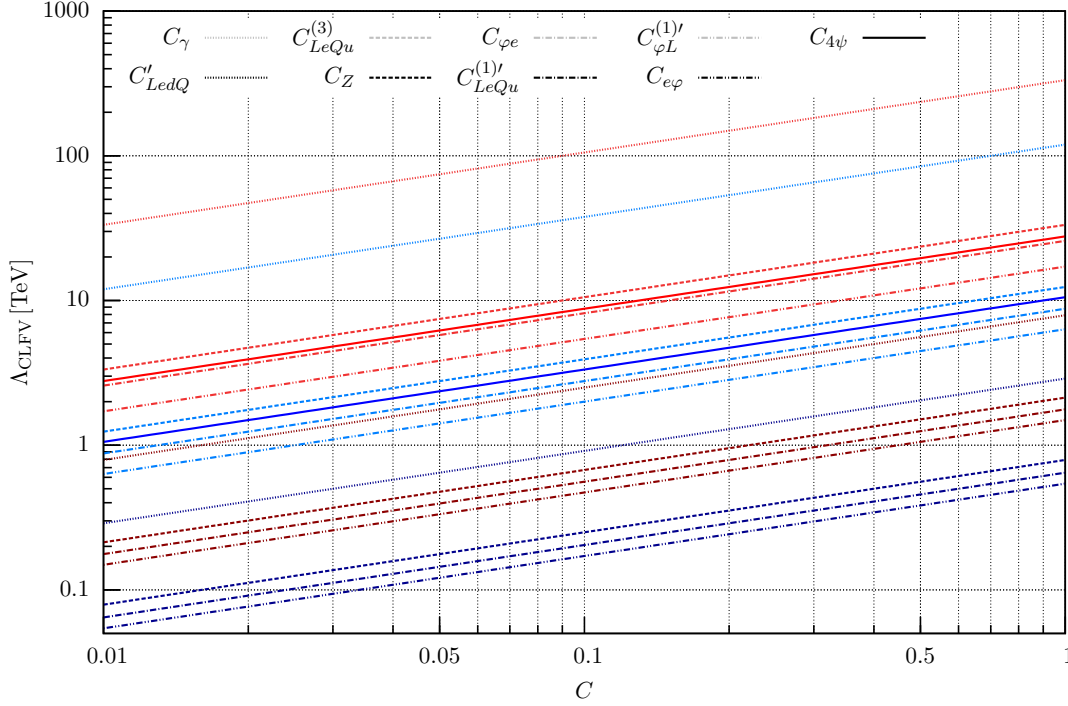
FIGURE 7.1:   Restriccions sobre Λ_{CLFV} respecte als valors dels WCs, basades en els límits actuals de Belle (tons en blau) i en els límits esperats de Belle II (tons en roig) i donades al $99.8\,\%$ nivell de confiança. Els WCs amb quatre fermions es representen en conjunt com a $C_{4\psi}$. Per a un conjunt donat de límits (distinguits per tons blaus i rojos), els tons més clars corresponen als WCs llistats en la fila de dalt de la llegenda (sense contar el comú als WCs amb 4 fermions $C_{4\psi}$), i els tons més obscurs corresponen als WCs de la fila de baix.

Finalment, al capítol 3 també mostrem les fortes restriccions sobre l'escala d'energia de nova física, que el límit actual (i esperat) de Belle (Belle II) sobre el procés $\tau \to \mu\gamma$ pot possar. En concret, el límit és sobre el paràmetre Λ associat a l'operador de dipol

$$\Lambda_{C_\gamma \approx 1} \gtrsim \begin{cases} 720\,\text{TeV [Belle]}\,, \\ 1100\,\text{TeV [Belle II]}\,. \end{cases} \tag{7.3.9}$$

Com es pot observar, l'estudi de processos de CLFV amb leptons tau és de gran rellevància, ja que poden constrenyir fortament l'espai de paràmetres de la teoria efectiva del Model Estàndard. En l'actualitat, Belle II ja està prenent dades i s'espera que millore els límits en, almenys, un ordre de magnitud. Finalment, hem estudiat la interrelació entre els decaïments hadrònics del tau i la conversió en nucli ℓ-τ i, encara que el segon procés encara no pot competir en sensibilitat amb el primer, trobem que en cas d'una millora d'un par d'ordres de magnitud, la conversió en nucli podria trencar les correlacions obtingudes dels límits de Belle i Belle II sobre els paràmetres de la SMEFT. Per tant, en cas de mesurar algun d'estos processos prohibits al SM, la conversió en nucli podria ajudar a discernir l'origen real de la nova física involucrada.
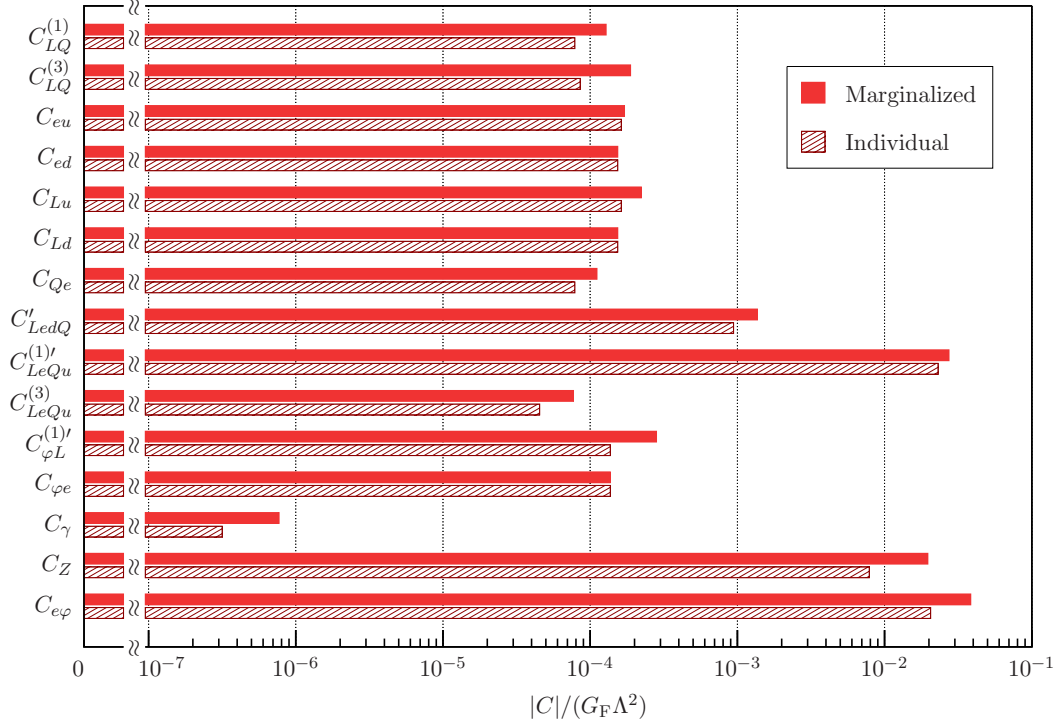
FIGURE 7.2: Valors permesos de $C/(G_F\Lambda^2)$, basat en els límits esperats de Belle II, on es comparen l'anàlisi marginalitzada i la individual per als decaïments hadrònics del tau. Els resultats es donen al 99% de nivell de confiança.

7.3.2 Leptoquarks

Al capítol 4 hem estudiat les contribucions del marc més genèric de leptoquarks als processos de CLFV amb leptons tau analitzats al capítol 3. Per a fer-ho es consideren els acoblaments dels leptoquarks a la matèria fermiònica del SM, als bosons gauge (γ i Z) i al Higgs. Trobem que les contribucions rellevants a estos observables ocorren a través dels acoblaments al contingut de matèria del SM i al photó i que, conseqüentment, els acoblaments al Z i al Higgs es poden menysprear de forma segura.

Per altra banda, degut a la gran quantitat de paràmetres lliures i al poc nombre de restriccions que tenim, separem l'anàlisi en dos escenaris: un on considerem tots els leptoquarks escalars al mateix temps i altre amb tots els leptoquarks vectorials. En ambós casos els leptoquarks són integrats i s'identifiquen els paràmetres del model amb els coeficients de Wilson, constrenyits anteriorment mitjançant els processos de CLFV amb taus.

Centrant-nos en el cas escalar (i considerant tots els leptoquars escalars al mateix temps en l'anàlisi) trobem les restriccions mostrades a la Taula 7.1. En aquesta taula es pot vore que el leptoquark que rep la restricció més forta és el S_3. No obstant, la majoria de leptoquarks escalars reben restriccions del mateix ordre, excepte per dos parells d'acoblaments de Yukawa que només són sensibles als límits de conversió en nucli de ℓ-τ i, per tant, reben restriccions més febles. L'anàlisi dels leptoquarks vectorials va donar resultats lleugerament més restrictius que els mostrats a la taula 7.1.

τ decays	Upper bounds on $\frac{\|yy'\|}{M_{\mathrm{S}}^2}$ $[10^{-3}\,\mathrm{TeV}^{-2}]$		Lower bounds on M_{S} [TeV]	
Yukawa pair	Belle	Belle II	Belle	Belle II
$\|y_3^{\mathrm{LL}} y_{3\,\tau}^{\mathrm{LL}}\|$	12	1.9	9.1	23
$\|y_2^{\mathrm{RL}} y_{2\,\tau}^{\mathrm{RL}}\|$	47	5.0	4.6	14
$\|y_2^{\mathrm{LR}} y_{2\,\tau}^{\mathrm{LR}}\|$	17	2.6	7.8	20
$\|y_2^{\mathrm{RL}} y_{2\,\tau}^{\mathrm{LR}}\|$	28	3.7	6.0	16
$\|\tilde{y}_2^{\mathrm{RL}} \tilde{y}_{2\,\tau}^{\mathrm{RL}}\|,\ \|\tilde{y}_1^{\mathrm{RR}} \tilde{y}_{1\,\tau}^{\mathrm{RR}}\|$	20	3.0	7.1	18
$\|y_1^{\mathrm{LL}} y_{1\,\tau}^{\mathrm{LL}}\|$	64	7.7	3.9	11
$\|y_1^{\mathrm{RR}} y_{1\,\tau}^{\mathrm{RR}}\|$	34	4.1	5.4	16
$\|y_1^{\mathrm{LL}} y_{1\,\tau}^{\mathrm{RR}}\|$	28	3.7	6.0	16

ℓ–τ conversion	Upper bounds on $\frac{\|yy'\|}{M_{\mathrm{S}}^2}$ $[10^{0}\,\mathrm{TeV}^{-2}]$		Lower bounds on M_{S} [TeV]	
Yukawa pair	e–τ	μ–τ	e–τ	μ–τ
$\|y_{2\,\tau}^{\mathrm{RL}} y_2^{\mathrm{LR}}\|$	350	2.3	0.054	0.66
$\|y_{1\,\tau}^{\mathrm{LL}} y_1^{\mathrm{RR}}\|$	250	1.8	0.063	0.75

TABLE 7.1: Límits obtinguts dels resultats presentats al capítol 3 per a l'escenari amb leptoquarks escalars. En la part esquerra de la taula presentem límits superiors en la relació $|yy'|/M_{\mathrm{S}}^2$; aquests números també corresponen a (amb la potència apropiada de 10) límits superiors en els parells de Yukawes $|yy'|$, assumint $M_{\mathrm{S}} = 1\,\mathrm{TeV}$. A la dreta, hi ha límits inferiors en l'escala d'energia provada dels leptoquarks escalars que medien els fenòmens de CLFV ($\Lambda_{\mathrm{CLFV}} = M_{\mathrm{S}}$), considerant $|yy'| \approx 1$. Es mostren els límits més forts, la majoria dels quals sorgeixen de l'anàlisi dels decaïments del tau (resultats de Belle i Belle II), amb les dos últimes files dedicades als Yukawes que només contribuixen a la conversió en nucli ℓ–τ sent l'excepció. Els valors es donen al 99.8 nivell de confiança.

Finalment, l'operador dipolar que a l'anàlisi del capítol 3 va rebre la restricció més forta, una volta es calcula la contribució dels leptoquarks a l'ordre predominant (que degut a l'acoblament dels leptoquarks al fotó ocorre a ordre de bucle), permet millorar, a nivell comparable amb les altres, les restriccions sobre els dos parells de Yukawes que, d'altra forma, reben restriccions molt fluixes del límits de conversió en nucli de taus.

7.3.3 Dispersió coherent i elàstica de neutrins en nuclis

En aquest treball, tot i que l'anàlisi s'està acabant encara i els resultats són preliminars, podem destacar diversos aspectes importants.

Per una banda, la importància de caracteritzar bé dins del formalisme de teoria quàntica de camps les oscil·lacions de neutrins. Hem vist que a l'experiment CO-HERENT (o qualsevol experiment on les neutrins es produïsquen mitjançant interaccions de corrent carregada i es detecten via corrents neutres), en el càlcul del número d'esdeveniments observats, emprant el nostre formalisme es dona una barretja entre els coeficients (no diagonals en sabor) de nova física en producció i detecció (a segon ordre en aquests) que conté elements no presents quan s'utilitza un enfocament del

mateix càlcul basat en la factorització (usual) de (flux de neutrins)×(secció eficaç). Aquest resultat es veu de forma explícita quan comparem les dos equacions per al resultat del número d'esdeveniments esperats en COHERENT. Per exemple, per als neutrins provinents del decaïment del pió obtenim en el nostre formalisme:

$$\frac{dN_{\nu_\mu}}{dT} = n_{\text{POT}} r_{\nu/p} \frac{N_T M_\mathcal{N} G_F}{4\pi L^2} \left(1 - \frac{M_N T}{2(E_\nu^\pi)^2} - \frac{T}{E_\nu^\pi}\right) \sum_{\beta,\beta'} [\mathcal{P}]_{\mu\beta} \left[\mathcal{Q}^\dagger \mathcal{Q}\right]_{\beta\beta'} \left[\mathcal{P}^\dagger\right]_{\beta'\mu},$$
$$(7.3.10)$$

on hem recollit els paràmetres de nova física dins de les peces de producció ($\mathcal{P}$) i detecció ($\mathcal{Q}$). Aquest resultat s'ha de comparar amb el cas de la factorització:

$$\frac{dN_{\nu_\mu}}{dT} = n_{\text{POT}} r_{\nu/p} \frac{N_T M_\mathcal{N} G_F}{4\pi L^2} \left(1 - \frac{M_N T}{2(E_\nu^\pi)^2} - \frac{T}{E_\nu^\pi}\right) \sum_{\beta,\beta'} [\mathcal{P}]_{\mu\beta} \left[\mathcal{Q}^\dagger \mathcal{Q}\right]_{\beta\beta'} \left[\mathcal{P}^\dagger\right]_{\beta'\mu} \delta_{\beta\beta'},$$
$$(7.3.11)$$

on explícitament es veu que el terme amb la delta fa que no apareixen termes en la suma sobre β i β' que, en canvi, en l'Eq. (7.3.10) si estan.

Per altra banda, és important també l'exemple que posa l'experiment COHER-ENT sobre la importància de l'elecció de l'esquema de dades d'entrada, que hem comentat en la secció 7.2.2. En aquest cas, la contaminació de la nova física en els paràmetres observats del SM fa que, al corregir-la, es perda (pràcticament) la sensibilitat de l'experiment sobre els paràmetres de producció.

Finalment, destacar la importància d'incloure en l'anàlisi estadístic les distribu-cions energètiques i temporals del número d'esdeveniments observat en COHER-ENT. Sense aquestes distribucions, tan sols seríem sensibles a una combinació gen-eral dels paràmetres de nova física que entren en el càlcul. Gràcies a la combinació de les dos distribucions podem constrenyir diverses direccions en l'espai de paràmetres, les quals agrupem al capítol 5 com a càrregues febles modificades, en comparació a l'única càrrega feble present al Model Estàndard.

7.3.4   Model lineal de balancí i neutrins Quasi-Dirac

Al capítol 6 expliquem que el règim Quasi-Dirac dels neutrins pesats introduïts en el model lineal de balancí, es pot parametritzar mitjançant la relació entre el número d'esdeveniments $\ell\ell jj$, on ℓ es refereix a un leptó i j a un jet hadrònic (provinent de quarks), amb mateix signe i signe oposat i sense p_T no mesurat. A aquest observable se'l sol designar com $R_{\ell\ell}$. En el model lineal de balancí trobem que aquesta quantitat depén de la diferència de masses entre els dos neutrins pesats ΔM i la seua amplada de decaïment Γ (que és pràcticament la mateixa per als dos neutrins degut a la xicoteta diferència entre les seues masses) de la forma:

$$R_{\ell\ell} = \frac{\Delta M^2}{2\Gamma^2 + \Delta M^2}.$$
$$(7.3.12)$$

Per una banda, en aquest model se satisfà la relació $\Delta M_i \sim m_{\nu_i}$, on m_{ν_i} és la massa del neutrí lleuger i. Per l'altra, l'amplada de decaïment depén tant de la massa del neutrí pesat M_{N_1}, com de les mescles entre els neutrins pesats i lleugers

$U_{N_i\ell}$, on ℓ aquí marca el sabor del neutrí lleuger. Aquestes últimes venen donades tant per la massa dels neutrins lleugers com per l'ajust que implementem amb la parametrització màster explicada en la secció 7.2.3 dalt. En l'anàlisi estudiem dos escenaris ben motivats dins d'aquesta parametrització màster, els quals abasten tot l'espai rellevant de paràmetres. Cadascú introdueix un paràmetre extra: f' i g. Així, les mescles de dalt depenen també d'una d'estes dos quantitats. Per tant, l'observable $R_{\ell\ell}$ que controla el caràcter QD del neutrins pesats depén de tres paràmetres: M_{N_1}, la massa dels neutrins lleugers m_{ν_i} (que es poden reduir, mitjançant els valors mesurats de les diferencies de les masses al quadrat, a la dependència de tan sols la massa del neutrí més lleuger m_{ν_1}) i f' o g, depenent de l'escenari estudiat. En base a aquesta discussió, fem un escaneig en l'espai de paràmetres per a diversos valors de $R_{\ell\ell}$ i trobem les regions Quasi-Dirac (per a $R_{\ell\ell} \in [0.1, 0.9]$) mostrades a la Fig. 7.3. No obstant, s'ha de tindre en compte que la regió QD és un continu.
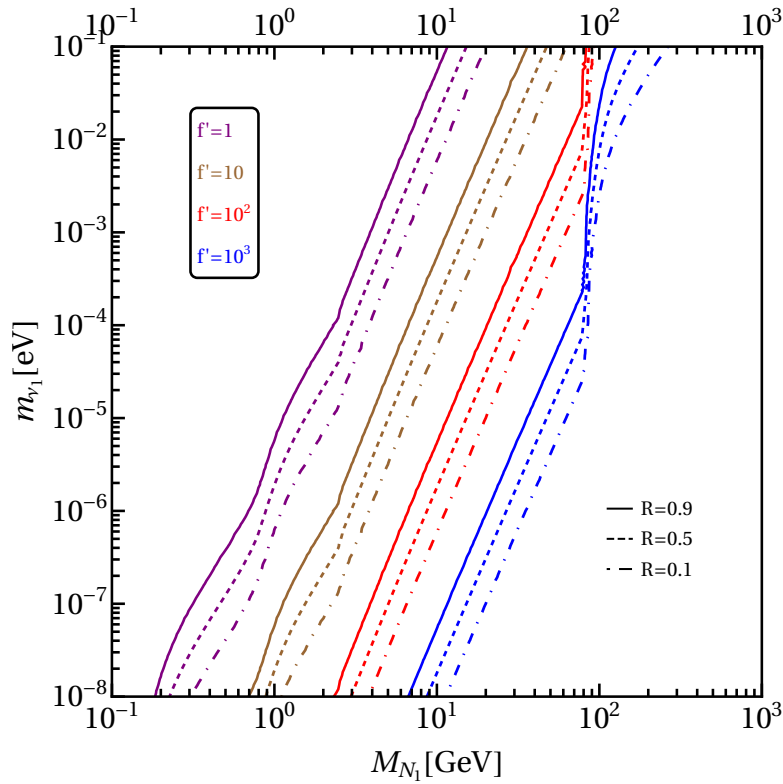
FIGURE 7.3: Línies m_{ν_1}–M_{N_1} corresponents a un valor específic de $R_{\ell\ell}$ i f'. Per a cada color, les tres línies corresponen a valors de $R_{\ell\ell} = 0.9$, 0.5 i 0.1 d'esquerra a dreta.

Al mateix capítol duem a terme una anàlisi fenomenològica en base als millors límits actuals i a les sensibilitats projectades d'experiments com ANUBIS, MATH-USLA, SHip, DUNE, FASER2, FCC-ee o AL3, per constrenyir el pla rellevant $|U_{N_1\ell}|^2$–M_{N_1} (búsquedes de processos de violació de sabor leptònic com $\mu \to e\gamma$ o de violació de número leptònic com neutrinoless double beta decay, es mostren com a no competitius en comparació). Els resultats de l'anàlisi es mostren en la

Fig. 7.4. Finalment, discutim com, estudiant la interrelació de les Figs. 7.3 i 7.4, els límits experimentals poden constrenyir també la regió Quasi-Dirac.
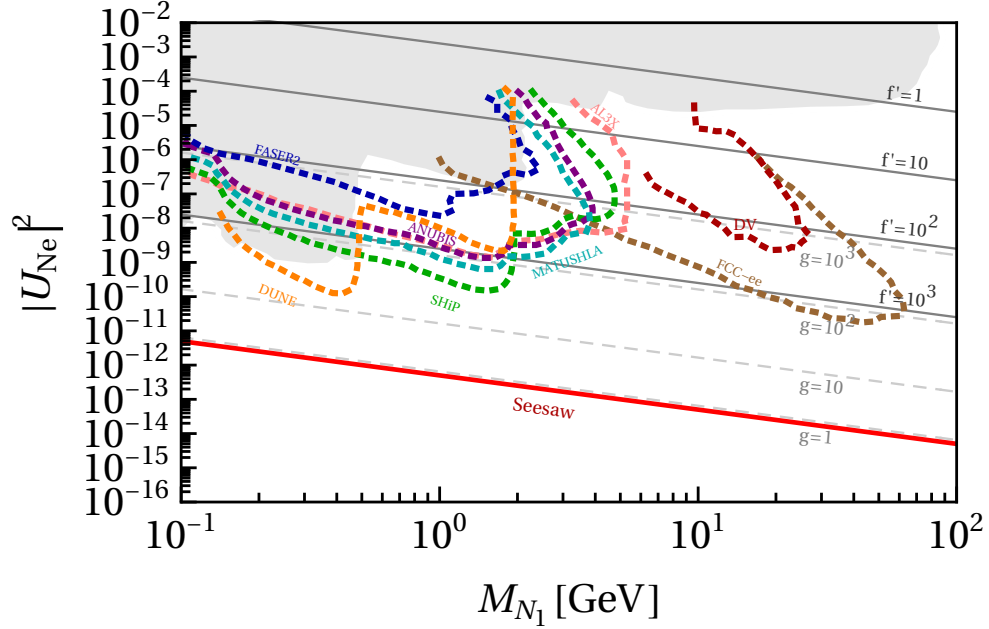
FIGURE 7.4: Barretja entre neutrins actius i estèrils $|U_{N_1 e}|^2$ versus la massa del neutrí pesat M_{N_1}, per a diferents valors dels paràmetres f' i g. Les línies de ratlles corresponen a les sensibilitats projectades d'experiments futurs, mentre que l'àrea sombrejada de gris indica la regió exclosa per les búsquedes actuals com es mostra en la Ref. [409]. La línia roja sòlida representa el model vanilla de balancí.

Appendix A

Nonets of resonances

Resonances are introduced by

$$R = \sum_{i=0}^{8} \frac{\lambda_i}{\sqrt{2}} \varphi_i \tag{A.0.1}$$

where the φ_i are taken from the phenomenologically observed resonances [48] and λ_i are the Gell-Mann matrices with $\lambda_0 = \sqrt{\frac{2}{n_f}} I_{n_f \times n_f}$, where $I_{n_f \times n_f}$ is the $n_f \times n_f$ identity matrix.

A.1   Scalar $(J^{PC} = 0^{++})$

There is still an ongoing discussion about the identification of the lowest-lying nonet of scalar resonances that survive in the large-N_C limit. We follow the work of Ref. [49] and choose the massive nonet $S_H = \{f_0(1370), K_0^*(1430), a_0(1450), f_0(1500)\}$:

$$S = \sum_{i=0}^{8} \frac{\lambda_i}{\sqrt{2}} \varphi_i = \begin{pmatrix} \frac{1}{\sqrt{2}} a_0^0 + \frac{1}{\sqrt{6}} f_0^8 + \frac{1}{\sqrt{3}} f_0^0 & a_0^+ & K_0^{*+} \\ a_0^- & -\frac{1}{\sqrt{2}} a_0^0 + \frac{1}{\sqrt{6}} f_0^8 + \frac{1}{\sqrt{3}} f_0^0 & K_0^{*0} \\ K_0^{*-} & \bar{K}_0^{*0} & -\frac{2}{\sqrt{6}} f_0^8 + \frac{1}{\sqrt{3}} f_0^0 \end{pmatrix}. \tag{A.1.2}$$

We consider no mixing between the light octet $f_0^8 = f_0(1370)$ and the heavy singlet $f_0^0 = f_0(1500)$.

A.2   Pseudoscalar $(J^{PC} = 0^{-+})$

The identification of the pseudoscalar nonet of resonances is as follows:

$$P = \sum_{i=0}^{8} \frac{\lambda_i}{\sqrt{2}} \varphi_i = \begin{pmatrix} \frac{1}{\sqrt{2}} \pi_p^0 + \frac{1}{\sqrt{6}} \eta_p^8 + \frac{1}{\sqrt{3}} \eta_p^0 & \pi_p^+ & K_p^+ \\ \pi_p^- & -\frac{1}{\sqrt{2}} \pi_p^0 + \frac{1}{\sqrt{6}} \eta_p^8 + \frac{1}{\sqrt{3}} \eta_p^0 & K_p^0 \\ K_p^- & \bar{K}_p^0 & -\frac{2}{\sqrt{6}} \eta_p^8 + \frac{1}{\sqrt{3}} \eta_p^0 \end{pmatrix}. \tag{A.2.3}$$

We consider no mixing between the light octet $\eta_p^8 = \eta(1295)$ and the heavy singlet $\eta_p^0 = \eta(1405)$.

A.3 Vectorial ($J^{PC} = 1^{--}$)

We use the antisymmetric tensor description of massive spin-1 fields [41]

$$V_{\mu\nu} = \sum_{i=0}^{8} \frac{\lambda_i}{\sqrt{2}} \varphi^i_{\mu\nu} = \begin{pmatrix} \frac{1}{\sqrt{2}}\rho^0 + \frac{1}{\sqrt{6}}\rho^8 + \frac{1}{\sqrt{3}}\rho^1 & \rho^+ & K^{*+} \\ \rho^- & -\frac{1}{\sqrt{2}}\rho^0 + \frac{1}{\sqrt{6}}\rho^8 + \frac{1}{\sqrt{3}}\rho^1 & K^{*0} \\ K^{*-} & \bar{K}^{*0} & -\frac{2}{\sqrt{6}}\rho^8 + \frac{1}{\sqrt{3}}\rho^1 \end{pmatrix}_{\mu\nu},$$

$$\text{(A.3.4)}$$

with the following mixing:

$$\begin{pmatrix} \rho^8_{\mu\nu} \\ \rho^1_{\mu\nu} \end{pmatrix} = \begin{pmatrix} \cos\theta_V & \sin\theta_V \\ -\sin\theta_V & \cos\theta_V \end{pmatrix} \begin{pmatrix} \phi_{\mu\nu} \\ \omega_{\mu\nu} \end{pmatrix}, \qquad \text{(A.3.5)}$$

where $\phi_{\mu\nu} = \phi(1020)$ and $\omega_{\mu\nu} = \omega(782)$. We consider ideal mixing: $\theta_V \sim 35^{\text{o}} \longrightarrow \cos\theta_V = \sqrt{2/3}, \sin\theta_V = \sqrt{1/3}$.

A.4 Axial ($J^{PC} = 1^{++}$)

We use again the antisymmetric tensor description of massive spin-1 fields [41]

$$A_{\mu\nu} = \sum_{i=0}^{8} \frac{\lambda_i}{\sqrt{2}} \varphi^i_{\mu\nu} = \begin{pmatrix} \frac{1}{\sqrt{2}}a_1^0 + \frac{1}{\sqrt{6}}f_1^8 + \frac{1}{\sqrt{3}}f_1^0 & a_1^+ & K_1^+ \\ a_1^- & -\frac{1}{\sqrt{2}}a_1^0 + \frac{1}{\sqrt{6}}f_1^8 + \frac{1}{\sqrt{3}}f_1^0 & K_1^0 \\ K_1^- & \bar{K}_1^0 & -\frac{2}{\sqrt{6}}f_1^8 + \frac{1}{\sqrt{3}}f_1^0 \end{pmatrix}_{\mu\nu}.$$

$$\text{(A.4.6)}$$

We consider no mixing between the light octet $f_1^8 = f_1(1285)$ and the heavy singlet $f_1^0 = f_1(1420)$.

A.5 Tensorial ($J^{PC} = 2^{++}$)

Spin-2 particles can only be described by symmetric tensor fields [46], the corresponding resonance nonet identification is:

$$T_{\mu\nu} = \sum_{i=0}^{8} \frac{\lambda_i}{\sqrt{2}} \varphi^i_{\mu\nu} = \begin{pmatrix} \frac{1}{\sqrt{2}}a_2^0 + \frac{1}{\sqrt{6}}f_2^8 + \frac{1}{\sqrt{3}}f_2^0 & a_2^+ & K_2^{*+} \\ a_2^- & -\frac{1}{\sqrt{2}}a_2^0 + \frac{1}{\sqrt{6}}f_2^8 + \frac{1}{\sqrt{3}}f_2^0 & K_2^{*0} \\ K_2^{*-} & \bar{K}_2^{*0} & -\frac{2}{\sqrt{6}}f_2^8 + \frac{1}{\sqrt{3}}f_2^0 \end{pmatrix}_{\mu\nu}.$$

$$\text{(A.5.7)}$$

We consider no mixing between the light octet $f_2^8 = f_2(1270)$ and the heavy singlet $f_2^0 = f_2(1430)$.

Appendix B

Numerical inputs

In this appendix, we collect the numerical inputs for our calculations: due to the hadronic incertitudes, we explain our choices for the related parameters; for the rest we take the PDG values [48].

For the masses of the hadrons, we take the values listed in Tab. B.1: for the pseudoscalar mesons, we take the isospin-averaged values. For the vectorial resonances, we take masses from Ref. [48]. For the rest of the resonances, we then consider a single mass for the whole multiplet chosen as the mass of the associated isotriplet.

m_π	m_K	m_η	$m_{\eta'}$	M_S	M_P	M_T
0.138	0.496	0.548	0.958	1.450	1.3	1.320

TABLE B.1: Masses (given in GeV) for the pseudoscalars and resonances.

Our knowledge of the hadron couplings in the RχT Lagrangian is rather sketchy. This is due to our poor insight about the final-state interactions, so relevant in strong processes. We use the values from Tab. B.2 together with the relations (2.4.56). It remains to comment on the γ coupling in the spin-2 resonance Lagrangian (2.4.50): there is no information on this coupling. However, we notice that its numerical relevance is rather suppressed since it accompanies the masses of the pseudoscalar mesons. Therefore, its specific value is not relevant in the numerical computations. For definiteness, we take $\gamma = \beta$.

F [GeV] [48]	F_V [GeV] [411]	c_d [GeV] [412]	g_T [GeV] [46, 412]	T_V (GeV^2)
0.092	0.206	0.030	0.028	0.115

TABLE B.2: Couplings involving hadron resonances. Their justification is based on the quoted references. For the value of T_V see the discussion at the end of Section 2.4.4.

We consider now the mixing angle between the octet (η_8) and singlet (η_0) strong-interaction eigenstates of the pseudoscalar meson multiplet giving the η and η' physical states. We define this angle via the following relation:

$$\left(\begin{array}{c} \eta \\ \eta' \end{array} \right) = \left(\begin{array}{cc} \cos\theta_P & -\sin\theta_P \\ \sin\theta_P & \cos\theta_P \end{array} \right) \left(\begin{array}{c} \eta_8 \\ \eta_0 \end{array} \right), \qquad (B.0.1)$$

and take $\theta_P = -20°$ arising in the large-N_C analyses [413, 414]. Finally, we define the analogous mixing angle for the vector resonances as

$$\begin{pmatrix} \phi(1020) \\ \omega(782) \end{pmatrix} = \begin{pmatrix} \cos\theta_V & -\sin\theta_V \\ \sin\theta_V & \cos\theta_V \end{pmatrix} \begin{pmatrix} V_8 \\ V_0 \end{pmatrix}. \tag{B.0.2}$$

We consider ideal mixing $\theta_V = 35°$.

Appendix C

Amplitudes generated by $d = 6$ operators

The $d = 6$ operators [58] of the SMEFT Lagrangian that are noninvariant under $U(1)_e \times U(1)_\mu \times U(1)_\tau$ rotations of the lepton fields while keeping the diagonal $U(1)_L$ symmetry (conserving the overall lepton number) generate CLFV processes. Within this setting, operators listed in Table 3.1 generate tree level and also some particular 1-loop amplitudes to those processes. The latter have been considered by other authors and we also include them in our study. All the relevant amplitudes are collected in this appendix.

C.1 The tree-level amplitudes for $\tau^- \to \ell^- \bar{q}q$ and $\ell^- q \to \tau^- q$, with $\ell = e, \mu$

The amplitudes for these processes with light quarks in the final state, namely $q = u, d, s$, can be divided into four structures:

$$\mathcal{M}_{\text{tree}} = \mathcal{M}_{\text{loc}} + \mathcal{M}_Z + \mathcal{M}_\gamma + \mathcal{M}_H. \tag{C.1.1}$$

$\mathcal{M}_{\text{loc}}$ corresponds to the contributions of four-fermion local operators (like those shown in Figs. 3.5(a) or 3.7(a)) and consists of the following matrix elements stemming from the respective operators (here we show the matrix elements for the $\ell_2 q \to \ell_1 q$ process; for different configurations, see the end of this section):

$$\mathcal{M}_{LQ}^{(1)} = \frac{C_{LQ}^{(1)}}{\Lambda_{\text{CLFV}}^2} [\bar{u}_{\ell_1} \gamma_\mu P_L u_{\ell_2}][(\bar{u}_u \gamma^\mu P_L u_u) + (\bar{u}_{d_x} \gamma^\mu P_L u_{d_x})],$$

$$\mathcal{M}_{LQ}^{(3)} = \frac{C_{LQ}^{(3)}}{\Lambda_{\text{CLFV}}^2} [\bar{u}_{\ell_1} \gamma_\mu P_L u_{\ell_2}][-(\bar{u}_u \gamma^\mu P_L u_u) + (\bar{u}_{d_x} \gamma^\mu P_L u_{d_x})],$$

$$\mathcal{M}_{eu} = \frac{C_{eu}}{\Lambda_{\text{CLFV}}^2} [\bar{u}_{\ell_1} \gamma_\mu P_R u_{\ell_2}][\bar{u}_u \gamma^\mu P_R u_u],$$

$$\mathcal{M}_{ed} = \frac{C_{ed}}{\Lambda_{\text{CLFV}}^2} [\bar{u}_{\ell_1} \gamma_\mu P_R u_{\ell_2}][\bar{u}_{d_x} \gamma^\mu P_R u_{d_x}],$$

$$\mathcal{M}_{Lu} = \frac{C_{Lu}}{\Lambda_{\text{CLFV}}^2} [\bar{u}_{\ell_1} \gamma_\mu P_L u_{\ell_2}][\bar{u}_u \gamma^\mu P_R u_u],$$

$$\mathcal{M}_{Ld} = \frac{C_{Ld}}{\Lambda_{\text{CLFV}}^2}[\bar{u}_{\ell_1}\gamma_\mu P_L u_{\ell_2}][\bar{u}_{d_x}\gamma^\mu P_R u_{d_x}]\,, \tag{C.1.2}$$

$$\mathcal{M}_{Qe} = \frac{C_{Qe}}{\Lambda_{\text{CLFV}}^2}[\bar{u}_{\ell_1}\gamma_\mu P_R u_{\ell_2}][(\bar{u}_u\gamma^\mu P_L u_u) + (\bar{u}_{d_x}\gamma^\mu P_L u_{d_x})]\,,$$

$$\mathcal{M}_{LedQ} = \frac{C_{LedQ}}{\Lambda_{\text{CLFV}}^2}\left\{[\bar{u}_{\ell_1}P_R u_{\ell_2}][\bar{u}_{d_x}P_L u_{d_x}] + [\bar{u}_{\ell_1}P_L u_{\ell_2}][\bar{u}_{d_x}P_R u_{d_x}]\right\}\,,$$

$$\mathcal{M}_{LeQu}^{(1)} = -\frac{C_{LeQu}^{(1)}}{\Lambda_{\text{CLFV}}^2}\left\{[\bar{u}_{\ell_1}P_R u_{\ell_2}][\bar{u}_u P_R u_u] + [\bar{u}_{\ell_1}P_L u_{\ell_2}][\bar{u}_u P_L u_u]\right\}\,,$$

$$\mathcal{M}_{LeQu}^{(3)} = -\frac{C_{LeQu}^{(3)}}{\Lambda_{\text{CLFV}}^2}\left\{[\bar{u}_{\ell_1}\sigma_{\mu\nu}P_R u_{\ell_2}][\bar{u}_u\sigma^{\mu\nu}P_R u_u] + [\bar{u}_{\ell_1}\sigma_{\mu\nu}P_L u_{\ell_2}][\bar{u}_u\sigma^{\mu\nu}P_L u_u]\right\}\,.$$

$\mathcal{M}_Z$ and $\mathcal{M}_\gamma$ encode the contributions mediated by Z and γ bosons, respectively, i.e. the processes $\tau \to \ell\{Z, \gamma\}$, followed by $\{Z, \gamma\} \to \bar{q}q$ (Figs. 3.5(b) and 3.7(b)):

$$\mathcal{M}_{\varphi e} = \frac{C_{\varphi e}M_Z^2}{\Lambda_{\text{CLFV}}^2}[\bar{u}_{\ell_1}\gamma^\mu P_R u_{\ell_2}]\frac{(-g_{\mu\nu} + q_\mu q_\nu/M_Z^2)}{q^2 - M_Z^2}$$
$$\times\left\{[\bar{u}_u\gamma^\nu(v_u - a_u\gamma_5)u_u] + [\bar{u}_{d_x}\gamma^\nu(v_d - a_d\gamma_5)u_{d_x}]\right\}\,,$$

$$\mathcal{M}_{\varphi L}^{(1)} = \frac{C_{\varphi L}^{(1)}M_Z^2}{\Lambda_{\text{CLFV}}^2}[\bar{u}_{\ell_1}\gamma^\mu P_L u_{\ell_2}]\frac{(-g_{\mu\nu} + q_\mu q_\nu/M_Z^2)}{q^2 - M_Z^2}$$
$$\times\left\{[\bar{u}_u\gamma^\nu(v_u - a_u\gamma_5)u_u] + [\bar{u}_{d_x}\gamma^\nu(v_d - a_d\gamma_5)u_{d_x}]\right\}\,,$$

$$\mathcal{M}_{\varphi L}^{(3)} = \frac{C_{\varphi L}^{(3)}M_Z^2}{\Lambda_{\text{CLFV}}^2}[\bar{u}_{\ell_1}\gamma^\mu P_L u_{\ell_2}]\frac{(-g_{\mu\nu} + q_\mu q_\nu/M_Z^2)}{q^2 - M_Z^2}$$
$$\times\left\{[\bar{u}_u\gamma^\nu(v_u - a_u\gamma_5)u_u] + [\bar{u}_{d_x}\gamma^\nu(v_d - a_d\gamma_5)u_{d_x}]\right\}\,,$$

$$\mathcal{M}_{eB}^{(Z)} = \frac{i\,C_{eB}s_W M_Z}{\sqrt{2}\Lambda_{\text{CLFV}}^2}[\bar{u}_{\ell_1}\sigma^{\mu\nu}u_{\ell_2}]\frac{\Omega_{\mu\nu\alpha}}{q^2 - M_Z^2}$$
$$\times\left\{[\bar{u}_u\gamma^\alpha(v_u - a_u\gamma_5)u_u] + [\bar{u}_{d_x}\gamma^\alpha(v_d - a_d\gamma_5)u_{d_x}]\right\}\,,$$

$$\mathcal{M}_{eW}^{(Z)} = \frac{i\,C_{eW}c_W M_Z}{\sqrt{2}\Lambda_{\text{CLFV}}^2}[\bar{u}_{\ell_1}\sigma^{\mu\nu}u_{\ell_2}]\frac{\Omega_{\mu\nu\alpha}}{q^2 - M_Z^2}$$
$$\times\left\{[\bar{u}_u\gamma^\alpha(v_u - a_u\gamma_5)u_u] + [\bar{u}_{d_x}\gamma^\alpha(v_d - a_d\gamma_5)u_{d_x}]\right\}\,,$$

$$\mathcal{M}_{eB}^{(\gamma)} = -\frac{i\,C_{eB}}{\Lambda_{\text{CLFV}}^2}\sqrt{2}s_W c_W^2 M_Z Q_q[\bar{u}_{\ell_1}\sigma^{\mu\nu}u_{\ell_2}]\frac{\Omega_{\mu\nu\alpha}}{q^2}\left\{[\bar{u}_u\gamma^\alpha u_u] + [\bar{u}_{d_x}\gamma^\alpha u_{d_x}]\right\}\,,$$

$$\mathcal{M}_{eW}^{(\gamma)} = \frac{i\,C_{eW}}{\Lambda_{\text{CLFV}}^2}\sqrt{2}s_W^2 c_W M_Z Q_q[\bar{u}_{\ell_1}\sigma^{\mu\nu}u_{\ell_2}]\frac{\Omega_{\mu\nu\alpha}}{q^2}\left\{[\bar{u}_u\gamma^\alpha u_u] + [\bar{u}_{d_x}\gamma^\alpha u_{d_x}]\right\}\,. \tag{C.1.3}$$

Note that we have separated the contribution of the operators $\mathcal{O}_{eB}$ and $\mathcal{O}_{eW}$ into those governed by the photon and the Z boson. In Eqs. (C.1.2) and (C.1.3), $c_W = \cos\theta_W$ and $s_W = \sin\theta_W$ are the trigonometric functions of the weak mixing angle and the index x at the d spinors refers to the first or second family, i.e. $d_x \in \{d, s\}$: note that in $\mathcal{M}_{\text{loc}}$ we assume that there are no FCNCs in the quark

bilinears. Further, we also used $P_{L,R} = \frac{1}{2}(1 \mp \gamma_5)$,

$$\Omega_{\mu\nu\alpha} = q_\mu \, g_{\nu\alpha} - q_\nu \, g_{\mu\alpha} \,, \tag{C.1.4}$$

and the SM weak couplings are

$$
\begin{aligned}
v_u &= \frac{1}{2} - \frac{4}{3} s_W^2 \,, & v_d &= -\frac{1}{2} + \frac{2}{3} s_W^2 \,, \\
a_u &= \frac{1}{2} \,, & a_d &= -\frac{1}{2} \,.
\end{aligned}
\tag{C.1.5}
$$

Finally, $\mathcal{M}_H$ corresponds to the intermediate-Higgs contribution: $\tau \to \ell H$, $H \to \bar{q}q$ (Figs. 3.5(c) and 3.7(c)). This is driven by $\mathcal{O}_{e\varphi}$ and by the Higgs–quark–quark coupling in $\mathcal{L}_{\text{eff}}$ that we have obtained in Eq. (D.1.6). As we are considering $m_u = m_d = 0$ and $m_s \neq 0$, we only have contribution to $\tau \to \ell\bar{s}s$ given by

$$\mathcal{M}_H = \frac{C_{e\varphi}}{\Lambda_{\text{CLFV}}^2} \frac{7v}{6\sqrt{2}} \frac{1}{(q^2 - M_H^2)} [\bar{u}_{\ell_1} u_{\ell_2}] \, m_s \bar{u}_s u_s \,, \tag{C.1.6}$$

with $v = (\sqrt{2} G_F)^{-1/2}$, which correspond to diagrams (c) in Figs. 3.5 and 3.7. Our results in Eqs. (C.1.2), (C.1.3) and (C.1.6) are relevant for both $\tau \to \ell\bar{q}q$ and $\ell q \to \tau q$, changing the u to v spinors appropriately and applying the following choices:

- For $\tau(k) \to \ell(k')\bar{q}(p')q(p)$, $\ell_1 = \ell$ and $\ell_2 = \tau$, with $q = k - k' = p + p'$.

- For $\ell(k)q(p) \to \tau(k')q(p')$, $\ell_1 = \tau$ and $\ell_2 = \ell$, with $q = k - k' = p' - p$.

C.2 The one-loop amplitude for $\boldsymbol{\tau^- \to \ell^- gg}$, with $\boldsymbol{\ell = e, \mu}$

We consider the gluon-involved contribution to the $\tau^- \to \ell^- \bar{P}P$ process (P stands for a pseudoscalar meson) upon hadronization of the two gluons from the $\tau^- \to \ell^- gg$ amplitude that, as pointed out in Ref. [154], can be represented via the dominant Higgs-exchange contribution shown in Fig. 3.6. The associated matrix element is generated by operator $\mathcal{O}_{e\varphi}$ from Table 3.1, together with the part of Eq. (D.1.6) related to the energy–momentum tensor that arises, essentially, from the gluon final state through the trace anomaly of QCD, as explained in Section D.1. The matrix element for the hadronization into a $\overline{P}P$ pair of pseudoscalar mesons reads

$$\mathcal{M}_{\tau gg} = \frac{C_{e\varphi}}{\Lambda_{\text{CLFV}}^2} \frac{v}{3\sqrt{2}} \frac{1}{(q^2 - M_H^2)} [\bar{u}_\ell \, u_\tau] \, \theta_P(q^2) \,, \tag{C.2.7}$$

where $\theta_P(q^2) \equiv \langle \, \overline{P}(p') \, P(p) \, | \, \theta_\mu^\mu \, | \, 0 \, \rangle$ and $q = p + p'$.

C.3 The one-loop amplitude for $\boldsymbol{\ell^- g \to \tau^- g}$, with $\boldsymbol{\ell = e, \mu}$

We include two one-loop diagrams contributing to the ℓ–τ conversion process; see Fig. 3.8. The Higgs contribution was already considered in Ref. [142], where it was claimed to represent the dominant Higgs amplitude to this process; in addition, we

consider the Z contribution. The peculiarities of the loop part of those diagrams are discussed in detail in Appendix D. The matrix element for the Higgs contribution to the $\ell g(p) \to \tau g(p')$ amplitude is

$$\mathcal{M}_{Hl} = \frac{C_{e\varphi}}{\Lambda^2_{\text{CLFV}}} \frac{3\,v}{\sqrt{2}} \left[\bar{u}_\tau u_\ell\right] \frac{g_{Hgg}}{q^2 - M_H^2} \left[q^2 g_{\mu\nu} - 2 p'_\mu p_\nu\right] \varepsilon_a^\mu(p)\,\varepsilon_a^{*\nu}(p')\,, \qquad \text{(C.3.8)}$$

where

$$g_{Hgg} = \sum_{Q=c,b,t} \frac{\alpha_S}{2\,\pi} \frac{m_q^2}{q^2} \left[1 - \frac{q^2}{2}\left(1 - \frac{4\,m_q^2}{q^2}\right) C_0(q^2, m_q^2)\right]. \qquad \text{(C.3.9)}$$

Above, the sum runs over the heavy quarks only (namely $Q = c, b, t$), $q = p' - p$ and $C_0(q^2, m_q^2)$ is given by Eq. (D.2.8). Notice that in Eq. (C.3.8) there is a sum over the color (a) in the gluon polarizations. The matrix element for the Z contribution is

$$
\begin{aligned}
\mathcal{M}_{Zl} = {} & \left(\frac{C_{\varphi e}}{\Lambda^2_{\text{CLFV}}}\left[\bar{u}_\tau \gamma_\sigma P_{\text{R}}\,u_\ell\right] + \left(\frac{C_{\varphi L}^{(1)}}{\Lambda^2_{\text{CLFV}}} + \frac{C_{\varphi L}^{(3)}}{\Lambda^2_{\text{CLFV}}}\right)\left[\bar{u}_\tau \gamma_\sigma P_{\text{L}}\,u_\ell\right]\right) \\
& \times \frac{\alpha_S}{\pi}\frac{q^\sigma}{q^2} \varepsilon_{\alpha\beta\mu\nu}\,q^\alpha\,(p+p')^\beta\,\varepsilon_a^\mu(p)\,\varepsilon_a^{*\nu}(p') \sum_q I^3_{\text{w},q}\,m_q^2\,C_0(q^2, m_q^2)\,,
\end{aligned}
\qquad \text{(C.3.10)}
$$

where the sum now runs over all quark flavors and $I^3_{\text{w},q} = \pm\frac{1}{2}$ is the quark weak isospin (eigenvalue of the $\sigma_3/2$ generator) same for each quark family. For completeness, we use the $\epsilon_{0123} = -1$ convention for the Levi-Civita tensor, even though the phase of the last equation has no physical effect on the resulting cross section.

Appendix D

Triangle diagrams

The computation of diagrams involving gluons in Figs. 3.6 and 3.8 imply several features that we intend to explain in this appendix, and are due to the trace anomaly of QCD [415–418] and the Landau–Yang theorem [419, 420].

D.1   SVV Green function

The Hgg vertex at one loop contributes both to the $H \to gg$ decay in Fig. 3.6 and the $gH \to g$ dynamical vertex in diagram (a) of Fig. 3.8. In the latter case, it is a part of the computation of the μ–τ conversion in nuclei, and the gluon hadronization at $E \gg m_\tau$ will then be carried out through the nucleon PDFs. We are interested here in the hadronization mechanism that involves '$gg \to$ hadrons' in the contribution to tau decays in Fig. 3.6, in particular, into a pseudoscalar pair.

The Higgs interaction with quarks is given, after spontaneous breaking of the electroweak symmetry, by the Standard Model Lagrangian

$$\mathcal{L} = -\sum_q \frac{m_q}{v}\, h\, \bar{\psi}_q \psi_q \,, \tag{D.1.1}$$

where $v = (\sqrt{2}G_F)^{-1/2} \approx 246\,\mathrm{GeV}$ and the sum extends on light $q_\ell = u, d, s$ and heavy quarks $Q = c, b, t$. With the quark-gluon vertices of the QCD Lagrangian, we can now compute the diagram in Fig. D.1 for an off-shell Higgs field with $q^2 \lesssim m_\tau^2$ by including only the (dominant) heavy quarks Q in the loop. For large quark masses $m_Q \gg m_\tau$ we have a low-energy local effective Lagrangian independent of the heavy quark mass [155]:

$$\mathcal{L}_{\mathrm{eff}} = \frac{\alpha_{\mathrm{S}}\, n_Q}{12\pi\, v}\, h\, G_{\mu\nu}^a G^{\mu\nu\, a} - \sum_{q=u,d,s} \frac{m_q}{v}\, h\, \bar{\psi}_q \psi_q \,, \tag{D.1.2}$$

where n_Q is the number of heavy quarks in the loop and $G_{\mu\nu}^a$ is the strength field tensor of the QCD gluon. In order to get the matrix element of the gluon operator in $\mathcal{L}_{\mathrm{eff}}$ for a two-pseudoscalar-mesons final state, we use the relation of that operator with the trace of the energy–momentum tensor of QCD. The latter has an anomaly and reads [415–418]

$$\theta_\mu^\mu = \frac{\beta(\alpha_{\mathrm{S}})}{4\,\alpha_{\mathrm{S}}}\, G_{\mu\nu}^a G^{\mu\nu\, a} + \sum_q m_q \left(1 + \gamma_{m_q}\right) \bar{\psi}_q \psi_q \,, \tag{D.1.3}$$
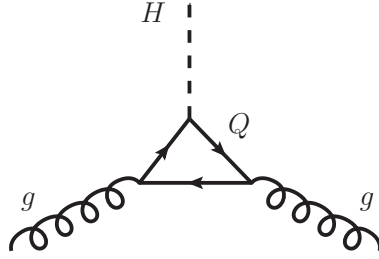
FIGURE D.1:   Triangle diagram contributing to $H \to gg$. Q indicates a heavy quark, $Q = c, b, t$. For the final contribution one needs to add an analogous (cross) contribution with the gluons interchanged (or, equivalently, reversed quark momenta in the loop).

where $q = u, d, c, s, b, t$. Above,

$$\gamma_{m_q}(\mu) = \mu \, \frac{\mathrm{d}\ln m_q}{\mathrm{d}\mu} \,, \qquad \beta(\alpha_{\mathrm{S}}) = -\left(9 - \frac{2}{3} \, n_Q \right) \frac{\alpha_{\mathrm{S}}^2}{2\pi} + \mathcal{O}(\alpha_{\mathrm{S}}^3) \,. \tag{D.1.4}$$

Note that θ_μ^μ is a scale-independent composite operator [421].

The gluon part of the effective action in Eq. (D.1.2) arises from the contribution of the heavy quarks Q in the loop shown in Fig. D.1, using for the Higgs–quark–quark vertex the interaction term from Eq. (D.1.1). Hence, neglecting the higher-order γ_m terms in θ_μ^μ, we can integrate out the heavy quarks obtaining

$$\theta_\mu^\mu = \frac{\beta(\alpha_{\mathrm{S}})}{4 \, \alpha_{\mathrm{S}}} \, G_{\mu\nu}^a G^{\mu\nu\, a} - \frac{\alpha_{\mathrm{S}}}{12\pi} \, n_Q G_{\mu\nu}^a G^{\mu\nu\, a} + \sum_{q=u,d,s} m_q \overline{\psi}_q \psi_q \,, \tag{D.1.5}$$

and the n_Q dependence cancels. Finally, we can rewrite our effective action as

$$\mathcal{L}_{\mathrm{eff}} = -\frac{h}{9 \, v} \left(2 \, \theta_\mu^\mu + 7 \sum_{q=u,d,s} m_q \overline{\psi}_q \psi_q \right) \,. \tag{D.1.6}$$

D.2   AVV Green function

In order to compute the diagram (*b*) in Fig. 3.8 contributing to the μ–τ conversion in nuclei, we need to consider the subdiagram in Fig. D.2. Because the $V - A$ structure of the Z–quark–quark vertex, it contributes both to the VVV and AVV Green functions. The Landau–Yang theorem [419, 420] states that a massive vector ($J = 1$) cannot decay into two on-shell identical massless vectors; hence, we cannot have $Z \to \gamma\gamma$ or $Z \to gg$ (as the gluons have identical color in this process). For any off-shell vector, the theorem does not apply. In our case we notice that the VVV contribution vanishes identically and independently of the on- or off-shellness of the Z boson: surely, a consequence of Furry's theorem. For the AVV component, we observe that the two-gluon system catches the scalar part ($J = 0$) of the off-shell Z boson, i.e. its longitudinal component Z_L that, accordingly, does not give a pole. Hence, the only non-vanishing contribution is given by $Z_L \to gg$.
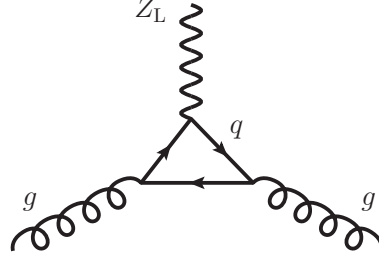
FIGURE D.2: Triangle diagram contributing to $Z_L \to gg$. Here, q is a generic quark, $q = u, d, c, s, t, b$. The final contribution comes from adding to this diagram the analogous one with the quark momenta in the loop reversed.

We recall that the *AVV* Green function carries the axial (Adler–Bell–Jackiw) anomaly [94, 422, 423]. Using the diagram in Fig. D.2 to compute $T_{\alpha\mu\nu}(p,p') \equiv i\mathcal{M}\big(g_\mu(p)\, Z_\alpha(q) \to g_\nu(p')\big)$ for on-shell gluons we obtain

$$T_{\alpha\mu\nu} = \frac{\alpha_{\mathrm{S}}}{2\pi} \frac{e}{\sin 2\theta_{\mathrm{W}}} \frac{q_\alpha}{q^2}\, \varepsilon_{\mu\nu\kappa\lambda}\, q^\kappa\, (p+p')^\lambda \sum_q I^3_{\mathrm{w},q}\, [1 + 2m_q^2 C_0(q^2, m_q^2)], \qquad \text{(D.2.7)}$$

where the sum extends to all quarks, $I^3_{\mathrm{w},q}$ is the weak isospin of a quark of flavor q and $C_0(q^2, m_q^2)$ is the Passarino–Veltman scalar triangle function [424]

$$C_0(q^2, m_q^2) \equiv C_0(0, 0, q^2, m_q^2, m_q^2, m_q^2) = \frac{1}{2q^2}\, \ln^2\left[\frac{\sqrt{1-\tau}-1}{\sqrt{1-\tau}+1} + i\varepsilon\right], \qquad \text{(D.2.8)}$$

with $\tau \equiv 4m_q^2/q^2$. The first term in $[1 + 2m_q^2 C_0(q^2, m_q^2)]$ in Eq. (D.2.7) is the contribution of the axial anomaly. Note, however, that as this term is multiplied by the $I^3_{\mathrm{w},q} = \pm\frac{1}{2}$ factor, the anomalous term cancels when adding the two members of each family of quarks, which results in the anomalous-free amplitude, as is desirable. In addition, and as commented above, $T_{\alpha\mu\nu} \propto q_\alpha$, where q_α is the 4-momentum of the Z boson. Accordingly, when contracted with the gauge-boson propagator, the pole in the latter cancels, as corresponds to the fact that the longitudinal component (scalar part) of a spin-1 boson is the only one contributing here.

Appendix E

Ω coefficients from the hadronization of quark currents

In this appendix, we collect the values for the Ω coefficients arising in the hadronization of quark currents in Chapters 3 and 6.

E.1 Ω coefficients for neutral quark bilinears

In this section, we collect the values for the Ω coefficients used in Eq. (3.3.6) for every final- and intermediate-state contribution. Note that the quark-type symbols used in the table header as ud, stand for the field content of the quark bilinear under hadronization, while the symbols representing mesons — either Goldstone bosons or resonances — stand for the actual physical states. We define $\sin\theta_P \equiv s_P$, $\cos\theta_P \equiv c_P$, $\sin\theta_V \equiv s_V$, $\cos\theta_V \equiv c_V$, with $\sin 2\theta_P \equiv s_{2P}$ and so on, and $m_{\pi/K} \equiv m_\pi/m_K$. Furthermore, θ_P has been defined in Eq. (B.0.1) and θ_V in Eq. (B.0.2).

P	$\Omega_P^{(1)}(ij)$				
	uu	dd	ss	ds	sd
π^0	$\frac{1}{2}$	$-\frac{1}{2}$	0	0	0
K^0	0	0	0	$\frac{1}{\sqrt{2}}$	0
$\overline{K}^0$	0	0	0	0	$\frac{1}{\sqrt{2}}$
η	$\frac{c_P-\sqrt{2}s_P}{2\sqrt{3}}$	$\frac{c_P-\sqrt{2}s_P}{2\sqrt{3}}$	$-\frac{2\sqrt{3}c_P+\sqrt{6}s_P}{6}$	0	0
η'	$\frac{s_P+\sqrt{2}c_P}{2\sqrt{3}}$	$\frac{s_P+\sqrt{2}c_P}{2\sqrt{3}}$	$\frac{\sqrt{6}c_P-2\sqrt{3}s_P}{6}$	0	0

TABLE E.1: Factor $\Omega_P^{(1)}(ij)$.

$\Omega_P^{(2)}(ij)$					
P	uu	dd	ss	ds	sd
π^0	$-4m_{\pi/K}^2$	$4m_{\pi/K}^2$	0	0	0
K^0	0	0	0	$-4\sqrt{2}$	0
$\overline{K}^0$	0	0	0	0	$-4\sqrt{2}$
η	$-\frac{4m_{\pi/K}^2\left(c_P-\sqrt{2}s_P\right)}{\sqrt{3}}$	$-\frac{4m_{\pi/K}^2\left(c_P-\sqrt{2}s_P\right)}{\sqrt{3}}$	$\frac{4(2-m_{\pi/K}^2)\left(2c_P+\sqrt{2}s_P\right)}{\sqrt{3}}$	0	0
η'	$-\frac{4m_{\pi/K}^2\left(s_P+c_P\sqrt{2}\right)}{\sqrt{3}}$	$-\frac{4m_{\pi/K}^2\left(s_P+c_P\sqrt{2}\right)}{\sqrt{3}}$	$\frac{4(2-m_{\pi/K}^2)\left(2s_P-\sqrt{2}c_P\right)}{\sqrt{3}}$	0	0

TABLE E.2:   Factor $\Omega_P^{(2)}(ij)$.

$\Omega_A^{(1)}(ij)$					
P	uu	dd	ss	ds	sd
π^0	$\frac{1}{2}$	$-\frac{1}{2}$	0	0	0
K^0	0	0	0	$\frac{1}{\sqrt{2}}$	0
$\overline{K}^0$	0	0	0	0	$\frac{1}{\sqrt{2}}$
η	$\frac{1}{6}\left(\sqrt{3}c_P-\sqrt{6}s_P\right)$	$\frac{1}{6}\left(\sqrt{3}c_P-\sqrt{6}s_P\right)$	$-\frac{\sqrt{2}c_P+s_P}{\sqrt{6}}$	0	0
η'	$\frac{s_P+\sqrt{2}c_P}{2\sqrt{3}}$	$\frac{s_P+\sqrt{2}c_P}{2\sqrt{3}}$	$\frac{c_P-\sqrt{2}s_P}{\sqrt{6}}$	0	0

TABLE E.3:   Factor $\Omega_A^{(1)}(ij)$.

$\Omega_V^{(1)}(ij)$					$\Omega_T^{(1)}(ij)$				
V	uu	dd	ss	ds	sd	uu	dd	ss	ds	sd
ρ^0	$-\frac{1}{2}$	$\frac{1}{2}$	0	0	0	$\frac{1}{\sqrt{2}}$	0	0	0	0
ϕ	$\frac{\sqrt{6}s_V-\sqrt{3}c_V}{6}$	$\frac{\sqrt{6}s_V-\sqrt{3}c_V}{6}$	$\frac{\sqrt{2}c_V+s_V}{\sqrt{6}}$	0	0	$\frac{c_V-\sqrt{2}s_V}{\sqrt{6}}$	0	0	0	0
ω	$-\frac{s_V+\sqrt{2}c_V}{2\sqrt{3}}$	$-\frac{s_V+\sqrt{2}c_V}{2\sqrt{3}}$	$\frac{\sqrt{2}s_V-c_V}{\sqrt{6}}$	0	0	$\frac{\sqrt{2}c_V+s_V}{\sqrt{6}}$	0	0	0	0
K^{0*}	0	0	0	$-\frac{1}{\sqrt{2}}$	0	0	0	0	0	0
$\overline{K}^{0*}$	0	0	0	0	$-\frac{1}{\sqrt{2}}$	0	0	0	0	0

TABLE E.4:   Factors $\Omega_V^{(1)}(ij)$ and $\Omega_T^{(1)}(ij)$.

$P_1 P_2$	$\Omega_S^{(1)}(ij)$				
	uu	dd	ss	ds	sd
$\pi^0\pi^0$	$\frac{1}{4}$	$\frac{1}{4}$	0	0	0
$\pi^+\pi^-$	$\frac{1}{2}$	$\frac{1}{2}$	0	0	0
$K^0\overline{K}^0$	0	$\frac{1}{2}$	$\frac{1}{2}$	0	0
K^+K^-	$\frac{1}{2}$	0	$\frac{1}{2}$	0	0
$\eta\eta$	$\frac{-c_{2P}-2\sqrt{2}s_{2P}+3}{24}$	$\frac{-c_{2P}-2\sqrt{2}s_{2P}+3}{24}$	$\frac{c_{2P}+2\sqrt{2}s_{2P}+3}{12}$	0	0
$\pi^0 K^0$	0	0	0	$-\frac{1}{2\sqrt{2}}$	0
$\pi^0\overline{K}^0$	0	0	0	0	$-\frac{1}{2\sqrt{2}}$
$\pi^+ K^-$	0	0	0	0	$\frac{1}{2}$
$K^+\pi^-$	0	0	0	$\frac{1}{2}$	0
$\pi^0\eta$	$\frac{\sqrt{3}c_P-\sqrt{6}s_P}{6}$	$\frac{\sqrt{6}s_P-\sqrt{3}c_P}{6}$	0	0	0
$\pi^0\eta'$	$\frac{s_P+\sqrt{2}c_P}{2\sqrt{3}}$	$-\frac{s_P+\sqrt{2}c_P}{2\sqrt{3}}$	0	0	0
$K^0\eta$	0	0	0	$-\frac{4s_P+\sqrt{2}c_P}{4\sqrt{3}}$	0
$K^0\eta'$	0	0	0	$\frac{2\sqrt{2}c_P-s_P}{2\sqrt{6}}$	0
$\overline{K}^0\eta$	0	0	0	0	$-\frac{4s_P+\sqrt{2}c_P}{4\sqrt{3}}$
$\overline{K}^0\eta'$	0	0	0	0	$\frac{2\sqrt{2}c_P-s_P}{2\sqrt{6}}$
$\eta\eta'$	$\frac{2\sqrt{2}c_{2P}-s_{2P}}{12}$	$\frac{2\sqrt{2}c_{2P}-s_{2P}}{12}$	$\frac{s_{2P}-2\sqrt{2}c_{2P}}{6}$	0	0

TABLE E.5: Factors $\Omega_S^{(1)}(ij)$.

P_1P_2	uu	dd	ss	ds	sd
			$\Omega_S^{(2)}(ij)$		
$\pi^0\pi^0$	$-4m_{\pi/K}^2$	$-4m_{\pi/K}^2$	0	0	0
$\pi^+\pi^-$	$-8m_{\pi/K}^2$	$-8m_{\pi/K}^2$	0	0	0
$K^0\overline{K}^0$	0	-8	-8	0	0
K^+K^-	-8	0	-8	0	0
$\eta\eta$	$\dfrac{m_{\pi/K}^2(4\sqrt{2}s_{2P}+2c_{2P}-6)}{3}$	$\dfrac{m_{\pi/K}^2(4\sqrt{2}s_{2P}+2c_{2P}-6)}{3}$	$\dfrac{(4m_{\pi/K}^2-8)(2\sqrt{2}s_{2P}+c_{2P}+3)}{3}$	0	0
π^0K^0	0	0	0	$2\sqrt{2}(1+m_{\pi/K}^2)$	0
$\pi^0\overline{K}^0$	0	0	0	0	$2\sqrt{2}(1+m_{\pi/K}^2)$
π^+K^-	0	0	0	0	$-4(1+m_{\pi/K}^2)$
$K^+\pi^-$	0	0	0	$-4(1+m_{\pi/K}^2)$	0
$\pi^0\eta$	$\dfrac{8m_{\pi/K}^2(\sqrt{2}s_P-c_P)}{\sqrt{3}}$	$-\dfrac{8m_{\pi/K}^2(\sqrt{2}s_P-c_P)}{\sqrt{3}}$	0	0	0
$\pi^0\eta'$	$-\dfrac{8m_{\pi/K}^2(s_P+\sqrt{2}c_P)}{\sqrt{3}}$	$\dfrac{8m_{\pi/K}^2(s_P+\sqrt{2}c_P)}{\sqrt{3}}$	0	0	0
$K^0\eta$	0	0	0	$\dfrac{2(\sqrt{2}c_P(5-3m_{\pi/K}^2)+8s_P)}{\sqrt{3}}$	0
$K^0\eta'$	0	0	0	$\dfrac{2(\sqrt{2}s_P(5-3m_{\pi/K}^2)-8c_P)}{\sqrt{3}}$	0
$\overline{K}^0\eta$	0	0	0	0	$\dfrac{2(8s_P+\sqrt{2}c_P(5-3m_{\pi/K}^2))}{\sqrt{3}}$
$\overline{K}^0\eta'$	0	0	0	0	$\dfrac{2(\sqrt{2}s_P(5-3m_{\pi/K}^2)-8c_P)}{\sqrt{3}}$
$\eta\eta'$	$\dfrac{4m_{\pi/K}^2(s_{2P}-2\sqrt{2}c_{2P})}{3}$	$\dfrac{4m_{\pi/K}^2(s_{2P}-2\sqrt{2}c_{2P})}{3}$	$\dfrac{(8m_{\pi/K}^2-16)(s_{2P}-2\sqrt{2}c_{2P})}{3}$	0	0

TABLE E.6: Factors $\Omega_S^{(2)}(ij)$.

P	$\Omega_S^{(3)}(ij)$				
	uu	dd	ss	ds	sd
a_0^0	$-\sqrt{2}$	$\sqrt{2}$	0	0	0
f_0^8	$-\sqrt{\frac{2}{3}}$	$-\sqrt{\frac{2}{3}}$	$2\sqrt{\frac{2}{3}}$	0	0
f_0^0	$-\frac{2}{\sqrt{3}}$	$-\frac{2}{\sqrt{3}}$	$-\frac{2}{\sqrt{3}}$	0	0
$K_0^{0\,*}$	0	0	0	-2	0
$\overline{K}_0^{0\,*}$	0	0	0	0	-2

TABLE E.7: Factor $\Omega_S^{(3)}(ij)$.

P_1P_2	$\Omega_S^{(4)},\ \Omega_T^{(3)}/2,\ \Omega_T^{(4)}$									
	a_0^0	a_2^0	f_0^8	f_2^8	f_0^0	f_2^0	$K_0^{0\,*}$	$K_2^{0\,*}$	$\overline{K}_0^{0\,*}$	$\overline{K}_2^{0\,*}$
$\pi^0\pi^0$	0		$\sqrt{\frac{2}{3}}$		$\frac{2}{\sqrt{3}}$		0		0	
$\pi^+\pi^-$	0		$2\sqrt{\frac{2}{3}}$		$\frac{4}{\sqrt{3}}$		0		0	
$K^0\overline{K}^0$	$-\sqrt{2}$		$-\sqrt{\frac{2}{3}}$		$\frac{4}{\sqrt{3}}$		0		0	
K^+K^-	$\sqrt{2}$		$-\sqrt{\frac{2}{3}}$		$\frac{4}{\sqrt{3}}$		0		0	
$\eta\eta$	0		$-\frac{c_P(4s_P+\sqrt{2}c_P)}{\sqrt{3}}$		$\frac{2}{\sqrt{3}}$		0		0	
π^0K^0	0		0		0		$-\sqrt{2}$		0	
$\pi^0\overline{K}^0$	0		0		0		0		$-\sqrt{2}$	
π^+K^-	0		0		0		0		2	
$K^+\pi^-$	0		0		0		2		0	
$\pi^0\eta$	$\frac{2(\sqrt{2}c_P-2s_P)}{\sqrt{3}}$		0		0		0		0	
$\pi^0\eta'$	$\frac{2(2c_P+\sqrt{2}s_P)}{\sqrt{3}}$		0		0		0		0	
$K^0\eta$	0		0		0		$-\frac{4s_P+\sqrt{2}c_P}{\sqrt{3}}$		0	
$K^0\eta'$	0		0		0		$\frac{4c_P-\sqrt{2}s_P}{\sqrt{3}}$		0	
$\overline{K}^0\eta$	0		0		0		0		$-\frac{4s_P+\sqrt{2}c_P}{\sqrt{3}}$	
$\overline{K}^0\eta'$	0		0		0		0		$\frac{4c_P-\sqrt{2}s_P}{\sqrt{3}}$	
$\eta\eta'$	0		$\frac{4c_{2P}-\sqrt{2}s_{2P}}{\sqrt{3}}$		0		0		0	

TABLE E.8: Factors $\Omega_S^{(4)}$, $\Omega_T^{(3)}$ and $\Omega_T^{(4)}$.

$$\Omega_S^{(5)}\ ,\ \Omega_T^{(5)}$$

P_1P_2	a_0^0	a_2^0	f_0^8	f_2^8	f_0^0	f_2^0	K_0^{0*}	K_2^{0*}	$\overline{K}_0^{0*}$	$\overline{K}_2^{0*}$
$\pi^0\pi^0$	0	0	$\sqrt{\tfrac{2}{3}}m_{\pi/K}^2$	0	$\dfrac{2m_{\pi/K}^2}{\sqrt{3}}$	0	0	0	0	0
$\pi^+\pi^-$	0	0	$2\sqrt{\tfrac{2}{3}}m_{\pi/K}^2$	0	$\dfrac{4m_{\pi/K}^2}{\sqrt{3}}$	0	0	0	0	0
$K^0\overline{K}^0$	$-\sqrt{2}$	0	$-\sqrt{\tfrac{2}{3}}$	0	$\dfrac{4}{\sqrt{3}}$	0	0	0	0	0
K^+K^-	$\sqrt{2}$	0	$-\sqrt{\tfrac{2}{3}}$	0	$\dfrac{4}{\sqrt{3}}$	0	0	0	0	0
$\eta\eta$	0	0	$\dfrac{(m_{\pi/K}^2-4)(2\sqrt{2}s_{2P}+c_{2P})+9m_{\pi/K}^2-12}{3\sqrt{6}}$	0	$\dfrac{(1-m_{\pi/K}^2)(4\sqrt{2}s_{2P}+2c_{2P})+6}{3\sqrt{3}}$	0	0	0	0	0
$\pi^0 K^0$	0	0	0	0	0	0	$-\dfrac{1+m_{\pi/K}^2}{\sqrt{2}}$	$-\dfrac{1+m_{\pi/K}^2}{\sqrt{2}}$	0	0
$\pi^0\overline{K}^0$	0	0	0	0	0	0	0	0	$-\dfrac{1+m_{\pi/K}^2}{\sqrt{2}}$	$-\dfrac{1+m_{\pi/K}^2}{\sqrt{2}}$
π^+K^-	0	0	0	0	0	0	$1+m_{\pi/K}^2$	$1+m_{\pi/K}^2$	0	0
$K^+\pi^-$	0	0	0	0	0	0	0	0	$1+m_{\pi/K}^2$	$1+m_{\pi/K}^2$
$\pi^0\eta$	$\dfrac{2m_{\pi/K}^2(\sqrt{2}c_P-2s_P)}{\sqrt{3}}$	0	0	0	0	0	0	0	0	0
$\pi^0\eta'$	$\dfrac{2m_{\pi/K}^2(2c_P+\sqrt{2}s_P)}{\sqrt{3}}$	0	0	0	0	0	0	0	0	0
$K^0\eta$	0	0	0	0	0	0	$\dfrac{c_P(3m_{\pi/K}^2-5)-4\sqrt{2}s_P}{\sqrt{6}}$	0	0	0
$K^0\eta'$	0	0	0	0	0	0	$\dfrac{s_P(3m_{\pi/K}^2-5)+4\sqrt{2}c_P}{\sqrt{6}}$	0	0	0
$\overline{K}^0\eta$	0	0	0	0	0	0	0	0	$\dfrac{c_P(3m_{\pi/K}^2-5)-4\sqrt{2}s_P}{\sqrt{6}}$	0
$\overline{K}^0\eta'$	0	0	0	0	0	0	0	0	$\dfrac{s_P(3m_{\pi/K}^2-5)+4\sqrt{2}c_P}{\sqrt{6}}$	0
$\eta\eta'$	0	0	$\dfrac{(4-m_{\pi/K}^2)(4c_{2P}-\sqrt{2}s_{2P})}{3\sqrt{3}}$	0	$\dfrac{4(1-m_{\pi/K}^2)(s_{2P}-2\sqrt{2}c_{2P})}{3\sqrt{3}}$	0	0	0	0	0

TABLE E.9: Factors $\Omega_S^{(5)}$ and $\Omega_T^{(5)}$.

T	$\Omega_T^{(2)}(ij)$				
	uu	dd	ss	ds	sd
a_2^0	$-\sqrt{2}$	$\sqrt{2}$	0	0	0
f_2^8	$-\sqrt{\frac{2}{3}}$	$-\sqrt{\frac{2}{3}}$	$2\sqrt{\frac{2}{3}}$	0	0
f_2^0	$-\frac{2}{\sqrt{3}}$	$-\frac{2}{\sqrt{3}}$	$-\frac{2}{\sqrt{3}}$	0	0
K_2^{0*}	0	0	0	-2	0
$\overline{K}_2^{0*}$	0	0	0	0	-2

TABLE E.10: Factor $\Omega_T^{(2)}(ij)$.

$P_1 P_2$	$\Omega_V^{(2)}(ij)$					$\Omega_T^{(6)}(ij)$				
	uu	dd	ss	ds	sd	uu	dd	ss	ds	sd
$\pi^+\pi^-$	$\frac{1}{2}$	$-\frac{1}{2}$	0	0	0	2	0	0	0	0
$K^0\overline{K}^0$	0	$\frac{1}{2}$	$-\frac{1}{2}$	0	0	0	0	0	0	0
K^+K^-	$\frac{1}{2}$	0	$-\frac{1}{2}$	0	0	2	0	0	0	0
π^0K^0	0	0	0	$\frac{1}{2\sqrt{2}}$	0	0	0	0	0	0
$\pi^0\overline{K}^0$	0	0	0	0	$-\frac{1}{2\sqrt{2}}$	0	0	0	0	0
π^+K^-	0	0	0	0	$\frac{1}{2}$	0	0	0	0	0
$K^+\pi^-$	0	0	0	$\frac{1}{2}$	0	0	0	0	0	0
$K^0\eta$	0	0	0	$-\sqrt{\frac{3}{2}}\frac{c_P}{2}$	0	0	0	0	0	0
$K^0\eta'$	0	0	0	$-\sqrt{\frac{3}{2}}\frac{s_P}{2}$	0	0	0	0	0	0
$\overline{K}^0\eta$	0	0	0	0	$\sqrt{\frac{3}{2}}\frac{c_P}{2}$	0	0	0	0	0
$\overline{K}^0\eta'$	0	0	0	0	$\sqrt{\frac{3}{2}}\frac{s_P}{2}$	0	0	0	0	0

TABLE E.11: Factors $\Omega_V^{(2)}(ij)$ and $\Omega_T^{(6)}(ij)$.

$P_1 P_2$	$\Omega_V^{(3)}$				
	ρ^0	ϕ	ω	K^{0*}	$\overline{K}^{0*}$
$\pi^+\pi^-$	$-\sqrt{2}$	0	0	0	0
$K^0\overline{K}^0$	$\frac{1}{\sqrt{2}}$	$-\sqrt{\frac{3}{2}}\,c_V$	$-\sqrt{\frac{3}{2}}\,s_V$	0	0
K^+K^-	$-\frac{1}{\sqrt{2}}$	$-\sqrt{\frac{3}{2}}\,c_V$	$-\sqrt{\frac{3}{2}}\,s_V$	0	0
π^0K^0	0	0	0	$-\frac{1}{\sqrt{2}}$	0
$\pi^0\overline{K}^0$	0	0	0	0	$\frac{1}{\sqrt{2}}$
π^+K^-	0	0	0	0	-1
$K^+\pi^-$	0	0	0	-1	0
$K^0\eta$	0	0	0	$\sqrt{\frac{3}{2}}\,c_P$	0
$K^0\eta'$	0	0	0	$\sqrt{\frac{3}{2}}\,s_P$	0
$\overline{K}^0\eta$	0	0	0	0	$-\sqrt{\frac{3}{2}}\,c_P$
$\overline{K}^0\eta'$	0	0	0	0	$-\sqrt{\frac{3}{2}}\,s_P$

TABLE E.12: Factors $\Omega_V^{(3)}$.

E.2   Ω coefficients for charged quark bilinears

In Tables E.13 and E.14 we present the values of the Ω coefficients found in Eq. (6.4.14), for the different final and intermediate-state contributions. Same definitions as above apply.

P	V	$\Omega_{A-C}^{(1)}(ij),\ -\Omega_{V-C}^{(1)}(ij)$			
		ud	du	us	su
π^+	ρ^+	$\frac{1}{\sqrt{2}}$	0	0	0
π^-	ρ^-	0	$\frac{1}{\sqrt{2}}$	0	0
K^+	K^{*+}	0	0	$\frac{1}{\sqrt{2}}$	0
K^-	K^{*-}	0	0	0	$\frac{1}{\sqrt{2}}$

TABLE E.13: Factors $\Omega_{A-C}^{(1)}(ij)$ and $\Omega_{V-C}^{(1)}(ij)$.

$P_1 P_2$	$-2\Omega^{(2)}_{V-C}(ij),\ \ \Omega^{(3)}_{V-C}$			
	ud $\|$ ρ^+	du $\|$ ρ^-	us $\|$ K^{*+}	su $\|$ K^{*-}
$\pi^0\pi^+$	$\sqrt{2}$	0	0	0
$\pi^-\pi^0$	0	$\sqrt{2}$	0	0
$K^+\overline{K}^0$	1	0	0	0
$K^0 K^-$	0	1	0	0
$\pi^0 K^+$	0	0	$\frac{1}{\sqrt{2}}$	0
$K^-\pi^0$	0	0	0	$\frac{1}{\sqrt{2}}$
$\pi^+ K^0$	0	0	1	0
$\overline{K}^0\pi^-$	0	0	0	1
ηK^+	0	0	$\sqrt{\frac{3}{2}}c_P$	0
$K^-\eta$	0	0	0	$\sqrt{\frac{3}{2}}c_P$
$\eta' K^+$	0	0	$\sqrt{\frac{3}{2}}s_P$	0
$K^-\eta'$	0	0	0	$\sqrt{\frac{3}{2}}s_P$

TABLE E.14: Factors $\Omega^{(2)}_{V-C}(ij)$ and $\Omega^{(3)}_{V-C}$.

Appendix F

Kinematics of ℓ-τ conversion in nuclei

ℓ–τ conversion in nuclei is a two-body to two-body process described at tree level within the SMEFT framework by the perturbative diagrams in Section 3.4.1. Hence, the squared unpolarized amplitudes as well as the phase space can be described by just two invariant variables. In our case, we choose ξ and Q^2 (see Section 3.4.2). The perturbative cross sections are then given (in terms of these invariant variables) by Eq. (3.4.17), where the phase-space factor is written in terms of the Källén's triangle function λ.

The total cross section of the process is given by Eq. (3.4.18), where the integration limits for ξ and Q^2 are as follows: As usual, we consider that the parton cannot (or it is very unlikely to) have a momentum larger than the nucleus in which it is confined, which leads to

$$\xi_{\max} = 1 \,. \tag{F.0.1}$$

Considering massive quarks and leptons modifies the typically assumed vanishing lower limit of ξ to

$$\xi_{\min} = \frac{\sqrt{E_\ell^2 - m_\ell^2 + (m_\tau + m_j)^2} - E_\ell}{M} \,. \tag{F.0.2}$$

For the variable Q^2, we have

$$Q_\pm^2 = \frac{\xi M E_\ell(m_\ell^2 - m_\tau^2 + \xi^2 M^2) + 2E_\ell^2 \xi^2 M^2 - m_j^2(E_\ell \xi M + m_\ell^2) - \xi^2 M^2 m_\tau^2 \pm \xi M \sqrt{XY}}{M\xi(2E_\ell + M\xi) + m_\ell^2} \,, \tag{F.0.3}$$

where

$$X = E_\ell^2 - m_\ell^2 \,, \tag{F.0.4}$$

and

$$Y = m_j^4 + [m_\ell^2 - m_\tau^2 + \xi M(2E_\ell + \xi M)]^2 - 2m_j^2[m_\ell^2 + m_\tau^2 + \xi M(2E_\ell + \xi M)] \,. \tag{F.0.5}$$

However, since the parton distribution functions provided by the nCTEQ15 group are expected not to be reliable below $Q = 1.3$ GeV, we take the square of this value as the lower limit of our integral (3.4.18). This leads to a small underestimation of the total cross section and thus more conservative resulting constraints on the Wilson coefficients.

Appendix G

τ decay width

In this appendix, we collect expressions for the branching ratios of the decays of the tau lepton into pseudoscalars:

$$\mathcal{B}(\tau \to \ell P) = \frac{\lambda^{1/2}(m_\tau^2, m_\ell^2, m_P^2)}{16\,\pi\,m_\tau^3\,\Gamma_\pi}\,\frac{1}{2}\sum_{i,f}|\mathcal{M}(P)|^2\,, \tag{G.0.1}$$

$$\mathcal{B}(\tau \to \ell P_1 P_2) = \frac{1}{256\,\pi^3\,m_\tau^3\,\Gamma_\tau}\int_{s_{\min}}^{s_{\max}}\mathrm{d}s\int_{t_{\min}}^{t_{\max}}\mathrm{d}t\,\frac{1}{2}\sum_{i,f}|\mathcal{M}(P_1,P_2)|^2\,, \tag{G.0.2}$$

with

$$t_{\min}^{\max} = \frac{1}{4\,s}\left[(m_\tau^2 - m_\ell^2 + m_{P_1}^2 - m_{P_2}^2)^2 - \left(\lambda^{1/2}(s, m_{P_1}^2, m_{P_2}^2) \mp \lambda^{1/2}(m_\tau^2, s, m_\ell^2)\right)^2\right],$$
$$s_{\min} = (m_{P_1} + m_{P_2})^2\,,$$
$$s_{\max} = (m_\tau - m_\ell)^2\,,$$
$$\tag{G.0.3}$$

where $\lambda(a, b, c)$ is the Källén's triangle function.

The calculation of observables involving hadron resonances as external states is not properly defined within quantum field theory because hadron resonances decay strongly and are not proper asymptotic states, as is required in that framework. Hence, in order to describe the $\tau \to \ell V$ decays, we need to provide an appropriate definition. We intend to study the processes with $V = \rho^0(770), \omega(782), \phi(1020), K^{*0}(892), \bar{K}^{*0}(892)$. All but the $\omega(782)$ decay strongly into two pseudoscalars. For these cases we can use the definition that has already been employed in Refs. [161] and [404]:

$$\mathcal{B}(\tau \to \ell V) = \sum_{P_1 P_2} \mathcal{B}(\tau \to \ell P_1 P_2)\Big|_V\,. \tag{G.0.4}$$

In the above equation, the branching ratios for the $P_1 P_2$ decays from Eq. (G.0.2) have the same t limits as shown in Eq. (G.0.3), but the s limits are now restricted to

$$s_{\min} = M_V^2 - \frac{1}{2}M_V\Gamma_V\,, \qquad\qquad s_{\max} = M_V^2 + \frac{1}{2}M_V\Gamma_V\,. \tag{G.0.5}$$

In Eq. (G.0.4), $P_1 P_2$, from a chiral point of view, are indistinguishable from the V resonance, i.e. the pair of pseudoscalar mesons have the same J and I quantum numbers. Accordingly, they are the dominant strong-decay channel of the resonance

V. This definition is based on the fact that, experimentally, no V resonance is observed, only its decay products (pairs $P_1 P_2$). The correspondence is $\{\rho, \phi, K^*\} \leftrightarrow \{\pi\pi, K\overline{K}, K\pi\}$, where a sum of contributions is understood: for instance, for the ϕ resonance we have to sum over the $K^+ K^-$ and $K^0 \overline{K}^0$ decay modes.

The $\omega(782)$ decays dominantly into three pions. Hence, the procedure above does not work for this decay. As the ratio between its width and mass is around 1 %, we will consider the $\omega(782)$ as an asymptotic state and proceed as in the case of one pseudoscalar. An analogous check with the $\phi(1020)$ case shows that, within this approach, we should get the right order of magnitude for the $\tau \to \ell\omega$ decay width.

Appendix H

Correlation matrices of the marginalized numerical analysis

In this section, we present the main correlation matrices of our numerical analysis using `HEPfit`. For the hadronic τ decays, the correlation matrix of all the Wilson coefficients obtained from the numerical analysis considering only the Belle limits and including (excluding) FCNCs is shown in Fig. H.1 (H.2). We regard it interesting to compare these two matrices, as is described in detail in Section 3.5.2.
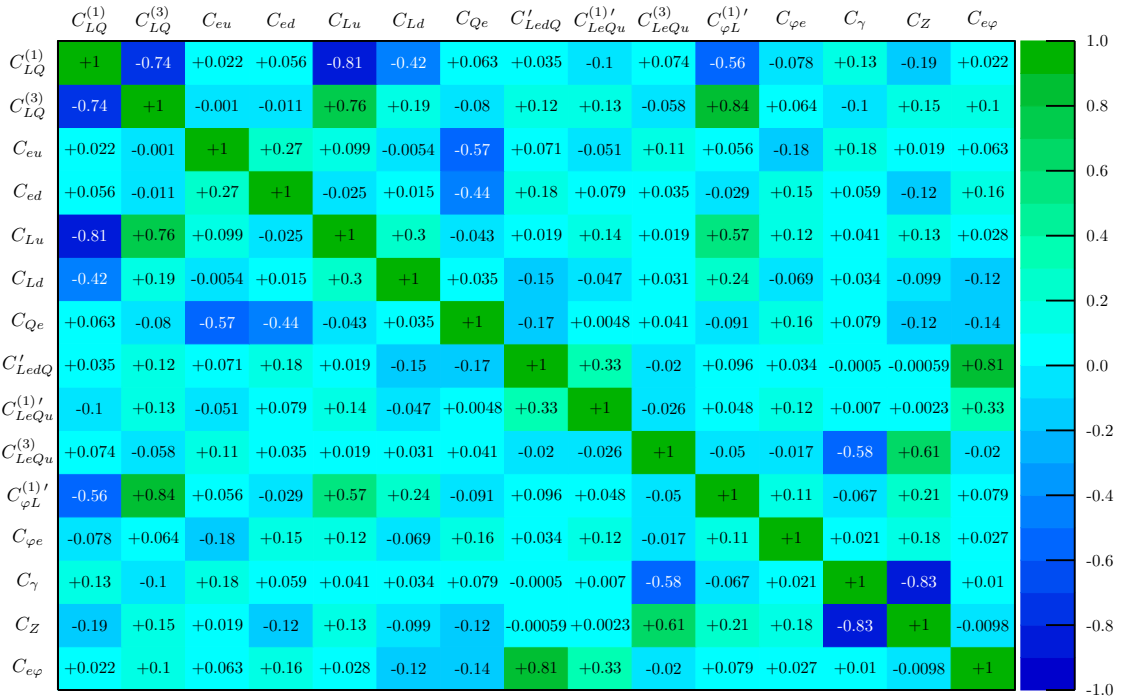
FIGURE H.1: Correlations among all the Wilson coefficients from the numerical analysis considering Belle limits and *including* FCNCs.

The correlation matrix obtained from the numerical analysis considering only the limits of ℓ–τ conversion in nuclei and including FCNCs is presented in Fig. H.3.
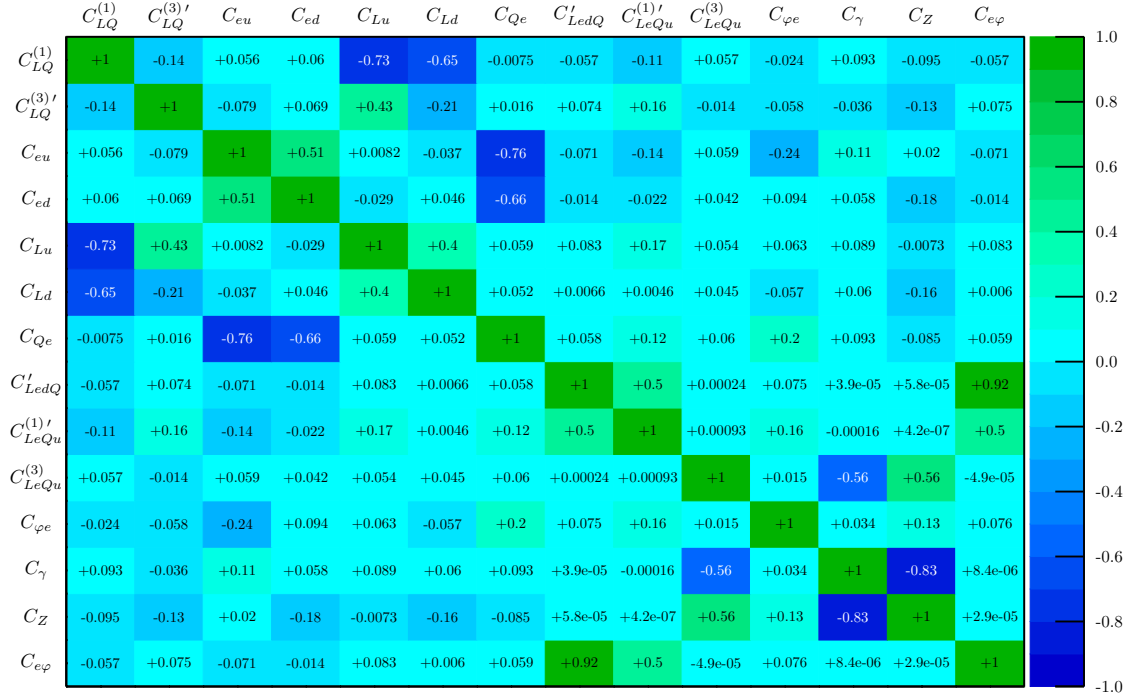
FIGURE H.2: Correlations among all the Wilson coefficients from the numerical analysis considering Belle limits and *excluding* FCNCs.

FIGURE H.3: Correlations among all the Wilson coefficients from the numerical analysis considering ℓ–τ limits and including FCNCs.

Appendix I

Identification of the SMEFT operator basis

In this appendix, for completeness, we list the identities and relations used to identify the $d = 6$ four-fermion operators of the basis in Ref. [56] from those resulting from the integration of the leptoquark fields. Then, we provide the corresponding identification in Table I.1.

Regarding the *scalar* Fierz identities, we have in our case for anticommuting fields

$$(\bar{a}_R b_L)(\bar{c}_L d_R) = (\bar{a}P_L b)(\bar{c}P_R d) = -\frac{1}{2}(\bar{a}_R \gamma_\mu d_R)(\bar{c}_L \gamma^\mu b_L) \,, \tag{I.0.1}$$

$$(\bar{a}_R b_L)(\bar{c}_R d_L) = (\bar{a}P_L b)(\bar{c}P_L d) = -\frac{1}{2}\left[(\bar{a}_R d_L)(\bar{c}_R b_L) + \frac{1}{4}(\bar{a}_R \sigma_{\mu\nu} d_L)(\bar{c}_R \sigma^{\mu\nu} b_L)\right] \,, \tag{I.0.2}$$

with $\sigma_{\mu\nu} \equiv \frac{i}{2}[\gamma_\mu, \gamma_\nu]$ and projectors $P_{R,L} = \frac{1}{2}(1 \pm \gamma_5)$. The *vector* Fierz identities then read

$$(\bar{a}_L \gamma_\mu b_L)(\bar{c}_L \gamma^\mu d_L) = (\bar{a}\gamma_\mu P_L b)(\bar{c}\gamma^\mu P_L d) = (\bar{a}_L \gamma_\mu d_L)(\bar{c}_L \gamma^\mu b_L) \,, \tag{I.0.3}$$

$$(\bar{a}_L \gamma_\mu b_L)(\bar{c}_R \gamma^\mu d_R) = (\bar{a}\gamma_\mu P_L b)(\bar{c}\gamma^\mu P_R d) = -2(\bar{a}_L d_R)(\bar{c}_R b_L) \,. \tag{I.0.4}$$

The fields in the charge-conjugation basis are defined as $\psi^{\mathrm{C}} \equiv C\overline{\psi}^T = C\gamma_0^T \psi^*$ (and consequently $\overline{\psi^{\mathrm{C}}} = -\psi^T C^{-1}$), with C being the charge-conjugation operator (in standard representation, $C = i\gamma_2\gamma_0$).

For the left-handed ($\psi_L = P_L\psi$) and right-handed ($\psi_R = P_R\psi$) components of Dirac fields, using $C^{-1}\gamma_5 C = +\gamma_5^T$, we then have[1]

$$\psi_L = P_L\psi \,, \qquad \psi_R = P_R\psi \,, \qquad \overline{\psi_L} = \overline{\psi}P_R \,, \qquad \overline{\psi_R} = \overline{\psi}P_L \,, \tag{I.0.5}$$

$$\psi_L^{\mathrm{C}} = P_R\psi^{\mathrm{C}} \,, \qquad \psi_R^{\mathrm{C}} = P_L\psi^{\mathrm{C}} \,, \qquad \overline{\psi_L^{\mathrm{C}}} = \overline{\psi^{\mathrm{C}}}P_L \,, \qquad \overline{\psi_R^{\mathrm{C}}} = \overline{\psi^{\mathrm{C}}}P_R \,. \tag{I.0.6}$$

Using $C^{-1}\gamma_\mu C = -\gamma_\mu^T$, for anticommutating ψ_1 and ψ_2 (and thus including an additional minus sign) we arrive at

$$\overline{\psi_1^{\mathrm{C}}}\psi_2^{\mathrm{C}} = +\overline{\psi_2}\psi_1 \,, \tag{I.0.7}$$

$$\overline{\psi_1^{\mathrm{C}}}\gamma_\mu\psi_2^{\mathrm{C}} = -\overline{\psi_2}\gamma_\mu\psi_1 \,, \tag{I.0.8}$$

---

[1]We write $\psi_{L,R}^{\mathrm{C}} \equiv (\psi_{L,R})^{\mathrm{C}}$.

$$\overline{\psi_1^{\mathrm{C}}}\sigma_{\mu\nu}\psi_2^{\mathrm{C}} = -\overline{\psi_2}\sigma_{\mu\nu}\psi_1\,. \tag{I.0.9}$$

With any representation in which $C^\dagger = C^{-1}$, we have employed $\left(\overline{\psi_1^{\mathrm{C}}}\,\Gamma\,\psi_2\right)^\dagger = \overline{\psi_2}\,\Gamma\,\psi_1^{\mathrm{C}}$, with $\Gamma \in \{\mathbb{1}, \gamma_\mu, \sigma_{\mu\nu}\}$.

For the SU(2) indices we make use of the following manipulations:

$$\sum_{k=1}^{3}(\varepsilon\!\cdot\!\tau_k)_{ab}(\varepsilon\!\cdot\!\tau_k)^\dagger_{cd} = \sum_{k=0,1,3}\tau_{k,ab}\tau_{k,cd} = 2\delta_{ad}\delta_{bc}-\tau_{2,ab}\tau_{2,cd} = 2\delta_{ad}\delta_{bc}+\varepsilon_{ab}\varepsilon_{cd}\,, \tag{I.0.10}$$

where $\varepsilon = i\tau_2$, and we have used the completeness relation $\sum_{k=0}^{3}\tau_{k,ab}\tau_{k,cd} = 2\delta_{ad}\delta_{bc}$. Combining $\varepsilon_{ab}\varepsilon_{cd} = \delta_{ac}\delta_{bd}-\delta_{ad}\delta_{bc}$ and $\sum_{k=1}^{3}\tau_{k,cb}\tau_{k,da} = 2\delta_{ca}\delta_{bd}-\delta_{cb}\delta_{da}$, it is apparent that

$$\varepsilon_{ab}\varepsilon_{cd} = \frac{1}{2}\left[\left(\sum_{k=1}^{3}\tau_{k,cb}\tau_{k,da}\right) - \delta_{ad}\delta_{bc}\right], \tag{I.0.11}$$

so we find

$$\sum_{k=1}^{3}(\varepsilon\cdot\tau_k)_{ab}(\varepsilon\cdot\tau_k)^\dagger_{cd} = \delta_{ac}\delta_{bd} + \delta_{ad}\delta_{bc} = \frac{3}{2}\delta_{ad}\delta_{bc} + \frac{1}{2}\sum_{k=1}^{3}\tau_{k,cb}\tau_{k,da}\,. \tag{I.0.12}$$

Eqs. (I.0.11) and (I.0.12) get handy when rewriting the expressions in terms of the operators from the SMEFT basis [56] we work with.

Finally, the matching between the $d = 6$ four-fermion operators and the lepto-quark Yukawa couplings are provided in Table I.1.

LQ	$C_{LQ}^{(1),klmn}$	$C_{LQ}^{(3),klmn}$	$C_{LeQu}^{(1),klmn}$	$C_{LeQu}^{(3),klmn}$	C_{Qe}^{klmn}	C_{Lu}^{klmn}	C_{Ld}^{klmn}	C_{eu}^{klmn}	C_{ed}^{klmn}	C_{LedQ}^{klmn}
S_3	$+\frac{3}{4}Y_{3,nl}^{LL}Y_{3,mk}^{LL}$	$+\frac{1}{4}Y_{3,nl}^{LL}Y_{3,mk}^{LL}$	×	×	×	×	×	×	×	×
R_2	×	×	$-\frac{1}{2}Y_{2,nk}^{RL}Y_{2,lm}^{LR}$	$-\frac{1}{8}Y_{2,nk}^{RL}Y_{2,lm}^{LR}$	$-\frac{1}{2}Y_{2,ml}^{LR}Y_{2,nk}^{LR}$	$-\frac{1}{2}Y_{2,ml}^{RL}Y_{2,nk}^{RL}$	×	×	×	×
$\tilde{R}_2$	×	×	×	×	×	×	$-\frac{1}{2}\tilde{Y}_{2,ml}^{RL}\tilde{Y}_{2,nk}^{RL}$	×	×	×
$\tilde{S}_1$	×	×	×	×	×	×	×	×	$+\frac{1}{2}\tilde{Y}_{1,nl}^{RR}\tilde{Y}_{1,mk}^{RR}$	×
S_1	$+\frac{1}{4}Y_{1,nl}^{LL}Y_{1,mk}^{LL}$	$-\frac{1}{4}Y_{1,nl}^{LL}Y_{1,mk}^{LL}$	$+\frac{1}{2}Y_{1,mk}^{LL}Y_{1,nl}^{RR}$	$-\frac{1}{8}Y_{1,mk}^{LL}Y_{1,nl}^{RR}$	×	×	×	$+\frac{1}{2}Y_{1,nl}^{RR}Y_{1,mk}^{RR}$	×	×
U_3	$-\frac{3}{2}X_{3,ml}^{LL}X_{3,nk}^{LL}$	$+\frac{1}{2}X_{3,ml}^{LL}X_{3,nk}^{LL}$	×	×	×	×	×	×	×	×
V_2	×	×	×	×	$+X_{2,ln}^{LR}X_{2,km}^{LR}$	×	$+X_{2,nl}^{RL}X_{2,mk}^{RL}$	×	×	$-2X_{2,mk}^{RL}X_{2,nl}^{LR}$
$\tilde{V}_2$	×	×	×	×	×	$+\tilde{X}_{2,nl}^{RL}\tilde{X}_{2,mk}^{RL}$	×	×	×	×
$\tilde{U}_1$	×	×	×	×	×	×	×	$-\tilde{X}_{1,ml}^{RR}\tilde{X}_{1,nk}^{RR}$	×	×
U_1	$-\frac{1}{2}X_{1,ml}^{LL}X_{1,nk}^{LL}$	$-\frac{1}{2}X_{1,ml}^{LL}X_{1,nk}^{LL}$	×	×	×	×	×	×	$-X_{1,ml}^{RR}X_{1,nk}^{RR}$	$+2X_{1,nk}^{LL}X_{1,ml}^{RR}$

TABLE I.1: Results of the matching of pairs of Yukawa couplings stemming from each leptoquark type listed in Table 4.1 to the Wilson coefficients of the four-fermion operators of SMEFT from Table 4.2. Notice that, owing to the Fierz rearrangement, we also obtain contributions containing tensorial operators, i.e. $C_{LeQu}^{(3)}$.

Appendix J

Single Yukawas of vector leptoquarks

The integration of leptoquarks and the following matching to the SMEFT lead to relations between the Wilson coefficients of this EFT and products of Yukawa leptoquark couplings. However, due to the rich variety of contributions of the Yukawas to the WCs, and the current and expected bounds on the latter from CLFV-τ processes, one can do better than just constraining pairs of Yukawas. Under a choice of a few free Yukawas, the rest can be related to these and the WCs. The most general leptoquark–matter interacting model provides, for vector leptoquarks, fourteen Yukawa couplings. These are reduced, upon LQ integration, to eight different WCs which receive a total of nine bounds from the charged-lepton-flavor-violating τ processes considered in this work. Therefore, by choosing $\tilde{x}_2^{\mathrm{RL}}$ and $\tilde{x}_1^{\mathrm{RR}}$ on one hand and x_3^{LL}, x_1^{LL} and x_2^{LR} on the other to be free, we find the trivial relations

$$\tilde{x}_{2\tau}^{\mathrm{RL}} = \frac{C_{Lu}}{\tilde{x}_2^{\mathrm{RL}}}, \qquad \tilde{x}_{1\tau}^{\mathrm{RR}} = -\frac{C_{eu}}{\tilde{x}_1^{\mathrm{RR}}}, \tag{J.0.1}$$

$$x_{3\tau}^{\mathrm{LL}} = \frac{C_{LQ}^{(3)} - C_{LQ}^{(1)}}{2x_3^{\mathrm{LL}}}, \qquad x_{1\tau}^{\mathrm{LL}} = -\frac{C_{LQ}^{(1)} + 3C_{LQ}^{(3)}}{2x_1^{\mathrm{LL}}}, \qquad x_{2\tau}^{\mathrm{LR}} = \frac{C_{Qe}}{x_2^{\mathrm{LR}}}, \tag{J.0.2}$$

and two different solutions for

$$
\begin{aligned}
x_{2\pm}^{\mathrm{RL}} &= \frac{2C_{ed}C_{LQ}^{(1)} - C_{LedQ}^{\ell-\tau}C_{LedQ}^{\tau h} + 6C_{ed}C_{LQ}^{(3)} - 4C_{Ld}C_{Qe} \mp \sqrt{A}}{4C_{LedQ}^{\ell-\tau}C_{Qe}} x_2^{\mathrm{LR}}, \\
x_{2\tau\pm}^{\mathrm{RL}} &= \frac{2C_{ed}C_{LQ}^{(1)} - C_{LedQ}^{\ell-\tau}C_{LedQ}^{\tau h} + 6C_{ed}C_{LQ}^{(3)} - 4C_{Ld}C_{Qe} \pm \sqrt{A}}{4C_{LedQ}^{\tau h}} \frac{1}{x_2^{\mathrm{LR}}}, \\
x_{1\pm}^{\mathrm{RR}} &= -\frac{2C_{ed}C_{LQ}^{(1)} + C_{LedQ}^{\ell-\tau}C_{LedQ}^{\tau h} + 6C_{ed}C_{LQ}^{(3)} - 4C_{Ld}C_{Qe} \pm \sqrt{A}}{2C_{LedQ}^{\tau h}(C_{LQ}^{(1)} + 3C_{LQ}^{(3)})} x_1^{\mathrm{LL}}, \\
x_{1\tau\pm}^{\mathrm{RR}} &= \frac{2C_{ed}C_{LQ}^{(1)} + C_{LedQ}^{\ell-\tau}C_{LedQ}^{\tau h} + 6C_{ed}C_{LQ}^{(3)} - 4C_{Ld}C_{Qe} \mp \sqrt{A}}{4C_{LedQ}^{\ell-\tau}} \frac{1}{x_1^{\mathrm{LL}}},
\end{aligned} \tag{J.0.3}
$$

where either all the positive or negative solutions are to be chosen, with

$$A = \left[C_{LedQ}^{\ell-\tau}C_{LedQ}^{\tau h} - 2C_{ed}(C_{LQ}^{(1)} + 3C_{LQ}^{(3)}) + 4C_{Ld}C_{Qe}\right]^2 - 16C_{Ld}C_{LedQ}^{\ell-\tau}C_{LedQ}^{\tau h}C_{Qe}. \tag{J.0.4}$$

Note that (usually stronger) limits on the five free variables $\tilde{x}_2^{\mathrm{RL}}$, $\tilde{x}_1^{\mathrm{RR}}$, x_3^{LL}, x_1^{LL} and x_2^{LR} can be found elsewhere, since they involve just the e and μ leptons. These can then be used, under the assumptions taken in this work, to constrain the rest of the Yukawas.

Appendix K

Translating the bounds

In this appendix, we show straightforwardly how, numerically, the WC bounds are translated into limits on Yukawa pairs according to Eqs. (4.3.31) and (4.3.35). The Wilson coefficients were given in the previous work as normal (Gaussian) probability distributions with mean μ and variance σ^2, i.e. $C = \mathcal{N}(\mu, \sigma^2)$. The non-vanishing correlations among these were collected in the covariance matrix W_{ij}.

In general, given a set of functions of the WCs for which we do not know their probability distribution functions, namely $(zz')_k = F_k(\vec{C})$, with $\vec{C} = (C_{Q_1}, C_{Q_2}, \dots)$ containing all WCs considered in this work and where the symbolic notation zz' can stand both for scalar (y) and vector (x) Yukawa pairs, one can approximate the expectation value of F_k and its covariance matrix through

$$E\big[F_k(\vec{C})\big] \simeq F_k(\vec{\mu}), \tag{K.0.1}$$

and

$$U_{km} \equiv \text{cov}\big[F_k F_m\big] \simeq \sum_{i,j=1}^{n} \left[\frac{\partial F_k}{\partial C_{Q_i}} \frac{\partial F_m}{\partial C_{Q_j}} \right]_{\vec{C}=\vec{\mu}} W_{ij}. \tag{K.0.2}$$

Above, the derivatives should be evaluated at the mean values of the WCs collected within the vector $\vec{\mu}$, which is, in our case, just a zero-valued vector $\vec{\mu} = \vec{0}$.

For the simple case of Eqs. (4.3.31) and (4.3.35), the resulting combinations of the WCs contributing to the Yukawa pairs $zz' = \sum_Q a_Q C_Q$ lead again to a Gaussian pdf for the latter, and Eqs. (K.0.1) and Eqs. (K.0.2) give

$$zz' = \mathcal{N}\left(\sum_Q a_Q \mu_Q, \ \sum_Q a_Q^2 \sigma_Q^2 \right) \tag{K.0.3}$$

for non-correlated WC, and

$$zz' = \mathcal{N}\left(\sum_Q a_Q \mu_Q, \ \sum_Q a_Q^2 \sigma_Q^2 + 2 \sum_{Q_1 < Q_2} a_{Q_1} \sigma_{Q_1} \rho_{Q_1 Q_2} a_{Q_2} \sigma_{Q_2} \right) \tag{K.0.4}$$

for the correlated ones, with $\rho_{Q_1 Q_2}$ being the WC correlation matrix.

Bibliography

[1] M. E. Peskin and D. V. Schroeder, *An Introduction to quantum field theory*. Addison-Wesley, Reading, USA, 1995.

[2] F. J. Yndurain, *The Theory of Quark and Gluon Interactions*, Theoretical and Mathematical Physics. Springer, Berlin, Germany, 2006, 10.1007/3-540-33210-3.

[3] M. Gell-Mann, *The Eightfold Way: A Theory of strong interaction symmetry*, .

[4] M. Gell-Mann, *A Schematic Model of Baryons and Mesons*, *Phys. Lett.* **8** (1964) 214.

[5] G. Zweig, *An SU(3) model for strong interaction symmetry and its breaking. Version 1*, .

[6] S. L. Glashow, J. Iliopoulos and L. Maiani, *Weak Interactions with Lepton-Hadron Symmetry*, *Phys. Rev. D* **2** (1970) 1285.

[7] C. Amsler, *The Quark Structure of Hadrons: An Introduction to the Phenomenology and Spectroscopy*, vol. 949. Springer, Cham, 2018, 10.1007/978-3-319-98527-5.

[8] S. Weinberg, *A Model of Leptons*, *Phys. Rev. Lett.* **19** (1967) 1264.

[9] S. L. Glashow, *Partial Symmetries of Weak Interactions*, *Nucl. Phys.* **22** (1961) 579.

[10] A. Salam, *Weak and Electromagnetic Interactions*, *Conf. Proc. C* **680519** (1968) 367.

[11] A. Pich, *The Standard Model of Electroweak Interactions*, in *2010 European School of High Energy Physics*, pp. 1–50, 1, 2012, 1201.0537.

[12] F. Englert and R. Brout, *Broken Symmetry and the Mass of Gauge Vector Mesons*, *Phys. Rev. Lett.* **13** (1964) 321.

[13] G. S. Guralnik, C. R. Hagen and T. W. B. Kibble, *Global Conservation Laws and Massless Particles*, *Phys. Rev. Lett.* **13** (1964) 585.

[14] P. W. Higgs, *Broken Symmetries and the Masses of Gauge Bosons*, *Phys. Rev. Lett.* **13** (1964) 508.

[15] Y. Nambu, *Quasiparticles and Gauge Invariance in the Theory of Superconductivity*, *Phys. Rev.* **117** (1960) 648.

[16] J. Goldstone, *Field Theories with Superconductor Solutions*, *Nuovo Cim.* **19** (1961) 154.

[17] ATLAS collaboration, G. Aad et al., *Observation of a new particle in the search for the Standard Model Higgs boson with the ATLAS detector at the LHC*, *Phys. Lett. B* **716** (2012) 1 [`1207.7214`].

[18] CMS collaboration, S. Chatrchyan et al., *Observation of a New Boson at a Mass of 125 GeV with the CMS Experiment at the LHC*, *Phys. Lett. B* **716** (2012) 30 [`1207.7235`].

[19] N. Cabibbo, *Unitary Symmetry and Leptonic Decays*, *Phys. Rev. Lett.* **10** (1963) 531.

[20] M. Kobayashi and T. Maskawa, *CP Violation in the Renormalizable Theory of Weak Interaction*, *Prog. Theor. Phys.* **49** (1973) 652.

[21] B. Pontecorvo, *Inverse beta processes and nonconservation of lepton charge*, *Zh. Eksp. Teor. Fiz.* **34** (1957) 247.

[22] Z. Maki, M. Nakagawa and S. Sakata, *Remarks on the unified model of elementary particles*, *Prog. Theor. Phys.* **28** (1962) 870.

[23] S. Weinberg, *Phenomenological Lagrangians*, *Physica A* **96** (1979) 327.

[24] S. Sakata, H. Umezawa and S. Kamefuchi, *On the structure of the interaction of the elementary particles. I: The renormalizability of the interaction*, *Prog. Theor. Phys.* **7** (1952) 377.

[25] S. Weinberg, *On the Development of Effective Field Theory*, *Eur. Phys. J. H* **46** (2021) 6 [`2101.04241`].

[26] M. D. Schwartz, *Quantum Field Theory and the Standard Model*. Cambridge University Press, 3, 2014.

[27] T. Appelquist and J. Carazzone, *Infrared Singularities and Massive Fields*, *Phys. Rev. D* **11** (1975) 2856.

[28] M. Neubert, *Renormalization Theory and Effective Field Theories*, `1901.06573`.

[29] H. Georgi, *On-shell effective field theory*, *Nucl. Phys. B* **361** (1991) 339.

[30] C. Arzt, *Reduced effective Lagrangians*, *Phys. Lett. B* **342** (1995) 189 [`hep-ph/9304230`].

[31] J. Gasser and H. Leutwyler, *Chiral Perturbation Theory to One Loop*, *Annals Phys.* **158** (1984) 142.

[32] J. Gasser and H. Leutwyler, *Chiral Perturbation Theory: Expansions in the Mass of the Strange Quark*, *Nucl. Phys.* **B250** (1985) 465.

[33] H. Leutwyler, *On the foundations of chiral perturbation theory*, *Annals Phys.* **235** (1994) 165 [`hep-ph/9311274`].

[34] S. Weinberg, *Dynamical approach to current algebra*, *Phys. Rev. Lett.* **18** (1967) 188.

[35] S. Weinberg, *Nonlinear realizations of chiral symmetry*, *Phys. Rev.* **166** (1968) 1568.

[36] S. R. Coleman, J. Wess and B. Zumino, *Structure of phenomenological Lagrangians. 1.*, *Phys. Rev.* **177** (1969) 2239.

[37] C. G. Callan, Jr., S. R. Coleman, J. Wess and B. Zumino, *Structure of phenomenological Lagrangians. 2.*, *Phys. Rev.* **177** (1969) 2247.

[38] A. Pich, *Effective Field Theory with Nambu-Goldstone Modes*, `1804.05664`.

[39] O. Cata and V. Mateu, *Chiral perturbation theory with tensor sources*, *JHEP* **09** (2007) 078 [`0705.2948`].

[40] J. Bijnens, G. Colangelo and G. Ecker, *The Mesonic chiral Lagrangian of order p**6*, *JHEP* **02** (1999) 020 [`hep-ph/9902437`].

[41] G. Ecker, J. Gasser, A. Pich and E. de Rafael, *The Role of Resonances in Chiral Perturbation Theory*, *Nucl. Phys.* **B321** (1989) 311.

[42] G. Ecker, J. Gasser, H. Leutwyler, A. Pich and E. de Rafael, *Chiral Lagrangians for Massive Spin 1 Fields*, *Phys. Lett.* **B223** (1989) 425.

[43] V. Cirigliano, G. Ecker, M. Eidemueller, R. Kaiser, A. Pich and J. Portolés, *Towards a consistent estimate of the chiral low-energy constants*, *Nucl. Phys.* **B753** (2006) 139 [`hep-ph/0603205`].

[44] G. 't Hooft, *A Planar Diagram Theory for Strong Interactions*, *Nucl. Phys. B* **72** (1974) 461.

[45] E. Witten, *Baryons in the 1/n Expansion*, *Nucl. Phys. B* **160** (1979) 57.

[46] G. Ecker and C. Zauner, *Tensor meson exchange at low energies*, *Eur. Phys. J. C* **52** (2007) 315 [`0705.0624`].

[47] V. Mateu and J. Portoles, *Form-factors in radiative pion decay*, *Eur. Phys. J. C* **52** (2007) 325 [`0706.1039`].

[48] PARTICLE DATA GROUP collaboration, P. A. Zyla et al., *Review of Particle Physics*, *PTEP* **2020** (2020) 083C01.

[49] L.-Y. Dai, J. Fuentes-Martín and J. Portolés, *Scalar-involved three-point Green functions and their phenomenology*, *Phys. Rev. D* **99** (2019) 114015 [`1902.10411`].

[50] M. Knecht and A. Nyffeler, *Resonance estimates of O(p**6) low-energy constants and QCD short distance constraints*, *Eur. Phys. J. C* **21** (2001) 659 [`hep-ph/0106034`].

[51] A. Pich, *Colorless mesons in a polychromatic world*, in *The Phenomenology of Large N(c) QCD*, pp. 239–258, 5, 2002, `hep-ph/0205030`, DOI.

[52] J. Bijnens, E. Gamiz, E. Lipartia and J. Prades, *QCD short distance constraints and hadronic approximations*, *JHEP* **04** (2003) 055 [`hep-ph/0304222`].

[53] G. P. Lepage and S. J. Brodsky, *Exclusive Processes in Perturbative Quantum Chromodynamics*, *Phys. Rev. D* **22** (1980) 2157.

[54] S. Gonzàlez-Solís, A. Miranda, J. Rendón and P. Roig, *Effective-field theory analysis of the* $\tau^- \to K^-(\eta^{(\prime)}, K^0)\nu_\tau$ *decays*, *Phys. Rev. D* **101** (2020) 034010 [`1911.08341`].

[55] F.-Z. Chen, X.-Q. Li, Y.-D. Yang and X. Zhang, *CP asymmetry in* $\tau \to K_S \pi \nu_\tau$ *decays within the Standard Model and beyond*, *Phys. Rev. D* **100** (2019) 113006 [`1909.05543`].

[56] B. Grzadkowski, M. Iskrzynski, M. Misiak and J. Rosiek, *Dimension-Six Terms in the Standard Model Lagrangian*, *JHEP* **10** (2010) 085 [`1008.4884`].

[57] S. Weinberg, *Baryon and Lepton Nonconserving Processes*, *Phys. Rev. Lett.* **43** (1979) 1566.

[58] W. Buchmüller and D. Wyler, *Effective Lagrangian Analysis of New Interactions and Flavor Conservation*, *Nucl. Phys. B* **268** (1986) 621.

[59] L. Lehman, *Extending the Standard Model Effective Field Theory with the Complete Set of Dimension-7 Operators*, *Phys. Rev. D* **90** (2014) 125023 [`1410.4193`].

[60] I. Brivio, Y. Jiang and M. Trott, *The SMEFTsim package, theory and tools*, *JHEP* **12** (2017) 070 [`1709.06492`].

[61] E. E. Jenkins, A. V. Manohar and M. Trott, *Renormalization Group Evolution of the Standard Model Dimension Six Operators I: Formalism and lambda Dependence*, *JHEP* **10** (2013) 087 [`1308.2627`].

[62] E. E. Jenkins, A. V. Manohar and M. Trott, *Renormalization Group Evolution of the Standard Model Dimension Six Operators II: Yukawa Dependence*, *JHEP* **01** (2014) 035 [`1310.4838`].

[63] R. Alonso, E. E. Jenkins, A. V. Manohar and M. Trott, *Renormalization Group Evolution of the Standard Model Dimension Six Operators III: Gauge Coupling Dependence and Phenomenology*, *JHEP* **04** (2014) 159 [`1312.2014`].

[64] E. E. Jenkins, A. V. Manohar and P. Stoffer, *Low-Energy Effective Field Theory below the Electroweak Scale: Operators and Matching*, *JHEP* **03** (2018) 016 [`1709.04486`].

[65] E. E. Jenkins, A. V. Manohar and P. Stoffer, *Low-Energy Effective Field Theory below the Electroweak Scale: Anomalous Dimensions*, *JHEP* **01** (2018) 084 [`1711.05270`].

[66] W. Dekens and P. Stoffer, *Low-energy effective field theory below the electroweak scale: matching at one loop*, *JHEP* **10** (2019) 197 [`1908.05295`].

[67] H. K. Dreiner, H. E. Haber and S. P. Martin, *Two-component spinor techniques and Feynman rules for quantum field theory and supersymmetry*, *Phys. Rept.* **494** (2010) 1 [0812.1594].

[68] M. Raidal et al., *Flavour physics of leptons and dipole moments*, *Eur. Phys. J. C* **57** (2008) 13 [0801.1826].

[69] A. de Gouvea and P. Vogel, *Lepton Flavor and Number Conservation, and Physics Beyond the Standard Model*, *Prog. Part. Nucl. Phys.* **71** (2013) 75 [1303.4097].

[70] L. Calibbi and G. Signorelli, *Charged Lepton Flavour Violation: An Experimental and Theoretical Introduction*, *Riv. Nuovo Cim.* **41** (2018) 71 [1709.00294].

[71] BELLE-II collaboration, W. Altmannshofer et al., *The Belle II Physics Book*, *PTEP* **2019** (2019) 123C01 [1808.10567].

[72] A. Pich, *Challenges for tau physics at the TeraZ*, *Eur. Phys. J. Plus* **136** (2021) 1117 [2012.07099].

[73] S. Banerjee et al., *Snowmass 2021 White Paper: Charged lepton flavor violation in the tau sector*, 2203.14919.

[74] T. Husek, K. Monsálvez-Pozo and J. Portolés, *Lepton-flavour violation in hadronic tau decays and $\mu - \tau$ conversion in nuclei*, *JHEP* **01** (2021) 059 [2009.10428].

[75] CMS collaboration, A. M. Sirunyan et al., *Combined measurements of Higgs boson couplings in proton–proton collisions at $\sqrt{s} = 13\,TeV$*, *Eur. Phys. J. C* **79** (2019) 421 [1809.10733].

[76] S. H. Neddermeyer and C. D. Anderson, *Note on the Nature of Cosmic Ray Particles*, *Phys. Rev.* **51** (1937) 884.

[77] H. Yukawa, *On the Interaction of Elementary Particles I*, *Proc. Phys. Math. Soc. Jap.* **17** (1935) 48.

[78] M. Conversi, E. Pancini and O. Piccioni, *On the Disintegration of Negative Mesons*, *Phys. Rev.* **71** (1947) 209.

[79] C. M. G. Lattes, H. Muirhead, G. P. S. Occhialini and C. F. Powell, *PROCESSES INVOLVING CHARGED MESONS*, *Nature* **159** (1947) 694.

[80] L. M. Brown, *The idea of the neutrino*, *Phys. Today* **31N9** (1978) 23.

[81] C. L. Cowan, F. Reines, F. B. Harrison, H. W. Kruse and A. D. McGuire, *Detection of the free neutrino: A Confirmation*, *Science* **124** (1956) 103.

[82] G. Feinberg, *Decays of the mu Meson in the Intermediate-Meson Theory*, *Phys. Rev.* **110** (1958) 1482.

[83] C. S. Wu, E. Ambler, R. W. Hayward, D. D. Hoppes and R. P. Hudson, *Experimental Test of Parity Conservation in β Decay*, *Phys. Rev.* **105** (1957) 1413.

[84] B. Pontecorvo, *Electron and Muon Neutrinos*, *Zh. Eksp. Teor. Fiz.* **37** (1959) 1751.

[85] G. Danby, J. M. Gaillard, K. A. Goulianos, L. M. Lederman, N. B. Mistry, M. Schwartz et al., *Observation of High-Energy Neutrino Reactions and the Existence of Two Kinds of Neutrinos*, *Phys. Rev. Lett.* **9** (1962) 36.

[86] G. D. Rochester and C. C. Butler, *Evidence for the Existence of New Unstable Elementary Particles*, *Nature* **160** (1947) 855.

[87] SLAC-SP-017 collaboration, J. E. Augustin et al., *Discovery of a Narrow Resonance in e^+e^- Annihilation*, *Phys. Rev. Lett.* **33** (1974) 1406.

[88] E598 collaboration, J. J. Aubert et al., *Experimental Observation of a Heavy Particle J*, *Phys. Rev. Lett.* **33** (1974) 1404.

[89] J. H. Christenson, J. W. Cronin, V. L. Fitch and R. Turlay, *Evidence for the 2π Decay of the K_2^0 Meson*, *Phys. Rev. Lett.* **13** (1964) 138.

[90] S. W. Herb et al., *Observation of a Dimuon Resonance at 9.5-GeV in 400-GeV Proton-Nucleus Collisions*, *Phys. Rev. Lett.* **39** (1977) 252.

[91] CDF collaboration, F. Abe et al., *Observation of top quark production in $\bar{p}p$ collisions*, *Phys. Rev. Lett.* **74** (1995) 2626 [`hep-ex/9503002`].

[92] D0 collaboration, S. Abachi et al., *Search for high mass top quark production in $p\bar{p}$ collisions at $\sqrt{s}$ = 1.8 TeV*, *Phys. Rev. Lett.* **74** (1995) 2422 [`hep-ex/9411001`].

[93] S. L. Adler, *Axial vector vertex in spinor electrodynamics*, *Phys. Rev.* **177** (1969) 2426.

[94] J. Bell and R. Jackiw, *A PCAC puzzle: $\pi^0 \to \gamma\gamma$ in the σ model*, *Nuovo Cim. A* **60** (1969) 47.

[95] C. Bouchiat, J. Iliopoulos and P. Meyer, *An Anomaly Free Version of Weinberg's Model*, *Phys. Lett. B* **38** (1972) 519.

[96] Y.-S. Tsai, *Decay Correlations of Heavy Leptons in e+ e- —> Lepton+ Lepton-*, *Phys. Rev. D* **4** (1971) 2821.

[97] M. L. Perl et al., *Evidence for Anomalous Lepton Production in e+ - e- Annihilation*, *Phys. Rev. Lett.* **35** (1975) 1489.

[98] PLUTO collaboration, J. Burmester et al., *Anomalous Muon Production in e+ e- Annihilation as Evidence for Heavy Leptons*, *Phys. Lett. B* **68** (1977) 297.

[99] ARGUS collaboration, H. Albrecht et al., *Determination of the Michel parameter in tau decay*, *Phys. Lett. B* **246** (1990) 278.

[100] DONUT collaboration, K. Kodama et al., *Observation of tau neutrino interactions*, *Phys. Lett. B* **504** (2001) 218 [`hep-ex/0012035`].

[101] CLEO collaboration, S. Ahmed et al., *Update of the search for the neutrinoless decay tau —> muon gamma*, *Phys. Rev. D* **61** (2000) 071101 [`hep-ex/9910060`].

[102] BaBar collaboration, D. Boutigny et al., *The BABAR physics book: Physics at an asymmetric B factory.* 10, 1998, 10.2172/979931.

[103] Belle collaboration, A. Abashian et al., *The Belle Detector*, *Nucl. Instrum. Meth. A* **479** (2002) 117.

[104] Belle collaboration, K. Miyabayashi, *B physics at BELLE, Acta Phys. Polon. B* **32** (2001) 1663.

[105] Belle collaboration, A. Matyja et al., *Observation of $B^0 \to D^{*-}\tau^+\nu_\tau$ decay at Belle*, *Phys. Rev. Lett.* **99** (2007) 191807 [`0706.4429`].

[106] BaBar collaboration, J. Lees et al., *Evidence for an excess of $\bar{B} \to D^{(*)}\tau^-\bar{\nu}_\tau$ decays*, *Phys. Rev. Lett.* **109** (2012) 101802 [`1205.5442`].

[107] BaBar collaboration, J. Lees et al., *Measurement of an Excess of $\bar{B} \to D^{(*)}\tau^-\bar{\nu}_\tau$ Decays and Implications for Charged Higgs Bosons*, *Phys. Rev. D* **88** (2013) 072012 [`1303.0571`].

[108] Belle collaboration, M. Huschle et al., *Measurement of the branching ratio of $\bar{B} \to D^{(*)}\tau^-\bar{\nu}_\tau$ relative to $\bar{B} \to D^{(*)}\ell^-\bar{\nu}_\ell$ decays with hadronic tagging at Belle*, *Phys. Rev. D* **92** (2015) 072014 [`1507.03233`].

[109] LHCb collaboration, R. Aaij et al., *Measurement of the ratio of branching fractions $\mathcal{B}(\bar{B}^0 \to D^{*+}\tau^-\bar{\nu}_\tau)/\mathcal{B}(\bar{B}^0 \to D^{*+}\mu^-\bar{\nu}_\mu)$, *Phys. Rev. Lett.* **115** (2015) 111803 [`1506.08614`].

[110] LHCb collaboration, R. Aaij et al., *Test of Lepton Flavor Universality by the measurement of the $B^0 \to D^{*-}\tau^+\nu_\tau$ branching fraction using three-prong τ decays*, *Phys. Rev. D* **97** (2018) 072013 [`1711.02505`].

[111] LHCb collaboration, R. Aaij et al., *Measurement of the ratio of the $B^0 \to D^{*-}\tau^+\nu_\tau$ and $B^0 \to D^{*-}\mu^+\nu_\mu$ branching fractions using three-prong τ-lepton decays*, *Phys. Rev. Lett.* **120** (2018) 171802 [`1708.08856`].

[112] Belle collaboration, A. Abdesselam et al., *Measurement of $\mathcal{R}(D)$ and $\mathcal{R}(D^*)$ with a semileptonic tagging method*, `1904.08794`.

[113] LHCb collaboration, R. Aaij et al., *Test of lepton universality using $B^+ \to K^+\ell^+\ell^-$ decays*, *Phys. Rev. Lett.* **113** (2014) 151601 [`1406.6482`].

[114] CMS, LHCB collaboration, V. Khachatryan et al., *Observation of the rare $B_s^0 \to \mu^+\mu^-$ decay from the combined analysis of CMS and LHCb data*, *Nature* **522** (2015) 68 [1411.4413].

[115] LHCB collaboration, R. Aaij et al., *Angular analysis of the $B^0 \to K^{*0}\mu^+\mu^-$ decay using 3 fb^{-1} of integrated luminosity*, *JHEP* **02** (2016) 104 [1512.04442].

[116] BELLE collaboration, A. Abdesselam et al., *Angular analysis of $B^0 \to K^*(892)^0\ell^+\ell^-$*, in *LHC Ski 2016: A First Discussion of 13 TeV Results*, 4, 2016, 1604.04042.

[117] LHCB collaboration, R. Aaij et al., *Test of lepton universality with $B^0 \to K^{*0}\ell^+\ell^-$ decays*, *JHEP* **08** (2017) 055 [1705.05802].

[118] LHCB collaboration, R. Aaij et al., *Search for lepton-universality violation in $B^+ \to K^+\ell^+\ell^-$ decays*, *Phys. Rev. Lett.* **122** (2019) 191801 [1903.09252].

[119] LHCB collaboration, R. Aaij et al., *Measurement of CP-Averaged Observables in the $B^0 \to K^{*0}\mu^+\mu^-$ Decay*, *Phys. Rev. Lett.* **125** (2020) 011802 [2003.04831].

[120] P. F. Perez, C. Murgui and A. D. Plascencia, *Leptoquarks and matter unification: Flavor anomalies and the muon g-2*, *Phys. Rev. D* **104** (2021) 035041 [2104.11229].

[121] LHCB collaboration, R. Aaij et al., *Tests of lepton universality using $B^0 \to K_S^0\ell^+\ell^-$ and $B^+ \to K^{*+}\ell^+\ell^-$ decays*, 2110.09501.

[122] D. London and J. Matias, *B Flavour Anomalies: 2021 Theoretical Status Report*, 2110.13270.

[123] MUON G-2 collaboration, G. Bennett et al., *Final Report of the Muon E821 Anomalous Magnetic Moment Measurement at BNL*, *Phys. Rev. D* **73** (2006) 072003 [hep-ex/0602035].

[124] MUON G-2 collaboration, B. Abi et al., *Measurement of the Positive Muon Anomalous Magnetic Moment to 0.46 ppm*, *Phys. Rev. Lett.* **126** (2021) 141801 [2104.03281].

[125] CMS collaboration, A. M. Sirunyan et al., *Search for resonant and nonresonant new phenomena in high-mass dilepton final states at $\sqrt{s}$ = 13 TeV*, *JHEP* **07** (2021) 208 [2103.02708].

[126] F. Cei, *Status and perspectives of Lepton Flavour Violation experiments with muons.*, *J. Phys. Conf. Ser.* **1526** (2020) 012020.

[127] A. Schöning, "LFV experiments." https://indico.cern.ch/event/667965/contributions/2787021/attachments/1584557/2504921/LFV_Experiments.pdf, 1, 2018.

[128] MEG collaboration, A. M. Baldini et al., *Search for the lepton flavour violating decay $\mu^+ \to e^+\gamma$ with the full dataset of the MEG experiment*, *Eur. Phys. J. C* **76** (2016) 434 [1605.05081].

[129] SINDRUM collaboration, U. Bellgardt et al., *Search for the Decay mu+ —>
e+ e+ e-*, *Nucl. Phys. B* **299** (1988) 1.

[130] SINDRUM II collaboration, W. H. Bertl et al., *A Search for muon to electron
conversion in muonic gold*, *Eur. Phys. J. C* **47** (2006) 337.

[131] S. Mihara, *cLFV/g-2/EDM Experiments*, *PoS* **ICHEP2018** (2019) 714.

[132] MEG II collaboration, A. M. Baldini et al., *The design of the MEG II experiment*, *Eur. Phys. J. C* **78** (2018) 380 [`1801.04688`].

[133] A. Blondel et al., *Research Proposal for an Experiment to Search for the Decay
$\mu \to eee$*, `1301.6113`.

[134] Mu2e collaboration, L. Bartoszek et al., *Mu2e Technical Design Report*,
`1501.05241`.

[135] COMET collaboration, Y. Kuno, *A search for muon-to-electron conversion at
J-PARC: The COMET experiment*, *PTEP* **2013** (2013) 022C01.

[136] Mu2e collaboration, F. Abusalma et al., *Expression of Interest for Evolution
of the Mu2e Experiment*, `1802.02599`.

[137] R. J. Barlow, *The PRISM/PRIME project*, *Nucl. Phys. B Proc. Suppl.* **218**
(2011) 44.

[138] S. Gninenko, S. Kovalenko, S. Kuleshov, V. E. Lyubovitskij and A. S.
Zhevlakov, *Deep inelastic $e - \tau$ and $\mu - \tau$ conversion in the NA64 experiment at the CERN SPS*, *Phys. Rev. D* **98** (2018) 015007 [`1804.05550`].

[139] S. N. Gninenko, M. M. Kirsanov, N. V. Krasnikov and V. A. Matveev, *Probing
lepton flavor violation in $\nu_\mu N \to \tau...$ scattering and $\mu \to \tau$ conversion on
nucleons*, *Mod. Phys. Lett.* **A17** (2002) 1407 [`hep-ph/0106302`].

[140] M. Sher and I. Turan, *$\mu N \to \tau N$ at a muon or neutrino factory*, *Phys. Rev.*
D69 (2004) 017302 [`hep-ph/0309183`].

[141] A. Abada, V. De Romeri, J. Orloff and A. M. Teixeira, *In-flight cLFV conversion: $e - \mu$, $e - \tau$ and $\mu - \tau$ in minimal extensions of the standard model
with sterile fermions*, *Eur. Phys. J.* **C77** (2017) 304 [`1612.05548`].

[142] M. Takeuchi, Y. Uesaka and M. Yamanaka, *Higgs mediated CLFV processes $\mu N(eN) \to \tau X$ via gluon operators*, *Phys. Lett.* **B772** (2017) 279
[`1705.01059`].

[143] J.-P. Delahaye et al., *Enabling Intensity and Energy Frontier Science with a
Muon Accelerator Facility in the U.S.: A White Paper Submitted to the 2013
U.S. Community Summer Study of the Division of Particles and Fields of the
American Physical Society*, in *Proceedings, 2013 Community Summer Study on
the Future of U.S. Particle Physics: Snowmass on the Mississippi (CSS2013):
Minneapolis, MN, USA, July 29-August 6, 2013*, 2013, `1308.0494`,
http://www.slac.stanford.edu/econf/C1307292/docs/submittedArxivFiles/1308.0494.pdf.

[144] EIC collaboration, A. Deshpande, *Physics of an Electron Ion Collider*, *Nucl. Phys. A* **904-905** (2013) 302c.

[145] J. L. Zhang et al., *Search for $e \to \tau$ Charged Lepton Flavor Violation at the EIC with the ECCE Detector*, 2207.10261.

[146] H. Baer, T. Barklow, K. Fujii, Y. Gao, A. Hoang, S. Kanemura et al., *The International Linear Collider Technical Design Report - Volume 2: Physics*, 1306.6352.

[147] Y. C. Acar, A. N. Akay, S. Beser, A. C. Canbay, H. Karadeniz, U. Kaya et al., *Future circular collider based lepton–hadron and photon–hadron colliders: Luminosity and physics*, *Nucl. Instrum. Meth.* **A871** (2017) 47 [1608.02190].

[148] T.-P. Cheng and L.-F. Li, *Muon Number Nonconservation Effects in a Gauge Theory with $V + A$ Currents and Heavy Neutral Leptons*, *Phys. Rev.* **D16** (1977) 1425.

[149] S. T. Petcov, *The Processes $\mu \to e\gamma$, $\mu \to ee\bar{e}$, $\nu' \to \nu\gamma$ in the Weinberg-Salam Model with Neutrino Mixing*, *Sov. J. Nucl. Phys.* **25** (1977) 340.

[150] S. M. Bilenky, S. T. Petcov and B. Pontecorvo, *Lepton Mixing, $\mu \to e\gamma$ Decay and Neutrino Oscillations*, *Phys. Lett. B* **67** (1977) 309.

[151] W. J. Marciano and A. I. Sanda, *Exotic Decays of the Muon and Heavy Leptons in Gauge Theories*, *Phys. Lett. B* **67** (1977) 303.

[152] B. W. Lee and R. E. Shrock, *Natural Suppression of Symmetry Violation in Gauge Theories: Muon - Lepton and Electron Lepton Number Nonconservation*, *Phys. Rev. D* **16** (1977) 1444.

[153] D. N. Dinh, A. Ibarra, E. Molinaro and S. T. Petcov, *The $\mu - e$ Conversion in Nuclei, $\mu \to e\gamma$, $\mu \to 3e$ Decays and TeV Scale See-Saw Scenarios of Neutrino Mass Generation*, *JHEP* **08** (2012) 125 [1205.4671].

[154] A. Celis, V. Cirigliano and E. Passemar, *Lepton flavor violation in the Higgs sector and the role of hadronic τ-lepton decays*, *Phys. Rev.* **D89** (2014) 013008 [1309.3564].

[155] J. F. Donoghue, J. Gasser and H. Leutwyler, *The Decay of a Light Higgs Boson*, *Nucl. Phys.* **B343** (1990) 341.

[156] D. Gómez Dumm, A. Pich and J. Portolés, *The Hadronic off-shell width of meson resonances*, *Phys. Rev. D* **62** (2000) 054014 [hep-ph/0003320].

[157] F. Guerrero and A. Pich, *Effective field theory description of the pion form-factor*, *Phys. Lett. B* **412** (1997) 382 [hep-ph/9707347].

[158] A. Pich and J. Portolés, *The Vector form-factor of the pion from unitarity and analyticity: A Model independent approach*, *Phys. Rev. D* **63** (2001) 093005 [hep-ph/0101194].

[159] D. Gómez Dumm and P. Roig, *Dispersive representation of the pion vector form factor in $\tau \to \pi\pi\nu_\tau$ decays*, *Eur. Phys. J. C* **73** (2013) 2528 [`1301.6973`].

[160] P. Masjuan, S. Peris and J. Sanz-Cillero, *Vector Meson Dominance as a first step in a systematic approximation: The Pion vector form-factor*, *Phys. Rev. D* **78** (2008) 074028 [`0807.4893`].

[161] E. Arganda, M. J. Herrero and J. Portolés, *Lepton flavour violating semileptonic tau decays in constrained MSSM-seesaw scenarios*, *JHEP* **06** (2008) 079 [`0803.2039`].

[162] SINDRUM II collaboration, W. H. Bertl et al., *A Search for muon to electron conversion in muonic gold*, *Eur. Phys. J. C* **47** (2006) 337.

[163] J. Rojo, *The Partonic Content of Nucleons and Nuclei*, `1910.03408`.

[164] European Muon collaboration, J. Aubert et al., *The ratio of the nucleon structure functions $F2_n$ for iron and deuterium*, *Phys. Lett. B* **123** (1983) 275.

[165] K. Kovarik et al., *nCTEQ15 - Global analysis of nuclear parton distributions with uncertainties in the CTEQ framework*, *Phys. Rev. D* **93** (2016) 085037 [`1509.00792`].

[166] D. Clark, E. Godat and F. Olness, *ManeParse : A Mathematica reader for Parton Distribution Functions*, *Comput. Phys. Commun.* **216** (2017) 126 [`1605.08012`].

[167] E. Leader and E. Predazzi, *An Introduction to gauge theories and modern particle physics. Vol. 2: CP violation, QCD and hard processes*, vol. 4. Cambridge University Press, 3, 1996.

[168] J. F. Owens and W.-K. Tung, *Parton distribution functions of hadrons*, *Ann. Rev. Nucl. Part. Sci.* **42** (1992) 291.

[169] J. de Blas et al., `HEPfit`: *a Code for the Combination of Indirect and Direct Constraints on High Energy Physics Models*, `1910.14012`.

[170] A. Caldwell, D. Kollar and K. Kroninger, *BAT: The Bayesian Analysis Toolkit*, *Comput. Phys. Commun.* **180** (2009) 2197 [`0808.2552`].

[171] A. C. Caldwell, D. Kollar and K. Kroninger, *BAT: The Bayesian analysis toolkit*, *J. Phys. Conf. Ser.* **219** (2010) 032013.

[172] F. Beaujean, A. Caldwell, D. Kollar and K. Kroninger, *BAT: The Bayesian analysis toolkit*, *J. Phys. Conf. Ser.* **331** (2011) 072040.

[173] HFLAV collaboration, Y. S. Amhis et al., *Averages of b-hadron, c-hadron, and τ-lepton properties as of 2018*, `1909.12524`.

[174] V. de Alfaro, S. Fubini, G. Furlan and C. Rossetti, *Currents in Hadron Physics*. North-Holland Publishing Company, 1973.

[175] D. Lurié, *Particles and Fields*. Interscience Publishers, John Wyley & Sons, 1968.

[176] S. Fubini and G. Furlan, *Renormalization effects for partially conserved currents*, *Physics Physique Fizika* **1** (1965) 229.

[177] M. Ademollo and R. Gatto, *Nonrenormalization Theorem for the Strangeness Violating Vector Currents*, *Phys. Rev. Lett.* **13** (1964) 264.

[178] M. Jamin, J. A. Oller and A. Pich, *Strangeness changing scalar form-factors*, *Nucl. Phys. B* **622** (2002) 279 [`hep-ph/0110193`].

[179] J. C. Pati and A. Salam, *Unified Lepton-Hadron Symmetry and a Gauge Theory of the Basic Interactions*, *Phys. Rev. D* **8** (1973) 1240.

[180] J. C. Pati and A. Salam, *Lepton Number as the Fourth Color*, *Phys. Rev. D* **10** (1974) 275.

[181] H. Georgi and S. L. Glashow, *Unity of All Elementary Particle Forces*, *Phys. Rev. Lett.* **32** (1974) 438.

[182] H. Georgi, *The State of the Art—Gauge Theories*, *AIP Conf. Proc.* **23** (1975) 575.

[183] H. Fritzsch and P. Minkowski, *Unified Interactions of Leptons and Hadrons*, *Annals Phys.* **93** (1975) 193.

[184] E. Witten, *Symmetry Breaking Patterns in Superstring Models*, *Nucl. Phys. B* **258** (1985) 75.

[185] J. L. Hewett and T. G. Rizzo, *Low-Energy Phenomenology of Superstring Inspired E(6) Models*, *Phys. Rept.* **183** (1989) 193.

[186] S. Dimopoulos and L. Susskind, *Mass Without Scalars*, *Nuclear Physics B* **155** (1979) 237.

[187] J. R. Ellis, M. K. Gaillard, D. V. Nanopoulos and P. Sikivie, *Can One Test Technicolor?*, *Nucl. Phys. B* **182** (1981) 529.

[188] E. Farhi and L. Susskind, *Technicolor*, *Phys. Rept.* **74** (1981) 277.

[189] B. Schrempp and F. Schrempp, *Light Leptoquarks*, *Phys. Lett. B* **153** (1985) 101.

[190] W. Buchmüller, *Composite Quarks and Leptons*, *Acta Phys. Austriaca Suppl.* **27** (1985) 517.

[191] B. Gripaios, *Composite Leptoquarks at the LHC*, *JHEP* **02** (2010) 045 [`0910.1789`].

[192] A. Davies and X.-G. He, *Tree Level Scalar Fermion Interactions Consistent With the Symmetries of the Standard Model*, *Phys. Rev. D* **43** (1991) 225.

[193] J. M. Arnold, B. Fornal and M. B. Wise, *Phenomenology of scalar leptoquarks*, *Phys. Rev. D* **88** (2013) 035009 [1304.6119].

[194] I. Doršner, S. Fajfer, A. Greljo, J. Kamenik and N. Košnik, *Physics of leptoquarks in precision experiments and at particle colliders*, *Phys. Rept.* **641** (2016) 1 [1603.04993].

[195] O. Popov and G. A. White, *One Leptoquark to unify them? Neutrino masses and unification in the light of $(g-2)_\mu$, $R_{D^{(\star)}}$ and R_K anomalies*, *Nucl. Phys. B* **923** (2017) 324 [1611.04566].

[196] K. Cheung, T. Nomura and H. Okada, *A Three-loop Neutrino Model with Leptoquark Triplet Scalars*, *Phys. Lett. B* **768** (2017) 359 [1701.01080].

[197] A. Crivellin, D. Müller and T. Ota, *Simultaneous explanation of $R(D^{(*)})$ and $b \to s\mu^+\mu^-$: the last scalar leptoquarks standing*, *JHEP* **09** (2017) 040 [1703.09226].

[198] Y. Cai, J. Gargalionis, M. A. Schmidt and R. R. Volkas, *Reconsidering the One Leptoquark solution: flavor anomalies and neutrino mass*, *JHEP* **10** (2017) 047 [1704.05849].

[199] D. Buttazzo, A. Greljo, G. Isidori and D. Marzocca, *B-physics anomalies: a guide to combined explanations*, *JHEP* **11** (2017) 044 [1706.07808].

[200] S. Sahoo and R. Mohanta, *Impact of vector leptoquark on $\bar{B} \to \bar{K}^* l^+ l^-$ anomalies*, *J. Phys. G* **45** (2018) 085003 [1806.01048].

[201] D. Bečirević, I. Doršner, S. Fajfer, N. Košnik, D. A. Faroughy and O. Sumensari, *Scalar leptoquarks from grand unified theories to accommodate the B-physics anomalies*, *Phys. Rev. D* **98** (2018) 055003 [1806.05689].

[202] A. Crivellin, C. Greub, D. Müller and F. Saturnino, *Importance of Loop Effects in Explaining the Accumulated Evidence for New Physics in B Decays with a Vector Leptoquark*, *Phys. Rev. Lett.* **122** (2019) 011805 [1807.02068].

[203] A. Biswas, D. Kumar Ghosh, N. Ghosh, A. Shaw and A. K. Swain, *Collider signature of U_1 Leptoquark and constraints from $b \to c$ observables*, *J. Phys. G* **47** (2020) 045005 [1808.04169].

[204] A. Angelescu, D. Bečirević, D. Faroughy and O. Sumensari, *Closing the window on single leptoquark solutions to the B-physics anomalies*, *JHEP* **10** (2018) 183 [1808.08179].

[205] S. Bansal, R. M. Capdevilla and C. Kolda, *Constraining the minimal flavor violating leptoquark explanation of the $R_{D^{(*)}}$ anomaly*, *Phys. Rev. D* **99** (2019) 035047 [1810.11588].

[206] S. Iguro, T. Kitahara, Y. Omura, R. Watanabe and K. Yamamoto, *D^* polarization vs. $R_{D^{(*)}}$ anomalies in the leptoquark models*, *JHEP* **02** (2019) 194 [1811.08899].

[207] J. Aebischer, A. Crivellin and C. Greub, *QCD improved matching for semileptonic B decays with leptoquarks*, *Phys. Rev. D* **99** (2019) 055002 [1811.08907].

[208] C. Cornella, J. Fuentes-Martín and G. Isidori, *Revisiting the vector leptoquark explanation of the B-physics anomalies*, *JHEP* **07** (2019) 168 [1903.11517].

[209] H. Yan, Y.-D. Yang and X.-B. Yuan, *Phenomenology of $b \to c\tau\bar{\nu}$ decays in a scalar leptoquark model*, *Chin. Phys. C* **43** (2019) 083105 [1905.01795].

[210] O. Popov, M. A. Schmidt and G. White, *R_2 as a single leptoquark solution to $R_{D^{(*)}}$ and $R_{K^{(*)}}$*, *Phys. Rev. D* **100** (2019) 035028 [1905.06339].

[211] A. Crivellin and F. Saturnino, *Explaining the Flavor Anomalies with a Vector Leptoquark (Moriond 2019 update)*, *PoS* **DIS2019** (2019) 163 [1906.01222].

[212] A. Crivellin, D. Müller and F. Saturnino, *Flavor Phenomenology of the Leptoquark Singlet-Triplet Model*, *JHEP* **06** (2020) 020 [1912.04224].

[213] S. Saad, *Combined explanations of $(g - 2)_\mu$, $R_{D^{(*)}}$, $R_{K^{(*)}}$ anomalies in a two-loop radiative neutrino mass model*, *Phys. Rev. D* **102** (2020) 015019 [2005.04352].

[214] V. Gherardi, D. Marzocca and E. Venturini, *Low-energy phenomenology of scalar leptoquarks at one-loop accuracy*, *JHEP* **01** (2021) 138 [2008.09548].

[215] K. S. Babu, P. S. B. Dev, S. Jana and A. Thapa, *Unified framework for B-anomalies, muon $g - 2$ and neutrino masses*, *JHEP* **03** (2021) 179 [2009.01771].

[216] M. Bordone, O. Catà, T. Feldmann and R. Mandal, *Constraining flavour patterns of scalar leptoquarks in the effective field theory*, *JHEP* **03** (2021) 122 [2010.03297].

[217] A. Crivellin, C. Greub, D. Müller and F. Saturnino, *Scalar Leptoquarks in Leptonic Processes*, *JHEP* **02** (2021) 182 [2010.06593].

[218] S. Davidson, D. C. Bailey and B. A. Campbell, *Model independent constraints on leptoquarks from rare processes*, *Z. Phys. C* **61** (1994) 613 [hep-ph/9309310].

[219] K. Babu and J. Julio, *Two-Loop Neutrino Mass Generation through Leptoquarks*, *Nucl. Phys. B* **841** (2010) 130 [1006.1092].

[220] A. Crivellin, M. Hoferichter and P. Schmidt-Wellenburg, *Combined explanations of $(g - 2)_{\mu,e}$ and implications for a large muon EDM*, *Phys. Rev. D* **98** (2018) 113002 [1807.11484].

[221] K. Kowalska, E. M. Sessolo and Y. Yamamoto, *Constraints on charmphilic solutions to the muon g-2 with leptoquarks*, *Phys. Rev. D* **99** (2019) 055007 [1812.06851].

[222] R. Mandal and A. Pich, *Constraints on scalar leptoquarks from lepton and kaon physics*, *JHEP* **12** (2019) 089 [1908.11155].

[223] I. Doršner, S. Fajfer and O. Sumensari, *Muon g − 2 and scalar leptoquark mixing*, *JHEP* **06** (2020) 089 [`1910.03877`].

[224] I. Bigaran and R. R. Volkas, *Getting chirality right: Single scalar leptoquark solutions to the* $(g−2)_{e,\mu}$ *puzzle*, *Phys. Rev. D* **102** (2020) 075037 [`2002.12544`].

[225] I. Bigaran and R. R. Volkas, *Reflecting on Chirality: CP-violating extensions of the single scalar-leptoquark solutions for the* $(g − 2)_{e,\mu}$ *puzzles and their implications for lepton EDMs*, `2110.03707`.

[226] M. Davier, A. Hoecker, B. Malaescu and Z. Zhang, *A new evaluation of the hadronic vacuum polarisation contributions to the muon anomalous magnetic moment and to* $\boldsymbol{\alpha(m_Z^2)}$, *Eur. Phys. J. C* **80** (2020) 241 [`1908.00921`].

[227] L. Delle Rose, C. Marzo and L. Marzola, *Simplified leptoquark models for precision* $l_i \to l_f \gamma$ *experiments: two-loop structure of* $O(\alpha_S Y^2)$ *corrections*, *Phys. Rev. D* **102** (2020) 115020 [`2005.12389`].

[228] D. Zhang, *Radiative neutrino masses, lepton flavor mixing and muon g − 2 in a leptoquark model*, *JHEP* **07** (2021) 069 [`2105.08670`].

[229] P. Bandyopadhyay and R. Mandal, *Revisiting scalar leptoquark at the LHC*, *Eur. Phys. J. C* **78** (2018) 491 [`1801.04253`].

[230] G. Hiller, D. Loose and I. Nišandžić, *Flavorful leptoquarks at hadron colliders*, *Phys. Rev. D* **97** (2018) 075004 [`1801.09399`].

[231] A. Monteux and A. Rajaraman, *B Anomalies and Leptoquarks at the LHC: Beyond the Lepton-Quark Final State*, *Phys. Rev. D* **98** (2018) 115032 [`1803.05962`].

[232] A. Crivellin, D. Müller and F. Saturnino, *Leptoquarks in oblique corrections and Higgs signal strength: status and prospects*, *JHEP* **11** (2020) 094 [`2006.10758`].

[233] M. Schmaltz and Y.-M. Zhong, *The leptoquark Hunter's guide: large coupling*, *JHEP* **01** (2019) 132 [`1810.10017`].

[234] A. Cerri et al., *Report from Working Group 4: Opportunities in Flavour Physics at the HL-LHC and HE-LHC*, *CERN Yellow Rep. Monogr.* **7** (2019) 867 [`1812.07638`].

[235] T. Faber, M. Hudec, H. Kolešová, Y. Liu, M. Malinský, W. Porod et al., *Collider phenomenology of a unified leptoquark model*, *Phys. Rev. D* **101** (2020) 095024 [`1812.07592`].

[236] J. Zhang, C.-X. Yue, C.-H. Li and S. Yang, *Constraints on scalar and vector leptoquarks from the LHC Higgs data*, `1905.04074`.

[237] K. Chandak, T. Mandal and S. Mitra, *Hunting for scalar leptoquarks with boosted tops and light leptons*, *Phys. Rev. D* **100** (2019) 075019 [`1907.11194`].

[238] B. Allanach, T. Corbett and M. Madigan, *Sensitivity of Future Hadron Colliders to Leptoquark Pair Production in the Di-Muon Di-Jets Channel*, *Eur. Phys. J. C* **80** (2020) 170 [1911.04455].

[239] C. Borschensky, B. Fuks, A. Kulesza and D. Schwartländer, *Scalar leptoquark pair production at hadron colliders*, *Phys. Rev. D* **101** (2020) 115017 [2002.08971].

[240] L. Buonocore, U. Haisch, P. Nason, F. Tramontano and G. Zanderighi, *Lepton-Quark Collisions at the Large Hadron Collider*, *Phys. Rev. Lett.* **125** (2020) 231804 [2005.06475].

[241] ATLAS collaboration, G. Aad et al., *Search for pairs of scalar leptoquarks decaying into quarks and electrons or muons in $\sqrt{s} = 13$ TeV pp collisions with the ATLAS detector*, *JHEP* **10** (2020) 112 [2006.05872].

[242] A. Bhaskar, T. Mandal, S. Mitra and M. Sharma, *Improving third-generation leptoquark searches with combined signals and boosted top quarks*, *Phys. Rev. D* **104** (2021) 075037 [2106.07605].

[243] U. Mahanta, *Neutrino masses and mixing angles from leptoquark interactions*, *Phys. Rev. D* **62** (2000) 073009 [hep-ph/9909518].

[244] F. Deppisch, S. Kulkarni, H. Päs and E. Schumacher, *Leptoquark patterns unifying neutrino masses, flavor anomalies, and the diphoton excess*, *Phys. Rev. D* **94** (2016) 013003 [1603.07672].

[245] I. Bigaran, J. Gargalionis and R. R. Volkas, *A near-minimal leptoquark model for reconciling flavour anomalies and generating radiative neutrino masses*, *JHEP* **10** (2019) 106 [1906.01870].

[246] P. S. Bhupal Dev, R. Mohanta, S. Patra and S. Sahoo, *Unified explanation of flavor anomalies, radiative neutrino masses, and ANITA anomalous events in a vector leptoquark model*, *Phys. Rev. D* **102** (2020) 095012 [2004.09464].

[247] R. Mandal, *Fermionic dark matter in leptoquark portal*, *Eur. Phys. J. C* **78** (2018) 726 [1808.07844].

[248] A. Mohamadnejad, *Accidental scale-invariant Majorana dark matter in leptoquark-Higgs portals*, *Nucl. Phys. B* **949** (2019) 114793 [1904.03857].

[249] C. Hati and U. Sarkar, *$B − L$ violating nucleon decays as a probe of leptoquarks and implications for baryogenesis*, *Nucl. Phys. B* **954** (2020) 114985 [1805.06081].

[250] B. Chauhan and S. Mohanty, *Leptoquark solution for both the flavor and ANITA anomalies*, *Phys. Rev. D* **99** (2019) 095018 [1812.00919].

[251] T. Husek, K. Monsalvez-Pozo and J. Portoles, *Constraints on leptoquarks from lepton-flavour-violating tau-lepton processes*, *JHEP* **04** (2022) 165 [2111.06872].

[252] B. W. Lee, S. Pakvasa, R. E. Shrock and H. Sugawara, *Muon and Electron Number Nonconservation in a V-A Gauge Model*, *Phys. Rev. Lett.* **38** (1977) 937.

[253] J. Bernigaud, M. Blanke, I. d. M. Varzielas, J. Talbert and J. Zurita, *LHC Signatures of τ-Flavoured Vector Leptoquarks*, 2112.12129.

[254] L. Allwicher, *B-physics anomalies: EFT analyses and simplified models*, in *32nd Rencontres de Blois on Particle Physics and Cosmology*, 1, 2022, 2201.04995.

[255] HFLAV collaboration, Y. S. Amhis et al., *Averages of b-hadron, c-hadron, and τ-lepton properties as of 2018*, *Eur. Phys. J. C* **81** (2021) 226 [1909.12524].

[256] A. Crivellin and L. Schnell, *Complete Lagrangian and set of Feynman rules for scalar leptoquarks*, *Comput. Phys. Commun.* **271** (2022) 108188 [2105.04844].

[257] E. Gabrielli, L. Marzola, M. Raidal and H. Veermäe, *Dark matter and spin-1 milli-charged particles*, *JHEP* **08** (2015) 150 [1507.00571].

[258] M. Gonderinger and M. J. Ramsey-Musolf, *Electron-to-Tau Lepton Flavor Violation at the Electron-Ion Collider*, *JHEP* **11** (2010) 045 [1006.5063].

[259] M. Hirsch, H. V. Klapdor-Kleingrothaus and S. G. Kovalenko, *New low-energy leptoquark interactions*, *Phys. Lett. B* **378** (1996) 17 [hep-ph/9602305].

[260] ATLAS collaboration, G. Aad et al., *Search for pair production of third-generation scalar leptoquarks decaying into a top quark and a τ-lepton in pp collisions at $\sqrt{s}$ = 13 TeV with the ATLAS detector*, *JHEP* **06** (2021) 179 [2101.11582].

[261] CMS collaboration, A. M. Sirunyan et al., *Constraints on models of scalar and vector leptoquarks decaying to a quark and a neutrino at $\sqrt{s}$ = 13 TeV*, *Phys. Rev. D* **98** (2018) 032005 [1805.10228].

[262] D. G. Boulware and L. S. Brown, *Tree Graphs and Classical Fields*, *Phys. Rev.* **172** (1968) 1628.

[263] A. L. Koshkarov, *Method of steepest descent for path integrals*, *Theoretical and Mathematical Physics* **102, No 2** (1995) 153.

[264] L. Lavoura, *General formulae for $f_1 \to f_2\gamma$*, *Eur. Phys. J. C* **29** (2003) 191 [hep-ph/0302221].

[265] A. Dedes and K. Mantzaropoulos, *Universal Scalar Leptoquark Action for Matching*, 2108.10055.

[266] M. Beneke and V. A. Smirnov, *Asymptotic expansion of Feynman integrals near threshold*, *Nucl. Phys. B* **522** (1998) 321 [hep-ph/9711391].

[267] V. A. Smirnov, *Applied asymptotic expansions in momenta and masses*, *Springer Tracts Mod. Phys.* **177** (2002) 1.

[268] B. Jantzen, *Foundation and generalization of the expansion by regions*, *JHEP* **12** (2011) 076 [`1111.2589`].

[269] J. Fuentes-Martín, J. Portolés and P. Ruíz-Femenía, *Integrating out heavy particles with functional methods: a simplified framework*, *JHEP* **09** (2016) 156 [`1607.02142`].

[270] J. De Blas et al., `HEPfit`: *a code for the combination of indirect and direct constraints on high energy physics models*, *Eur. Phys. J. C* **80** (2020) 456 [`1910.14012`].

[271] T. Aoyama et al., *The anomalous magnetic moment of the muon in the Standard Model*, *Phys. Rept.* **887** (2020) 1 [`2006.04822`].

[272] T. Ohlsson and H. Zhang, *Non-Standard Interaction Effects at Reactor Neutrino Experiments*, *Phys. Lett. B* **671** (2009) 99 [`0809.4835`].

[273] A. Falkowski, M. González-Alonso and Z. Tabrizi, *Consistent QFT description of non-standard neutrino interactions*, *JHEP* **11** (2020) 048 [`1910.02971`].

[274] V. Bresó-Pla, A. Falkowski, M. González-Alonso and K. Monsalvez-Pozo, *EFT description of the COHERENT experiment*, `In progress`.

[275] D. Z. Freedman, *Coherent Neutrino Nucleus Scattering as a Probe of the Weak Neutral Current*, *Phys. Rev. D* **9** (1974) 1389.

[276] COHERENT collaboration, D. Akimov et al., *Observation of Coherent Elastic Neutrino-Nucleus Scattering*, *Science* **357** (2017) 1123 [`1708.01294`].

[277] C. Giunti, C. W. Kim, J. A. Lee and U. W. Lee, *On the treatment of neutrino oscillations without resort to weak eigenstates*, *Phys. Rev. D* **48** (1993) 4310 [`hep-ph/9305276`].

[278] GARGAMELLE NEUTRINO collaboration, F. J. Hasert et al., *Observation of Neutrino Like Interactions Without Muon Or Electron in the Gargamelle Neutrino Experiment*, *Phys. Lett. B* **46** (1973) 138.

[279] F. J. Hasert et al., *Search for Elastic ν_μ Electron Scattering*, *Phys. Lett. B* **46** (1973) 121.

[280] M. Abdullah et al., *Coherent elastic neutrino-nucleus scattering: Terrestrial and astrophysical applications*, in *2022 Snowmass Summer Study*, 3, 2022, `2203.07361`.

[281] B. C. Cañas, E. A. Garcés, O. G. Miranda and A. Parada, *Future perspectives for a weak mixing angle measurement in coherent elastic neutrino nucleus scattering experiments*, *Phys. Lett. B* **784** (2018) 159 [`1806.01310`].

[282] M. Cadeddu and F. Dordei, *Reinterpreting the weak mixing angle from atomic parity violation in view of the Cs neutron rms radius measurement from COHERENT*, *Phys. Rev. D* **99** (2019) 033010 [`1808.10202`].

[283] M. Cadeddu, C. Giunti, Y. F. Li and Y. Y. Zhang, *Average CsI neutron density distribution from COHERENT data*, *Phys. Rev. Lett.* **120** (2018) 072501 [1710.02730].

[284] E. Ciuffoli, J. Evslin, Q. Fu and J. Tang, *Extracting nuclear form factors with coherent neutrino scattering*, *Phys. Rev. D* **97** (2018) 113003 [1801.02166].

[285] M. Cadeddu, F. Dordei, C. Giunti, Y. F. Li and Y. Y. Zhang, *Neutrino, electroweak, and nuclear physics from COHERENT elastic neutrino-nucleus scattering with refined quenching factor*, *Phys. Rev. D* **101** (2020) 033004 [1908.06045].

[286] D. K. Papoulias, T. S. Kosmas, R. Sahu, V. K. B. Kota and M. Hota, *Constraining nuclear physics parameters with current and future COHERENT data*, *Phys. Lett. B* **800** (2020) 135133 [1903.03722].

[287] A. N. Khan and W. Rodejohann, *New physics from COHERENT data with an improved quenching factor*, *Phys. Rev. D* **100** (2019) 113003 [1907.12444].

[288] X.-R. Huang and L.-W. Chen, *Neutron Skin in CsI and Low-Energy Effective Wek Mixing Angle from COHERENT Data*, *Phys. Rev. D* **100** (2019) 071301 [1902.07625].

[289] B. C. Canas, E. A. Garces, O. G. Miranda, A. Parada and G. Sanchez Garcia, *Interplay between nonstandard and nuclear constraints in coherent elastic neutrino-nucleus scattering experiments*, *Phys. Rev. D* **101** (2020) 035012 [1911.09831].

[290] M. Cadeddu, F. Dordei, C. Giunti, Y. F. Li, E. Picciau and Y. Y. Zhang, *Physics results from the first COHERENT observation of coherent elastic neutrino-nucleus scattering in argon and their combination with cesium-iodide data*, *Phys. Rev. D* **102** (2020) 015030 [2005.01645].

[291] O. G. Miranda, D. K. Papoulias, G. Sanchez Garcia, O. Sanders, M. Tórtola and J. W. F. Valle, *Implications of the first detection of coherent elastic neutrino-nucleus scattering (CEvNS) with Liquid Argon*, *JHEP* **05** (2020) 130 [2003.12050].

[292] P. Coloma, I. Esteban, M. C. Gonzalez-Garcia and J. Menendez, *Determining the nuclear neutron distribution from Coherent Elastic neutrino-Nucleus Scattering: current results and future prospects*, *JHEP* **08** (2020) 030 [2006.08624].

[293] T. W. Donnelly, J. Dubach and I. Sick, *Isospin Dependences in Parity Violating Electron Scattering*, *Nucl. Phys. A* **503** (1989) 589.

[294] T. W. Donnelly and I. Sick, *ELASTIC MAGNETIC ELECTRON SCATTERING FROM NUCLEI*, *Rev. Mod. Phys.* **56** (1984) 461.

[295] I. Angeli and K. P. Marinova, *Table of experimental nuclear ground state charge radii: An update*, *Atom. Data Nucl. Data Tabl.* **99** (2013) 69.

[296] P. Coloma, P. B. Denton, M. C. Gonzalez-Garcia, M. Maltoni and T. Schwetz, *Curtailing the Dark Side in Non-Standard Neutrino Interactions*, *JHEP* **04** (2017) 116 [1701.04828].

[297] P. Coloma, M. C. Gonzalez-Garcia, M. Maltoni and T. Schwetz, *COHERENT Enlightenment of the Neutrino Dark Side*, *Phys. Rev. D* **96** (2017) 115007 [1708.02899].

[298] J. Liao and D. Marfatia, *COHERENT constraints on nonstandard neutrino interactions*, *Phys. Lett. B* **775** (2017) 54 [1708.04255].

[299] J. B. Dent, B. Dutta, S. Liao, J. L. Newstead, L. E. Strigari and J. W. Walker, *Accelerator and reactor complementarity in coherent neutrino-nucleus scattering*, *Phys. Rev. D* **97** (2018) 035009 [1711.03521].

[300] I. M. Shoemaker, *COHERENT search strategy for beyond standard model neutrino interactions*, *Phys. Rev. D* **95** (2017) 115028 [1703.05774].

[301] I. Esteban, M. C. Gonzalez-Garcia, M. Maltoni, I. Martinez-Soler and J. Salvado, *Updated constraints on non-standard interactions from global analysis of oscillation data*, *JHEP* **08** (2018) 180 [1805.04530].

[302] D. Aristizabal Sierra, V. De Romeri and N. Rojas, *COHERENT analysis of neutrino generalized interactions*, *Phys. Rev. D* **98** (2018) 075018 [1806.07424].

[303] J. Billard, J. Johnston and B. J. Kavanagh, *Prospects for exploring New Physics in Coherent Elastic Neutrino-Nucleus Scattering*, *JCAP* **11** (2018) 016 [1805.01798].

[304] P. B. Denton, Y. Farzan and I. M. Shoemaker, *Testing large non-standard neutrino interactions with arbitrary mediator mass after COHERENT data*, *JHEP* **07** (2018) 037 [1804.03660].

[305] D. K. Papoulias, *COHERENT constraints after the COHERENT-2020 quenching factor measurement*, *Phys. Rev. D* **102** (2020) 113004 [1907.11644].

[306] C. Giunti, *General COHERENT constraints on neutrino nonstandard interactions*, *Phys. Rev. D* **101** (2020) 035039 [1909.00466].

[307] P. Coloma, I. Esteban, M. C. Gonzalez-Garcia and M. Maltoni, *Improved global fit to Non-Standard neutrino Interactions using COHERENT energy and timing data*, *JHEP* **02** (2020) 023 [1911.09109].

[308] L. J. Flores, N. Nath and E. Peinado, *Non-standard neutrino interactions in U(1)' model after COHERENT data*, *JHEP* **06** (2020) 045 [2002.12342].

[309] P. Coloma, I. Esteban, M. C. Gonzalez-Garcia, L. Larizgoitia, F. Monrabal and S. Palomares-Ruiz, *Bounds on new physics with data of the Dresden-II reactor experiment and COHERENT*, *JHEP* **05** (2022) 037 [2202.10829].

[310] M. Atzori Corona, M. Cadeddu, N. Cargioli, F. Dordei, C. Giunti, Y. F. Li et al., *Impact of the Dresden-II and COHERENT neutrino scattering data on neutrino electromagnetic properties and electroweak physics*, 2205.09484.

[311] D. K. Papoulias and T. S. Kosmas, *COHERENT constraints to conventional and exotic neutrino physics*, *Phys. Rev. D* **97** (2018) 033003 [1711.09773].

[312] M. Cadeddu, C. Giunti, K. A. Kouzakov, Y.-F. Li, Y.-Y. Zhang and A. I. Studenikin, *Neutrino Charge Radii From Coherent Elastic Neutrino-nucleus Scattering*, *Phys. Rev. D* **98** (2018) 113010 [1810.05606].

[313] O. G. Miranda, D. K. Papoulias, M. Tórtola and J. W. F. Valle, *Probing neutrino transition magnetic moments with coherent elastic neutrino-nucleus scattering*, *JHEP* **07** (2019) 103 [1905.03750].

[314] C. Hati, P. Bolton, F. F. Deppisch, K. Fridell, J. Harz and S. Kulkarni, *Distinguishing Dirac vs Majorana Neutrinos at CEνNS experiments*, *PoS* **EPS-HEP2021** (2022) 225.

[315] A. J. Anderson, J. M. Conrad, E. Figueroa-Feliciano, C. Ignarra, G. Karagiorgi, K. Scholberg et al., *Measuring Active-to-Sterile Neutrino Oscillations with Neutral Current Coherent Neutrino-Nucleus Scattering*, *Phys. Rev. D* **86** (2012) 013004 [1201.3805].

[316] T. S. Kosmas, D. K. Papoulias, M. Tortola and J. W. F. Valle, *Probing light sterile neutrino signatures at reactor and Spallation Neutron Source neutrino experiments*, *Phys. Rev. D* **96** (2017) 063013 [1703.00054].

[317] C. Blanco, D. Hooper and P. Machado, *Constraining Sterile Neutrino Interpretations of the LSND and MiniBooNE Anomalies with Coherent Neutrino Scattering Experiments*, *Phys. Rev. D* **101** (2020) 075051 [1901.08094].

[318] O. G. Miranda, D. K. Papoulias, O. Sanders, M. Tórtola and J. W. F. Valle, *Future CEvNS experiments as probes of lepton unitarity and light-sterile neutrinos*, *Phys. Rev. D* **102** (2020) 113014 [2008.02759].

[319] S.-F. Ge and I. M. Shoemaker, *Constraining Photon Portal Dark Matter with Texono and Coherent Data*, *JHEP* **11** (2018) 066 [1710.10889].

[320] V. Brdar, W. Rodejohann and X.-J. Xu, *Producing a new Fermion in Coherent Elastic Neutrino-Nucleus Scattering: from Neutrino Mass to Dark Matter*, *JHEP* **12** (2018) 024 [1810.03626].

[321] J. B. Dent, B. Dutta, S. Liao, J. L. Newstead, L. E. Strigari and J. W. Walker, *Probing light mediators at ultralow threshold energies with coherent elastic neutrino-nucleus scattering*, *Phys. Rev. D* **96** (2017) 095007 [1612.06350].

[322] M. Abdullah, J. B. Dent, B. Dutta, G. L. Kane, S. Liao and L. E. Strigari, *Coherent elastic neutrino nucleus scattering as a probe of a Z' through kinetic and mass mixing effects*, *Phys. Rev. D* **98** (2018) 015005 [1803.01224].

[323] CONNIE collaboration, A. Aguilar-Arevalo et al., *Search for light mediators in the low-energy data of the CONNIE reactor neutrino experiment*, *JHEP* **04** (2020) 054 [1910.04951].

[324] P. Coloma, M. C. Gonzalez-Garcia and M. Maltoni, *Neutrino oscillation constraints on U(1)' models: from non-standard interactions to long-range forces*, *JHEP* **01** (2021) 114 [2009.14220].

[325] CONUS collaboration, H. Bonet et al., *Novel constraints on neutrino physics beyond the standard model from the CONUS experiment*, *JHEP* **05** (2022) 085 [2110.02174].

[326] L. M. G. de la Vega, L. J. Flores, N. Nath and E. Peinado, *Complementarity between dark matter direct searches and CEνNS experiments in U(1)' models*, *JHEP* **09** (2021) 146 [2107.04037].

[327] M. Atzori Corona, M. Cadeddu, N. Cargioli, F. Dordei, C. Giunti, Y. F. Li et al., *Probing light mediators and $(g - 2)_\mu$ through detection of coherent elastic neutrino nucleus scattering at COHERENT*, *JHEP* **05** (2022) 109 [2202.11002].

[328] M. Cadeddu, N. Cargioli, F. Dordei, C. Giunti, Y. F. Li, E. Picciau et al., *Constraints on light vector mediators through coherent elastic neutrino nucleus scattering data from COHERENT*, *JHEP* **01** (2021) 116 [2008.05022].

[329] Y. Farzan, M. Lindner, W. Rodejohann and X.-J. Xu, *Probing neutrino coupling to a light scalar with coherent neutrino scattering*, *JHEP* **05** (2018) 066 [1802.05171].

[330] J. Barranco, O. G. Miranda and T. I. Rashba, *Low energy neutrino experiments sensitivity to physics beyond the Standard Model*, *Phys. Rev. D* **76** (2007) 073008 [hep-ph/0702175].

[331] COHERENT collaboration, D. Akimov et al., *First Measurement of Coherent Elastic Neutrino-Nucleus Scattering on Argon*, *Phys. Rev. Lett.* **126** (2021) 012002 [2003.10630].

[332] COHERENT collaboration, D. Akimov et al., *COHERENT Collaboration data release from the first detection of coherent elastic neutrino-nucleus scattering on argon*, 2006.12659.

[333] D. Akimov et al., *Measurement of the Coherent Elastic Neutrino-Nucleus Scattering Cross Section on CsI by COHERENT*, 2110.07730.

[334] D. Baxter et al., *Coherent Elastic Neutrino-Nucleus Scattering at the European Spallation Source*, *JHEP* **02** (2020) 123 [1911.00762].

[335] TEXONO collaboration, S. Kerman, V. Sharma, M. Deniz, H. T. Wong, J. W. Chen, H. B. Li et al., *Coherency in Neutrino-Nucleus Elastic Scattering*, *Phys. Rev. D* **93** (2016) 113006 [1603.08786].

[336] J. Colaresi, J. I. Collar, T. W. Hossbach, A. R. L. Kavner, C. M. Lewis, A. E. Robinson et al., *First results from a search for coherent elastic neutrino-nucleus scattering at a reactor site*, *Phys. Rev. D* **104** (2021) 072003 [2108.02880].

[337] J. Colaresi, J. I. Collar, T. W. Hossbach, C. M. Lewis and K. M. Yocum, *Suggestive evidence for Coherent Elastic Neutrino-Nucleus Scattering from reactor antineutrinos*, 2202.09672.

[338] R. Rapp, "SNS Neutrino Flux." https://conference.sns.gov/event/171/attachments/258/1358/fpsts2019_rapp.pdf, 7, 2019.

[339] G. C. Rich, *Measurement of Low-Energy Nuclear-Recoil Quenching Factors in CsI[Na] and Statistical Analysis of the First Observation of Coherent, Elastic Neutrino-Nucleus Scattering*, Ph.D. thesis, North Carolina U., 2017. 10.17615/972g-w286.

[340] COHERENT collaboration, D. Akimov et al., *Simulating the neutrino flux from the Spallation Neutron Source for the COHERENT experiment*, 2109.11049.

[341] R. H. Helm, *Inelastic and Elastic Scattering of 187-Mev Electrons from Selected Even-Even Nuclei*, *Phys. Rev.* **104** (1956) 1466.

[342] J. D. Lewin and P. F. Smith, *Review of mathematics, numerical factors, and corrections for dark matter experiments based on elastic nuclear recoil*, *Astropart. Phys.* **6** (1996) 87.

[343] D. Akimov, J. Albert, P. An, C. Awe, P. Barbeau, B. Becker et al., *COHERENT Collaboration data release from the first observation of coherent elastic neutrino-nucleus scattering*, Apr., 2018. 10.5281/zenodo.1228631.

[344] D. Akimov, J. Albert, P. An, C. Awe, P. Barbeau, B. Becker et al., *COHERENT Collaboration data release from the first detection of coherent elastic neutrino-nucleus scattering on argon*, June, 2020. 10.5281/zenodo.3903810.

[345] D. Akimov, P. An, C. Awe, P. S. Barbeau, B. Becker, V. Belov et al., *Measurement of the coherent elastic neutrino-nucleus scattering cross section on csi by coherent*, 2021. 10.48550/ARXIV.2110.07730.

[346] J. I. Collar, A. R. L. Kavner and C. M. Lewis, *Response of CsI[Na] to Nuclear Recoils: Impact on Coherent Elastic Neutrino-Nucleus Scattering (CEνNS)*, *Phys. Rev. D* **100** (2019) 033003 [1907.04828].

[347] J. B. Birks, *Scintillations from Organic Crystals: Specific Fluorescence and Relative Response to Different Radiations*, *Proc. Phys. Soc. A* **64** (1951) 874.

[348] A. Falkowski, M. González-Alonso and K. Mimouni, *Compilation of low-energy constraints on 4-fermion operators in the SMEFT*, *JHEP* **08** (2017) 123 [1706.03783].

[349] SUPER-KAMIOKANDE collaboration, Y. Fukuda et al., *Evidence for oscillation of atmospheric neutrinos*, *Phys. Rev. Lett.* **81** (1998) 1562 [`hep-ex/9807003`].

[350] SNO collaboration, Q. R. Ahmad et al., *Direct evidence for neutrino flavor transformation from neutral current interactions in the Sudbury Neutrino Observatory*, *Phys. Rev. Lett.* **89** (2002) 011301 [`nucl-ex/0204008`].

[351] P. F. de Salas, D. V. Forero, S. Gariazzo, P. Martínez-Miravé, O. Mena, C. A. Ternes et al., *2020 Global reassessment of the neutrino oscillation picture*, `2006.11237`.

[352] P. Minkowski, $\mu \to e\gamma$ *at a rate of one out of 109 muon decays?*, *Physics Letters B* **67** (1977) 421.

[353] R. N. Mohapatra and G. Senjanović, *Neutrino mass and spontaneous parity nonconservation*, *Phys. Rev. Lett.* **44** (1980) 912.

[354] J. Schechter and J. W. F. Valle, *Neutrino masses in su(2)* $\bigotimes$ *u(1) theories*, *Phys. Rev. D* **22** (1980) 2227.

[355] T. P. Cheng and L.-F. Li, *Neutrino masses, mixings, and oscillations in su(2)xu(1) models of electroweak interactions*, *Phys. Rev. D* **22** (1980) 2860.

[356] D. Wyler and L. Wolfenstein, *Massless Neutrinos in Left-Right Symmetric Models*, *Nucl. Phys. B* **218** (1983) 205.

[357] R. N. Mohapatra and J. W. F. Valle, *Neutrino Mass and Baryon Number Nonconservation in Superstring Models*, *Phys. Rev. D* **34** (1986) 1642.

[358] J. Bernabeu, A. Santamaria, J. Vidal, A. Mendez and J. W. F. Valle, *Lepton Flavor Nonconservation at High-Energies in a Superstring Inspired Standard Model*, *Phys. Lett. B* **187** (1987) 303.

[359] S. Khalil, *TeV-scale gauged B-L symmetry with inverse seesaw mechanism*, *Phys. Rev. D* **82** (2010) 077702 [`1004.0013`].

[360] A. Das, P. S. Bhupal Dev and N. Okada, *Direct bounds on electroweak scale pseudo-Dirac neutrinos from* $\sqrt{s} = 8$ *TeV LHC data*, *Phys. Lett. B* **735** (2014) 364 [`1405.0177`].

[361] A. Das and N. Okada, *Improved bounds on the heavy neutrino productions at the LHC*, *Phys. Rev. D* **93** (2016) 033003 [`1510.04790`].

[362] G. Anamiati, M. Hirsch and E. Nardi, *Quasi-Dirac neutrinos at the LHC*, *JHEP* **10** (2016) 010 [`1607.05641`].

[363] A. Das, P. S. B. Dev and R. N. Mohapatra, *Same Sign versus Opposite Sign Dileptons as a Probe of Low Scale Seesaw Mechanisms*, *Phys. Rev. D* **97** (2018) 015018 [`1709.06553`].

[364] E. K. Akhmedov, M. Lindner, E. Schnapka and J. W. F. Valle, *Left-right symmetry breaking in NJL approach*, *Phys. Lett. B* **368** (1996) 270 [`hep-ph/9507275`].

[365] M. Malinsky, J. C. Romao and J. W. F. Valle, *Novel supersymmetric SO(10) seesaw mechanism*, *Phys. Rev. Lett.* **95** (2005) 161801 [`hep-ph/0506296`].

[366] C. O. Dib, G. R. Moreno and N. A. Neill, *Neutrinos with a linear seesaw mechanism in a scenario of gauged B-L symmetry*, *Phys. Rev. D* **90** (2014) 113003 [`1409.1868`].

[367] C. Arbeláez, C. Dib, K. Monsálvez-Pozo and I. Schmidt, *Quasi-Dirac neutrinos in the linear seesaw model*, *JHEP* **07** (2021) 154 [`2104.08023`].

[368] J. Gluza and T. Jeliński, *Heavy neutrinos and the pp → lljj CMS data*, *Phys. Lett. B* **748** (2015) 125 [`1504.05568`].

[369] ATLAS collaboration, G. Aad et al., *Search for heavy Majorana neutrinos with the ATLAS detector in pp collisions at $\sqrt{s} = 8$ TeV*, *JHEP* **07** (2015) 162 [`1506.06020`].

[370] CMS collaboration, V. Khachatryan et al., *Search for heavy Majorana neutrinos in $\mu^{\pm}\mu^{\pm}+$ jets events in proton-proton collisions at $\sqrt{s} = 8$ TeV*, *Phys. Lett. B* **748** (2015) 144 [`1501.05566`].

[371] CMS collaboration, *Search for heavy Majorana neutrinos in the same-sign dilepton channel in proton-proton collisions at sqrt(s) = 13 TeV*, .

[372] E. Izaguirre and B. Shuve, *Multilepton and Lepton Jet Probes of Sub-Weak-Scale Right-Handed Neutrinos*, *Phys. Rev. D* **91** (2015) 093010 [`1504.02470`].

[373] F. del Aguila and J. A. Aguilar-Saavedra, *Electroweak scale seesaw and heavy Dirac neutrino signals at LHC*, *Phys. Lett. B* **672** (2009) 158 [`0809.2096`].

[374] F. del Aguila, J. A. Aguilar-Saavedra and J. de Blas, *Trilepton signals: the golden channel for seesaw searches at LHC*, *Acta Phys. Polon. B* **40** (2009) 2901 [`0910.2720`].

[375] C.-Y. Chen and P. S. B. Dev, *Multi-Lepton Collider Signatures of Heavy Dirac and Majorana Neutrinos*, *Phys. Rev. D* **85** (2012) 093018 [`1112.6419`].

[376] S. Dube, D. Gadkari and A. M. Thalapillil, *Lepton-Jets and Low-Mass Sterile Neutrinos at Hadron Colliders*, *Phys. Rev. D* **96** (2017) 055031 [`1707.00008`].

[377] CMS collaboration, A. M. Sirunyan et al., *Search for heavy neutral leptons in events with three charged leptons in proton-proton collisions at $\sqrt{s} = 13$ TeV*, *Phys. Rev. Lett.* **120** (2018) 221801 [`1802.02965`].

[378] C. O. Dib, C. S. Kim, K. Wang and J. Zhang, *Distinguishing Dirac/Majorana Sterile Neutrinos at the LHC*, *Phys. Rev. D* **94** (2016) 013005 [`1605.01123`].

[379] C. O. Dib, C. S. Kim and K. Wang, *Signatures of Dirac and Majorana sterile neutrinos in trilepton events at the LHC*, *Phys. Rev. D* **95** (2017) 115020 [`1703.01934`].

[380] C. O. Dib, C. S. Kim and K. Wang, *Search for Heavy Sterile Neutrinos in Trileptons at the LHC*, *Chin. Phys. C* **41** (2017) 103103 [`1703.01936`].

[381] C. Arbeláez, C. Dib, I. Schmidt and J. C. Vásquez, *Probing the Dirac or Majorana nature of the Heavy Neutrinos in pure leptonic decays at the LHC*, *Phys. Rev. D* **97** (2018) 055011 [1712.08704].

[382] C. O. Dib, C. S. Kim and S. Tapia Araya, *Search for light sterile neutrinos from $W^{\pm}$ decays at the LHC*, *Phys. Rev. D* **101** (2020) 035022 [1903.04905].

[383] C. O. Dib, C. S. Kim, N. A. Neill and X.-B. Yuan, *Search for sterile neutrinos decaying into pions at the LHC*, *Phys. Rev. D* **97** (2018) 035022 [1801.03624].

[384] A. B. Balantekin, A. de Gouvêa and B. Kayser, *Addressing the Majorana vs. Dirac Question with Neutrino Decays*, *Phys. Lett. B* **789** (2019) 488 [1808.10518].

[385] A. de Gouvea, P. J. Fox, B. J. Kayser and K. J. Kelly, *Three-Body Decays of Heavy Dirac and Majorana Fermions*, 2104.05719.

[386] A. Blondel, A. de Gouvêa and B. Kayser, *Z-Boson Decays into Majorana or Dirac (Heavy) Neutrinos*, 2105.06576.

[387] J. Gluza, T. Jelinski and R. Szafron, *Lepton number violation and 'Diracness' of massive neutrinos composed of Majorana states*, *Phys. Rev. D* **93** (2016) 113017 [1604.01388].

[388] P. S. Bhupal Dev and R. N. Mohapatra, *Unified explanation of the eejj, diboson and dijet resonances at the LHC*, *Phys. Rev. Lett.* **115** (2015) 181803 [1508.02277].

[389] F. F. Deppisch, P. S. Bhupal Dev and A. Pilaftsis, *Neutrinos and Collider Physics*, *New J. Phys.* **17** (2015) 075019 [1502.06541].

[390] J. De Vries, H. K. Dreiner, J. Y. Günther, Z. S. Wang and G. Zhou, *Long-lived Sterile Neutrinos at the LHC in Effective Field Theory*, *JHEP* **03** (2021) 148 [2010.07305].

[391] M. Hirsch and Z. S. Wang, *Heavy neutral leptons at ANUBIS*, *Phys. Rev. D* **101** (2020) 055034 [2001.04750].

[392] G. Cottin, J. C. Helo and M. Hirsch, *Displaced vertices as probes of sterile neutrino mixing at the LHC*, *Phys. Rev. D* **98** (2018) 035012 [1806.05191].

[393] ATLAS collaboration, M. Aaboud et al., *Search for long-lived, massive particles in events with displaced vertices and missing transverse momentum in $\sqrt{s} = 13$ TeV pp collisions with the ATLAS detector*, *Phys. Rev. D* **97** (2018) 052012 [1710.04901].

[394] ATLAS collaboration, G. Aad et al., *Search for massive, long-lived particles using multitrack displaced vertices or displaced lepton pairs in pp collisions at $\sqrt{s} = 8$ TeV with the ATLAS detector*, *Phys. Rev. D* **92** (2015) 072004 [1504.05162].

[395] D. Zhu, *Search for Long-Lived Heavy Neutral Leptons and Detector Modules for the CMS Pixel Phase 1 Upgrade*, Ph.D. thesis, Zurich, ETH, 2020. 10.3929/ethz-b-000447851.

[396] I. Cordero-Carrión, M. Hirsch and A. Vicente, *General parametrization of Majorana neutrino mass models*, *Phys. Rev. D* **101** (2020) 075032 [1912.08858].

[397] Y. Cai, J. Herrero-García, M. A. Schmidt, A. Vicente and R. R. Volkas, *From the trees to the forest: a review of radiative neutrino mass models*, *Front. in Phys.* **5** (2017) 63 [1706.08524].

[398] S. Ray, *Renormalization group evolution of neutrino masses and mixing in seesaw models: A Review*, *Int. J. Mod. Phys. A* **25** (2010) 4339 [1005.1938].

[399] S. Antusch, E. Cazzato and O. Fischer, *Resolvable heavy neutrino–antineutrino oscillations at colliders*, *Mod. Phys. Lett. A* **34** (2019) 1950061 [1709.03797].

[400] A. Atre, T. Han, S. Pascoli and B. Zhang, *The Search for Heavy Majorana Neutrinos*, *JHEP* **05** (2009) 030 [0901.3589].

[401] J. C. Helo, S. Kovalenko and I. Schmidt, *Sterile neutrinos in lepton number and lepton flavor violating decays*, *Nucl. Phys. B* **853** (2011) 80 [1005.1607].

[402] K. Bondarenko, A. Boyarsky, D. Gorbunov and O. Ruchayskiy, *Phenomenology of GeV-scale Heavy Neutral Leptons*, *JHEP* **11** (2018) 032 [1805.08567].

[403] G. Cvetic, C. Dib, C. S. Kim and J. Zamora-Saa, *Probing the Majorana neutrinos and their CP violation in decays of charged scalar mesons π, K, D, D_s, B, B_c*, *Symmetry* **7** (2015) 726 [1503.01358].

[404] A. Lami, J. Portolés and P. Roig, *Lepton flavor violation in hadronic decays of the tau lepton in the simplest little Higgs model*, *Phys. Rev.* **D93** (2016) 076008 [1601.07391].

[405] I. Cordero-Carrión, M. Hirsch and A. Vicente, *Master Majorana neutrino mass parametrization*, *Phys. Rev. D* **99** (2019) 075019 [1812.03896].

[406] P. de Salas, D. Forero, C. Ternes, M. Tortola and J. Valle, *Status of neutrino oscillations 2018: 3σ hint for normal mass ordering and improved CP sensitivity*, *Phys. Lett. B* **782** (2018) 633 [1708.01186].

[407] M. Gell-Mann, P. Ramond and R. Slansky, *Complex Spinors and Unified Theories*, *Conf. Proc. C* **790927** (1979) 315 [1306.4669].

[408] J. C. Helo, M. Hirsch and Z. S. Wang, *Heavy neutral fermions at the high-luminosity LHC*, *JHEP* **07** (2018) 056 [1803.02212].

[409] P. D. Bolton, F. F. Deppisch and P. S. Bhupal Dev, *Neutrinoless double beta decay versus other probes of heavy sterile neutrinos*, *JHEP* **03** (2020) 170 [1912.03058].

[410] BELLE-II collaboration, W. Altmannshofer et al., *The Belle II Physics Book*, *PTEP* **2019** (2019) 123C01 [1808.10567].

[411] D. G. Dumm, P. Roig, A. Pich and J. Portolés, *tau —> pi pi pi nu(tau) decays and the a(1)(1260) off-shell width revisited*, *Phys. Lett. B* **685** (2010) 158 [`0911.4436`].

[412] J. J. Sanz-Cillero and O. Shekhovtsova, *Refining the scalar and tensor contributions in $\tau \to \pi\pi\pi\nu_\tau$ decays*, *JHEP* **12** (2017) 080 [`1707.01137`].

[413] P. Herrera-Siklódy, J. Latorre, P. Pascual and J. Tarón, *Eta - eta-prime mixing from U(3)(L) x U(3)(R) chiral perturbation theory*, *Phys. Lett. B* **419** (1998) 326 [`hep-ph/9710268`].

[414] R. Kaiser and H. Leutwyler, *Pseudoscalar decay constants at large N(c)*, in *Nonperturbative methods in quantum field theory. Proceedings, Workshop, Adelaide, Australia, February 2-13, 1998*, pp. 15–29, 6, 1998, `hep-ph/9806336`.

[415] R. J. Crewther, *Nonperturbative evaluation of the anomalies in low-energy theorems*, *Phys. Rev. Lett.* **28** (1972) 1421.

[416] M. S. Chanowitz and J. R. Ellis, *Canonical Anomalies and Broken Scale Invariance*, *Phys. Lett.* **40B** (1972) 397.

[417] J. C. Collins, A. Duncan and S. D. Joglekar, *Trace and Dilatation Anomalies in Gauge Theories*, *Phys. Rev.* **D16** (1977) 438.

[418] M. A. Shifman, A. I. Vainshtein and V. I. Zakharov, *Remarks on Higgs Boson Interactions with Nucleons*, *Phys. Lett.* **78B** (1978) 443.

[419] L. D. Landau, *On the angular momentum of a system of two photons*, *Dokl. Akad. Nauk SSSR* **60** (1948) 207.

[420] C.-N. Yang, *Selection Rules for the Dematerialization of a Particle Into Two Photons*, *Phys. Rev.* **77** (1950) 242.

[421] X.-D. Ji, *Breakup of hadron masses and energy - momentum tensor of QCD*, *Phys. Rev.* **D52** (1995) 271 [`hep-ph/9502213`].

[422] J. Hořejší, *Ultraviolet and infrared aspects of the axial anomaly. 1*, *Czech. J. Phys.* **42** (1992) 241.

[423] J. Hořejší, *Ultraviolet and infrared aspects of the axial anomaly. 2*, *Czech. J. Phys.* **42** (1992) 345.

[424] G. Passarino and M. J. G. Veltman, *One Loop Corrections for e+ e- Annihilation Into mu+ mu- in the Weinberg Model*, *Nucl. Phys.* **B160** (1979) 151.